Progress of Theoretical Physics, Vol. 74, No. 6, December 1985

Microscopic Description of Anharmonic Gamma-Vibrations by Means of the Selfconsistent-Collective-Coordinate Method. I

Masayuki MATSUO and Kenichi MATSUYANAGI

Department of Physics, Kyoto University, Kyoto 606

(Received March 4, 1985)

We investigate, in a fully microscopic way, the double gamma-vibrational states in ^{168}Er by means of the selfconsistent-collective-coordinate (SCC) method proposed by Marumori, Maskawa, Sakata and Kuriyama. In applying the SCC method, we propose a new prescription to derive a quantized collective Hamiltonian. The collective potential is defined in terms of the Wigner transform of the quantized collective Hamiltonian. It is different from the potential defined by the energy expectation values with respect to the time-even Slater determinants, and we find that it acquires a much stronger tendency toward the triaxial equilibrium shape than the latter. Numerical calculations show that ^{168}Er is situated just in the transitional region toward the triaxial equilibrium shape.

§ 1. Introduction

The nuclear anharmonicities associated with low-frequency vibrational modes have been an outstanding subject in nuclear many-body problems. We encounter genuine non-linear vibrations, for instance, in transitional nuclei lying in the intermediate region between the spherical and deformed equilibrium shapes. For the aim of constructing a fully microscopic theory capable of describing the large-amplitude collective motions such as the non-linear nuclear vibrations, Marumori, Maskawa, Sakata and Kuriyama[1] have proposed a new theory called the selfconsistent-collective-coordinate (SCC) method.

The quadrupole collective modes associated with the γ-degree of freedom have been thought to constitute another typical example of large-amplitude, nuclear non-linear phenomena.[2] But, it is only recently that significant anharmonic character of the γ vibrations is demonstrated in a clear-cut way.[3]

In this paper, we shall analyse the microscopic structure of the anharmonicities associated with the γ-vibrational modes by means of the SCC method.[1] For this aim, we shall propose a new prescription to quantize the classical collective Hamiltonian derived by the SCC method. We also propose a new procedure to relate the resulting quantized Hamiltonian with the phenomenological Bohr Hamiltonian.[4]

We start in § 2 with the Nilsson model with the pairing plus quadrupole residual interactions, and review in § 3 the SCC method in a specialized form convenient to the description of the anharmonic γ vibrations. In § 4, we quantize the collective Hamiltonian obtained in § 3, and derive an approximate Bohr collective Hamiltonian in a fully microscopic way. We then present in § 5 the result of numerical calculation focussing our attention on the problem of current issue,[5)~9)] i.e., on the nature of double excitations of the γ-vibrational quanta in ^{168}Er. Our result will be compared in detail with the phenomenological analysis carried out by Dumitrescu and Hamamoto[5] in terms of the Bohr collective Hamiltonian. In § 6, we add some arguments to justify our procedure for deriving the quantized collective Hamiltonian.

For convenience of publication, a detailed analysis of the mode-mode couplings between different RPA-vibrations will be separately presented in Part II of this series of

paper.[10] A preliminary version of this work was previously reported in this journal.[11]

§ 2. The Hamiltonian and the RPA modes

We start with a Hamiltonian describing nucleons moving in the axially symmetric Nilsson potential. The residual interaction consists of the monopole-pairing and the doubly-stretched quadrupole forces:

$$\hat{H}=\hat{h}_{\rm def}+\hat{H}_{\rm int}\,, \tag{2·1}$$

$$\hat{h}_{\rm def}=\sum_{\mu>0}(\epsilon_\mu-\lambda)(c_\mu^\dagger c_\mu+c_{\bar\mu}^\dagger c_{\bar\mu})\,, \tag{2·2}$$

$$\hat{H}_{\rm int}=-G_0\hat{P}_{00}^\dagger\hat{P}_{00}-\frac{1}{2}\chi\sum_{K=-2}^{2}(-1)^K\hat{Q}''_{2K}\hat{Q}''_{2-K}\,, \tag{2·3}$$

where

$$\hat{P}_{00}^\dagger=\sum_{\mu>0}c_\mu^\dagger c_{\bar\mu}^\dagger\,, \tag{2·4}$$

$$\hat{Q}''_{2K}=\sum_{\mu\nu}\langle\mu|(r^2Y_{2K})''|\nu\rangle c_\mu^\dagger c_\nu\,. \tag{2·5}$$

Here the double prime in $\hat{Q}''_{2K}$ denotes that the coordinates x_i in r^2Y_{2K} are replaced by the doubly-stretched coordinates $x_i''=(\omega_i/\omega_0)x_i$, ω_i being the frequencies of the harmonic-oscillator (h.o.) potential (in the axially symmetric case, $\omega_1=\omega_2\equiv\omega_\perp$ and $\omega_3\equiv\omega_\parallel$). The other notations used above are familiar ones and would be self-explanatory.

The $Q''Q''$ force is the residual interaction for the fluctuations around the deformed equilibrium shape, which is naturally derived[12),13),26)] by applying the Landau-Migdal prescription to the h.o. potential model which satisfies the selfconsistency between the potential and the density. It is known that this force explains well the K-dependence of the ordinary QQ force-strengths for the β, γ vibrations, and the K-splitting of the isoscalar quadrupole giant resonances in deformed nuclei.*)

After the Bogoliubov transformation, we obtain the quasiparticle Hamiltonian in the Nilsson basis:

$$\hat{H}=\hat{H}_0+\hat{H}'_{\rm int}\,, \tag{2·6}$$

$$\hat{H}_0=\sum_{\mu>0}E_\mu(a_\mu^\dagger a_\mu+a_{\bar\mu}^\dagger a_{\bar\mu})\,, \tag{2·7}$$

$$\hat{H}'_{\rm int}=-\frac{1}{4}G_0(\tilde{P}_{00}^{(+)\dagger}\tilde{P}_{00}^{(+)}+\tilde{P}_{00}^{(-)\dagger}\tilde{P}_{00}^{(-)})-\frac{1}{2}\chi\sum_{K=-2}^{2}(-1)^K\tilde{Q}''_{2K}\tilde{Q}''_{2-K}\,, \tag{2·8}$$

where

$$\tilde{P}_{00}^{(\pm)\dagger}=\hat{P}_{00}^\dagger\pm\hat{P}_{00}-\langle\phi_0|\hat{P}_{00}^\dagger\pm\hat{P}_{00}|\phi_0\rangle \tag{2·9}$$

with $|\phi_0\rangle$ being the vacuum for the quasiparticles ($a_\mu^\dagger$, $a_{\bar\mu}^\dagger$). Owing to the selfconsistency

*) With the selfconsistently determined value of the force-strength χ, the $Q''Q''$ force automatically guarantees the zero-energy solutions of the RPA as the Nambu-Goldstone modes with respect to the rotational symmetry.[12),13),26)] When the selfconsistency and the symmetry are required in higher-order treatments, many-body forces (the three-body force, etc.) derived by the prescription should be added in the Hamiltonian. However, in this paper, we drop the higher-order interactions for simplicity.

condition, the expectation values $\langle\phi_0|\hat{Q}''_{2K}|\phi_0\rangle$ are zero at the equilibrium deformation so that $\tilde{Q}''_{2K}\equiv\hat{Q}''_{2K}-\langle\phi_0|\hat{Q}''_{2K}|\phi_0\rangle=\hat{Q}''_{2K}$. For simplicity of notations, we write $\hat{H}'_{\rm int}$ as follows:

$$\hat{H}'_{\rm int}=-\frac{1}{2}\sum_{\rho=1}^{9}\chi_\rho\hat{R}_\rho^{\dagger}\hat{R}_\rho\,, \tag{2·10}$$

where

$$\hat{R}_\rho=\{\tilde{P}_{00}^{(+n)}\tilde{P}_{00}^{(-n)},\ \tilde{P}_{00}^{(+p)},\ \tilde{P}_{00}^{(-p)},\ \tilde{Q}''^{\dagger}_{2K}\}\,, \tag{2·11}$$

$$\chi_\rho=\frac{1}{2}\{G_0^{(n)},\ G_0^{(n)},\ G_0^{(p)},\ G_0^{(p)},\ 2\varkappa\}\,, \tag{2·12}$$

and the letters n and p in the superscripts denote the neutron and proton parts of the pairing operators $P_{00}^{(\pm)}$.

The harmonic vibrational excitations

$$\hat{X}_\lambda^{\dagger}=\sum_{\mu<\nu}\{\psi_\lambda(\mu\nu)\,a_\mu^{\dagger}a_\nu^{\dagger}+\varphi_\lambda(\mu\nu)\,a_{\bar{\nu}}a_{\bar{\mu}}\} \tag{2·13}$$

are obtained by solving the RPA equation of motion

$$[\hat{H},\ \hat{X}_\lambda^{\dagger}]_{\rm RPA}=\omega_\lambda\hat{X}_\lambda^{\dagger} \tag{2·14}$$

under the normalization condition

$$\langle\phi_0|[\hat{X}_\lambda,\ \hat{X}_{\lambda'}^{\dagger}]|\phi_0\rangle=\sum_{\mu<\nu}\{\psi_\lambda(\mu\nu)\psi_{\lambda'}(\mu\nu)-\varphi_\lambda(\mu\nu)\varphi_{\lambda'}(\mu\nu)\}=\delta_{\lambda\lambda'}\,. \tag{2·15}$$

To deal with the situation where some of the eigenvalues ω_λ become zero or imaginary, we adopt the RPA formalism in the coordinate and momentum representation instead of Eqs. (2·14) and (2·15): The RPA coordinate and momentum operators,

$$\begin{aligned}\hat{Q}_\lambda&=\sum_{\mu<\nu}q_\lambda(\mu\nu)(a_\mu^{\dagger}a_\nu^{\dagger}+a_{\bar{\nu}}a_{\bar{\mu}})\,,\\ \hat{P}_\lambda^{\dagger}&=i\sum_{\mu<\nu}p_\lambda(\mu\nu)(a_\mu^{\dagger}a_\nu^{\dagger}-a_{\bar{\nu}}a_{\bar{\mu}})\,,\end{aligned} \tag{2·16}$$

are determined by

$$\left.\begin{aligned}[\hat{H},\ \hat{Q}_\lambda]_{\rm RPA}&=-\frac{i}{B_\lambda}\hat{P}_\lambda^{\dagger}\,,\\ [\hat{H},\ \hat{P}_\lambda^{\dagger}]_{\rm RPA}&=iC_\lambda\hat{Q}_\lambda\,,\end{aligned}\right\} \tag{2·17}$$

$$\langle\phi_0|[\hat{Q}_\lambda,\ \hat{P}_\lambda]|\phi_0\rangle=i\,, \tag{2·18}$$

where B_λ and C_λ are the mass and the restoring-force parameters, respectively. It is convenient in this case to introduce the phonon operators through

$$\hat{X}_\lambda^{\dagger}=\frac{1}{\sqrt{2}}(\hat{Q}_\lambda-i\hat{P}_\lambda^{\dagger}),\qquad \hat{X}_{\bar{\lambda}}=\frac{1}{\sqrt{2}}(\hat{Q}_\lambda^{\dagger}+i\hat{P}_\lambda)\,. \tag{2·19}$$

Since our Hamiltonian is axial symmetric and time-reversal invariant, the projection K of the angular momentum on the symmetry axis is a good quantum number, i.e.,

$$[\hat{J}_z,\ \hat{X}_\lambda^{\dagger}]=K_\lambda\hat{X}_\lambda^{\dagger}\,, \tag{2·20}$$

and the RPA modes appear in doublets, $\hat{X}_\lambda^{\dagger}$ and its time-reversed partner $\hat{X}_{\bar{\lambda}}^{\dagger}$, except for

$K_\lambda=0$. Below, we shall specifically denote the γ-vibrational modes in the RPA with $K=2$ and -2 as $\hat{X}_\gamma{}^\dagger$ and $\hat{X}_{\bar{\gamma}}{}^\dagger$, respectively.

§3. The SCC method for anharmonic γ vibrations

3.1. *The basic equations*

Let the total number of physical RPA modes be Ω, and let us consider the general time-dependent Hartree-Bogoliubov (TDHB) state vector

$$|\phi(t)\rangle=\exp\sum_{\lambda=1}^{\Omega}(G_\lambda(t)\hat{X}_\lambda{}^\dagger-G_\lambda{}^*(t)\hat{X}_\lambda)|\phi_0\rangle\,. \tag{3·1}$$

The time evolution of $|\phi(t)\rangle$ is described as a classical trajectory in the 2Ω dimensional phase space parametrized by $G_\lambda(t)$ and $G_\lambda{}^*(t)$, which are determined by the well-known TDHB equation. Our aim is to dynamically extract the collective submanifold, which is optimal to describe the anharmonic γ-vibrational modes, from this huge-dimensional phase space.

Since the number of the RPA operators $(\hat{X}_\gamma{}^\dagger, \hat{X}_\gamma, \hat{X}_{\bar{\gamma}}{}^\dagger, \hat{X}_{\bar{\gamma}})$ creating and annihilating the γ-vibrational modes in the harmonic limit is four, let us assume that the number of collective coordinates describing the anharmonic γ vibrations is also four.*) Denoting these collective coordinates as $(\eta^*, \eta, \tilde{\eta}^*, \tilde{\eta})$, let us consider the TDHB state whose time-evolution is entirely described by η's:

$$|\phi(\eta_i{}^*, \eta_i)\rangle=e^{i\hat{G}(\eta_i{}^*,\ \eta_i)}|\phi_0\rangle\equiv\hat{U}^{-1}(\eta_i{}^*, \eta_i)|\phi_0\rangle\,, \tag{3·2}$$

$$i\hat{G}(\eta_i{}^*, \eta_i)=\sum_\lambda(G_\lambda(\eta_i{}^*, \eta_i)\hat{X}_\lambda{}^\dagger-G_\lambda{}^*(\eta_i{}^*, \eta_i)\hat{X}_\lambda)\,, \tag{3·3}$$

where η_i $(i=1, 2)$ are defined by

$$\eta_1\equiv\eta \qquad \text{and} \qquad \eta_2\equiv\tilde{\eta}\,. \tag{3·4}$$

We set $\hat{U}^{-1}=1$ at $\eta_i=0$.

The basic principle of the SCC method is the "invariance principle of the Schrödinger equation."[14] This principle requires that the collective subspace and the time-evolution of the collective coordinates $(\eta_i{}^*, \eta_i)$ be determined such that the TDHB equation holds also for $|\phi(\eta_i{}^*, \eta_i)\rangle$:

$$\delta\langle\phi(\eta_i{}^*, \eta_i)|i\frac{\partial}{\partial t}-\hat{H}|\phi(\eta_i{}^*, \eta_i)\rangle=0\,. \tag{3·5}$$

The trajectories of $|\phi(\eta_i{}^*, \eta_i)\rangle$ thus determined constitute the collective subspace (submanifold) which is expected to be an invariant subspace of the TDHB phase space.

The basic equations of the SCC method to determine the unknown functions $G_\lambda(\eta_i{}^*, \eta_i)$ are summarized as follows:

*) Here we assume that the coupling between the γ vibration and the collective rotation is weak so that it is not necessary to take into account the degrees of freedom of the collective rotation explicitly. This assumption may be justified in the case of the well-deformed nuclei such as ^{168}Er investigated in § 5.

i) *the equation of collective subspace*

$$\delta\langle\phi_0|\Big\{\hat{U}(\eta_i^*,\eta_i)\hat{H}\hat{U}^{-1}(\eta_i^*,\eta_i)-\sum_i\Big(\frac{\partial\mathcal{H}}{\partial\eta_i^*}\hat{O}_i^{\dagger}(\eta_j^*,\eta_j)+\frac{\partial\mathcal{H}}{\partial\eta_i}\hat{O}_i(\eta_j^*,\eta_j)\Big)\Big\}|\phi_0\rangle=0\,, \quad (3\cdot6)$$

which is derived from Eq. (3·5). Here

$$\hat{O}_i^{\dagger}(\eta_j^*,\eta_j)=\hat{U}(\eta_j^*,\eta_j)\frac{\partial}{\partial\eta_i}\hat{U}^{-1}(\eta_j^*,\eta_j)\,,$$

$$\hat{O}_i(\eta_j^*,\eta_j)=-\hat{U}(\eta_j^*,\eta_j)\frac{\partial}{\partial\eta_i^*}\hat{U}^{-1}(\eta_j^*,\eta_j)\,, \quad (3\cdot7)$$

and the collective Hamiltonian $\mathcal{H}$ is defined by

$$\mathcal{H}(\eta_i^*,\eta_i)=\langle\phi_0|\hat{U}(\eta_i^*,\eta_i)\hat{H}\hat{U}^{-1}(\eta_i^*,\eta_i)|\phi_0\rangle-\langle\phi_0|\hat{H}|\phi_0\rangle\,. \quad (3\cdot8)$$

ii) *the canonical-variables conditions*

$$\langle\phi_0|\hat{O}_i^{\dagger}(\eta_j^*,\eta_j)|\phi_0\rangle=\frac{1}{2}\eta_i^* \quad \text{and} \quad \langle\phi_0|\hat{O}_i(\eta_j^*,\eta_j)|\phi_0\rangle=\frac{1}{2}\eta_i\,. \quad (3\cdot9)$$

It is then easily confirmed that the time-development of η's is determined by the canonical equation

$$\dot{\eta}_i=\frac{1}{i}\frac{\partial\mathcal{H}}{\partial\eta_i^*}=\{\eta_i,\mathcal{H}\}_{\text{P.B.}} \quad \text{and} \quad \text{c.c.} \quad (3\cdot10)$$

with the Poisson bracket being defined by

$$\{A,B\}_{\text{P.B.}}=\frac{1}{i}\sum_{i=1}^{2}\Big\{\frac{\partial A}{\partial\eta_i}\frac{\partial B}{\partial\eta_i^*}-\frac{\partial B}{\partial\eta_i}\frac{\partial A}{\partial\eta_i^*}\Big\}\,. \quad (3\cdot11)$$

The collective representation of an operator $\hat{F}$ is defined by

$$\mathcal{F}(\eta_i^*,\eta_i)=\langle\phi_0|\hat{U}(\eta_i^*,\eta_i)\hat{F}\hat{U}^{-1}(\eta_i^*,\eta_i)|\phi_0\rangle-\langle\phi_0|\hat{F}|\phi_0\rangle\,. \quad (3\cdot12)$$

In the following, we shall always neglect the Fock term in accordance with the use of the separable-type residual interactions. This means that the expectation values of $\hat{H}'_{\text{int}}$ are evaluated as

$$\langle\phi(\eta_i^*,\eta_i)|\hat{H}'_{\text{int}}|\phi(\eta_i^*,\eta_i)\rangle=-\frac{1}{2}\sum_{\rho}\chi_{\rho}\mathcal{R}_{\rho}^*(\eta_i^*,\eta_i)\mathcal{R}_{\rho}(\eta_i^*,\eta_i)\,, \quad (3\cdot13)$$

$$\mathcal{R}_{\rho}(\eta_i^*,\eta_i)=\langle\phi_0|\hat{U}(\eta_i^*,\eta_i)\hat{R}_{\rho}\hat{U}^{-1}(\eta_i^*,\eta_i)|\phi_0\rangle\,. \quad (3\cdot14)$$

In this approximation, the equation of collective subspace (3·6) can be written as

$$\langle\phi_0|\Big[\hat{U}\hat{H}_0\hat{U}^{-1}-\frac{1}{2}\sum_{\rho}\chi_{\rho}(\mathcal{R}_{\rho}(\eta_i^*,\eta_i)\hat{U}\hat{R}_{\rho}^{\dagger}\hat{U}^{-1}+\mathcal{R}_{\rho}^*(\eta_i^*,\eta_i)\hat{U}\hat{R}_{\rho}\hat{U}^{-1})$$

$$-\sum_i\Big(\frac{\partial\mathcal{H}}{\partial\eta_i^*}\hat{U}\frac{\partial}{\partial\eta_i}\hat{U}^{-1}-\frac{\partial\mathcal{H}}{\partial\eta_i}\hat{U}\frac{\partial}{\partial\eta_i^*}\hat{U}^{-1}\Big),\quad \hat{X}_{\lambda}\Big]|\phi_0\rangle=0$$

and c.c. for all λ. $(3\cdot15)$

3.2. *The (η^*,η) expansion with an optimized RPA boundary condition*

To solve the basic equations (3·6) and (3·9), let us expand the unknown functions $G_{\lambda}(\eta_i^*,\eta_i)$ in a power series of η_i^* and η_i as

$$G_\lambda=\sum_{n=1}^{\infty} G_\lambda^{(n)} \quad \text{with} \quad G_\lambda^{(n)}=\sum_{i+j+k+l=n} g_\lambda^{(ijkl)}\eta^{*i}\eta^{j}\tilde{\eta}^{*k}\tilde{\eta}^{l}\,. \tag{3·16}$$

Correspondingly, the collective Hamiltonian $\mathcal{H}$ is expanded as

$$\mathcal{H}=\sum_{n=1}^{\infty}\mathcal{H}^{(n+1)} \quad \text{with} \quad \mathcal{H}^{(n+1)}=\sum_{i+j+k+l=n+1} h^{(ijkl)}\eta^{*i}\eta^{j}\tilde{\eta}^{*k}\tilde{\eta}^{l}\,, \tag{3·17}$$

where the $(n+1)$-th order term is determined by $G_\lambda^{(k)}$'s with $k\leq n$. The unknown coefficients $g_\lambda^{(ijkl)}$ are determined such that Eqs. (3·6) and (3·9) are satisfied order by order with respect to the powers of (η_i^*, η_i) specified by n. Then $h^{(ijkl)}$ are immediately obtained. Note that $\mathcal{H}^{(1)}=0$ due to the Hartree-Bogoliubov condition $\delta\langle\phi_0|\hat{H}|\phi_0\rangle=0$.

It is very important to set up a proper boundary condition for the lowest-order term; i.e., for $n=1$. Since we want to describe the anharmonic γ vibrations, we require that they reduce to the harmonic γ vibrations in the small amplitude limit; i.e., we require that the lowest-order term of $i\hat{G}$ consists of the RPA γ-vibrational phonon operators. Then we obtain from Eq. (3·9)

$$i\hat{G}^{(1)}=\sum_{\lambda=\gamma,\tilde{\gamma}}(G_\lambda^{(1)}\hat{X}_\lambda^{\dagger}-G_\lambda^{(1)*}\hat{X}_\lambda)\,, \tag{3·18}$$

$$G_\lambda^{(1)}=\sum_i(\sigma_{\lambda i}\eta_i+\tau_{\lambda i}\eta_i^*)\,, \qquad (\lambda=\gamma,\ \tilde{\gamma}) \tag{3·19}$$

where $\sigma_{\lambda i}$ and $\tau_{\lambda i}$ are arbitrary complex numbers satisfying

$$\left.\begin{aligned}&\sum_{\lambda=\gamma,\tilde{\gamma}}(\sigma_{\lambda i}\sigma_{\lambda j}^*-\tau_{\lambda i}^*\tau_{\lambda j})=\delta_{ij}\,,\\ &\sum_{\lambda=\gamma,\tilde{\gamma}}(\sigma_{\lambda i}\tau_{\lambda j}^*-\tau_{\lambda i}^*\sigma_{\lambda j})=0\,.\end{aligned}\right\} \tag{3·20}$$

It is immediately confirmed that the equation of collective subspace (3·6) is satisfied in this order. There remains an ambiguity for the solutions of Eq. (3·20), which is connected with the invariance property of the fundamental equations (3·6)~(3·9) with respect to linear canonical transformations of the collective coordinates (η_i^*, η_i).[15]

We fix the coefficients $\sigma_{\lambda i}$ and $\tau_{\lambda i}$ by the following procedure. In order to guarantee that the (η^*, η) transfer the K-quantum number by $(2, -2)$ and that $(\tilde{\eta}^*, \tilde{\eta})$ coincide with the time-reversal of (η^*, η), we restrict the general solution (3·19) to

$$\left.\begin{aligned}&G_\gamma^{(1)}=\sigma\,\eta+\tau\tilde{\eta}^*\,,\\ &G_{\tilde{\gamma}}^{(1)}=\sigma^*\tilde{\eta}+\tau^*\eta^* \quad \text{with} \quad |\sigma|^2-|\tau|^2=1\,.\end{aligned}\right\} \tag{3·21}$$

We then fix the remaining arbitrary coefficients σ and τ by the condition

$$\langle\phi_0|\hat{Y}_{\tilde{\gamma}}\hat{Y}_\gamma|\phi_0\rangle=0\,, \tag{3·22}$$

where

$$\hat{Y}_\gamma\equiv\sigma\hat{X}_\gamma-\tau\hat{X}_{\tilde{\gamma}}^{\dagger}, \qquad \hat{Y}_{\tilde{\gamma}}\equiv\sigma^*\hat{X}_{\tilde{\gamma}}-\tau^*\hat{X}_\gamma^{\dagger}\,. \tag{3·23}$$

The solution of Eq. (3·22) is readily found to be

$$\sigma=\frac{1}{2}(s+s^{-1}), \qquad \tau=\frac{1}{2}(s-s^{-1}), \tag{3·24}$$

$$s^4=\sum_{\mu<\nu}\{\psi_\gamma(\mu\nu)+\varphi_\gamma(\mu\nu)\}^2/\sum_{\mu<\nu}\{\psi_\gamma(\mu\nu)-\varphi_\gamma(\mu\nu)\}^2. \tag{3·25}$$

Thus the lowest-order term of $1\hat{G}$ is completely determined as

$$i\hat{G}^{(1)}=(\eta\hat{Y}_\gamma{}^\dagger-\eta^*\hat{Y}_\gamma)+(\tilde{\eta}\hat{Y}_{\tilde{\gamma}}{}^\dagger-\tilde{\eta}^*\hat{Y}_{\tilde{\gamma}}). \tag{3·26}$$

This expression shows that we can consider the collective coordinates $(\eta^*, \eta, \tilde{\eta}^*, \tilde{\eta})$ to correspond to the operators $(\hat{Y}_\gamma{}^\dagger, \hat{Y}_\gamma, \hat{Y}_{\tilde{\gamma}}{}^\dagger, \hat{Y}_{\tilde{\gamma}})$ in the lowest order. The choice (3·26) with the values given by (3·24) is called "an optimized RPA boundary condition", since it is designed to be optimally suited to the quantization procedure with the normal ordering (see Ref. 16) and § 6 of this paper). The collective Hamiltonian in this order is given by

$$\mathcal{H}^{(2)}=\alpha(\eta^*\eta+\tilde{\eta}^*\tilde{\eta})+\beta(\eta^*\tilde{\eta}^*+\eta\tilde{\eta}) \tag{3·27}$$

with

$$\alpha=\frac{1}{2}(s^2C_\gamma+s^{-2}B_\gamma{}^{-1}),$$

$$\beta=\frac{1}{2}(s^2C_\gamma-s^{-2}B_\gamma{}^{-1}). \tag{3·28}$$

The next-order ($n=2$) solution of the (η^*, η) expansion is then obtained as

$$\left.\begin{aligned} G_\lambda{}^{(2)}=&\left\{\omega_\lambda-\alpha\sum_{i=1,2}\left(\eta_i\frac{\partial}{\partial\eta_i}-\eta_i{}^*\frac{\partial}{\partial\eta_i{}^*}\right)\right.\\ &\left.-\beta\left(\tilde{\eta}^*\frac{\partial}{\partial\eta}+\eta^*\frac{\partial}{\partial\tilde{\eta}}-\tilde{\eta}\frac{\partial}{\partial\eta^*}-\eta\frac{\partial}{\partial\tilde{\eta}^*}\right)\right\}^{-1}B_\lambda{}^{(2)} \text{ for } K_\lambda=0 \text{ and } \pm4,\\ G_\lambda{}^{(2)}=&0 \qquad\qquad \text{otherwise}, \end{aligned}\right\} \tag{3·29}$$

$$\mathcal{H}^{(3)}=0, \tag{3·30}$$

where

$$\begin{aligned} B_\lambda{}^{(2)}=-\frac{1}{2}\sum_\rho\chi_\rho\Big\{&\frac{1}{2}\langle\phi_0|[\hat{R}_\rho{}^\dagger, \hat{X}_\lambda]|\phi_0\rangle\langle\phi_0|[[\hat{R}_\rho, i\hat{G}^{(1)}], i\hat{G}^{(1)}]|\phi_0\rangle\\ &+\langle\phi_0|[[\hat{R}_\rho{}^\dagger, i\hat{G}^{(1)}], \hat{X}_\lambda]|\phi_0\rangle\langle\phi_0|[\hat{R}_\rho, i\hat{G}^{(1)}]|\phi_0\rangle+(\hat{R}_\rho{}^\dagger\leftrightarrow\hat{R}_\rho)\Big\}, \end{aligned} \tag{3·31}$$

$$i\hat{G}^{(n)}\equiv\sum_\lambda(G_\lambda{}^{(n)}\hat{X}_\lambda{}^\dagger-G_\lambda{}^{(n)*}\hat{X}_\lambda). \tag{3·32}$$

In the third-order ($n=3$), we obtain

$$G_\gamma{}^{(3)}=\frac{1}{2}\sum_\lambda\left(\frac{\partial G_\lambda{}^{(2)}}{\partial\eta^*}G_\lambda{}^{(2)*}-\frac{\partial G_\lambda{}^{(2)*}}{\partial\eta^*}G_\lambda{}^{(2)}\right)-\frac{1}{4!}\langle\phi_0|[[[X_\gamma, iG^{(1)}], iG^{(1)}], iG^{(1)}]|\phi_0\rangle, \tag{3·33}$$

$$G_{\tilde{\gamma}}{}^{(3)}(\eta^*, \eta, \tilde{\eta}^*, \tilde{\eta})=(G_\gamma{}^{(3)}(\tilde{\eta}, \tilde{\eta}^*, \eta, \eta^*))^*, \tag{3·34}$$

$$\mathcal{H}^{(4)}=\mathcal{H}_0{}^{(4)}-\frac{1}{2}\sum_\rho\chi_\rho\{\mathcal{R}_\rho{}^{(1)*}\mathcal{R}_\rho{}^{(3)}+\mathcal{R}_\rho{}^{(3)*}\mathcal{R}_\rho{}^{(1)}+\mathcal{R}_\rho{}^{(2)*}\mathcal{R}_\rho{}^{(2)}\}, \tag{3·35}$$

$$\mathcal{H}_0^{(4)}=\frac{1}{4!}\langle\phi_0|[[[[\hat{H}_0, i\hat{G}^{(1)}], i\hat{G}^{(1)}], i\hat{G}^{(1)}], i\hat{G}^{(1)}]|\phi_0\rangle$$

$$+\frac{1}{2!}\langle\phi_0|[[\hat{H}_0, i\hat{G}^{(2)}], i\hat{G}^{(2)}]|\phi_0\rangle+\langle\phi_0|[[\hat{H}_0, i\hat{G}^{(1)}], i\hat{G}^{(3)}]|\phi_0\rangle\,, \tag{3·36}$$

where

$$\mathcal{R}_\rho^{(1)}=\langle\phi_0|[\hat{R}_\rho, i\hat{G}^{(1)}]|\phi_0\rangle\,, \tag{3·37}$$

$$\mathcal{R}_\rho^{(2)}=\langle\phi_0|[\hat{R}_\rho, i\hat{G}^{(2)}]|\phi_0\rangle+\frac{1}{2!}\langle\phi_0|[[\hat{R}_\rho, i\hat{G}^{(1)}], i\hat{G}^{(1)}]|\phi_0\rangle\,, \tag{3·38}$$

$$\mathcal{R}_\rho^{(3)}=\langle\phi_0|[\hat{R}_\rho, i\hat{G}^{(3)}]|\phi_0\rangle+\langle\phi_0|[[\hat{R}_\rho, i\hat{G}^{(1)}], i\hat{G}^{(2)}]|\phi_0\rangle$$

$$+\frac{1}{3!}\langle\phi_0|[[[\hat{R}_\rho, i\hat{G}^{(1)}], i\hat{G}^{(1)}], i\hat{G}^{(1)}]|\phi_0\rangle\,. \tag{3·39}$$

Here, the expression for $G_\lambda^{(3)}$ with $\lambda\mp\gamma$ or $\tilde{\gamma}$ is omitted since these terms do not contribute to $\mathcal{H}^{(4)}$.

In the same manner, the collective representation (3·12) of an operator $\hat{F}$ is expanded as

$$\mathcal{F}(\eta_i^*, \eta_i)=\mathcal{F}^{(1)}(\eta_i^*, \eta_i)+\mathcal{F}^{(2)}(\eta_i^*, \eta_i)+\mathcal{F}^{(3)}(\eta_i^*, \eta_i)+\cdots\,, \tag{3·40}$$

where $\mathcal{F}^{(1)}$, $\mathcal{F}^{(2)}$, $\cdots$ are determined by equations similar to (3·37)$\sim$(3·39).

3.3. *Symmetry properties*

The Hamiltonian (2·1) and the BCS ground state $|\phi_0\rangle$ are invariant under 1) the rotation about the symmetry axis (z-axis) and 2) the time reversal $\mathcal{T}$:

$$[\hat{J}_z, \hat{H}]=0, \qquad \hat{J}_z|\phi_0\rangle=0\,, \tag{3·41}$$

$$[\mathcal{T}, \hat{H}]=0, \qquad \mathcal{T}|\phi_0\rangle=|\phi_0\rangle\,. \tag{3·42}$$

Accordingly, the collective subspace and the collective coordinates determined by the (η^*, η) expansion method with the boundary condition (3·26) possess the symmetry properties described below. As is proved in the Appendix, the symmetry transformations of the TDHB state vectors can be equivalently expressed by the linear canonical transformations of the collective coordinates,

$$e^{-i\theta\hat{J}_z}|\phi(\eta_i^*, \eta_i)\rangle=|\phi(\eta_i^{\theta*}, \eta_i^{\theta})\rangle\,, \tag{3·43}$$

$$\mathcal{T}|\phi(\eta_i^*, \eta_i)\rangle=|\phi(\eta_i^T, \eta_i^{T*})\rangle\,, \tag{3·44}$$

where

$$(\eta^{\theta*}, \eta^{\theta}, \tilde{\eta}^{\theta*}, \tilde{\eta}^{\theta})=(e^{2i\theta}\eta^*, e^{-2i\theta}\eta, e^{-2i\theta}\tilde{\eta}^*, e^{2i\theta}\tilde{\eta})\,, \tag{3·45}$$

$$(\eta^{T*}, \eta^T, \tilde{\eta}^{T*}, \tilde{\eta}^T)=(\tilde{\eta}^*, \tilde{\eta}, \eta^*, \eta)\,. \tag{3·46}$$

The above equations mean that the collective coordinates (η^*, η) are the time-reversal of $(\tilde{\eta}^*, \tilde{\eta})$, and they transfer the K-quantum numbers by $(2, -2)$ and $(-2, 2)$, respectively. From Eqs. (3·43) and (3·44) it follows that transformation properties of the collective representation $\mathcal{F}(\eta_i^*, \eta_i)$ under the transformations of the operator $\hat{F}$

$$\hat{F}\to e^{i\theta\hat{J}_z}\hat{F}e^{-i\theta\hat{J}_z}\ , \tag{3·47}$$

$$\hat{F}\to\hat{\mathcal{I}}^{-1}\hat{F}\hat{\mathcal{I}} \tag{3·48}$$

are

$$\mathcal{F}(\eta^*,\eta,\tilde{\eta}^*,\tilde{\eta})\to\mathcal{F}(e^{2i\theta}\eta^*,e^{-2i\theta}\eta,e^{-2i\theta}\tilde{\eta}^*,e^{2i\theta}\tilde{\eta})\ , \tag{3·49}$$

$$\mathcal{F}(\eta^*,\eta,\tilde{\eta}^*,\tilde{\eta})\to(\mathcal{F}(\tilde{\eta},\tilde{\eta}^*,\eta,\eta^*))^*\ . \tag{3·50}$$

It also follows that the correspondence

$$[\hat{J}_z,\hat{F}]\iff i\{\mathcal{J}_z,\mathcal{F}\}_{\text{P.B.}} \tag{3·51}$$

holds with $\mathcal{J}_z$ given by

$$\begin{aligned}\mathcal{J}_z&=\langle\phi(\eta_i^*,\eta_i)|\hat{J}_z|\phi(\eta_i^*,\eta_i)\rangle-\langle\phi_0|\hat{J}_z|\phi_0\rangle\\&=2(\eta^*\eta-\tilde{\eta}^*\tilde{\eta})\ .\end{aligned} \tag{3·52}$$

Consequently, $\mathcal{F}(\eta_i^*,\eta_i)$ can be generally expressed as

$$\mathcal{F}(\eta_i^*,\eta_i)=\sum_{i-j-k+l=K/2}\mathcal{F}^{(ijkl)}\eta^{*i}\eta^j\tilde{\eta}^{*k}\tilde{\eta}^l\ , \tag{3·53}$$

if the K-quantum number transferred by $\hat{F}$ is even, and $\mathcal{F}=0$ otherwise. Owing to this property, we obtain $\mathcal{H}^{(3)}=0$, and the $K=1$ components of the residual interaction (2·8) do not contribute to the collective Hamiltonian. It is also evident that only the RPA modes with $K=0$ and ±4 contribute to $G_\lambda^{(2)}$ given by Eq. (3·29).

§ 4. Microscopic Bohr Hamiltonian for anharmonic γ vibrations

4.1. *Quantization with normal ordering*

To the fourth order in the power series of (η_i^*,η_i) the collective Hamiltonian $\mathcal{H}$ is expressed as

$$\begin{aligned}\mathcal{H}=&\alpha(\eta^*\eta+\tilde{\eta}^*\tilde{\eta})+\beta(\eta^*\tilde{\eta}^*+\tilde{\eta}\eta)\\&+b_1(\eta^*\eta^*\tilde{\eta}^*\tilde{\eta}^*+\text{c.c.})+b_2(\eta^*\tilde{\eta}^*\eta^*\eta+\eta^*\tilde{\eta}^*\tilde{\eta}^*\tilde{\eta}+\text{c.c.})\\&+b_3(\eta^*\eta^*\eta\eta+\tilde{\eta}^*\tilde{\eta}^*\tilde{\eta}\tilde{\eta})+b_4\eta^*\eta\tilde{\eta}^*\tilde{\eta}\ ,\end{aligned} \tag{4·1}$$

where the coefficients $b_1\sim b_4$ are related to the microscopic quantities through Eqs. (3·34) $\sim$(3·39).

To obtain quantum spectra and transition probabilities, we have to quantize the classical Hamiltonian (4·1). According to the arguments presented in Ref. 16), we shall adopt the canonical quantization method with the normal ordering. Namely, we replace the classical canonical variables $(\eta^*,\eta,\tilde{\eta}^*,\tilde{\eta})$ with the boson operators $(B^\dagger,B,\tilde{B}^\dagger,\tilde{B})$ and take the normal ordering,

$$\mathcal{H}(\eta^*,\eta,\tilde{\eta}^*,\tilde{\eta})\to H_B\equiv:\mathcal{H}(B^\dagger,B,\tilde{B}^\dagger,\tilde{B}):\ . \tag{4·2}$$

This applies also for the collective representation $\mathcal{F}$ of an arbitrary operator:

$$\mathcal{F}(\eta^*,\eta,\tilde{\eta}^*,\tilde{\eta})\to F_B\equiv:\mathcal{F}(B^\dagger,B,\tilde{B}^\dagger,\tilde{B}):\ . \tag{4·3}$$

Then, as is evident from (3·52) and (3·48),

$$[(J_z)_B, B^\dagger]=2B^\dagger, \quad \mathcal{T}_B B^\dagger \mathcal{T}_B{}^{-1}=\tilde{B}^\dagger, \quad \text{etc}. \tag{4·4}$$

The excitation spectra and transition probabilities are easily calculated by diagonalizing H_B in the boson space

$$\left\{|n, \tilde{n})=\frac{1}{\sqrt{n!\,\tilde{n}!}}(B^\dagger)^n(\tilde{B}^\dagger)^{\tilde{n}}|0); \quad \begin{matrix} n=0, 1, 2, \cdots, \\ \tilde{n}=0, 1, 2, \cdots, \end{matrix}\right\} \tag{4·5}$$

where $B|0)=\tilde{B}|0)=0$, and by evaluating the matrix element of F_B between the resulting eigenstates.

4.2. *Derivation of approximate Bohr Hamiltonian for the anharmonic γ vibrations*

In order to make physical interpretation of the quantized collective Hamiltonian H_B clear, let us next try to establish the correspondence with the Bohr Hamiltonian for the γ-vibrational degrees of freedom. For this purpose we first rewrite H_B in terms of the position and momentum operators defined by

$$\left.\begin{aligned} Q&=\frac{z}{\sqrt{2}}(B^\dagger+\tilde{B}), \quad \tilde{Q}=Q^\dagger, \\ P&=\frac{i}{\sqrt{2}z}(\tilde{B}^\dagger-B), \quad \tilde{P}=P^\dagger, \end{aligned}\right\} \tag{4·6}$$

where z is a scaling parameter, and rearrange the operators (Q, P) and $(\tilde{Q}, \tilde{P})$ into the Weyl ordering:

$$\begin{aligned} H_B=&e_1P\tilde{P}+\frac{1}{4}e_2\{(P^2Q^2+2PQ^2P+Q^2P^2)+(\tilde{P}^2\tilde{Q}^2+2\tilde{P}\tilde{Q}^2\tilde{P}+\tilde{Q}^2\tilde{P}^2)\} \\ &+e_3\frac{1}{2}(PQ+QP)\frac{1}{2}(\tilde{P}\tilde{Q}+\tilde{Q}\tilde{P})+e_4+e_5Q\tilde{Q}+e_6Q^2\tilde{Q}^2+e_7P^2\tilde{P}^2, \end{aligned} \tag{4·7}$$

where the coefficients e_i are connected with α, β, $b_1\sim b_4$ in Eq. (4·1) and z. We define the collective potential by the terms independent of P and $\tilde{P}$ in this Weyl-ordered form.

Noticing the similarity to the two-dimensional harmonic oscillator, we can easily find the representation of Q and P in the polar coordinates (γ, φ):*)

$$\left.\begin{aligned} P&=\frac{\hbar}{i}\frac{1}{\sqrt{2}}e^{-i\varphi}\left(\frac{1}{\sqrt{\gamma}}\frac{\partial}{\partial\gamma}\sqrt{\gamma}-\frac{i}{2\gamma}\frac{\partial}{\partial\varphi}\right)e^{-i\varphi}, \\ Q&=\frac{1}{\sqrt{2}}\gamma e^{2i\varphi}. \end{aligned}\right\} \tag{4·8}$$

Accordingly, the scaling parameter z is fixed such that the ordinary definition of the triaxial deformation γ, i.e., $\tan\gamma=\sqrt{2}\langle\hat{Q}_{22}\rangle/\langle\hat{Q}_{20}\rangle$, holds in the lowest order of the collective representation. Thus, we obtain the collective Hamiltonian of the following form:

$$\begin{aligned} H_{\text{coll}}=&-\frac{\hbar^2}{2D}\left(\frac{\partial^2}{\partial\gamma^2}+\frac{1}{\gamma}\frac{\partial}{\partial\gamma}+\frac{1}{4\gamma^2}\frac{\partial^2}{\partial\varphi^2}\right)+\epsilon_1\frac{\hbar^2}{2D}\left(\gamma^2\frac{\partial^2}{\partial\gamma^2}+3\gamma\frac{\partial}{\partial\gamma}+1\right)+\epsilon_2\frac{\hbar^2}{2D}\frac{1}{4}\frac{\partial^2}{\partial\varphi^2} \\ &+\epsilon_3\left(\frac{\hbar^2}{2D}\right)^2\left(\frac{\partial^2}{\partial\gamma^2}+\frac{1}{\gamma}\frac{\partial}{\partial\gamma}+\frac{1}{4\gamma^2}\frac{\partial^2}{\partial\varphi^2}\right)^2+V_{\text{coll}}(\gamma), \end{aligned} \tag{4·9}$$

*) From now on, we explicitly write $\hbar$.

Table I.

$D^{-1}=(2\alpha-2\beta+4b_2-4b_3-b_4)z^2/2$
$C_2=(2\alpha+2\beta-4b_2-4b_3-b_4)/(2z^2)$
$C_4=(2b_1+4b_2+2b_3+b_4)/(16z^4)$
$\varepsilon_1=D(6b_1-2b_3-b_4)/4$
$\varepsilon_2=D(2b_1-6b_3+b_4)/4$
$\varepsilon_3=D^2(2b_1-4b_2+2b_3+b_4)z^4/4$

$$V_{\rm coll}(\gamma)=\frac{1}{2}C_2\gamma^2+C_4\gamma^4\,, \qquad (4\cdot10)$$

where an unimportant constant term in $V_{\rm coll}$ is dropped. If we put $\varepsilon_3=0$, this $H_{\rm coll}$ is reduced to the approximated version of the Bohr Hamiltonian investigated by Dumitrescu and Hamamoto.[5] Thus, we have determined the mass parameter D, the restoring-force parameter C_2, and the anharmonicity coefficients ($\varepsilon_1\sim\varepsilon_3$, C_4) in a completely microscopic way. In Table I, we list their relations to the quantities α, β and $b_1\sim b_4$ appearing in Eq. (4·1).

It should be emphasized that the potential $V_{\rm coll}$ (γ) defined above differs from the conventional Hartree-Bogoliubov potential which is defined by the energy expectation values with respect to the time-even Slater determinants, because it contains the contraction terms which arise when the operators (Q, P) and ($\tilde{Q}, \tilde{P}$) are rearranged into the Weyl-form. Thus, the restoring-force parameter C_2 depends, not only on α and β, but also on b_2, b_3 and b_4 which represent the fourth order contributions in the (η_i^*, η_i) expansion. We shall give in § 6 some arguments in favor of our definition of $V_{\rm coll}$, and show that these contributions in fact play a crucial role.

§ 5. Analysis of the double γ-vibrational states in ^{168}Er

5.1. *Procedure of numerical calculation*

In the numerical calculation, we parametrized the Nilsson potential in $\hat{h}_{\rm def}$ in the same way as Bohr and Mottelson,[4] except that the coordinates x_i in the $\boldsymbol{l}^2$- and $\boldsymbol{l}\cdot\boldsymbol{s}$-terms are also replaced by the doubly-stretched coordinates (see Ref. 17) for further details). As for the deformed shell-model space, we explicitly take into account three major shells for both neutrons and protons; i.e., $N_{\rm osc}=4, 5$ and 6 for neutrons, and $N_{\rm osc}=3, 4$ and 5 for protons. The pairing-force strengths G_0 are determined as usual to reproduce the experimental values for odd-even mass differences $\Delta_{\rm oe}$.

Thus, only the quadrupole-force strength χ is treated as a parameter, and we are interested in how the properties of the anharmonic γ vibrations change with the increase of χ. To treat the situations where the values of χ exceed the RPA critical point, we solve the RPA equation in the position-momentum representation (2·17). As a matter of course, we can fix the value of χ to reproduce the empirical energies of the single γ-vibrational states.

In the computation of the anharmonicity coefficients $b_1\sim b_4$, we take into account only the G_γ and $G_{\tilde{\gamma}}$ terms neglecting the other G_λ terms with $\lambda\neq\gamma$ and $\tilde{\gamma}$ (see Eqs. (3·29) and (3·36)). The neglected terms represent the coupling effects between different RPA modes; for instance, the couplings between the γ vibrations and the pairing vibrations. In fact, one of the most attractive features of the SCC method is its ability of incorporating these mode-mode couplings (in determining the microscopic structure of collective coordinates η_i^* and η_i) through the sum $\sum_\lambda$ in Eq. (3·36); and hence, their roles will be separately discussed in Part II.[10]

After computing these anharmonicity coefficients, the excitation spectra and the

transition probabilities are calculated in the boson space (4·5) by utilizing the lowest 20 basis states for each K.

5.2. *Result of numerical calculation*

Since the central issue of current investigation[3),5)~9)] toward understanding the anharmonic γ vibrations is the nature of the double γ excitations in ^{168}Er, we shall focus our attention on it.

Figure 1 shows the calculated excitation energies of the single and the double γ-vibrational states as functions of the quadrupole-force strength χ. To clearly indicate the anharmonicities of this spectrum, we plotted in Fig. 2 the ratios of the excitation energies and of the transition amplitudes of the double γ-vibrational states to those of the single γ-vibrational state. These figures demonstrate that our model is able to describe not only the weakly anharmonic vibrations but also the strongly anharmonic motions which prominently appear beyond the RPA critical point. As is easily understood from the behaviour of the collective potential displayed in Fig. 3, the anharmonicities are originated from the instability of the axially symmetric shape toward the triaxial equilibrium deformation. Thus with the increase of the force-strength χ we obtain the minimum at $\gamma \neq 0$, and the spectrum aquires the properties of the triaxial rotor.

The above figures illustrate rather general predictions of our theory which are valid

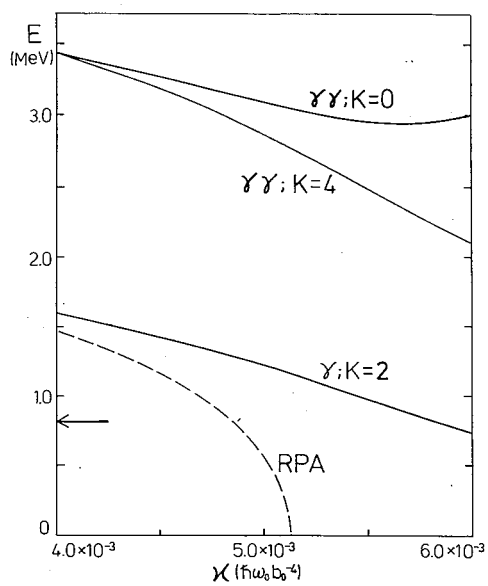

Fig. 1. Excitation energies of the single and double γ-vibrational states calculated as functions of the (doubly-stretched) quadrupole-force strength χ. The RPA excitation energies $\hbar\omega_\lambda$ are also plotted. The arrow indicates the experimental value for the single γ-vibrational state in ^{168}Er. For the quadrupole-deformation parameter $\delta_{\rm osc}$ and the odd-even mass differences for protons and neutrons, $\Delta_{\rm oe}^{(p)}$ and $\Delta_{\rm oe}^{(n)}$, the values appropriate to ^{168}Er are used: $\delta_{\rm osc}=0.271$, $\Delta_{\rm oe}^{(p)}=0.830$ MeV and $\Delta_{\rm oe}^{(n)}=0.775$ MeV.

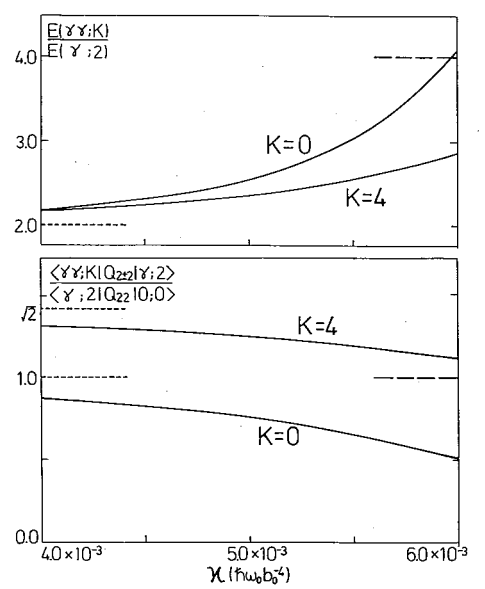

Fig. 2. The upper part: The ratios of the excitation energies of the double γ-vibrational states ($K=0$ and 4) to that of the single γ-vibrational state are plotted as functions of the quadrupole-force strength χ. The broken and dotted lines indicate the triaxial rigid-rotor limit for the $K=4$ state and the harmonic-vibrational limit for both the $K=0$ and $K=4$ states, respectively. The lower part: The same as above, but for the quadrupole-transition amplitudes between the single- and double-γ-vibrational states.

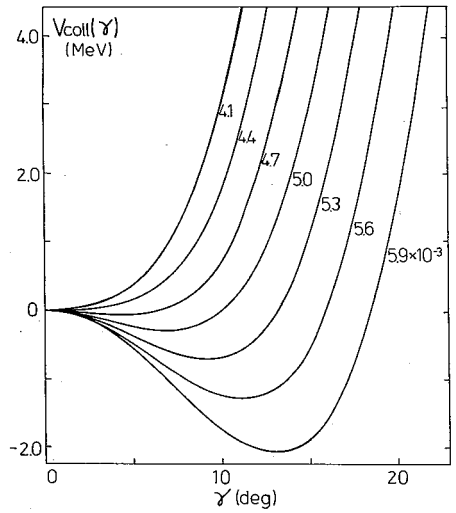

Fig. 3. Collective potential evaluated for various quadrupole-force strength χ. The unit for χ is $\hbar\omega_0 \cdot b_0^{-4}$. The other parameters are fixed at the values listed in the caption of Fig. 1.

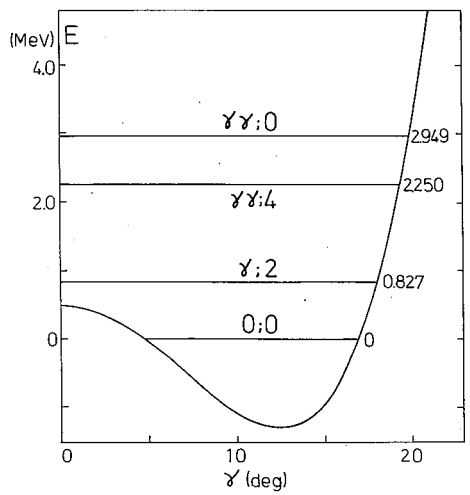

Fig. 4. The collective potential and the excitation energies of the single and double γ-vibrational states in ^{168}Er, which are calculated by using $\chi = 5.80 \times 10^{-3} \hbar\omega_0 b_0^{-4}$. The other parameters are the same as in Fig. 1.

also for other nuclei. We next specify our discussion on ^{168}Er. Figure 4 shows the solution of the Schrödinger equation for the collective Hamiltonian and the potential energy function for this nucleus. We also present in Table II the calculated values of the transition amplitudes for the quadrupole operators $\hat{Q}''_{2\pm2}$. Here, the value of χ is fixed such that the calculated energy of the single γ-vibrational state reproduce the experimental value for ^{168}Er. According to this result, we can expect the double γ-vibrational states to appear in the 2.2~3.0 MeV region which is just above the energy region investigated in the experiment by Davidson et al.[9] It is quite interesting that the microscopically calculated potential does exhibit a tendency toward the triaxial minimum in accordance with the results of Dumitrescu and Hamamoto[5] based on the phenomenological analysis in terms of the Bohr Hamiltonian. Our calculated anharmonicity parameters are $\varepsilon_1 = -6.4$ and $\varepsilon_2 = -7.1$, which are qualitatively similar to their values ($\varepsilon_1 = -4$ and $\varepsilon_2 = -12$). Furthermore, we have found that the effect of the ε_3 term in $H_{\rm coll}$, which is absent in the Bohr Hamiltonian, is rather small (see Table III).

Finally, we note that Figs. 2~4 above are slightly different from the corresponding figures in Ref. 11), since a different boundary condition ($\sigma = 1$ and $\tau = 0$) and a different

Table II. Calculated excitation energies in [MeV] of the γ-vibrational states in ^{168}Er and their transition amplitudes in $[b_0^2]$ for the quadrupole operators. Values in parentheses are the ratios to those for the single γ-vibrational states. The parameters used are the same as in Fig. 4.

	$\gamma;\ K=2$	$\gamma\gamma;\ K=4$	$\gamma\gamma;\ K=0$
excitation energy	0.827	2.250 (2.72)	2.949 (3.56)
$\langle\gamma;\ 2\|Q''_{22}\|0;\ 0\rangle$ or $\langle\gamma\gamma;\ K\|Q''_{2\pm2}\|\gamma;\ 2\rangle$	16.7	19.2 (1.15)	9.6 (0.57)

Table III. Coefficients of the quantized collective Hamiltonian (4·9), of the collective representation of the quadrupole operator (6·2) in $[b_0^2]$, and of the classical collective Hamiltonian (4·1) in $[\hbar\omega_0]$. The parameters used in this microscopic calculation for these coefficients are the same as in Fig. 4.

D	$2.79\times10^2[(\hbar\omega_0)^{-1}\cdot\hbar^2]$	$q_{22}^{(1000)}$	8.82	α	1.58×10^{-1}
C_2	$-1.02\times10^1[\hbar\omega_0]$	$q_{22}^{(2100)}$	-1.19×10^{-1}	β	-2.48×10^{-1}
C_4	$1.08\times10^2[\hbar\omega_0]$	$q_{22}^{(2010)}$	1.69×10^{-2}	b_1	-3.90×10^{-3}
ε_1	-6.43	$q_{22}^{(1101)}$	-1.18×10^{-1}	b_2	2.07×10^{-2}
ε_2	-7.05			b_3	2.03×10^{-2}
ε_3	$-3.48\times10^{-2}[\hbar^{-1}\omega_0^{-1}]$			b_4	2.83×10^{-2}

quadrupole-force strength $\varkappa$ were used in the latter.

5·3. *Comparison with other works*

Soloviev and Shirikova[6] evaluated the anharmonicities of the two-phonon states in deformed nuclei by means of their quasiparticle-phonon model. They concluded that, because of the Pauli-principle effects, the two-phonon states are shifted up by 1~3 MeV in energy resulting in a strong fragmentation of their collectivities. For ^{168}Er, they found that the main parts of the strengths of the double γ-vibrational states with $K=0$ and 4 were located at 3.5 MeV and 4.3 MeV, respectively. The extremely strong anharmonicity effects they obtained are significantly different from our result presented in § 5.2.

On the other hand, in the phenomenological analysis by Warner, Casten and Davidson[8] on the low-energy spectrum of ^{168}Er in terms of the $SU(3)$ symmetry (and its breaking) of the interacting boson model (IBM),[18] the double γ-vibrational states with $K=0$ and 4 are predicted to appear at about 1.5 MeV and 1.6 MeV, respectively. As was pointed out by Bohr and Mottelson,[3] however, there is no experimental evidence for such double γ-vibrational states below 2 MeV. Evidently, the very weak anharmonicity, which is considered to be inherent to the IBM,[18] also contradicts our results obtained from the microscopic calculation.

Certainly, the numerical values presented in § 5.2 depend on the details of the boundary conditions chosen, of the parameters used, and of the truncation adopted in numerical calculations. However, the difference between our prediction and those of Refs. 6) and 8) is of qualitative nature so that the conclusion stated above will not be affected by such quantitative modifications.

§ 6. Discussion

In this section, we present some arguments to justify our quantization procedure adopted in deriving the quantized collective Hamiltonian $H_{\rm coll}$.

6·1. *The boundary condition and quantization with normal ordering*

Although our basic equations are invariant under linear canonical transformations, we have to choose a specific canonical coordinate system to carry out the quantization procedure. For this purpose, we have fixed the values of σ and τ (whose arbitrariness stems from the invariance mentioned above) by imposing the condition (3·22). This condition is equivalent to the requirement that the expectation value $\langle\phi_0|\hat{Y}_\gamma^\dagger\hat{Y}_\gamma|\phi_0\rangle$ be minimum: Using the parametrization (3·24) for σ and τ we can evaluate it as

$$f(s)\equiv\langle\phi_0|\hat{Y}_\gamma{}^\dagger\hat{Y}_\gamma|\phi_0\rangle=\sum_{\mu<\nu}\{\sigma\varphi_\gamma(\mu\nu)-\tau\psi_\gamma(\mu\nu)\}^2$$

$$=\frac{1}{4}s^2\sum_{\mu<\nu}\{\psi_\gamma(\mu\nu)-\varphi_\gamma(\mu\nu)\}^2+\frac{1}{4}s^{-2}\sum_{\mu<\nu}\{\psi_\gamma(\mu\nu)+\varphi_\gamma(\mu\nu)\}^2-\frac{1}{2}$$

$$\geqq\frac{1}{2}\sqrt{\left(\sum_{\mu<\nu}\{\psi_\gamma(\mu\nu)+\varphi_\gamma(\mu\nu)\}^2\right)\cdot\left(\sum_{\mu<\nu}\{\psi_\gamma(\mu\nu)-\varphi_\gamma(\mu\nu)\}^2\right)}-\frac{1}{2}. \qquad (6\cdot1)$$

Obviously, the equality holds when s takes the value given by (3·25). We can thus regard the condition (3·22) as a requirement to minimize the sum of the squares of the backward amplitudes $\varphi_\gamma'(\mu\nu)=\sigma\varphi_\gamma(\mu\nu)-\tau\psi_\gamma(\mu\nu)$ of the operator $\hat{Y}_\gamma{}^\dagger$. As is discussed in Ref. 16), for the TDHB state space constructed from a specific phonon operator determined by the Tamm-Dancoff approximation (TDA), we can justify (albeit not complete) our quantization procedure by making a comparison with the modified-Marumori boson-expansion method.[19)~21)] It is easily confirmed that the operator $\hat{Y}_\gamma{}^\dagger$ with the parameter s given by (3·25) coincides with the TDA-phonon operator in the limit that all the single-particle energies are degenerate. In general cases, however, the operator $\hat{Y}_\gamma{}^\dagger$ is different from the TDA-phonon operators which do not necessarily fulfill the lowest-order equation of the collective subspace. Namely, the two requirements (i.e., the agreement with the boson-expansion method in a certain limit and the fulfilment of the equation of collective subspace) are not always compatible. Thus, Eq. (3·22) may be regarded as a condition to optimize the values of σ and τ such that the operators $\hat{Y}_\gamma{}^\dagger$ and $\hat{Y}_{\bar{\gamma}}{}^\dagger$ best resemble, within the RPA-type boundary condition (3·18), the TDA-phonon operators for the γ vibrations.

6.2. *Definition of collective potential*

In § 4.2, we defined the collective potential by rearranging the position and momentum operators (Q, P) and $(\tilde{Q}, \tilde{P})$ into the Weyl ordered form. The main reason why we prefer this definition is that the functional form of its Wigner transform (which is usually used to give a semiclassical interpretation of the quantum system) is the same as the expression of the original quantum Hamiltonian in the Weyl ordered form.[22),23)] Thanks to this property of the Weyl-Wigner correspondence, we are able to give a clear semiclassical interpretation of our calculated results by analyzing the potential defined in § 4.2. To quantitatively see to which extent the collective potential defined above differs from the Hartree-Bogoliubov potential, which corresponds to the momentum-independent terms of the classical collective Hamiltonian (4·1), we present a numerical example in Fig. 5. We see a significant difference between the two: The former potential displays a much stronger tendency toward the triaxial minimum with $\gamma\neq0$ than the latter potential. In this connection, it is interesting to quote Refs. 24) and 25) in which they have shown that some essential features of the semiclassical nucleus-nucleus potentials derived by the WKB method applied to the Wigner transform are lost in the potentials that are averaged out by the widths of the Hartree-Fock wave packet.

It should be emphasized that the Weyl correspondence[22),23)] is used here as a means of transforming the operators into the functions in phase space in order to make the geometrical interpretation clear. Hence, the choice of the ordering of the operators (Q, P)

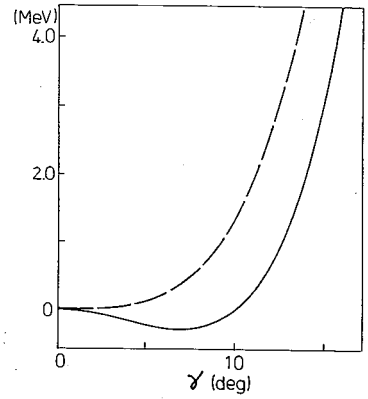

Fig. 5. Comparison between the collective potential (solid line) defined by Eq. (4·10) and the conventional Hartree-Bogoliubov potential (broken line). Both are calculated by using $\varkappa=5.00\times10^{-3}\hbar\omega_0 b_0^{-4}$. The other parameters are the same as in Fig. 1.

and $(\tilde{Q}, \tilde{P})$ discussed here has nothing to do with the choice of the quantization procedure discussed before. Namely, the results for all observable quantities like quantum spectra remain, of course, unaffected by the manner to define the potential term in the already quantized collective Hamiltonian.

6.3. *Convergence of the* (η^*, η) *expansion*

We present in Table III the numerical values for the anharmonicity coefficients in the collective representation of the quadrupole operator $\hat{Q}''_{2K}$:

$$Q''_{22}=Q^{(1)}_{22}+Q^{(3)}_{22}+\cdots, \tag{6·2}$$

$$Q^{(1)}_{22}=q^{(1000)}_{22}(\eta^*+\tilde{\eta}), \tag{6·3}$$

$$Q^{(3)}_{22}=q^{(2100)}_{22}(\eta^*\eta^*\eta+\tilde{\eta}^*\tilde{\eta}\tilde{\eta})+q^{(2010)}_{22}(\eta^*\eta^*\tilde{\eta}^*+\eta\tilde{\eta}\tilde{\eta})+q^{(1101)}_{22}(\eta^*\eta\tilde{\eta}+\eta^*\tilde{\eta}^*\tilde{\eta}). \tag{6·4}$$

We see that the third-order terms are one-order of magnitude smaller than the first-order term, suggesting a rather rapid convergence. In the same table, the fourth-order coefficients $b_1\sim b_4$ of the collective Hamiltonian (4·1) are also listed. Their values are rather small, and also suggest a fast convergence. It should be emphasized, however, that they determine the major characteristics of the excitation spectrum; in particular, they play a crucial role for the stability of the solutions of the collective Schrödinger equation in the region where the force-strength $\varkappa$ exceeds the RPA critical point. This result, however, does not necessarily imply that the (η^*, η) expansion converges fast in general cases. Namely, it is necessary to investigate further whether it converges rapidly when we selfconsistently determine the collective subspace by incorporating the mode-mode couplings.

§ 7. Concluding remarks

We have investigated the microscopic structure of anharmonicities associated with the double γ-vibrational states in ^{168}Er by means of the SCC method. To derive the quantized collective Hamiltonian on the basis of the SCC method, we have made special efforts to 1) find the optimal boundary condition suitable for the quantization procedure adopted, and 2) give an appropriate definition of the collective potential, which should be compared with that of the Bohr-Mottelson-type collective Hamiltonian. The microscopic calculation performed in this paper shows that the collective potential for ^{168}Er possesses the minimum at the triaxial shape, although the amplitude of the zero-point vibration is comparable to the magnitude of the equilibrium deformation. Thus, the nucleus ^{168}Er may be considered to be situated just in the transitional region between the axial and the triaxial equilibrium shapes. A more detailed study of the anharmonicities associated with the large-amplitude γ vibrations will be performed in a forthcoming paper,[10] in

which the mode-mode couplings between different RPA vibrations will also be taken into account.

Acknowledgements

We thank Dr. Y. R. Shimizu for providing us several subroutines which were used in the numerical calculation. The computer calculation for this work has been supported by the Grant-in-Aid for Scientific Research of the Ministry of Education, Science and Culture (No. 58540153).

Appendix

We here give a proof of Eq. (3·43). Let $|\phi(\eta_i^*, \eta_i)\rangle$ be the TDHB states satisfying the basic equations (3·6)~(3·9). Then, from the fact that the Hamiltonian and the BCS ground state $|\phi_0\rangle$ possess the axial symmetry property, Eq. (3·40), it immediately follows that the rotated TDHB states

$$e^{-i\theta\hat{J}_z}|\phi(\eta_i^*, \eta_i)\rangle = e^{i\hat{G}^\theta(\eta_i^*, \eta_i)}|\phi_0\rangle\,, \tag{A·1}$$

$$i\hat{G}^\theta(\eta_i^*, \eta_i) \equiv e^{-i\theta\hat{J}_z} i\hat{G}(\eta_i^*, \eta_i) e^{i\theta\hat{J}_z}\,, \tag{A·2}$$

also satisfy our basic equations. Now, the transformation property of the lowest-order term $i\hat{G}^{(1)}$ can be explicitly evaluated as

$$i\hat{G}^{\theta(1)}(\eta_i^*, \eta_i) = i\hat{G}^{(1)}(\eta_i^{\theta*}, \eta_i^\theta) \tag{A·3}$$

with $(\eta_i^{\theta*}, \eta_i^\theta)$ given by (3·45). Because the higher-order terms are uniquely constructed from the lowest-order term by means of the general procedure of the (η^*, η) expansion method, the property (A·3) propagates to all orders of the expansion; i.e., we obtain

$$i\hat{G}^{\theta(n)}(\eta_i^*, \eta_i) = i\hat{G}^{(n)}(\eta_i^{\theta*}, \eta_i^\theta) \tag{A·4}$$

in each order ($n=2, 3, \cdots$). Thus Eq. (3·43) holds. The time-reversal property (3·44) can also be proved in a similar manner.

References

1) T. Marumori, T. Maskawa, F. Sakata and A. Kuriyama, Prog. Theor. Phys. **64** (1980), 1294.
2) K. Kumar and M. Baranger, Nucl. Phys. **A122** (1968), 273.
3) A. Bohr and B. R. Mottelson, Physica Scripta **25** (1982), 28.
4) A. Bohr and B. R. Mottelson, *Nuclear Structure,* vol. II (Benjamin, New York, 1975).
5) T. S. Dumitrescu and I. Hamamoto, Nucl. Phys. **A383** (1982), 205.
I. Hamamoto, Prog. Theor. Phys. Suppl. Nos. 74 &75 (1983), 157.
6) V. G. Soloviev and N. Yu. Shirikova, Yadern. Fiz. **36** (1982), 1376 [Sov. J. Nucl. Phys. **36** (1982), 799].
7) R. V. Jolos, J. L. Molina and V. G. Soloviev, Z. Phys. **A295** (1980), 147.
8) D. D. Warner, R. F. Casten and W. F. Davidson, Phys. Rev. **C24** (1981), 1713.
9) W. F. Davidson et al., J. of Phys. **G7** (1981), 455, 843.
See also W. F. Davidson et al., Phys. Lett. **130B** (1983), 161.
10) M. Matsuo and K. Matsuyanagi, in preparation.
11) M. Matsuo, Prog. Theor. Phys. **72** (1984), 666.
12) T. Kishimoto, *Proc. 1980 RCNP Int. Symp. Highly Excited States in Nuclear Reactions, Osaka,* p. 145.
T. Kishimoto et al., Phys. Rev. Lett. **35** (1975), 552.
13) Y. R. Shimizu and K. Matsuyanagi, Prog. Theor. Phys. **72** (1984), 799.
14) T. Marumori, Prog. Theor. Phys. **57** (1977), 112.

T. Marumori, F. Sakata, T. Maskawa, T. Une and Y. Hashimoto, *"Nuclear Collective Dynamics", Lectures of 1982 International Summer School of Nuclear Physics, Poiana Brasov, Romania* (World Scientific Publishing Co. Pte. Ltd., 1983), p. 1.
15) M. Yamamura, A. Kuriyama and S. Iida, Prog. Theor. Phys. **71** (1984), 109.
16) M. Matsuo and K. Matsuyanagi, Prog. Theor. Phys. **74** (1985), 288.
17) Y. R. Shimizu and K. Matsuyanagi, Prog. Theor. Phys. **71** (1984), 960.
18) A. Arima and F. Iachello, Ann. of Phys. **111** (1978), 201.
19) S. G. Lie and G. Holzwarth, Phys. Rev. **C12** (1975), 1035.
20) For a review, see, e.g., T. Marumori, K. Takada and F. Sakata, Prog. Theor. Phys. Suppl. No. 71 (1981), 1.
21) K. Matsuyanagi, *Proceeding of the Nuclear Physics Workshop, ICTP, Trieste, 1981,* ed. C. H. Dasso, R. A. Broglia and A. Winther (North-Holland, Amsterdam, 1982), p. 29.
22) N. L. Balazs and B. K. Jennings, Phys. Rep. **104** (1984), 347.
23) M. Hillery, R. F. O'connell, M. O. Scully and E. P. Wigner, Phys. Rep. **106** (1984), 121.
24) H. Horiuchi, K. Aoki, T. Wada and K. Yabana, Prog. Theor. Phys. **70** (1983), 1599.
25) K. Aoki and H. Horiuchi, Prog. Theor. Phys. **69** (1983), 1154.
26) E. R. Malshalek, Phys. Rev. **C29** (1984), 640.

Prog. Theor. Phys. Vol. 74, No. 6, December 1985, Progress Letters

Diabatic Quasiparticle Representation for Rotating Shell Model

Yoshifumi R. SHIMIZU*) and Kenichi MATSUYANAGI
Department of Physics, Kyoto University, Kyoto 606
(Received April 18, 1985)

On the basis of the selfconsistent collective-coordinate method, we present a new powerful method for constructing the diabatic quasiparticle representation to be used in the rotating shell model for high-spin states in the yrast region. With the use of this method, clean separation between the aligned and collective angular momenta can be achieved.

We propose a new powerful method to construct a "diabatic quasiparticle representation" to be used in the rotating shell model (RSM)[1),2)] for high-spin states in the yrast region. Use of the diabatic representation enables us to unambiguously specify individual rotational bands in which internal structure of the quasiparticle state vectors smoothly changes as functions of the rotational frequency ω.

Our approach is based on the selfconsistent collective-coordinate (SCC) method which is proposed by Marumori et al.[3)] as a microscopic theory of large-amplitude collective motions. We start from the time-dependent Hartree-Bogoliubov state vector of the following form:

$$|\phi(\theta, I)\rangle = e^{-i\theta \hat{J}_x} e^{i\hat{G}} |\phi_0\rangle , \tag{1}$$

$$i\hat{G}(\omega) = \sum_{\alpha\beta} \{ (g_{\alpha\beta}(\omega)\, a_\alpha^\dagger a_\beta^\dagger - g_{\alpha\beta}^*(\omega)\, a_\beta a_\alpha \} , \tag{2}$$

where $\theta = \omega t$, $\hat{J}_x$ is the x-component of the angular momentum operator, and $|\phi_0\rangle$ is the vacuum for the quasiparticles $a_\alpha^\dagger$ which are obtained by diagonalizing the Nilsson plus BCS Hamiltonian $h = h_{\rm def} - \Delta(\hat{P}^\dagger + \hat{P}) - \lambda \hat{N}$. Our aim is to determine the unknowns $g_{\alpha\beta}(\omega)$ in the operator $i\hat{G}$ as functions of ω. The basic equations determining $g_{\alpha\beta}(\omega)$ are:

$$\delta \langle \phi_0 | e^{-i\hat{G}} (H - \omega \hat{J}_x) e^{i\hat{G}} | \phi_0 \rangle = 0 , \tag{3}$$

$$\langle \phi_0 | e^{-i\hat{G}} \frac{\partial}{\partial \omega} e^{i\hat{G}} | \phi_0 \rangle = 0 , \tag{4a}$$

$$\langle \phi_0 | e^{-i\hat{G}} \hat{J}_x e^{i\hat{G}} | \phi_0 \rangle = I(\omega) , \tag{4b}$$

$$I(\omega) = -\frac{\partial \mathcal{H}'(\omega)}{\partial \omega}$$

with

$$\mathcal{H}'(\omega) \equiv \langle \phi_0 | e^{-i\hat{G}} (H - \omega \hat{J}_x) e^{i\hat{G}} | \phi_0 \rangle , \tag{5}$$

where $\delta|\phi_0\rangle = a^\dagger{}_\alpha a_\beta^\dagger |\phi_0\rangle$ and $H = h + H_{\rm int}$, with $H_{\rm int}$ being the residual interaction. Let us expand the operator G in a power series of ω

$$\hat{G}(\omega) = \omega \hat{G}^{(1)} + \omega^2 \hat{G}^{(2)} + \omega^3 \hat{G}^{(3)} + \cdots , \tag{6}$$

$$i\hat{G}^{(n)} = \sum_{\alpha\beta} \{ g^{(n)}(\alpha\beta)\, a_\alpha^\dagger a_\beta^\dagger - g^{(n)*}_{(\alpha\beta)}\, a_\beta a_\alpha \} . \tag{7}$$

Inserting (6) into (3) and requiring that the resultant equations should be satisfied order by order with respect to the powers of ω, we obtain inhomogeneous RPA equations for determining $g^{(n)}(\alpha\beta)$:

$$\boldsymbol{K} \begin{pmatrix} g^{(n)} \\ -g^{(n)*} \end{pmatrix} = \begin{pmatrix} \lambda^{(n)} \\ -\lambda^{(n)*} \end{pmatrix} , \tag{8}$$

where $\boldsymbol{K}$ is the RPA matrix for the Hamiltonian H, and $\lambda^{(n)}$ is the quantity expressible by the lower-order terms of $g^{(m)}$ with $m \leqq n-1$. Owing to Eq. (4a), the solution of Eq. (8) can be uniquely determined. The quasiparticle energies in the rotating frame are obtained by diagonalizing

$$h'_c(\omega) \equiv \text{one body part of } e^{-i\hat{G}} (H - \omega \hat{J}_x) e^{i\hat{G}} = \sum_{\alpha\beta} \Big(\sum_{n \geq 0} \omega^n \mathcal{E}^{(n)}_{\alpha\beta} \Big) a_\alpha^\dagger a_\beta . \tag{9}$$

Note that $h_c'(\omega)$ contains no $a_\alpha^\dagger a_\beta^\dagger$ and $a_\beta a_\alpha$ terms according to the variational principle (3). Thus, the quasiparticle Hamiltonian in the rotating frame is given by

$$h'(\omega) = e^{i\hat{G}} h'_c(\omega)\, e^{-i\hat{G}} = \sum_\mu E_\mu'(\omega)\, a_\mu^\dagger(\omega)\, a_\mu(\omega) , \tag{10}$$

where

$$\begin{pmatrix} a_\mu(\omega) \\ a_\mu^\dagger(\omega) \end{pmatrix} = e^{i\hat{G}} \begin{pmatrix} \sum_\alpha D_{\mu\alpha}(\omega)\, a_\alpha \\ \sum_\alpha D^*_{\mu\alpha}(\omega)\, a_\alpha^\dagger \end{pmatrix} e^{-i\hat{G}} \tag{11}$$

and

$$\sum_\beta \Big(\sum_{n \geq 0} \omega^n \mathcal{E}^{(n)}_{\alpha\beta} \Big) D_{\mu\beta}(\omega) = E_\mu'(\omega)\, D_{\mu\alpha}(\omega) . \tag{12}$$

The lowest-order solution of Eq. (8) is readily

*) Present address: The Niels Bohr Institute, Blegdamsvej 17, DK-2100 Copenhagen.

found to be

$$i\hat{G}^{(1)}=\mathcal{J}_{\mathrm{TV}}\cdot i\hat{\theta}^{(\mathrm{RPA})},$$

$$I^{(1)}(\omega)=\omega\mathcal{J}_{\mathrm{TV}}, \tag{13}$$

$$h'_c{}^{(0)}+h'_c{}^{(1)}=h-\omega(\hat{J}_x-\hat{J}_x{}^{(\mathrm{RPA})}), \tag{14}$$

where $\hat{\theta}^{(\mathrm{RPA})}$ and $\hat{J}_x{}^{(\mathrm{RPA})}$ are the RPA angle and angular-momentum operators, and $\mathcal{J}_{\mathrm{TV}}$ is the Thouless-Valatin moment of inertia. It is clear from Eq. (14) that the Tanaka-Suekane method[4] for constructing the diabatic representation is the lowest-order approximation to the present approach.

The quasiparticle energy diagram obtained by the above procedure is presented in Fig. 1. The lowest, 2nd and 3rd order solutions are drawn by thin-solid lines, dashed lines, and dot-dashed lines, respectively. In this calculation, the residual interaction H_{int} is neglected in order to compare with the conventional adiabatic energy diagram (for fixed pairing and quadrupole deformation parameters) which is also drawn in Fig. 1 by thick-solid lines. This figure demonstrates that the cutoff of the ω-expansion at a finite order $n_{\max}$ results in the diabatic level diagram. The physical reason why we obtain the diabatic levels (in place of the adiabatic levels) may be explained as follows. It is possible to divide $h'(\omega)$ into two parts:

$$h'(\omega)=\bar{h}'(\omega)+\Delta h'(\omega), \tag{15}$$

where $\bar{h}'(\omega)$ represents the smoothly varying part

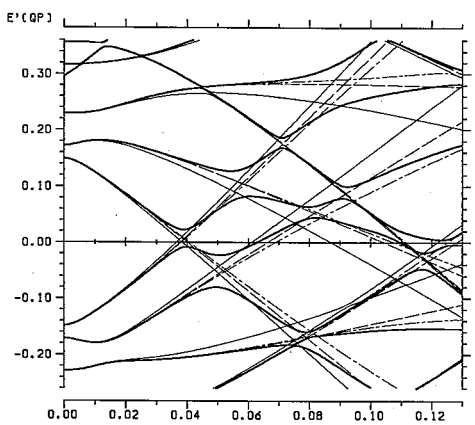

Fig. 1. Quasiparticle energy diagram for neutrons with signature $r=+i$. Only the levels resulting from the $i_{13/2}$ orbit are drawn. The unit is $\hbar\omega_0$. The mean-field parameters used are those suitable for ^{164}Er: $\delta_{\mathrm{osc}}=0.269$. $\Delta=1.032$ MeV, $\lambda=6.5293\hbar\omega_0$, $\hbar\omega_0=41.0A^{-1/3}=7.49$ MeV.

of $h'(\omega)$ expressible by the truncated ω-expansion, and the remaining part $\Delta h'(\omega)$ is connected with major change in the microscopic structure of yrast states caused by the alignment of the quasiparticle angular momenta. Thus, the ω-expansion provides us with a powerful means to extract the smooth part $\bar{h}'(\omega)$ from $h'(\omega)$. The result shown in Fig. 1 indicates that the calculations with $n_{\max}=2$ already give a satisfactory result. Determination of the optimal value of $n_{\max}$ remains as an important future problem, however.

An arbitrary one-body operator $\hat{F}$ can be expressed as

$$\hat{F}=e^{i\hat{G}}\Big(\sum_{n=0}^{n_{\max}}\omega^n\hat{F}^{(n)}\Big)e^{-i\hat{G}}$$

$$=\mathcal{F}+\hat{F}_A+\hat{F}_B, \tag{16}$$

where

$$\mathcal{F}=\langle\phi_0|e^{-i\hat{G}}\hat{F}e^{i\hat{G}}|\phi_0\rangle, \tag{17}$$

$$\hat{F}_B=\sum_{\mu\nu}\Big(\sum_{n=0}^{n_{\max}}\omega^n f_B{}^{(n)}(\mu\nu;\omega)\Big)a_\mu{}^\dagger(\omega)a_\nu(\omega), \tag{18}$$

$$f_B{}^{(n)}(\mu\nu;\omega)\equiv\sum_{\alpha\beta}D^*_{\mu\alpha}(\omega)f_B{}^{(n)}(\alpha\beta)D_{\nu\beta}(\omega), \tag{19}$$

and similar equations for $\hat{F}_A$ consisting of the $a_\mu{}^\dagger a_\nu{}^\dagger$ and $a_\nu a_\mu$ terms. Equations (18) and (19) explicitly show that there are two origins of the ω-dependence of the quasiparticle matrix elements: One is the direct mixing of quasiparticles $a_\alpha{}^\dagger$ (defined at $\omega=0$) which is caused by the Coriolis force and described by Eqs. (12) and (19), and the other is expressed by an ω-expansion up to $n_{\max}$ in Eq. (18) which comes from the transformation $e^{i\hat{G}}$ representing a smooth change of internal structure of the rotating nucleus as a whole.

The quantities $\mathcal{F}$ like angular momentum and pairing gaps of the g-band can be easily evaluated as

$$I(\omega)=\mathcal{J}_0\omega+\mathcal{J}_1\omega^3+\cdots, \tag{20}$$

$$\Delta(\omega)=\Delta_0+\Delta_1\omega^2+\cdots. \tag{21}$$

Thus, the phenomenological parameters like $\mathcal{J}_0$ and $\mathcal{J}_1$ of the Harris formula (20) are microscopically determined. It should be emphasized that these quantities change quite smoothly as functions of ω,when the diabatic basis is adopted.[2] A numerical example for the g-band of ^{164}Er is given in Table I. By comparing the results with and without including the residual pairing interaction, we see that the fourth-order Coriolis effect and the Coriolis-antipairing effect contribute to

Table I. The column with "cal 1" ("cal 2") lists the result calculated by neglecting (including) the residual pairing force.

	$\mathcal{J}_0$	$\mathcal{J}_1$	Δ_0 (neutron, proton)	Δ_1 (neutron, proton)
cal 1	24.0	35.0	1.032, 0.984	−0.51, −0.36
cal 2	24.0	74.4	1.032, 0.984	−1.70, −1.18
exp	32.6	93.3		
	$\hbar^2$/MeV	$\hbar^4$/(MeV)^3	MeV	$\hbar^2$/MeV

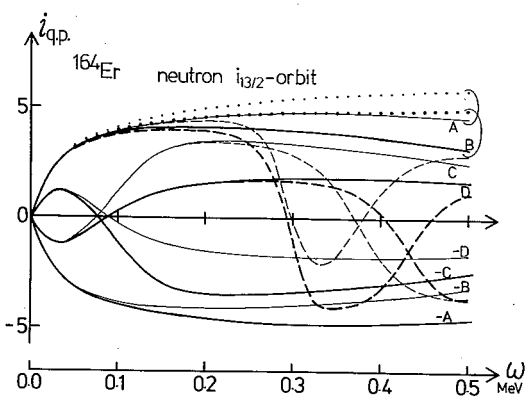

Fig. 2. Aligned angular momenta of the quasiparticle states (usually denoted by A, B, C and D) which result from the neutron $i_{13/2}$ orbit. The values calculated by the diabatic basis (solid lines) are compared with those by the adiabatic basis (dashed lines). The residual interaction H_{int} is neglected here. The dotted lines indicate the values obtained by the lowest-order approximation of the ω-expansion, i.e., by neglecting the $n=1$, 2, and 3 terms in Eq. (18).

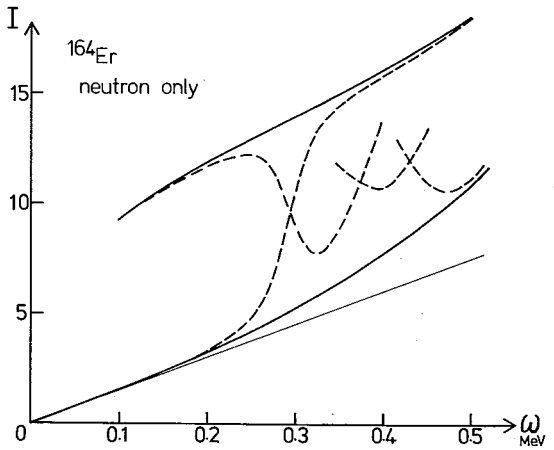

Fig. 3. Augular momenta of the g-band and the s-band in ^{164}Er calculated as functions of ω. The residual interaction is neglected and only the neutron contribution is displayed. The solid (dashed) lines show the values obtained by the diabatic (adiabatic) basis.

the value of $\mathcal{J}_1$ almost equally. The calculated values of $\mathcal{J}_0$ and $\mathcal{J}_1$ are 70~80% of the experimental values mainly due to the neglect of the quadrupole pairing force.

The usefulness of our method may be evidently seen in Fig. 2 which displays the aligned angular momenta. From a comparison between the calculation with $n_{\max}=3$ and that with $n_{\max}=0$ in Eq. (18), we can learn the important role of the $n=1$, 2 and 3 terms in reproducing the alignments. These terms represent the non-adiabatic effects of collective rotation. Figure 3 shows the neutron contribution to the angular momentum of the g-band and that of the s-band. By including the above non-adiabatic effects, we obtain the theoretical value 8.5$\hbar$ for the alignment of the s-band (at the band-crossing frequency) in agreement with the experimental value (if these effects are neglected, we would obtain 10.0$\hbar$). This figure furthermore indicates that the $\mathcal{J}_1$ value of the s-band is smaller than that of the g-band, again in agreement with experimental data. It should be emphasized that such a clean separation between the aligned and collective angular momenta would be extremely difficult, if the conventional adiabatic basis is used.

A detailed account of our method will be published after completing a more systematic calculations.

One of the authors (Y.R.S.) is indebted to Japan Society for the Promotion of Science for financial support. The computer calculation for this work has been supported by RCNP, Osaka University.

1) R. Bengtsson and S. Frauendorf, Nucl. Phys. **A327** (1979), 139.
2) Y. R. Shimizu and K. Matsuyanagi, Prog. Theor.

Phys. **70** (1983), 144; **72** (1984), 799.
3) T. Marumori, T. Maskawa, F. Sakata and A. Kuriyama, Prog. Theor. Phys. **64** (1980), 1294.
4) Y. Tanaka and S. Suekane, Prog. Theor. Phys. **66** (1981), 1639.

Progress of Theoretical Physics, Vol. 75, No. 5, May 1986

Monopole and Quadrupole Giant Resonances in Rotating Triaxially Deformed Nuclei. II

— *A Microscopic Description of the Isoscalar and Isovector Modes* —

Yoshifumi R. SHIMIZU*) and Kenichi MATSUYANAGI

Department of Physics, Kyoto University, Kyoto 606

(Received June 10, 1985)

Microscopic calculations are performed for the isoscalar and isovector monopole and quadrupole giant resonances built on high-spin yrast states. The results of the calculation show that the shapes of the strength functions for both the isoscalar and isovector vibrations are determined mainly by the deformation parameters of the mean field. The effects of rotation on the isoscalar and isovector quadrupole modes are found to be quite different: The rotation-splittings of the former become significant at very high-spins, while those of the latter remain small. It is also demonstrated that the transformation of the strength functions from the rotating frame into the laboratory frame is crucial to accurately evaluate the rotation-splittings of the quadrupole modes.

§ 1. Introduction

Recent experimental progress opens the great possibilities to study the properties of nuclei at high-spin states. One of the exciting findings is the detection of the high-energy γ-rays which are emitted from the isovector giant dipole resonances (IV-GDR) built on excited states with large angular momenta.[1),2)] Investigations of these giant resonances (GR) are expected to reveal various kinds of phase transitions which occur along and/or above the yrast line. Thus, many experimental[3),4)] and theoretical[5)~12)] works have been done on the GR in rapidly rotating nuclei. The experimental data seem to indicate that the excitation energies of the GDR shift to lower positions with increasing angular momentum and that the intrinsic widths become systematically broader in comparison with those of the GDR built on the ground states. There are several possible mechanisms responsible for these character-changes observed in the GDR built on states with large angular momenta; shape changes, rotation-splittings, temperature effects, etc. At the present stage of investigation, however, we have no definite conclusion about the origin (s).

In the previous paper[11)] (from now on referred to as I), we have performed RPA calculations based on the selfconsistent rotating shell model (RSM) for the isoscalar (IS) monopole and quadrupole giant resonances (GMR and GQR) in rapidly rotating, triaxially deformed nuclei. Quite recently the region of detected γ-ray spectra was extended and the bump around $E_\gamma \approx 27$ MeV was observed in ^{111}Sn,[13)] which may probably be attributed to the isovector (IV)-GQR. Encouraged by this new experimental development, we have extended our calculation of I in such a way that the strength functions for the IS and IV-modes of the GMR and GQR can be treated in a unified manner by employing essentially the full shell-model space. Furthermore, we have carried out a more detailed analysis of the rotation-splittings as well as the deformation-splittings of the GQR by giving special attention to the relations between the strength functions in the rotating frame and those in the laboratory frame.

*) Present address: Department of Physics, Kyushu University, Fukuoka 812.

After giving a brief account of our microscopic framework in § 2, the results of realistic calculation are presented for ^{158}Er and ^{164}Er in § 3: The former is a typical nucleus in which the prolate-oblate shape change occurs, and the latter approximately preserves a prolate shape. Section 4 is devoted to a summary and discussion.

§ 2. Formulations

In I the RPA response functions are derived in a general form by paying particular attention to the treatment of the Nambu-Goldstone (NG) modes. Since formulations of our approach are given in I and Refs. 14) and 15), we only mention what will be particularly needed in later sections.

2.1. *The Hamiltonian*

The deformation parameters (β, γ) and the pairing gaps (Δ_n, Δ_p) of the single-particle Hamiltonian H_0 of the Nilsson plus BCS type are determined selfconsistently as functions of the rotational frequency $\omega_{\rm rot}$, by using the isotropic velocity distribution (IVD) condition and the BCS equations. The residual interaction V between the quasiparticles in the rotating frame is composed of the monopole pairing force and the doubly-stretched monopole and quadrupole forces. The latter contains both the IS($T=0$) and IV($T=1$)-components. The doubly stretched multipole operators ($L=0, 2$) are obtained from

$$Q_{LK}^{(\pm)}=\frac{1}{\sqrt{2(1+\delta_{K0})}}\sum_{n=1}^{A}\left\{ r^2(Y_{LK}\pm Y_{L-K})\begin{pmatrix}1\\ \tau_0-\dfrac{N-Z}{A}\end{pmatrix}\right\}_n \quad \text{for} \quad \begin{pmatrix}T=0\\ T=1\end{pmatrix} \tag{2·1}$$

by the replacement $x_i\to x_i''\equiv(\omega_i^{\rm eff}/\omega_0)x_i$ with $\omega_i^{\rm eff}=\sqrt{\omega_i^2-(1-\delta_{i1})\omega_{\rm rot}^2}$. Here $(\pm)$ denotes the signature quantum number $r=\pm$, and K is the projection of L on the z axis (i.e., the symmetry axis in the ground state). The rotation axis is chosen to be the x axis.

The force strengths of the IS-part are determined by the Landau-Migdal prescription with the volume-conserving constraint and Kishimoto's saturation condition both applied to the harmonic oscillator (h.o.) potential model. The force strengths of the IV-part are obtained by assuming that transition densities are of volume-type and their rotational frequency dependences are the same as those of the IS-part. Thus, we get[16),17)]

$$\chi_{LK}^{(\pm)}(T=1)=a_L\cdot\chi_{LK}^{(\pm)}(T=0) \tag{2·2}$$

with

$$a_L=\frac{5}{4}\frac{V_1}{M\omega_0^2}\times\begin{cases}\langle r^2\rangle_0/(\langle r^4\rangle_0-\langle r^2\rangle_0^2) & \text{for } L=0,\\ \langle r^2\rangle_0/\langle r^4\rangle_0 & \text{for } L=2.\end{cases} \tag{2·3}$$

The values of $\langle r^2\rangle_0$ and $\langle r^4\rangle_0$ are taken from Bohr and Mottelson's textbook, which are $0.87\,A^{2/3}$fm^2 and $0.95\,A^{4/3}$ fm^4, respectively. As for the symmetry potential V_1, we have used the value -110 MeV which results in $a_0=-15.28$ and $a_2=-3.11$. In the limit of spherical h.o. potential, the excitation energies of the GMR and GQR are thus given as

$$\hbar\omega_M^{(\rm IS)}=73.3A^{-1/3}, \qquad \hbar\omega_Q^{(\rm IS)}=58.0A^{-1/3},$$

$$\hbar\omega_M^{(\mathrm{IV})}=165.1A^{-1/3}, \qquad \hbar\omega_Q^{(\mathrm{IV})}=131.1A^{-1/3}. \tag{2·4}$$

2.2. *Strength functions in the laboratory frame*

Let us define the RPA-strength function for an arbitrary one-body operator F:

$$S(F;\omega)\equiv\frac{1}{\pi}\mathrm{Im}\mathcal{R}(F^{\dagger},F;\omega+i\varepsilon)$$

$$\overset{\varepsilon\to 0+}{\longrightarrow}\sum_n\{\delta(\omega_n-\omega)|\langle n|F|0\rangle|^2-\delta(\omega_n+\omega)|\langle n|F^{\dagger}|0\rangle|^2\}, \tag{2·5}$$

where $\mathcal{R}(A,B;\omega)$ is the RPA-response function for operators A and B (for the definition of it, see I), and the summation $\sum_n$ in the second line should be performed over the physical RPA solutions.

Since all the calculations are carried out in the rotating frame, we should transform the calculated strength functions into those in the laboratory frame. We perform the transformation in the following two steps. First the strength functions for the operator $Q_{\lambda K}^{(\pm)}$ are linearly transformed to those for the multipole operator $Q_{\lambda\mu}$ whose quantization axis is *the rotation axis*. For the quadrupole operator under consideration, thus, we have

$$S(Q_{2,0})=\frac{1}{4}S(Q_{20}^{(+)})+\frac{3}{4}S(Q_{22}^{(+)})-\frac{\sqrt{3}}{2}\frac{1}{\pi}\mathrm{Im}\mathcal{R}(Q_{20}^{(+)},Q_{22}^{(+)}), \tag{2·6}$$

$$S(Q_{2,\pm1})=\frac{1}{2}S(Q_{21}^{(-)})+\frac{1}{2}S(Q_{22}^{(-)})\pm\frac{1}{\pi}\mathrm{Im}\mathcal{R}(Q_{21}^{(-)},Q_{22}^{(-)}), \tag{2·7}$$

$$S(Q_{2,\pm2})=\frac{3}{8}S(Q_{20}^{(+)})+\frac{1}{8}S(Q_{22}^{(+)})+\frac{1}{2}S(Q_{21}^{(+)})$$

$$+\frac{\sqrt{3}}{4}\frac{1}{\pi}\mathrm{Im}\mathcal{R}(Q_{20}^{(+)},Q_{22}^{(+)})\pm\frac{1}{2}\frac{1}{\pi}\mathrm{Im}(\mathcal{R}(Q_{20}^{(+)},Q_{21}^{(+)})+\mathcal{R}(Q_{22}^{(+)},Q_{21}^{(+)})). \tag{2·8}$$

Next, the strength functions above, $S^{(\mathrm{rot})}$, all of which are evaluated in the rotating frame, are transformed into those in the laboratory frame, $S^{(\mathrm{lab})}$, according to

$$S^{(\mathrm{lab})}(Q_{\lambda\mu};\omega)=S^{(\mathrm{rot})}(Q_{\lambda\mu};\omega-\mu\omega_{\mathrm{rot}}). \tag{2·9}$$

The above relation has been obtained by regarding the system under consideration as rotating uniformly about a fixed axis (the x-axis). This is known as a basic approximation of the cranking model, where the x-component of the angular momentum is identified with the magnitude of it and, accordingly, the energies in the uniformly rotating frame, $\hbar\omega'$, are related to those in the laboratory frame through $\hbar\omega'=\hbar\omega-\hbar\omega_{\mathrm{rot}}J_x$. In this approximation, the reduced matrix elements between high-spin states can be evaluated in terms of the intrinsic matrix elements $\langle\alpha'I'|Q_{\lambda\mu}|\alpha I\rangle^{(\mathrm{intri})}$ through the relation

$$\langle\alpha'I'\|Q_\lambda\|\alpha I\rangle\approx\sqrt{2I+1}\langle\alpha'I'|Q_{\lambda\mu}|\alpha I\rangle^{(\mathrm{intri})}\delta_{I',I+\mu},$$

which holds under the neglection of terms of order $1/I$.[18] Here $|\alpha I\rangle^{(\mathrm{intri})}$ is the state vector defined in the rotating frame, which satisfies the constraint $\langle\alpha I|J_x|\alpha I\rangle=I$. Notice that the relation $\Delta I\equiv I'-I=\mu$ is implied above. In general, Eq. (2·9) may be regarded as the lowest-order approximation of the $1/I$-expansion,[18] which is expected to be a good approximation for the states near the yrast line.

Since the laboratory strength functions $S^{(\mathrm{lab})}(Q_{\lambda\mu};\omega)$ describe the transitions from the

yrast states which are not the ground state, a careful treatment is necessary concerning the range of variable ω. As is illustrated in Fig. 1, the physically allowed transitions are those denoted by A, a and b, where the strength functions $S^{(\mathrm{lab})}$ are non-negative. Thus, we see that $\omega \geq -|\mu|\omega_{\mathrm{rot}}$ for the transitions with $\Delta I = -|\mu|$, while $\omega \geq |\mu|\omega_{\mathrm{rot}}$ for those with $\Delta I = |\mu|$. In the next section, nevertheless, we always show the $\omega \geq 0$ part of the calculated strength functions including the unphysical part denoted by B in Fig. 1. This is merely because of convenience of plotting figures. We note, however, that the strengths for the $\Delta I = -|\mu|$ transitions with $0 > \omega > -|\mu|\omega_{\mathrm{rot}}$ (i.e., the part b) can be easily obtained from those for the $\Delta I = |\mu|$ transitions with $|\mu|\omega_{\mathrm{rot}} \geq \omega > 0$ (i.e., the part B which are displayed in Figs. 3(b) and 5(b)) by means of the identity

$$S(F^{\dagger}; -\omega) = -S(F; \omega) . \tag{2·10}$$

We define the quantities related to the photo and/or electro-reaction cross sections in the long-wave length limit by

$$\tau(E0; \omega) = 2\pi^3 \left(\frac{e^2}{\hbar c}\right) \frac{(\hbar\omega_0)^3}{(\hbar c)^2} B(E0; \omega) ,$$

$$\tau(E\lambda; \omega) = \frac{8\pi^3(2\lambda+1)(\lambda+1)}{\lambda[(2\lambda+1)!!]^2} \left(\frac{e^2}{\hbar c}\right) \frac{(\hbar\omega_0)^{2\lambda-1}}{(\hbar c)^{2\lambda-2}} B(E\lambda; \omega) \quad \text{for } \lambda \geq 1 \tag{2·11}$$

with

$$B(E\lambda; \omega) = \sum_{\mu=-\lambda}^{+\lambda} S(Q_{\lambda\mu}(p); \omega) , \tag{2·12}$$

where $Q_{\lambda\mu}(p)$ denotes the proton part of the mass λ-pole operator whose quantization axis is the rotation axis. Note that the following identity holds in the rotating frame,

$$\sum_{\mu=-\lambda}^{+\lambda} S^{(\mathrm{rot})}(Q_{\lambda\mu}; \omega) = \sum_{\substack{K=0,1,\cdots\lambda \\ \tau=\pm}} S^{(\mathrm{rot})}(Q^{(\tau)}_{\lambda K}; \omega) . \tag{2·13}$$

For example, $E\lambda$-photo absorption cross section $\sigma(E\lambda; \omega)$ $(\lambda \geq 1)$ is obtained by $(\omega/\omega_0)^{2\lambda-1} \times \tau(E\lambda; \omega)$.

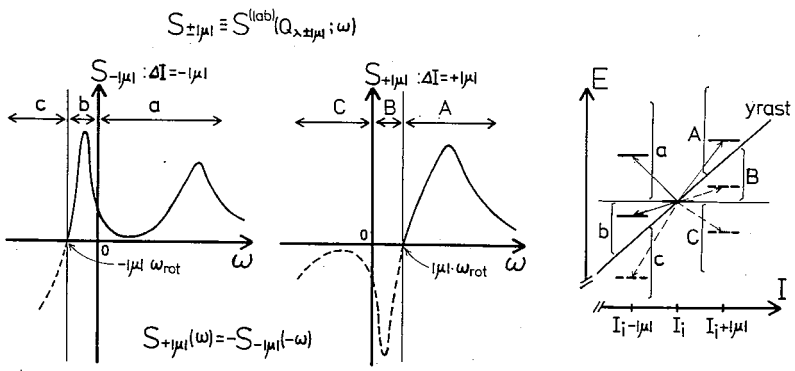

Fig. 1. A schematic illustration of physical transitions in the laboratory frame. Unphysical transitions are drawn by the dashed lines. In realistic calculations (Figs. 3 and 5), the values of ω at which $S_{+|\mu|}$ become zero slightly deviate from $|\mu| \cdot \omega_{\mathrm{rot}}$, because finite values of $\mathrm{Im}(\omega)$ are used there.

2.3. *Rotation-splittings in the h.o. potential model rotating about the symmetry axis*

In I, we presented the analytical solutions for the triaxially deformed but non-rotating h.o. potential model and found that they well explain the major properties of the GMR and GQR, especially deformation-splittings of the GQR, revealed by realistic calculations. However, the rotation-splittings will become increasingly important as the angular momentum increases. In order to estimate the rotational effects on the GQR, it would be instructive to consider the analytically solvable h.o. potential model rotating about the symmetry axis.[6] In this model all the calculations can be performed in the laboratory frame, and the modes with $\mu=0$, ±1 and ±2-components completely decouple. Since effects of rotation explicitly appear only for $\mu\neq0$-components, we have examined only the $\mu=\pm1$ and ±2-modes (for the GMR and the $\mu=0$-mode of the GQR, see I).

First let us introduce the quantities

$$f=\varkappa/\varkappa_{\rm self}\,,\quad x=1-f/2\,,\quad \eta=\frac{1}{4}\left(\frac{\omega_{/\!/}{}^2-\omega_\perp{}^2}{\omega_{/\!/}{}^2+\omega_\perp{}^2}\right)^2, \tag{2·14}$$

$$q_1=I_0/\left(\frac{\omega_{/\!/}{}^2+\omega_\perp{}^2}{2}\right)^{1/2}(\mathcal{J}_{/\!/})_{\rm rig}\,,\quad q_2=I_0/\omega_\perp(\mathcal{J}_\perp)_{\rm rig} \tag{2·15}$$

with the definitions $\omega_{/\!/}\equiv\omega_1$, $\omega_\perp\equiv\omega_2=\omega_3$ and $\varkappa_{\rm self}=(4\pi/5)M\omega_0{}^2/\langle\sum_{n=1}^{A}(x''{}^2)_n\rangle$, where I_0 is the angular momentum of the yrast state, $\varkappa$ is the strength of the doubly-stretched quadrupole interaction,*) $(\mathcal{J}_{/\!/})_{\rm rig}$ and $(\mathcal{J}_\perp)_{\rm rig}$ are the rigid moment of inertia with respect to the x and the z axis, respectively. Then, we can express the excitation energies and the transition strengths for the GQR in the laboratory frame as

$$\hbar\omega_{\pm\mu}\approx(2\hbar\omega_0)\sqrt{x}\,d_\mu\left(1\mp\frac{f}{4}\mu q_\mu/\sqrt{x^3}-\delta_{\mu1}(1-f)\eta/x^3\right), \tag{2·16}$$

$$|t(Q_{2\pm\mu})|^2\approx\frac{T_{\rm cl}}{2\sqrt{x}}\cdot\frac{d_\mu}{c_\mu{}^2}(1\pm\mu q_\mu/\sqrt{x^3}-\delta_{\mu1}(3-f)\eta/x^3)\,, \tag{2·17}$$

where

$$d_1=\omega_\perp/\omega_0\,,\qquad d_2=((\omega_{/\!/}{}^2+\omega_\perp{}^2)/2\omega_0{}^2)^{1/2}, \tag{2·18}$$

$$c_1=(\omega_\perp/\omega_0)^2\,,\qquad c_2=\omega_{/\!/}\omega_\perp/\omega_0{}^2\,, \tag{2·19}$$

and $T_{\rm cl}=\hbar\omega_0/\varkappa_{\rm self}$ is the classical value of the $r^2Y_{2\mu}$-transition strength in the spherical limit. Here d_μ represent the deformation-effects and c_μ the conversion coefficients between the doubly-stretched and the ordinary quadrupole operators. In Eqs. (2·16) and (2·17) we have used the lowest-order approximations with respect to q_μ and η. The exact expression can be obtained by solving the cubic (bi-quadratic) equation for the $\mu=2$ ($\mu=1$)-modes. However, since $q_\mu\approx\omega_{\rm rot}/\omega_0$ and $\eta\approx\varepsilon^2$(ε is the deformation parameter), this approximation is accurate even at the highest possible angular momentum in realistic situations.

Noting that $f=1$ ($x=1/2$) and $f\approx-3.1$ ($x\approx2.6$) for the IS and IV-GQR, respectively, we find from Eqs. (2·16) and (2·17) the following: (1) The excitation energy of the $+\mu$-mode is smaller (larger) than that of the $-\mu$-mode for the IS (IV)-GQR, while the

*) In our approach the force strength $\varkappa$ depends on μ, but its dependence is $|\varkappa_{\mu=2}-\varkappa_{\mu=1}|/\varkappa_{\mu=2}\approx(\omega_{\rm rot}/\omega_0)^2/2\varepsilon$ and is small in the realistic situations. Therefore, this effect is neglected in Eq. (2·14).

transition strength of the $+\mu$-mode is always larger than that of the $-\mu$-mode. (2) The amount of the splitting induced by the rotation for the excitation energy is smaller by about a factor $|f/4|$ than that for the transition strength. (3) The rotation-splittings (for both the excitation energies and the transition strengths) are about twice as large for the $\mu=2$-mode as those for the $\mu=1$-mode. (4) The rotation-splittings for the IS-GQR would increase with increasing angular momentum and become comparable with the deformation-splittings, while those for the IV-GQR remain always small.

§ 3. Results of calculation

3.1. *Details of calculation*

The calculational procedure is the same as in I except for the following improvement: Since the high-j orbits from the neutron $N_{\rm osc}=8$ and the proton $N_{\rm osc}=7$ shells come into play as the rotational frequency increases, we have extended the model space to 6-major shells, i.e., $N_{\rm osc}=3\sim8$ for neutrons and $N_{\rm osc}=2\sim7$ for protons. Indeed, we found that the shape of the strength function is affected considerably by the contributions from these orbits. In particular, we note that the order of the $+|\mu|$ and $-|\mu|$-components of the IV-GQR in the laboratory frame is reversed when these orbits are neglected. On the other hand, the effects on the IS-GQR are not so much important (compare Figs. 3~6 below with those of I). As a result, the number of the two-quasiparticle states employed in this paper becomes about 18,000 which is twice as large as that in I. It should be mentioned that the calculation using this very large model space is an almost complete one within our microscopic approach. In fact, the kinematical identities between the operators (J_x, iJ_y, J_z) and $(Q_{21}^{(+)}, Q_{21}^{(-)}, Q_{22}^{(-)})$, which are listed in Table II of Ref. 14), hold within 99.5~100% accuracy for any value of $\omega_{\rm rot}$ when this model space is used. In the 5 major-shells calculation of I, these identities are satisfied only with accuracy 93~98 % for neutrons and 87~92 % for protons.

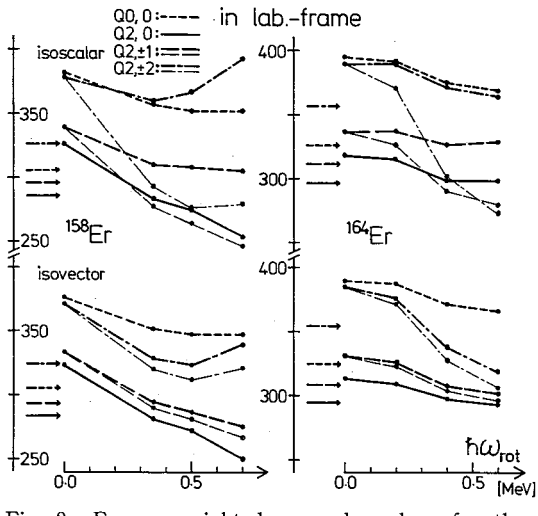

Fig. 2. Energy weighted sum-rule values for the operators $Q_{\lambda\mu}(\lambda=0, 2)$, which are evaluated in the laboratory frame by Eq. (3·1), are plotted as functions of the rotational frequency $\omega_{\rm rot}$ for ^{158}Er and ^{164}Er. Note that the quantization axis is chosen to be the rotating axis (the x axis) and those for Q_{00} are multiplied by a factor 5/2. The unit is $b_0^4\cdot\hbar\omega_0$. The allows at the left-hand side represent the classical sum-rule values for the ground states. See Figs. 2 and 4 for the mean-field parameters used in this calculation.

In addition to the effect of neutron excess explicitly shown in Eq. (2·1), we have taken into account the difference of the oscillator lengths between neutrons and protons. This does not affect the IS-modes practically, but slightly affects the IV-modes. The energy-averaging parameter $\mathrm{Im}(\hbar\omega)$ for the strength functions is chosen to be 1.0 MeV (except for Fig. 7), and the temperature-effects are neglected (see the argument in § 4).

In Fig. 2 we show the energy-weighted sum-rule values for the operator $Q_{\lambda\mu}(\lambda=0, 2)$ evaluated in the laboratory frame which are defined by

Table I. The calculated results for the low-lying $\beta(K=0)$, NG($K=1$) and $\gamma(K=2)$ modes built on the ground states of ^{158}Er and ^{164}Er. The 1st row lists the renormalization factors[14] defined as the ratios of the force strengths that reproduce the experimentally observed excitation energies, $\varkappa_{\rm exp}$, to the theoretical values for the h.o. potential, $\varkappa_{\rm self}$. The 2nd and 3rd (4th and 5th) rows list the excitation energies and the transition amplitudes calculated by using $\varkappa_{\rm exp}(\varkappa_{\rm self})$. The last row indicates the value of $\varkappa_{\rm self}$. See Figs. 2 and 4 for the mean-field parameters used.

	^{158}Er			^{164}Er		
	$K=0$	1	2	$K=0$	1	2
$f=\varkappa_{\rm exp}/\varkappa_{\rm self}$	1.100	1.009	1.054	1.179	1.006	1.032
$\hbar\omega_{\rm exp}$ (MeV)	0.806	0.0	0.820	1.246	0.0	0.860
$\lvert t(Q^{(+)}_{2K})\rvert$ (fm^2)	159	—	132	120	—	102
$\hbar\omega_{\rm theor}$ (MeV)	1.693	0.508	1.482	1.898	0.375	1.154
$\lvert t(Q^{(+)}_{2K})\rvert$ (fm^2)	87	192	89	42	219	83
$\varkappa_{\rm self}$ (MeV/fm^4)		0.008136			0.007719	

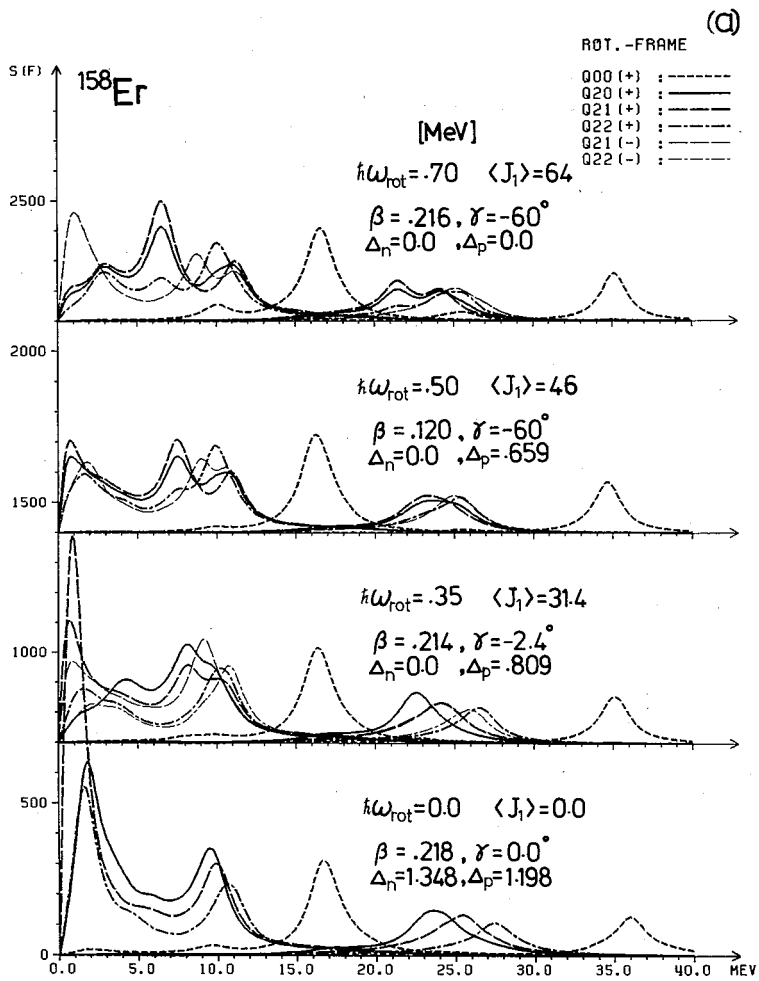

Fig. 3. (continued)

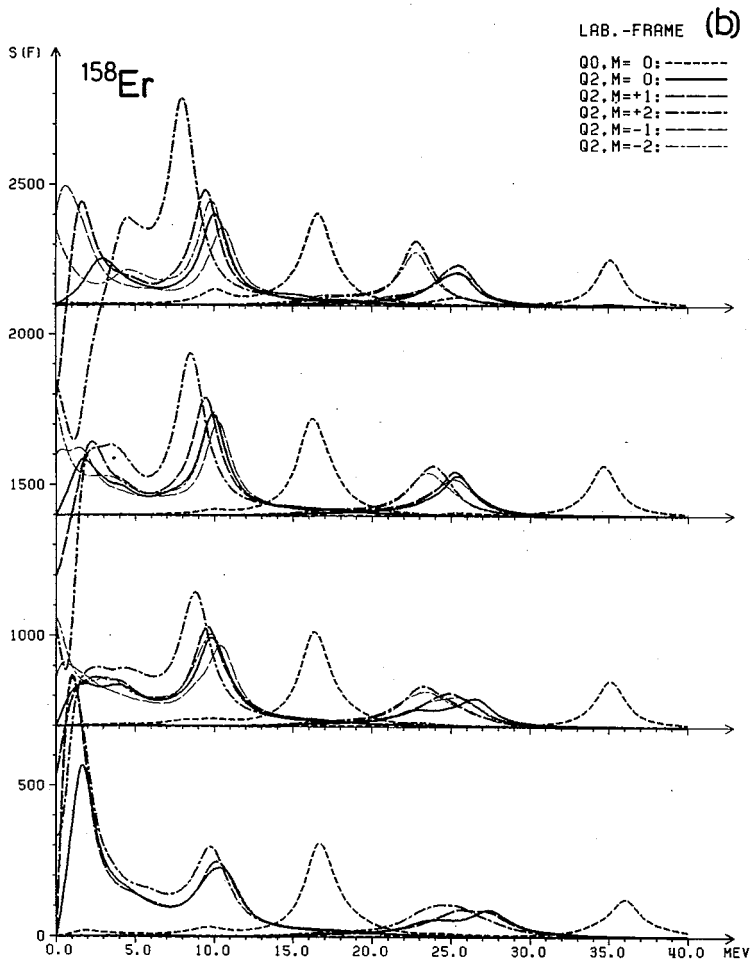

Fig. 3. Strength functions for the IS and IV monopole and quadrupole operators acting on the yrast states of ^{158}Er with $\hbar\omega_{\rm rot}=0.0$, 0.35, 0.5 and 0.7 MeV, each of which is shifted by 700 units from the bottom. The unit is $b_0^4/\hbar\omega_0$. The energy-averaging parameter $\mathrm{Im}(\hbar\omega)=1.0$ MeV is used. (a) is for the operators $Q_{\lambda K}^{(+)}$ in the rotating frame, while (b) is for the operators $Q_{\lambda\mu}$ in the laboratory frame. For interpretation of the latter (the laboratory strength function), see the comments in the text. The deformation parameters (β, γ), the pairing gaps (Δ_n, Δ_p) and the expectation value of J_x used in this calculation are also displayed as insets to (a). The monopole strength is multiplied by a factor 5/2.

$$S_1(Q_{\lambda\mu})=\hbar^2\int_0^\infty d\omega\cdot\omega S^{(\mathrm{lab})}(Q_{\lambda\mu};\omega)\ , \tag{3·1}$$

and are calculated for ^{158}Er and ^{164}Er as functions of the rotational frequency. These quantities show roughly how the rotation affects the GQR. Thus, from Fig. 2 we have found that the effects of rotation are a good deal larger on the IS-GQR than those on the IV-GQR. We note here that the energy-weighted sum-rule values for the monopole and quadrupole operators could differ considerably from the classical sum-rule values. This is due to the velocity-dependent components in the single-particle potential such as the static pairing deformation and the $\boldsymbol{l}^2$-term in the Nilsson potential. In our case, the pairing potential (at $\omega_{\rm rot}=0$) makes the sum-rule values for the operator $Q_{00}(Q_{2\mu})$ larger

than the classical value by about 5%(10%), and the $\boldsymbol{l}^2$-term increases (decreases) the value for $Q_{00}(Q_{2\mu})$ by about 20% (5%). This is the reason why the 5-major shells calculations in I already exhaust the classical sum-rule values. Therefore, it is dangerous to judge the sufficiency of the model space by a mere comparison between the calculated and the classical values of the energy-weighted sum-rules.

We present in Table I the result of RPA calculations for low-frequency vibrations built on the ground states of ^{158}Er and ^{164}Er. In the IV-sector, the strengths spread over many two-quasiparticle states and no $K^\pi=1^+$-collective states are found, in agreement with other realistic calculations.[19),20)] We note that NG modes do not decouple in the calculation with the force strength, χ_{self}, valid for the h.o. potential, because of the presence of the doubly-stretched $\boldsymbol{l}\cdot\boldsymbol{s}$ and $\boldsymbol{l}^2$-potentials which are, however, very important to obtain the correct equilibrium-deformation paramseters by the IVD condition.[15)]

3.2. *GMR and GQR built on high-spin yrast states*

Figure 3 shows the calculated strength functions for the monopole and quadrupole operators acting on the yrast states of ^{158}Er. They are evaluated for both the $T=0$ and $T=1$ modes at $\hbar\omega_{\text{rot}}=0.0$, 0.35, 0.5 and 0.7 MeV and are displayed as four sets of curves.

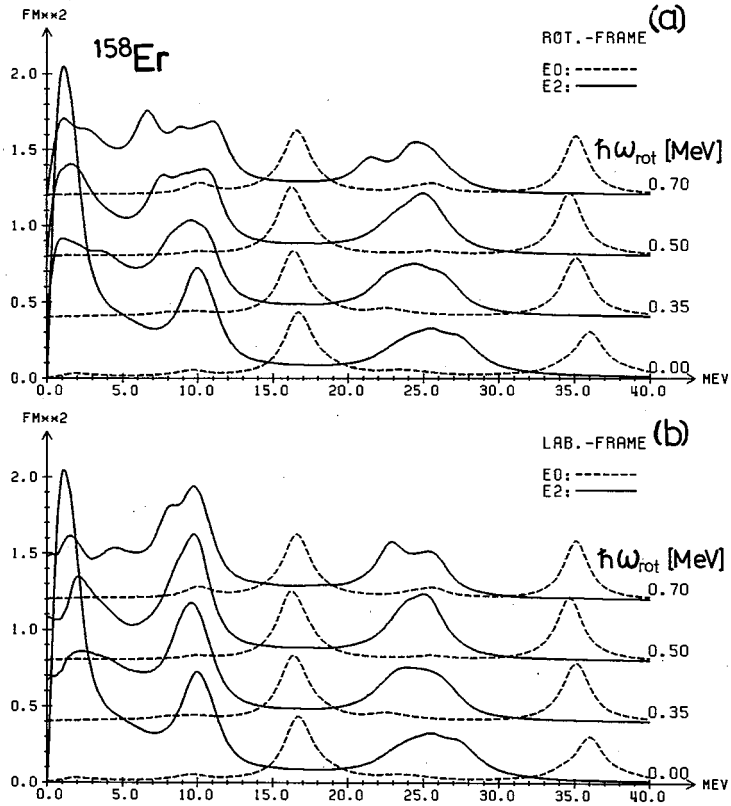

Fig. 4. The quantities $\tau(E0;\omega)$ and $\tau(E2;\omega)$ evaluated for ^{158}Er, which are defined by Eqs. (2·11) and (2·12) and are related to the photo and/or electro-reaction cross sections. The unit is fm^2. (a) is evaluated in the rotating frame, while (b) in the laboratory frame. Four sets of curves, to which the values of $\hbar\omega_{\text{rot}}$ are attached, correspond to those in Fig. 3 and each set of curves is shifted by 0.4 fm^2 from the bottom.

Figure 3(a) is the one for the operators $Q_{\lambda K}^{(\pm)}$, Eq. (2·1), which is calculated in the rotating frame, while Fig. 3(b) for the operators $Q_{\lambda\mu}$ transformed into the laboratory frame by Eqs. (2·6)~(2·9). Selfconsistently determined mean-field parameters (β, γ, Δ) and the expectation value of J_x at each value of $\omega_{\rm rot}$ are written in Fig. 3(a). We also present in Figs. 4(a) and (b) the quantities $\tau(E0;\omega)$ and $\tau(E2;\omega)$ defined by Eqs. (2·11) and (2·12) which respectively correspond to Figs. 3(a) and (b). The peaks seen at $\hbar\omega\approx 10$, 16, 26 and 35 MeV are related to the IS-GQR, IS-GMR, IV-GQR and IV-GMR, respectively. Note that the negative parts of the strength functions seen in the low-energy regions in Fig. 3(b) for the $\mu=+1$ and $+2$-operators should be converted, by means of Eq. (2·10), into the negative-energy transitions from the yrast state with $I=I_i$ to states with $I_f=I_i-1$ and I_i-2. These transitions are possible in the description in the laboratory frame. Since there exists a model-independent sum-rule between the non-energy-weighted strength with $+\mu$ and $-\mu$ components, i.e.,

$$\int_0^\infty d\omega S^{(\rm lab)}(Q_{\lambda\mu};\omega)=\int_0^\infty d\omega S^{(\rm lab)}(Q_{\lambda-\mu};\omega)\,, \tag{3·2}$$

the strength distributions for the GQR with $\mu\neq 0$ are somewhat affected by these negative-energy transitions.

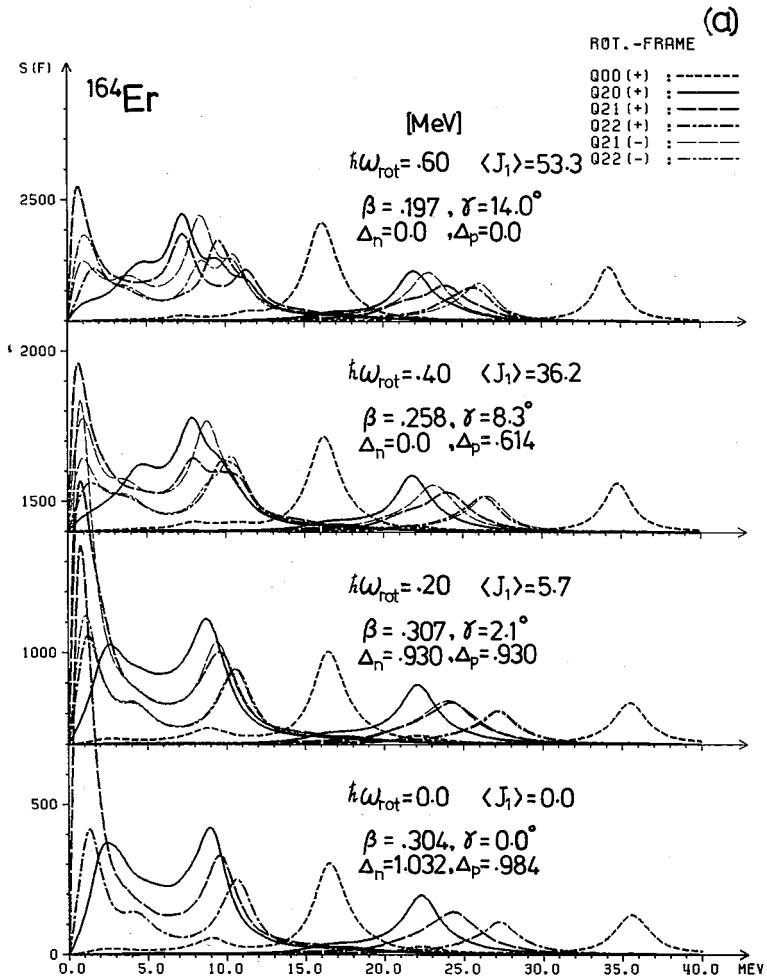

Fig. 5. (continued)

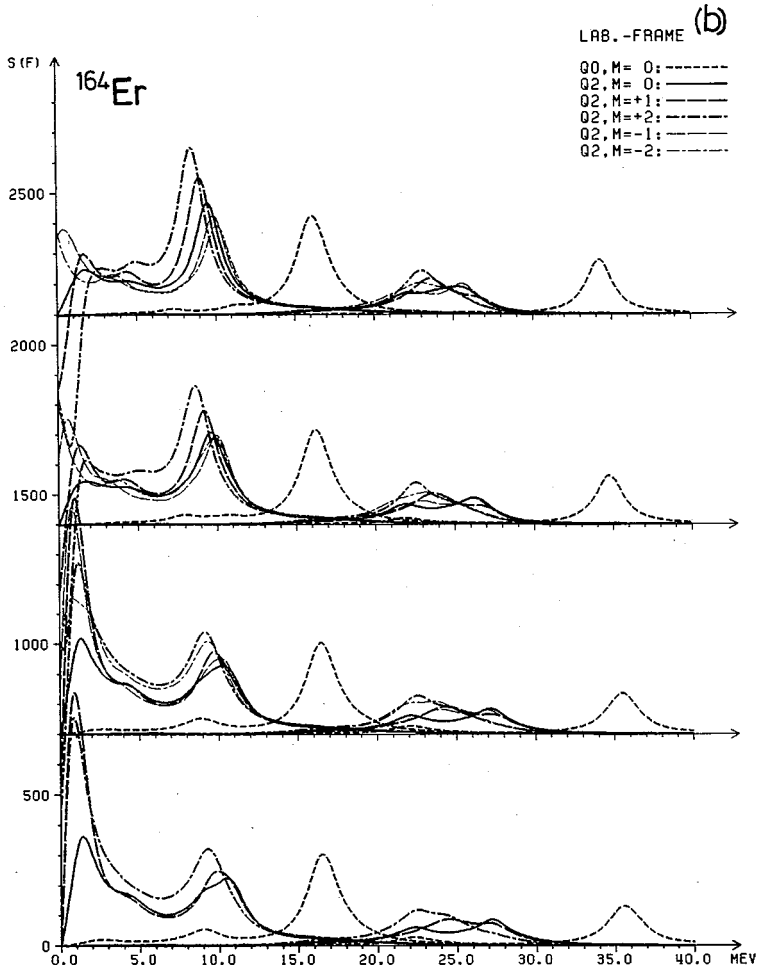

Fig. 5. The same as Fig. 3 but for ^{164}Er with $\hbar\omega_{\rm rot}=0.0$, 0.2, 0.4 and 0.6 MeV.

In this nucleus, the shape change occurs at $I\approx 45$ and the oblate limit is realized in the top two sets of curves in Figs. 3 and 4. From Figs. 3(a) and 4(a) we find that the $Q^{(\pm)}_{2K}$-strengths in the rotating frame spread over a wide energy-region due to the strong K-mixing induced by the Coriolis force. However, this spreading is somewhat misleading about the rotational effects. As seen in Figs. 3(b) and 4(b), the actual rotation-induced splittings are not so large in the laboratory frame and the qualitative features are well understood by the rotating h.o. potential model considered in § 2.3. In the laboratory frame, the width of the IS-GQR slightly increases as the rotational frequency increases, while that of the IV-GQR remains almost constant. On the other hand, the excitation energies of both modes are slightly shifted downwards. These direct effects of rotation are not drastic so that we can say that the total widths are mainly determined by the deformation-splittings.

In Figs. 5 and 6 we show the results for ^{164}Er with $\hbar\omega_{\rm rot}=0.0$, 0.2, 0.4 and 0.6 MeV. Similar observations to those for ^{158}Er hold here. This nucleus approximately preserves prolate shapes with small triaxial deformations up to considerably high angular momenta. For low-spin regions the characteristics of the triaxially deformed but non-rotating h.o. potential model described in I are well realized for both the IV and IS-modes, although for

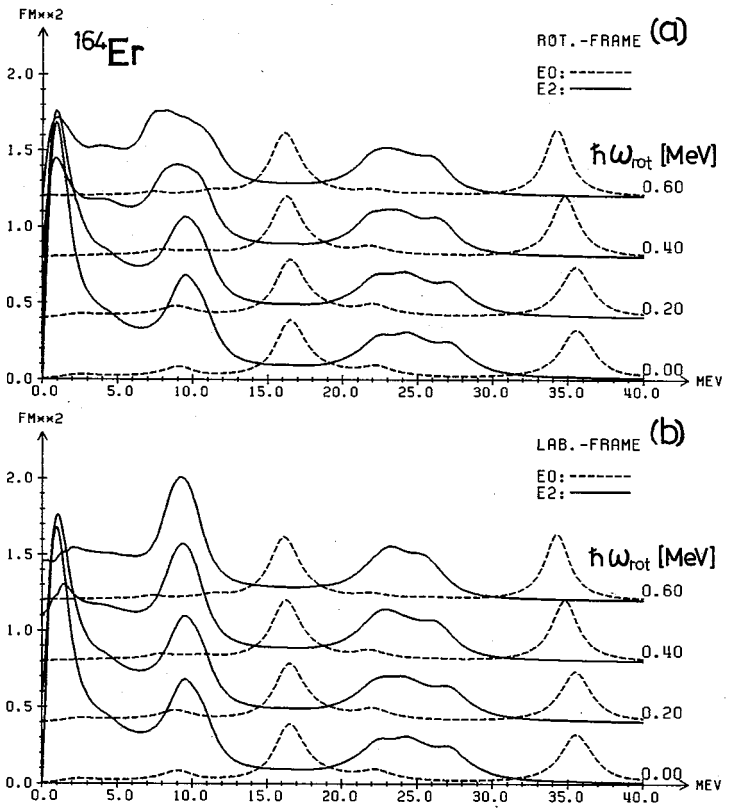

Fig. 6. The same as Fig. 4 but for ^{164}Er.

higher-spin regions the rotation-effects become non-negligible. It should be noticed that the deformation parameter decreases from $\beta\approx 0.3$ at $\hbar\omega_{\rm rot}=0.0$ MeV to $\beta\approx 0.2$ at $\hbar\omega_{\rm rot}=0.6$ MeV, so that the intrinsic width of the GQR does not increase with increasing $\omega_{\rm rot}$ for the IS-mode and rather becomes smaller for the IV-mode.

Another interesting point is that the rotational effects on the properties of the IS and IV-GQR at high-spins are quite different in this nucleus: For the IS-GQR the mixing effect between the $Q_{2\mu}$-strengths in the laboratory frame is negligiblly small. This fact indicates that the IS-GQR almost completely aligns its intrinsic angular momentum along the rotation-axis, although this nucleus is far from the oblate limit at the rotational frequency considered here. On the other hand, for the IV-GQR the coupling between the $Q^{(\pm)}_{2K}$-strengths in the rotating frame is rather weak. This difference can be understood as follows: The deformation-splitting of the excitation energies for the IS-modes (about 2 MeV) is small compared with those for the IV-modes (about 5 MeV), so that the Coriolis force is more effective on the former than the latter.

§ 4. Summary and discussion

By means of the RPA based on the selfconsistent rotating shell model, we have performed microscopic calculations for the GMR and GQR. Both the isoscalar and isovector modes built on high-spin yrast states have been treated in a unified manner by employing essentially the full shell-model space. We have found that the rotation-

splittings of the isoscalar GQR become comparable with the deformation-splittings at very high spin states, while those of the isovector GQR are rather small. We have also emphasized that it is crucial to correctly transform the strength functions from the rotating frame into the laboratory frame in order to accurately investigate the rotation-splittings. In fact, as shown in § 3 the gross features of the strength functions for the GQR are changed considerably by this transformation. A careful analysis is required to obtain this result because the transformation is performed in two steps and the non-diagonal elements of the response matrix play an important role in the second step where the transition energy $\hbar\omega$ is shifted *for each* μ*-component* according to Eq. (2·9). To explicitly indicate this point, we display in Fig. 7 an example for the $r=-1$-sector, i.e., for $Q_{2,\pm1}=i(Q_{21}^{(-)}\pm Q_{22}^{(-)})/\sqrt{2}$. This figure clearly demonstrates that the shapes of the strength functions would become quite different, if the non-diagonal elements of the response matrix, $\mathcal{R}(Q_{21}^{(-)}, Q_{22}^{(-)}; \omega)$, are neglected. Thus, contrary to the intuitive consideration,[9] the transformation does not necessarily lead to the broadening of the width.

In this paper, we have obtained the strength functions in the laboratory frame within the framework of the semiclassical approximation inherent in the cranking model, in

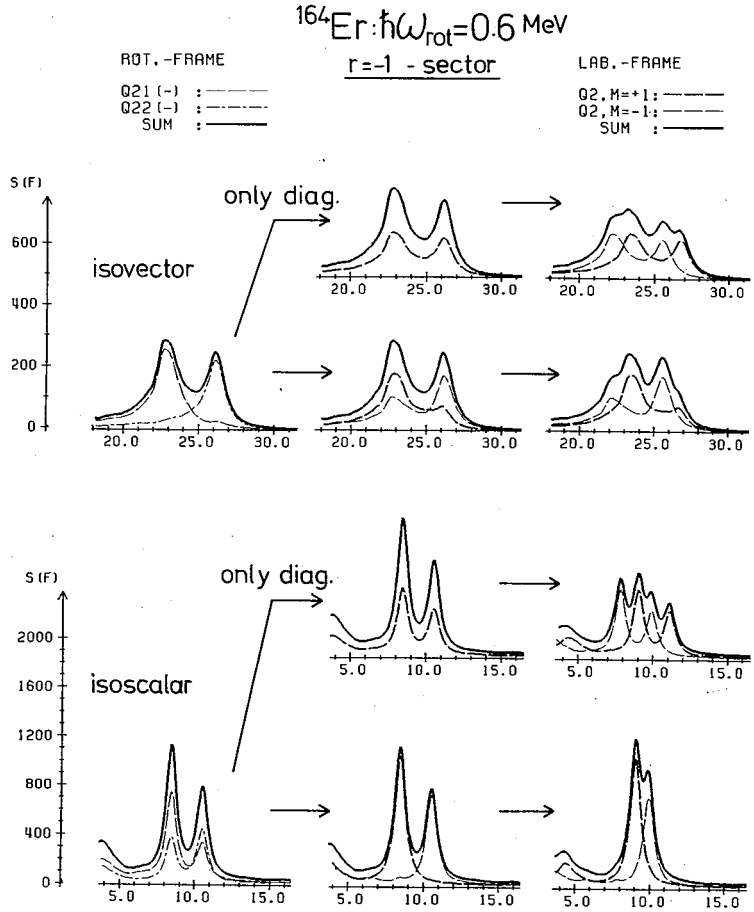

Fig. 7. The process of the two-step transformation, Eqs. (2·6)~(2·9), from the rotating frame into the laboratory frame. Only the $r=-1$-sector evaluated at $\hbar\omega_{rot}=0.6$ MeV in ^{164}Er is shown. In this figure $\mathrm{Im}(\hbar\omega)=0.4$ MeV is used. As a reference, those with neglecting the non-diagonal elements of the response matrix are also displayed.

which only the uniform rotations about a fixed axis are considered. For a more rigorous treatment of the transformation between the rotating- and laboratory frames, quantum-mechanical treatments of the collective rotation, like Ref. 18), along the line of the particle-rotor model should be developed further.

The temperature-effects should also be taken into account for a better comparison with experimental data. We note, however, that the observed γ-ray spectrum is constructed from the inclusive sum of the transitions that connect quite different regions above the yrast line, for which only one temperature could hardly be assigned. Therefore it seems to us that the applicability of the standard prescription[21] to the problem under consideration is an open subject of investigation. Moreover, it is reported[5),7),9)] that the inclusion of the temperature-effects by means of the standard prescription does not significantly change the results of the strength functions evaluated at zero temperature. We believe that the essential features of the strength functions for the GR's built on the high-spin states studied here would remain unchanged at least up to the region where the shell-structure effects are not largely diminished by the temperature-effects.

As is mentioned in the introduction, existence of the IV-GDR at high-spin states is confirmed and the change of its properties (peak positions, widths, etc.) as a function of angular momentum is now under investigation. As for the IV-GQR, angular momentum dependence of its properties is unknown at the present time. We hope that a detailed comparison between experimental data and theoretical calculations for the GQR will become possible in the near future.

Finally we should mention that the calculated excitation energies of the isoscalar GMR (GQR) are slightly higher (lower) than experimental values. There are two reasons for this: (i) The l^2-potential pushes up (down) the unperturbed two quasiparticle energies somewhat too strong, i.e., the shift is about 4 MeV (2 MeV) for the GMR (GQR) from those of the h.o. potential model (see figures of Ref. 11)).*) (ii) The velocity-dependence of the residual interactions (i.e., the effect of the effective mass $M^* \neq M$) is not included in our calculation. As is well known,[16] this velocity dependent effect pushes up the excitation energy by a factor $\sqrt{M/M^*}$, and can be incorporated along the line of Ref. 17).

Acknowledgements

We thank Dr. H. Kurasawa for valuable discussions. One of us (Y. R. S.) is indebted to Japan Society for the Promotion of Science for financial support. The computer calculation for this work has been supported in part by the Grant-in-Aid for Scientific Research of the Japan Ministry of Education, Science and Culture (No. 58540153), and in part by Research Center for Nuclear Physics, Osaka University.

References

1) J. O. Newton et al., Phys. Rev. Lett. **46** (1981), 1383.
2) J. E. Draper et al., Phys. Rev. Lett. **49** (1982), 434.
3) B. Haas et al., Phys. Lett. **120B** (1983), 79.
A. M. Sandorfi et al., Phys. Lett. **130B** (1983), 19.

*) We have used the newly determined N_{osc}-dependent parameters of Ref. 22). The use of them somewhat improves the result. The improvement is not sufficient, however.

W. Hennerici et al., Nucl. Phys. **A396** (1983), 329c.
4) J. J. Gaardhøje et al., Phys. Rev. Lett. **53** (1984), 148.
J. J. Gaardhøje et al., Phys. Lett. **139B** (1984), 273.
5) A. V. Ignatyuk and I. N. Mikhailov, Yadern. Fiz. **30** (1979), 665 [Sov. J. Nucl. Phys. **30** (1974), 343].
A. Akbarov, A. V. Ignatyuk, I. N. Mikhailov, Kh. L. Molina, R. G. Nazmitdinov and D. Janssen, Yadern. Fiz. **33** (1981), 1480 [Sov. J. Nucl. Phys. **33** (1981), 794].
E. B. Bal'butsev, Z. Vaishvila and I. N. Mikhailov, Yadern. Fiz. **35** (1982), 836 [Sov. J. Nucl. Phys. **35** (1982), 486].
S. N. Fedotkin, I. N. Mikhailov and R. G. Nazmitdinov, Phys. Lett. **121B** (1983), 15.
I. N. Mikhailov, R. G. Nazmitdinov and S. N. Fedotkin, Yadern. Fiz. **38** (1983), 24, 591 [Sov. J. Nucl. Phys. **38** (1983), 13, 351].
6) H. Kurasawa, Prog. Theor. Phys. **64** (1980), 2055; **66** (1981), 1317; **68** (1982), 1594.
7) J. L. Egido and P. Ring, Phys. Rev. **C25** (1982), 3239.
M. E. Faber, J. L. Egido and P. Ring, Phys. Lett. **127B** (1983), 5.
P. Ring, L. M. Robledo, J. L. Egido and M. Faber, Nucl. Phys. **A419** (1984), 261.
8) K. Neegaard, Phys. Lett. **110B** (1982), 7.
9) R. R. Hilton, Z. Phys. **A309** (1983), 233.
10) O. Civitarese, S. Furui, M. Ploszajczak and A. Faessler, Nucl. Phys. **A408** (1983), 61.
11) Y. R. Shimizu and K. Matsuyanagi, Prog. Theor. Phys. **72** (1984), 1017.
12) M. Di Nardo, M. Di Toro, G. Giansiracusa, U. Lombardo and G. Russo, Phys. Lett. **125B** (1983), 240; **132B** (1983), 11.
M. Di Toro, U. Lombardo and G. Russo, Nucl. Phys. **A435** (1985), 173.
13) J. J. Gaardhøje, C. Ellegard, B. Herskind, R. M. Diamond, M. A. Deleplanque, G. Dines, A. O. Macchiavelli and F. S. Stephens, submitted to Phys. Rev. Lett.
14) Y. R. Shimizu and K. Matsuyanagi, Prog. Theor. Phys. **70** (1983), 144.
15) Y. R. Shimizu and K. Matsuyanagi, Prog. Theor. Phys. **71** (1984), 960; **72** (1985), 799.
16) A. Bohr and B. R. Mottelson, *Nuclear Structure* (W. A. Benjamin Inc., 1975), vol. II.
17) E. Lipparini and S. Stringari, Nucl. Phys. **A371** (1981), 430.
S. Stringari and E. Lipparini, Nucl. Phys. **A371** (1981), 445.
18) E. R. Marshalek, Nucl. Phys. **A266** (1976), 317; **A275** (1977), 416.
See also A. Klein and M. G. Vassanji, Nucl. Phys. **A317** (1979), 116.
D. Janssen, Sov. J. Nucl. Phys. **25** (1977), 479.
H. Ichihashi and M. Yamamura, Prog. Theor. Phys. **60** (1978), 753.
19) S. Iwasaki and K. Hara, Phys. Lett. **144B** (1984), 9.
20) I. Hamamoto and S. Aberg, Phys. Lett. **145B** (1984), 163.
21) A. L. Fetter and J. D. Walecka, *Quantum Theory of Many Particle Systems* (McGraw-Hill Inc., 1971).
22) T. Bengtsson and I. Ragnarsson, Nucl. Phys. **A436** (1985), 14.

Progress of Theoretical Physics, Vol. 76, No. 1, July 1986

Microscopic Description of Anharmonic Gamma-Vibrations by Means of the Selfconsistent-Collective-Coordinate Method. II

Masayuki MATSUO and Kenichi MATSUYANAGI

Department of Physics, Kyoto University, Kyoto 606

(Received January 25, 1986)

Microscopic structures of the mode-mode couplings between the RPA γ vibrations and the other $K^\pi = 0^+$ and $\pm 4^+$ modes, which are incorporated in the fourth-order collective Hamiltonian for anharmonic γ vibrations, are analysed in detail. The conditions of the subshell structure of the Nilsson orbits near the Fermi surface for enhancement of these mode-mode couplings are clarified. It is predicted that the properties of the double γ vibrational states with $K^\pi = 0^+$ are especially sensitive to the dynamical anharmonicity effects arising from the mode-mode couplings. Numerical examples are presented for ^{164,166,168}Er.

§ 1. Introduction

In Part I[1] of this series of paper, we formulated a practical procedure for deriving, on the basis of the selfconsistent-collective-coordinate (SCC) method,[2] the Bohr-Mottelson-type collective Hamiltonian[3),4] for anharmonic γ-vibrational modes in deformed nuclei.

The SCC method provides us with a selfconsistent scheme to dynamically determine the collective coordinates and momenta which govern the time-evolution of the average potential. The scheme extracts the maximally-decoupled collective submanifold (for the large-amplitude collective vibrations) from the huge-dimensional phase space associated with the time-dependent Hartree-Bogoliubov (TDHB) state vectors. The mode-mode couplings between different RPA modes (which are the normal modes of the system in the small-amplitude limit) are incorporated in the determination of the collective submanifold. The (η^*, η) expansion method[2] for solving the basic equations of the SCC method does not presuppose the microscopic structures of the collective variables (η_i^*, η_i) and their boson correspondents $(B_i^\dagger, B_i)$. Thus, it may be considered as a dynamical extension of the familiar boson-expansion methods.

The aim of this paper, Part II, is to clarify the microscopic structure of the mode-mode couplings that are incorporated in the fourth-order collective Hamiltonian for anharmonic γ-vibrations. In § 2, the fourth-order anharmonicity terms derived in Part I by means of the (η^*, η) expansion method are rewritten in such a form that explicitly displays the mode-mode couplings. These expressions will provide us with a simple physical picture for the anharmonicity effects. As is well known, the properties of the collective β and γ vibrations are sensitively dependent on the subshell structure near the Fermi surface. Thus, for instance, a strong collectivity for the γ-degrees of freedom is realized in ^{164,166,168}Er with $Z=68$ and $N=96\sim100$ where both the proton subshell with the asymptotic quantum numbers $(N_{\rm osc}=4, n_3=1)$ and the neutron subshell with $(N_{\rm osc}=5, n_3=2)$ are partially occupied, since the Nilsson orbits belonging to these subshells have large single-particle matrix elements for the operators $r^2 Y_{2\pm2}$. In a similar manner, we will find in § 3 that the dynamical anharmonicity effects significantly change as the number of neutrons

changes. The reason for such a strong isotope dependence can be understood from a detailed analysis made in § 4, which clarifies the condition of the subshell structure near the Fermi surface for enhancement of the mode-mode coupling vertices. We solve in § 5 the fourth-order collective Hamiltonian for ^{164,166,168}Er, and discuss how the dynamical anharmonicity terms affect the properties of the double γ-vibrational states in these nuclei. In § 6 we add some remarks on future subjects.

A preliminary result of this work was previously reported in Ref. 6).

§ 2. Structure of the fourth-order collective Hamiltonian

2.1. *Classification of anharmonicities*

The TDHB state vector describing anharmonic γ-vibrations is written as

$$|\phi(\eta_i^*, \eta_i)\rangle = \exp i\hat{G}(\eta_i^*, \eta_i)|\phi_0\rangle\,, \tag{2·1}$$

$$i\hat{G}(\eta_i^*, \eta_i) = \sum_\lambda (G_\lambda(\eta_i^*, \eta_i)\hat{X}_\lambda^\dagger - G_\lambda^*(\eta_i^*, \eta_i)\hat{X}_\lambda)\,, \tag{2·2}$$

where $\eta_1^* \equiv \eta^*$ and $\eta_2^* \equiv \tilde{\eta}^*$ are the collective variables which transfer the K-quantum numbers by 2 and -2, respectively. The phonon operators $\hat{X}_\lambda^\dagger$ satisfy the RPA equations (2·14) and (2·15) of Part I, and are related to two-quasiparticle creation and annihilation operators as

$$\hat{X}_\lambda^\dagger = \sum_{\mu<\nu}\{\phi_\lambda(\mu\nu)a_\mu^\dagger a_\nu^\dagger + \varphi_\lambda(\mu\nu)a_\nu a_\mu\}\,. \tag{2·3}$$

We solve the basic equations of the SCC method by means of the (η^*, η) expansion under the boundary condition that anharmonic γ-vibrations reduce to the RPA γ-vibrations ($\hat{X}_\gamma^\dagger$ and its time-reversal partner $\hat{X}_{\tilde{\gamma}}^\dagger$) in the small amplitude limit. Then, the second-order term of the collective Hamiltonian $\mathcal{H} \equiv \langle\phi_0|e^{-i\hat{G}}\hat{H}e^{i\hat{G}}|\phi_0\rangle - \langle\phi_0|\hat{H}|\phi_0\rangle$ takes the following form:

$$\mathcal{H}^{(2)} = \alpha(\eta^*\eta + \tilde{\eta}^*\tilde{\eta}) + \beta(\eta^*\tilde{\eta}^* + \eta\tilde{\eta})\,, \tag{2·4}$$

and the lowest-order term of $i\hat{G}$ is given by

$$i\hat{G}^{(1)} = (\eta\hat{Y}_\gamma^\dagger - \eta^*\hat{Y}_\gamma) + (\tilde{\eta}\hat{Y}_{\tilde{\gamma}}^\dagger - \tilde{\eta}^*\hat{Y}_{\tilde{\gamma}})\,, \tag{2·5}$$

$$\hat{Y}_\gamma^\dagger = \sigma\hat{X}_\gamma^\dagger - \tau\hat{X}_{\tilde{\gamma}}\,, \qquad \hat{Y}_{\tilde{\gamma}}^\dagger = \sigma\hat{X}_{\tilde{\gamma}}^\dagger - \tau\hat{X}_\gamma\,. \qquad (\sigma^2 - \tau^2 = 1) \tag{2·6}$$

Here the real parameters σ and τ specify the canonical coordinate system for the collective submanifold, and can be chosen arbitrarily.

Because our original Hamiltonian conserves the K-quantum number, the third-order collective Hamiltonian $\mathcal{H}^{(3)}$ vanishes.

The fourth-order collective Hamiltonian takes the following form:

$$\begin{aligned}\mathcal{H}^{(4)} = {} & \omega_\gamma(G_\gamma^{(1)*}G_\gamma^{(3)} + G_\gamma^{(1)}G_\gamma^{(3)*} + G_{\tilde{\gamma}}^{(1)*}G_{\tilde{\gamma}}^{(3)} + G_{\tilde{\gamma}}^{(1)}G_{\tilde{\gamma}}^{(3)*}) \\ & + \sum_{\lambda;\,K=0,\pm4}\omega_\lambda G_\lambda^{(2)*}G_\lambda^{(2)} \\ & + \frac{1}{2}\langle\phi_0|[[[\hat{H}, i\hat{G}^{(1)}], i\hat{G}^{(1)}], i\hat{G}^{(2)}]|\phi_0\rangle\end{aligned}$$

$$+\frac{1}{4!}\langle\phi_0|[[[[\hat{H}, i\hat{G}^{(1)}], i\hat{G}^{(1)}], i\hat{G}^{(1)}], i\hat{G}^{(1)}]|\phi_0\rangle\,, \tag{2·7}$$

where $G_\gamma{}^{(1)}=\sigma\eta+\tau\tilde{\eta}^*$, $G_{\tilde{\gamma}}{}^{(1)}=\sigma\tilde{\eta}+\tau\eta^*$ and

$$G_\gamma{}^{(3)}=\frac{1}{2}\sum_{\lambda;K=0,\pm4}\left\{\left(\sigma\frac{\partial}{\partial\eta^*}-\tau\frac{\partial}{\partial\tilde{\eta}}\right)G_\lambda{}^{(2)}\cdot G_\lambda{}^{(2)*}-\left(\sigma\frac{\partial}{\partial\eta^*}-\tau\frac{\partial}{\partial\tilde{\eta}}\right)G_\lambda{}^{(2)*}\cdot G_\lambda{}^{(2)}\right\}$$

$$-\frac{1}{4!}\langle\phi_0|[[[\hat{X}_\gamma, i\hat{G}^{(1)}], i\hat{G}^{(1)}], i\hat{G}^{(1)}]|\phi_0\rangle\,, \tag{2·8}$$

$$G_{\tilde{\gamma}}{}^{(3)}(\eta^*, \eta, \tilde{\eta}^*, \tilde{\eta})=(G_\gamma{}^{(3)}(\tilde{\eta}, \tilde{\eta}^*, \eta, \eta^*))^*\,. \tag{2·9}$$

The functions $G_\lambda{}^{(2)}(\eta_i{}^*, \eta_i)$ appearing in the above equations are determined by the second-order part of the equation of the collective subspace, Eq. (3·15) of Part I:

$$(\omega_\lambda-\mathring{D})\,G_\lambda{}^{(2)}=B_\lambda{}^{(2)}\,, \tag{2·10}$$

$$B_\lambda{}^{(2)}=\frac{1}{2}\langle\phi_0|[[[\hat{H}, i\hat{G}^{(1)}], i\hat{G}^{(1)}], \hat{X}_\lambda]|\phi_0\rangle\,, \tag{2·11}$$

where ω_λ are the RPA frequencies and $\mathring{D}$ is a linear operator acting on polynomials of $(\eta_i{}^*, \eta_i)$, which is defined by

$$\mathring{D}=\sum_{i=1,2}\left(\frac{\partial\mathcal{H}^{(2)}}{\partial\eta_i{}^*}\frac{\partial}{\partial\eta_i}-\frac{\partial\mathcal{H}^{(2)}}{\partial\eta_i}\frac{\partial}{\partial\eta_i{}^*}\right). \tag{2·12}$$

It is convenient to formally write $G_\lambda{}^{(2)}$ as

$$G_\lambda{}^{(2)}=(\omega_\lambda-\mathring{D})^{-1}B_\lambda{}^{(2)}\,. \tag{2·13}$$

Note that $G_\lambda{}^{(2)}=0$ for the modes λ with $K=2$ and -2.

The fourth-order collective Hamiltonian $\mathcal{H}^{(4)}$ can be divided into two kinds:

$$\mathcal{H}^{(4)}=\mathcal{H}^{(4)}_{\rm tru}+\mathcal{H}^{(4)}_{\rm dyn}\,. \tag{2·14}$$

The first term $\mathcal{H}^{(4)}_{\rm tru}$ represents the anharmonicities that arise even when the TDHB state vector is truncated into the following restricted form:

$$|\phi(\eta_i{}^*, \eta_i)\rangle_{\rm tru}=\exp(G_\gamma\hat{X}_\gamma{}^\dagger+G_{\tilde{\gamma}}\hat{X}_{\tilde{\gamma}}{}^\dagger-G_\gamma{}^*\hat{X}_\gamma-G_{\tilde{\gamma}}{}^*\hat{X}_{\tilde{\gamma}})|\phi_0\rangle\,. \tag{2·15}$$

The second term $\mathcal{H}^{(4)}_{\rm dyn}$ represents the contributions from the RPA modes with $K^\pi=0^+$ and $\pm4^+$. We call them "dynamical anharmonicities".*) These effects are represented by the

*) The first term $\mathcal{H}^{(4)}_{\rm tru}$ can be further divided into two kinds: $\mathcal{H}^{(4)}_{\rm tru}=\mathcal{H}^{(4)}_{\rm kin}+\mathcal{H}^{(4)}_{\rm tru,dyn}$, where $\mathcal{H}^{(4)}_{\rm kin}$ represents the kinematical anharmonicities resulting from the Pauli principle between the quasiparticles constituting the phonons $\hat{X}_\gamma{}^\dagger$ and $\hat{X}_{\tilde{\gamma}}{}^\dagger$. On the other hand, $\mathcal{H}^{(4)}_{\rm tru,dyn}$ represents the effects due to the residual interactions which have been omitted in the RPA and can be taken into account within the truncated TDHB space defined by Eq. (2·15). Usually, the latter effects are also called "dynamical anharmonicities."[7] Thus, in order to distinguish $\mathcal{H}^{(4)}_{\rm tru,dyn}$ from $\mathcal{H}^{(4)}_{\rm dyn}$ defined by Eq. (2·16), we call the former "dynamical anharmonicity of the first kind" and the latter "the second kind". If the third-order collective Hamiltonian $\mathcal{H}^{(3)}$ exists, the first-kind dynamical anharmonicity would constitute an important part of it. For the anharmonic γ-vibrations under consideration, however, the $\mathcal{H}^{(3)}$ vanishes. Furthermore, the $\mathcal{H}^{(4)}_{\rm tru,dyn}$ plays a minor role in comparison with $\mathcal{H}^{(4)}_{\rm kin}$. Therefore, in this paper, we focus our attention on $\mathcal{H}^{(4)}_{\rm dyn}$ and simply call it dynamical anharmonicity. Also we sometimes call the effect resulting from $\mathcal{H}^{(4)}_{\rm tru}$ "kinematical anharmonicity" in quotation marks.

functions $G_\lambda^{(2)}$. Accordingly, making use of Eqs. (2·8)~(2·13), we can express $\mathcal{H}_{\rm dyn}^{(4)}$ in a compact form as

$$\mathcal{H}_{\rm dyn}^{(4)}=\sum_{\lambda\,;\,K=0,\pm4}\mathcal{H}_{{\rm dyn},\lambda}^{(4)}\,, \tag{2·16}$$

$$\begin{aligned}\mathcal{H}_{{\rm dyn},\lambda}^{(4)}&=-\frac{1}{2}(B_\lambda^{(2)*}G_\lambda^{(2)}+B_\lambda^{(2)}G_\lambda^{(2)*})\\&=-\frac{1}{2}\left(B_\lambda^{(2)*}\frac{1}{\omega_\lambda-\mathring{D}}B_\lambda^{(2)}+B_\lambda^{(2)}\frac{1}{\omega_\lambda+\mathring{D}}B_\lambda^{(2)*}\right).\end{aligned} \tag{2·17}$$

Evidently, each term $\mathcal{H}_{{\rm dyn},\lambda}^{(4)}$ represents the contribution from a particular RPA mode labelled by $\lambda\neq\gamma,\ \tilde{\gamma}$.

2.2. *Diagrammatic representation*

In this subsection, we fix the parameters in Eq. (2·6) as $\sigma=1$ and $\tau=0$. In this case, the operators $(\hat{Y}_\gamma{}^\dagger,\ \hat{Y}_\gamma,\ \hat{Y}_{\tilde{\gamma}}{}^\dagger,\ \hat{Y}_{\tilde{\gamma}})$ coincide with the RPA phonons $(\hat{X}_\gamma{}^\dagger,\ \hat{X}_\gamma,\ \hat{X}_{\tilde{\gamma}}{}^\dagger,\ \hat{X}_{\tilde{\gamma}})$, and therefore the collective variables $(\eta^*,\ \eta,\ \tilde{\eta}^*,\ \tilde{\eta})$ exactly correspond to these RPA creation and annihilation operators in the small-amplitude limit. Furthermore, the coefficients α and β of the second-order collective Hamiltonian (2·4) coincide with ω_γ and zero, respectively.

For the $K^\pi=0^+$ modes, the quantity $B_\lambda^{(2)}$ appearing in $\mathcal{H}_{{\rm dyn},\lambda}^{(4)}$ is decomposed into the following form:

$$-B_\lambda^{(2)}=V(\lambda\gamma;\,\gamma)\eta^*\eta+V(\lambda\tilde{\gamma};\,\tilde{\gamma})\tilde{\eta}^*\tilde{\eta}+V(\lambda;\,\gamma\tilde{\gamma})\eta\tilde{\eta}+V(\lambda\gamma\tilde{\gamma};)\eta^*\tilde{\eta}^*\,, \tag{2·18}$$

$$\left.\begin{aligned}&V(\lambda\gamma;\,\gamma)=\langle\phi_0|[\hat{X}_\lambda,\,[\hat{Y}_\gamma,\,[\hat{H},\,\hat{Y}_\gamma{}^\dagger]]]|\phi_0\rangle\,,\\&V(\lambda\tilde{\gamma};\,\tilde{\gamma})=\langle\phi_0|[\hat{X}_\lambda,\,[\hat{Y}_{\tilde{\gamma}},[\hat{H},Y_{\tilde{\gamma}}{}^\dagger]]]|\phi_0\rangle=V(\lambda\gamma;\,\gamma)\,,\\&V(\lambda;\,\gamma\tilde{\gamma})=\langle\phi_0|[\hat{X}_\lambda,\,[[\hat{H},\,\hat{Y}_\gamma{}^\dagger],\,\hat{Y}_{\tilde{\gamma}}{}^\dagger]]|\phi_0\rangle\,,\\&V(\lambda\gamma\tilde{\gamma};)=\langle\phi_0|[\hat{X}_\lambda,\,[\hat{Y}_\gamma,\,[\hat{Y}_{\tilde{\gamma}},\,\hat{H}]]]|\phi_0\rangle\,.\end{aligned}\right\} \tag{2·19}$$

For the $K^\pi=4^+$ modes, the $B_\lambda^{(2)}$ is decomposed as

$$-B_\lambda^{(2)}=V(\lambda\tilde{\gamma};\,\gamma)\eta\tilde{\eta}^*+V(\lambda;\,\gamma\,\gamma)\eta\eta+V(\lambda\tilde{\gamma}\tilde{\gamma};)\tilde{\eta}^*\tilde{\eta}^*\,, \tag{2·20}$$

$$\left.\begin{aligned}&V(\lambda\tilde{\gamma};\,\gamma)=\langle\phi_0|[\hat{X}_\lambda,\,[\hat{Y}_{\tilde{\gamma}},\,[\hat{H},\,\hat{Y}_\gamma{}^\dagger]]]|\phi_0\rangle\,,\\&V(\lambda;\,\gamma\gamma)=\frac{1}{2}\langle\phi_0|[\hat{X}_\lambda,\,[[\hat{H},\,\hat{Y}_\gamma{}^\dagger],\,\hat{Y}_\gamma{}^\dagger]]|\phi_0\rangle\,,\\&V(\lambda\tilde{\gamma}\tilde{\gamma};)=\frac{1}{2}\langle\phi_0|[\hat{X}_\lambda,\,[\hat{Y}_{\tilde{\gamma}},\,[\hat{Y}_{\tilde{\gamma}},\,\hat{H}]]]|\phi_0\rangle\,.\end{aligned}\right\} \tag{2·21}$$

For $K^\pi=-4^+$, similar expressions are readily obtained by taking the time-reversal of Eqs. (2·20) and (2·21). Apparently, the quantities defined above by Eqs. (2·19) and (2·21) express the mode-mode couplings between the RPA γ-vibrations and the other RPA modes $\hat{X}_\lambda{}^\dagger$ with $K^\pi=0^+$ or $\pm4^+$. These are diagrammatically represented in Fig. 1. Since the RPA modes are composed of two-quasiparticle operators, the mode-mode coupling vertices have the microscopic structure as illustrated in Fig. 2 for $V(\lambda\gamma;\,\gamma)$.

In the case under consideration, the operator $\mathring{D}$ defined by (2·12) acts on the polynomials of the collective variables as

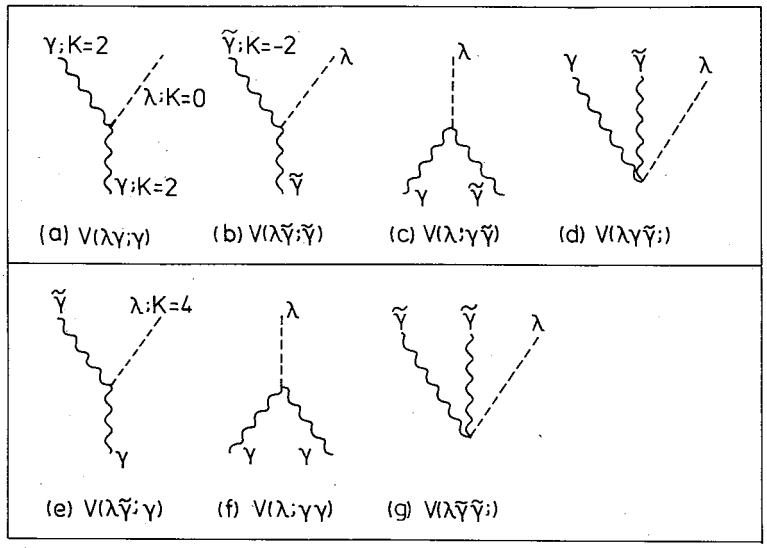

Fig. 1. Mode-mode coupling vertices between the RPA γ-vibrations (denoted by γ and $\tilde{\gamma}$) and the $K^\pi = 0^+, \pm 4^+$ modes (denoted by λ).

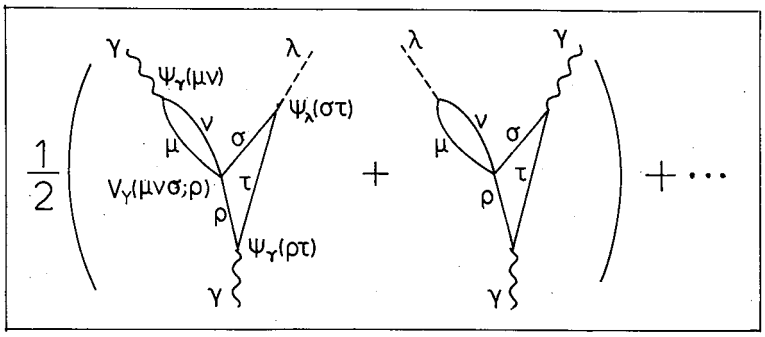

Fig. 2. Microscopic structure of the mode-mode coupling vertex $V(\lambda\gamma;\gamma)$ displayed in Fig. 1(a). The quantity $V_\gamma(\mu\nu\sigma;\rho)$ is a matrix element of the residual interaction between quasiparticles. Only the part associated with the forward-going amplitudes $\phi_\gamma(\mu\nu)$ of the RPA γ-vibration is illustrated.

$$\mathring{D}(\eta^*)^i(\eta)^j(\tilde{\eta}^*)^k(\tilde{\eta})^l=(-i+j+k-l)\omega_\gamma(\eta^*)^i(\eta)^j(\tilde{\eta}^*)^k(\tilde{\eta})^l \tag{2·22}$$

so that the quantities $G_\lambda^{(2)}$ in (2·13) are explicitly written as

$$G_\lambda^{(2)}=-\frac{V(\lambda\gamma;\gamma)}{\omega_\lambda}\eta^*\eta-\frac{V(\lambda\tilde{\gamma};\tilde{\gamma})}{\omega_\lambda}\tilde{\eta}^*\tilde{\eta}-\frac{V(\lambda;\gamma\tilde{\gamma})}{\omega_\lambda-2\omega_\gamma}\eta\tilde{\eta}-\frac{V(\lambda\gamma\tilde{\gamma};)}{\omega_\lambda+2\omega_\gamma}\eta^*\tilde{\eta}^*$$

$$\text{for}\quad K=0\,, \tag{2·23}$$

$$G_\lambda^{(2)}=-\frac{V(\lambda\tilde{\gamma};\gamma)}{\omega_\lambda}\eta\tilde{\eta}^*-\frac{V(\lambda\tilde{\gamma};\gamma)}{\omega_\lambda-2\omega_\gamma}\eta\eta+\frac{V(\lambda\tilde{\gamma}\tilde{\gamma};)}{\omega_\lambda+2\omega_\gamma}\tilde{\eta}^*\tilde{\eta}^*\qquad\text{for}\quad K=4\,. \tag{2·24}$$

Inserting the expressions (2·18), (2·20), (2·23) and (2·24) into Eq. (2·17) for $\mathcal{H}^{(4)}_{\mathrm{dyn},\lambda}$, we obtain the explicit expressions for the fourth-order dynamical anharmonicity terms, which are listed in Table I. Their physical meanings are diagrammatically illustrated in Fig. 3. A similarity between these expressions and those of the Nuclear Field Theory[8] is note-

Table I. Explicit expressions for the coefficients of different terms composing the fourth-order anharmonic Hamiltonian $\mathcal{H}^{(4)}_{\mathrm{qvn},\lambda}$ defined by Eq. (2·17). The upper part (a) represents the contributions from the couplings with the $K^\pi=0^+$ modes, while the lower part (b) those from the $K^\pi=4^+$ modes. Expressions for those terms that are readily obtained by using the hermiticity and the time-reversal invariance of the Hamiltonian are omitted in this table. Thus, for instance, the expressions for the contributions from the $K^\pi=-4^+$ modes are obtained by taking the time-reversal of the expressions listed in (b), i.e., by the replacement $\gamma\leftrightarrow\tilde{\gamma}$.

(a)

$\eta^*\eta^*\tilde{\eta}^*\tilde{\eta}^*$	$V(\lambda;\gamma\tilde{\gamma})^*V(\lambda\gamma\tilde{\gamma};)\frac{1}{2}\left(\frac{1}{2\omega_\gamma-\omega_\lambda}+\frac{1}{-2\omega_\gamma-\omega_\lambda}\right)$
$\eta^*\tilde{\eta}^*\eta^*\eta$	$V(\lambda;\gamma\tilde{\gamma})^*V(\lambda\gamma;\gamma)\frac{1}{2}\left(\frac{1}{-\omega_\lambda}+\frac{1}{2\omega_\gamma-\omega_\lambda}\right)$
	$+V(\lambda\gamma;\gamma)^*V(\lambda\gamma\tilde{\gamma};)\frac{1}{2}\left(\frac{1}{-\omega_\lambda}+\frac{1}{-2\omega_\gamma-\omega_\lambda}\right)$
$\eta^*\tilde{\eta}^*\tilde{\eta}^*\tilde{\eta}$	$V(\lambda\gamma;\gamma)^*V(\lambda\gamma;\gamma)\cdot\frac{1}{-\omega_\lambda}$
$\eta^*\tilde{\eta}^*\eta\tilde{\eta}$	$V(\lambda;\gamma\tilde{\gamma})^*V(\lambda;\gamma\tilde{\gamma})\cdot\frac{1}{2\omega_\gamma-\omega_\lambda}$
	$+V(\lambda\gamma;\gamma)^*V(\lambda\tilde{\gamma};\tilde{\gamma})\cdot\frac{1}{-\omega_\lambda}$
	$+V(\lambda\tilde{\gamma};\tilde{\gamma})^*V(\lambda\gamma;\gamma)\cdot\frac{1}{-\omega_\lambda}$
	$+V(\lambda\gamma\tilde{\gamma};)^*V(\lambda\gamma\tilde{\gamma};)\cdot\frac{1}{-2\omega_\gamma-\omega_\lambda}$

(b)

$\eta^*\eta^*\tilde{\eta}^*\tilde{\eta}^*$	$V(\lambda;\gamma\gamma)^*V(\lambda\tilde{\gamma}\tilde{\gamma};)\frac{1}{2}\left(\frac{1}{2\omega_\gamma-\omega_\lambda}+\frac{1}{-2\omega_\gamma-\omega_\lambda}\right)$
$\eta^*\eta^*\tilde{\eta}^*\eta$	$V(\lambda;\gamma\gamma)^*V(\lambda\tilde{\gamma};\gamma)\frac{1}{2}\left(\frac{1}{2\omega_\gamma-\omega_\lambda}+\frac{1}{-\omega_\lambda}\right)$
$\eta^*\tilde{\eta}^*\tilde{\eta}^*\tilde{\eta}$	$V(\lambda\tilde{\gamma};\gamma)^*V(\lambda\tilde{\gamma}\tilde{\gamma};)\frac{1}{2}\left(\frac{1}{-2\omega_\gamma-\omega_\lambda}+\frac{1}{-\omega_\lambda}\right)$
$\eta^*\eta^*\eta\eta$	$V(\lambda;\gamma\gamma)^*V(\lambda;\gamma\gamma)\cdot\frac{1}{2\omega_\gamma-\omega_\lambda}$
$\tilde{\eta}^*\tilde{\eta}^*\tilde{\eta}\tilde{\eta}$	$V(\lambda\tilde{\gamma}\tilde{\gamma};)^*V(\lambda\tilde{\gamma}\tilde{\gamma};)\cdot\frac{1}{-2\omega_\gamma-\omega_\lambda}$
$\eta^*\tilde{\eta}^*\eta\tilde{\eta}$	$V(\lambda\tilde{\gamma};\gamma)^*V(\lambda\tilde{\gamma};\gamma)\cdot\frac{1}{-\omega_\lambda}$

worthy.

2.3. (q, p) *representation*

To deal with general cases other than $\sigma=1$ and $\tau=0$, it is more convenient to adopt the representation in terms of the RPA coordinate and momentum operators $(\hat{Q}_\lambda,\ \hat{P}_\lambda,\ \hat{Q}_\lambda^\dagger,\ \hat{P}_\lambda^\dagger)$ defined by Eqs. (2·16)~(2·18) of Part I. Correspondingly, it is convenient to use the collective variables $(q,\ p,\ \tilde{q},\ \tilde{p})$ which are related to $(\eta,\ \eta^*,\ \tilde{\eta},\ \tilde{\eta}^*)$ by

$$\left.\begin{aligned} q&=\frac{1}{\sqrt{2}}(\eta^*+\tilde{\eta})\,, \qquad \tilde{q}=\frac{1}{\sqrt{2}}(\tilde{\eta}^*+\eta)=q^*\,,\\ p&=\frac{i}{\sqrt{2}}(\tilde{\eta}^*-\eta)\,, \qquad \tilde{p}=\frac{i}{\sqrt{2}}(\eta^*-\tilde{\eta})=p^*\,. \end{aligned}\right\} \tag{2·25}$$

It is easily seen that the linear canonical transformation, $\eta\to\sigma\eta+\tau\tilde{\eta}^*$ and $\tilde{\eta}^*\to\tau\eta+\sigma\tilde{\eta}^*$,

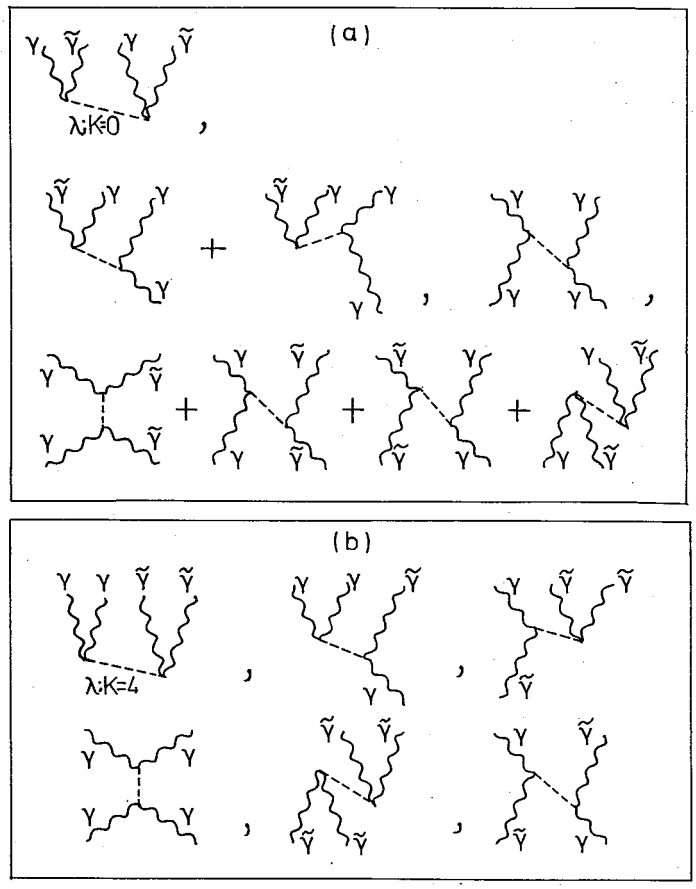

Fig. 3. Diagrammatic representation of the fourth-order dynamical anharmonicities. The terms resulting from the couplings with the $K^{\pi}=0^{+}$ modes are displayed in (a), while those associated with the $K^{\pi}=4^{+}$ modes are shown in (b). Each diagram corresponds one-to-one to each term listed in Table I.

discussed in Part I merely corresponds to the scale transformation

$$(q_i, p_i)\rightarrow(sq_i, s^{-1}p_i) \tag{2·26}$$

with $\sigma=(s+s^{-1})/2$ and $\tau=(s-s^{-1})/2$, where $(q_1, p_1)\equiv(q, p)$ and $(q_2, p_2)\equiv(\tilde{q}, \tilde{p})$. In this (q, p) representation, the operator $i\hat{G}^{(1)}$ is written as

$$i\hat{G}^{(1)}=i(p\hat{Q}_{\tau}'-q\hat{P}_{\tau}'+\tilde{p}\hat{Q}_{\tilde{\tau}}'-\tilde{q}\hat{P}_{\tilde{\tau}}'), \tag{2·27}$$

$$\left.\begin{aligned}\hat{Q}_{\tau}'&=s^{-1}\hat{Q}_{\tau}, \qquad \hat{Q}_{\tilde{\tau}}'=s^{-1}\hat{Q}_{\tilde{\tau}},\\ \hat{P}_{\tau}'&=s\hat{P}_{\tau} \quad , \qquad \hat{P}_{\tilde{\tau}}'=s\hat{P}_{\tilde{\tau}}\end{aligned}\right\} \tag{2·28}$$

with $\hat{Q}_{\tilde{\tau}}\equiv\hat{Q}_{\tau}^{\dagger}$ and $\hat{P}_{\tilde{\tau}}\equiv\hat{P}_{\tau}^{\dagger}$. We recall here that the RPA equations for $(\hat{Q}_{\tau}, \hat{P}_{\tau})$ are invariant with respect to the scale transformation (2·28). It is seen that the arbitrariness in the choice of the scale parameter s is connected with this invariance. The quantities $B_{\lambda}^{(2)}$ for the couplings with the $K^{\pi}=0^{+}$ modes are represented as

$$B_\lambda^{(2)} = -V_{q\tilde{q}}(\lambda) q\tilde{q} - V_{pq}(\lambda)(pq + \tilde{p}\tilde{q}) - V_{p\tilde{p}}(\lambda) p\tilde{p}\,, \tag{2·29}$$

where

$$\left.\begin{aligned} V_{q\tilde{q}}(\lambda) &= \langle\phi_0|[\hat{X}_\lambda, \hat{V}_{q\tilde{q}}]|\phi_0\rangle \quad \text{with} \quad \hat{V}_{q\tilde{q}} = -s^2[[\hat{H}, \hat{P}_\gamma], \hat{P}_{\tilde{\gamma}}]_A\,, \\ V_{pq}(\lambda) &= \langle\phi_0|[\hat{X}_\lambda, \hat{V}_{pq}]|\phi_0\rangle \quad \text{with} \quad \hat{V}_{pq} = [[\hat{H}, \hat{Q}_\gamma], \hat{P}_\gamma]_A\,, \\ V_{p\tilde{p}}(\lambda) &= \langle\phi_0|[\hat{X}_\lambda, \hat{V}_{p\tilde{p}}]|\phi_0\rangle \quad \text{with} \quad \hat{V}_{p\tilde{p}} = -s^{-2}[[\hat{H}, \hat{Q}_\gamma], \hat{Q}_{\tilde{\gamma}}]_A\,. \end{aligned}\right\} \tag{2·30}$$

Here the subscript A denotes a part of the double commutator that creates or annihilates two quasiparticles; thus, for instance, $\hat{V}_{q\tilde{q}}$ may be written as

$$\hat{V}_{q\tilde{q}} = \sum_{\mu<\nu}\left(V_{q\tilde{q}}(\mu\nu)\, a_\mu^\dagger a_\nu^\dagger + V_{q\tilde{q}}^*(\mu\nu)\, a_{\bar{\nu}} a_{\bar{\mu}}\right). \tag{2·31}$$

In a similar way, for the couplings with the $K^\pi = 4^+$ modes, the quantities $B_\lambda^{(2)}$ are written as

$$B_\lambda^{(2)} = -V_{\tilde{q}\tilde{q}}(\lambda)\,\tilde{q}\tilde{q} - V_{p\tilde{q}}(\lambda)\, p\tilde{q} - V_{pp}(\lambda)\, pp\,, \tag{2·32}$$

where

$$\left.\begin{aligned} V_{\tilde{q}\tilde{q}}(\lambda) &= \langle\phi_0|[\hat{X}_\lambda, \hat{V}_{\tilde{q}\tilde{q}}]|\phi_0\rangle \quad \text{with} \quad \hat{V}_{\tilde{q}\tilde{q}} = -\frac{1}{2}s^2[[\hat{H}, \hat{P}_{\tilde{\gamma}}], \hat{P}_{\tilde{\gamma}}]_A\,, \\ V_{p\tilde{q}}(\lambda) &= \langle\phi_0|[\hat{X}_\lambda, \hat{V}_{p\tilde{q}}]|\phi_0\rangle \quad \text{with} \quad \hat{V}_{p\tilde{q}} = [[\hat{H}, \hat{Q}_\gamma], \hat{P}_{\tilde{\gamma}}]_A\,, \\ V_{pp}(\lambda) &= \langle\phi_0|[\hat{X}_\lambda, \hat{V}_{pp}]|\phi_0\rangle \quad \text{with} \quad \hat{V}_{pp} = -\frac{1}{2}s^{-2}[[\hat{H}, \hat{Q}_\gamma], \hat{Q}_\gamma]_A\,. \end{aligned}\right\} \tag{2·33}$$

The expressions for $K^\pi = -4^+$ are readily obtained by taking the time-reversal of the above equations. Since the operators $\hat{V}_{q\tilde{q}}$, $\hat{V}_{pq}$, $\cdots$ etc. defined above produce the mode-mode couplings neglected in the RPA, we call them "coupling-source operators". It should be noted that the above equations, Eqs. (2·27) ~ (2·33), are valid even when the RPA frequency ω_γ for the γ-vibrations become zero or imaginary. This is an important merit of the (q, p) representation in comparison with Eqs. (2·18)~(2·21) discussed in § 2.2.

§ 3. Isotope dependence of dynamical anharmonicity effects

3.1. *Procedure of calculation*

Procedure of numerical calculation is the same as in Part I, except that we now take into account the dynamical anharmonicities resulting from $\mathcal{H}_{\rm dyn}^{(4)}$ (which were completely neglected in Part I). We start with the Nilsson-plus-BCS single-particle Hamiltonian and consider the quasiparticle interactions composed of the residual pairing and the doubly-stretched quadrupole-quadrupole (Q″Q″) forces. The Nilsson space is truncated to three major shells for both protons and neutrons. The parameter s which fixes the canonical coordinate system for describing the collective submanifold is determined also in the same way as in Part I, i.e., the optimized RPA boundary condition is used. Among the mode-mode couplings with $K^\pi = 0^+$, we neglect contributions from the pairing rotations.

To treat such Nambu-Goldstone modes with zero energy, we need to explicitly introduce the collective variables that correspond to them. Since these contributions do not appear essential to our present purpose, we postpone this task to a forthcoming paper (Part III).

It is expected that characteristics of the dynamical anharmonicities significantly depend on the subshell structure near the Fermi surface. Thus, we consider it indispensable to investigate isotope dependence of them. Numerical calculations are therefore done for a region of Er isotopes from $N=92$ to $N=102$, which is wider than the region $N=96\sim100$ exhibiting a strong collectivity for γ-vibrational modes, so that we can trace out how the properties of the mode-mode couplings change as the collectivity of the γ-vibrations decreases. To get a qualitative understanding of the dynamical anharmonicity effects, we present in §§ 3 and 4 the results of calculation with use of the Q″Q″ force-strength $\varkappa$ that makes the RPA γ-vibration frequency ω_γ zero. This choice of $\varkappa$ is convenient to study the isotope dependence of anharmonicities by suppressing that of the RPA frequency itself. Their adopted values are listed, together with other parameters of calculation, in Table II. Then, we shall present in § 5 the theoretical spectra for the double γ-vibrational states obtained by the use of $\varkappa$ values that reproduce the empirical excitation energies of the single γ-vibrational states.

3.2. *Isotope dependence of anharmonicity effects*

The fourth-order collective Hamiltonian takes the following form:

$$\begin{aligned}\mathcal{H}=&\alpha(\eta^*\eta+\tilde{\eta}^*\tilde{\eta})+\beta(\eta^*\tilde{\eta}^*+\eta\tilde{\eta})\\&+b_1(\eta^*\eta^*\tilde{\eta}^*\tilde{\eta}^*+\text{c.c.})+b_2(\eta^*\tilde{\eta}^*\eta^*\eta+\eta^*\tilde{\eta}^*\tilde{\eta}^*\tilde{\eta}+\text{c.c.})\\&+b_3(\eta^*\eta^*\eta\eta+\tilde{\eta}^*\tilde{\eta}^*\tilde{\eta}\tilde{\eta})+b_4\eta^*\eta\tilde{\eta}^*\tilde{\eta}\ .\end{aligned}\tag{3·1}$$

The values for the coefficients α, β and b_i evaluated for Er isotopes are presented in Fig. 4, where contributions to b_i from the "kinematical anharmonicities", the dynamical anharmonicities associated with the $K^\pi=0^+$ modes, and those associated with the $K^\pi=\pm4^+$ modes are separately displayed. It is seen that the dynamical anharmonicity effects strongly depend on the neutron number N whereas the "kinematical anharmonicity" effects depend on N rather weakly. In particular, we notice a strong variation of the contributions from the $K^\pi=0^+$ modes; they become extremely strong in ^{160}Er($N=92$) and ^{170}Er($N=102$), while they are relatively small in the nucleus ^{166}Er($N=98$) situated between them. Similar trend is seen also for the contributions from the $K^\pi=\pm4^+$ modes but in a smaller scale. It should be noted that the contributions to b_i from the dynamical anharmonicity effects are always comparable to (in magnitude) or larger than those from

Table II. Parameters used in the calculation of Figs. 4~8 and Table III.

	^{160}Er	^{162}Er	^{164}Er	^{166}Er	^{168}Er	^{170}Er
δ_{osc}	0.245	0.258	0.269	0.272	0.271	0.268
G_{0n}[MeV]	0.1239	0.1201	0.1203	0.1193	0.1122	0.1084
G_{0p}[MeV]	0.1669	0.1601	0.1563	0.1508	0.1480	0.1459
$\varkappa\times10^{-3}$ [MeVfm^4]	1.314	1.294	1.255	1.222	1.223	1.264

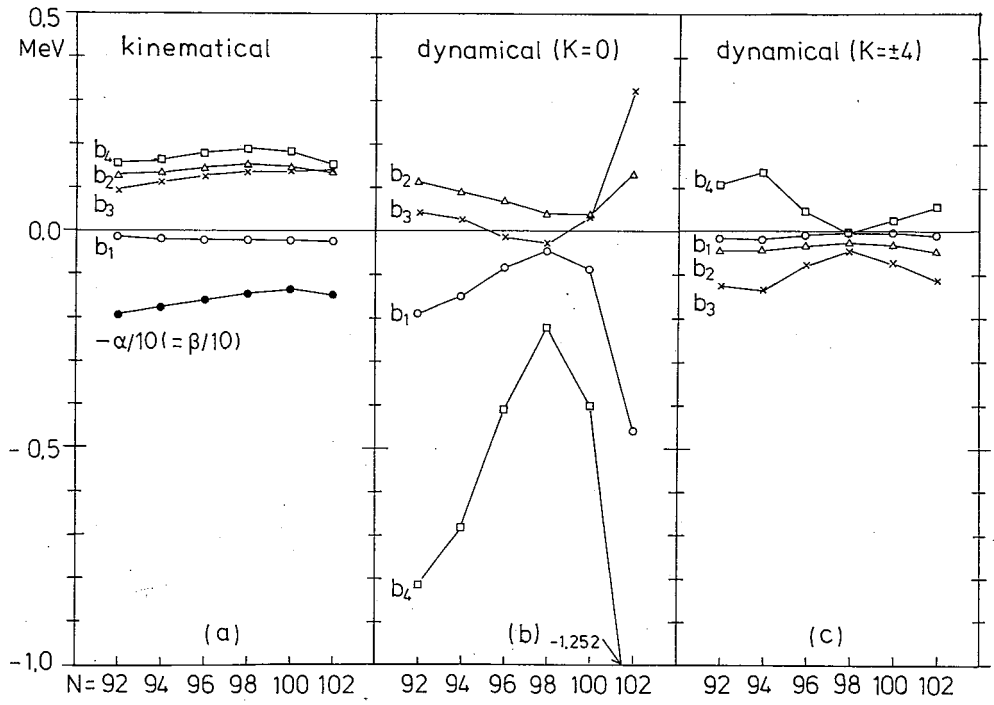

Fig. 4. The calculated coefficients b_i of the anharmonic Hamiltonian for Er isotopes are shown as functions of neutron number N. (a) The contributions from the "kinematical anharmonicities". (b) The contributions from the dynamical anharmonicities associated with the $K^\pi=0^+$ modes. (c) Those associated with the $K^\pi=\pm 4^+$ modes.

the "kinematical anharmonicity" effects.

In order to understand the origin of this strong isotope dependence, let us explicitly see the contributions to the anharmonicity coefficients b_i from individual RPA modes. Figure 5(a) displays the contributions to b_4 from the $K^\pi=0^+$ modes. In ^{160}Er, which lies near the transitional region between spherical and deformed shapes, we have both the low-lying β-vibration and the neutron pairing vibration. The two collective modes, together with several non-collective modes lying below 4 MeV, are the main contributors to b_4 in this nucleus. As the neutron number N approaches 98, the collectivity of the β-vibration diminishes and the contributions from the pairing vibrations are also reduced. With further increasing N, the neutron pairing vibration begins to play a predominant role and finally gives an extremely strong effect on b_4 in ^{170}Er. On the other hand, as for the anharmonicities associated with the $K^\pi=\pm 4^+$ modes, we see from Fig. 5(b) that the neutron two-quasiparticle mode $[521, 3/2]\otimes[523, 5/2]$ always gives the major contribution. Similarly to the case of the $K^\pi=0^+$ modes, the effect also becomes minimum at ^{166}Er.

Similar analysis can be made also for the coefficients b_i other than b_4 [see Ref. 9) for a more detailed report of our investigation].

3.3. *Accumulated effects from a large number of non-collective modes*

In the above subsection, we only discussed the RPA modes that give the major contributions to b_i. Although individual contributions from other RPA modes are small, it is possible that these small contributions accumulate to produce a non-negligible effect,

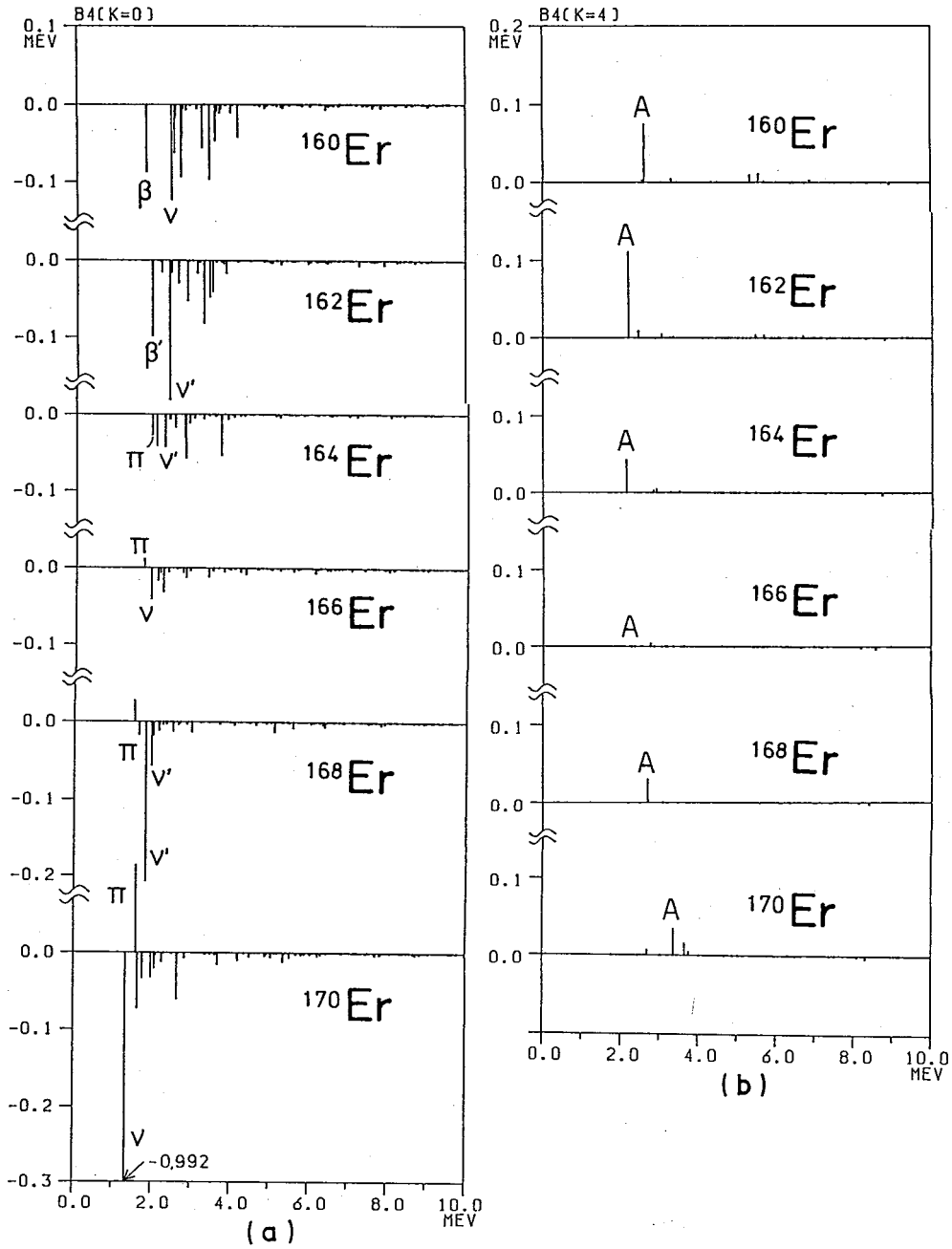

Fig. 5. Contributions from individual RPA modes λ to the anharmonicity coefficient b_4. The left-hand side represents the contributions from the $K^\pi=0^+$ modes, while the right-hand side those from the $K^\pi=\pm 4^+$ modes. From the upper part to the lower part are shown the calculated results for ^{160,162,164,166,168,170}Er. In each figure, the ordinate represents the values of $b_{4,\lambda}$ and the abscissa the excitation energies $\hbar\omega_\lambda$ of the RPA modes. The notation $\nu(\pi)$ represents the neutron (proton) pairing-vibrational mode, while $\nu'(\pi')$ denotes the noncollective mode with weak neutron (proton) pairing-vibrational character. The notation β is used for the β-vibrational mode, while A denotes a neutron two-quasiparticle mode composed of $[521, 3/2]\otimes[523, 5/2]$.

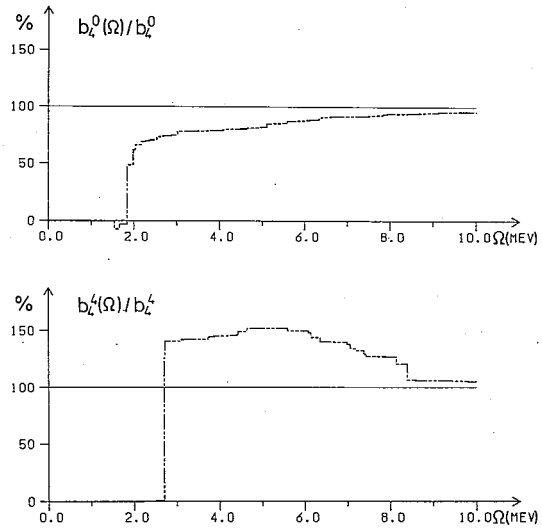

Fig. 6. Convergence of the calculated values of b_4 for ^{168}Er. The upper part shows the contributions from the couplings with the $K^\pi=0^+$ modes, while the lower part those from the $K^\pi=\pm 4^+$ modes. The values $b_4{}^K(\Omega)$ evaluated with the cutoff energy Ω approach the final values $b_4{}^K$ as Ω increases.

because the number of these modes is large (several hundreds in the case of the 3-major-shell calculation). To answer this question, we examined the convergence with respect to the upper cutoff Ω for the excitation energies of the RPA modes that are taken into account in the calculation of b_i. The result for b_4 is shown in Fig. 6. This result demonstrates that the accumulated effect is indeed very important, i.e., it is necessary to sum up these small contributions up to a sufficiently high excitation energy. This figure indicates that the value of b_4 saturates at the cutoff energy of about 10 MeV (it is desirable, however, to extend the Nilsson space used in the calculation, for a more detailed examination of the convergence property).

The values for b_i shown in Fig. 4 are, of course, those which take into account all the contributions discussed above.

§ 4. Microscopic structure of the mode-mode couplings

To get deeper understanding of the reason for the strong isotope dependence of the dynamical anharmonicity effects obtained in § 3, we investigate in this section microscopic structures of the mode-mode coupling vertices paying special attention to their relations with subshell structure near the Fermi surface.

4.1. *Explicit expressions for the coupling vertices*

For the Hamiltonian under consideration (see Eq. (2·6) of Part I), the coefficients of the coupling-source operators defined by Eqs. (2·30) and (2·33) are explicitly calculated as follows: For the coupling-source operators with $K^\pi=0^+$,

$$V_{q\tilde{q}}(\mu\nu)=-2\chi t_Q\{\sum_\sigma \mathcal{Y}_2(\mu\sigma)\eta(\mu\sigma)p_\tau(\tilde{\sigma}\tilde{\mu})-(\mu\leftrightarrow\nu)\}$$
$$-\chi^C\mathcal{V}_1\mathcal{Y}_0(\mu\tilde{\nu})\xi(\mu\nu)-\frac{1}{2}G_0\mathcal{W}_1\delta_{\mu\tilde{\nu}}\eta(\mu\nu)\,, \tag{4·1}$$

$$V_{pq}(\mu\nu)=-i\chi t_Q\{\sum_\sigma \mathcal{Y}_2(\mu\sigma)\eta(\mu\sigma)q_\tau(\tilde{\sigma}\tilde{\mu})-(\mu\leftrightarrow\nu)\}\,, \tag{4·2}$$

$$V_{p\tilde{p}}(\mu\nu)=-\chi^C\mathcal{V}_2\mathcal{Y}_0(\mu\tilde{\nu})\xi(\mu\nu)-\frac{1}{2}G_0\mathcal{W}_2\delta_{\mu\tilde{\nu}}\eta(\mu\nu)\,. \tag{4·3}$$

For the coupling-source operators with $K^\pi=4^+$,

$$V_{\tilde{q}\tilde{q}}(\mu\nu)=-\chi t_Q\{\sum_\sigma \mathcal{Y}_2(\mu\sigma)\eta(\mu\sigma)p_\tau(\sigma\nu)-(\mu\leftrightarrow\nu)\}\,, \tag{4·4}$$

$$V_{p\tilde{q}}(\mu\nu)=-i\chi t_Q\{\sum_\sigma \mathcal{Y}_2(\mu\sigma)\eta(\mu\sigma)q_\tau(\sigma\nu)-(\mu\leftrightarrow\nu)\}\,, \tag{4·5}$$

and $V_{pp}(\mu\nu)=0$. Here

$$t_Q=-i\langle\phi_0|[\tilde{Q}''_{22},\ \hat{P}_\gamma]|\phi_0\rangle=2\sum_{\mu<\nu}\mathcal{Q}_2(\mu\nu)\xi(\mu\nu)p_\gamma(\mu\tilde{\nu})\ , \tag{4·6}$$

$$\begin{pmatrix}\mathcal{V}_1\\ \mathcal{V}_2\end{pmatrix}=\langle\phi_0|[[\tilde{Q}''_{20},\begin{pmatrix}\hat{P}_\gamma\\ \hat{Q}_\gamma\end{pmatrix}],\begin{pmatrix}\hat{P}_{\tilde{\gamma}}\\ \hat{Q}_{\tilde{\gamma}}\end{pmatrix}]|\phi_0\rangle=-\sum_{\mu\nu\sigma}\mathcal{Q}_0(\mu\nu)\eta(\mu\nu)\begin{pmatrix}p_\gamma(\mu\sigma)p_\gamma(\nu\sigma)\\ q_\gamma(\mu\sigma)q_\gamma(\nu\sigma)\end{pmatrix}, \tag{4·7}$$

$$\begin{pmatrix}\mathcal{W}_1\\ \mathcal{W}_2\end{pmatrix}=\langle\phi_0|[[\tilde{P}^{(+)}_{00},\begin{pmatrix}\hat{P}_\gamma\\ \hat{Q}_\gamma\end{pmatrix}],\begin{pmatrix}\hat{P}_{\tilde{\gamma}}\\ \hat{Q}_{\tilde{\gamma}}\end{pmatrix}]|\phi_0\rangle=2\sum_{\mu\sigma}\xi(\mu\mu)\begin{pmatrix}p_\gamma(\mu\sigma)^2\\ q_\gamma(\mu\sigma)^2\end{pmatrix}, \tag{4·8}$$

where the pairing operator $\tilde{P}^{(+)}_{00}$ and the doubly-stretched quadrupole operators $\tilde{Q}''_{2K}$ are given as

$$\tilde{P}^{(+)\dagger}_{00}=\sum_{\mu>0}\eta(\mu\mu)(a_\mu{}^\dagger a_{\tilde{\mu}}{}^\dagger+a_{\tilde{\mu}}a_\mu)-\sum_\mu\xi(\mu\mu)a_\mu{}^\dagger a_\mu\ , \tag{4·9}$$

$$\tilde{Q}''_{2K}=-\sum_{\mu<\nu}\mathcal{Q}_K(\mu\tilde{\nu})\xi(\mu\nu)(a_\mu{}^\dagger a_\nu{}^\dagger+a_{\tilde{\nu}}a_{\tilde{\mu}})+\sum_{\mu\nu}\mathcal{Q}_K(\mu\nu)\eta(\mu\nu)a_\mu{}^\dagger a_\nu \tag{4·10}$$

with

$$\xi(\mu\nu)=u_\mu v_\nu+v_\mu u_\nu\ ,\qquad \eta(\mu\nu)=u_\mu u_\nu-v_\mu v_\nu\ , \tag{4·11}$$

$$\mathcal{Q}_K(\mu\nu)=\langle\mu|(r^2Y_{2K})''|\nu\rangle\ . \tag{4·12}$$

The explicit expressions for the coefficients $p_\gamma(\mu\nu)$ and $q_\gamma(\mu\nu)$ of the RPA coordinate and momentum operators $(\hat{Q}_\gamma,\ \hat{P}_\gamma,\ \hat{Q}_{\tilde{\gamma}},\ \hat{P}_{\tilde{\gamma}})$ are

$$p_\gamma(\mu\nu)=-\varkappa t_Q\frac{E_{\mu\nu}}{E^2_{\mu\nu}-\omega_\gamma{}^2}\mathcal{Q}_2(\mu\tilde{\nu})\xi(\mu\nu)\ , \tag{4·13}$$

$$q_\gamma(\mu\nu)=-\varkappa t_Q\frac{B_\gamma{}^{-1}}{E^2_{\mu\nu}-\omega_\gamma{}^2}\mathcal{Q}_2(\mu\tilde{\nu})\xi(\mu\nu) \tag{4·14}$$

with $E_{\mu\nu}=E_\mu+E_\nu$ (where E_μ is a quasiparticle energy). From Eqs. (4·1)~(4·5), we see that, for the $K^\pi=0^+$ couplings, the $K=2$ component of the Q″Q″ force contributes to the coupling-source operators $\hat{V}_{q\tilde{q}}$ and $\hat{V}_{pq}$, while the pairing force as well as the $K=0$ component of the Q″Q″ force to $\hat{V}_{q\tilde{q}}$ and $\hat{V}_{p\tilde{p}}$. As for the $K^\pi=4^+$ couplings, we see that only the $K=2$ component of the Q″Q″ force contributes to $\hat{V}_{q\tilde{q}}$ and $\hat{V}_{p\tilde{q}}$, and that $\hat{V}_{pp}$ vanishes.

The mode-mode coupling vertices are determined by the inner products between the RPA modes with $K^\pi=0^+,\ \pm4^+$ and the coupling-source operators $\hat{V}_{q\tilde{q}},\ \hat{V}_{pq},\ \cdots$, etc. For instance, $V_{q\tilde{q}}(\lambda)$ is given as

$$\begin{aligned}V_{q\tilde{q}}(\lambda)&=\langle\phi_0|[\hat{X}_\lambda,\ \hat{V}_{q\tilde{q}}]|\phi_0\rangle\\ &=\sum_{\mu<\nu}(V_{q\tilde{q}}(\mu\nu)\psi_\lambda(\mu\nu)-V^*_{q\tilde{q}}(\mu\nu)\varphi_\lambda(\mu\nu))\ .\end{aligned} \tag{4·15}$$

The above expression indicates that the properties of the mode-mode coupling vertices $V_{q\tilde{q}}(\lambda)$ are essentially dependent on the relationships between the matrix elements $V_{q\tilde{q}}(\mu\nu)$ and the RPA-phonon amplitudes $\psi_\lambda(\mu\nu)$ and $\varphi_\lambda(\mu\nu)$.

4.2. *Couplings with the $K^\pi=0^+$ modes*

Subshell structure effects on the coupling-source operators

As is easily confirmed, the major amplitudes of the RPA phonon operators with $K^\pi=0^+$ are diagonal with respect to the quasiparticle indices μ and ν, i.e., they are of the form $\psi_\lambda(\mu\tilde{\mu})$. Accordingly, for instance, for the coupling vertices $V_{q\bar{q}}(\lambda)$, only the diagonal elements $V_{q\bar{q}}(\mu\tilde{\mu})$ are important. Let us investigate in detail the contributions from the $K=2$ component of the Q″Q″ force to $V_{q\bar{q}}(\mu\tilde{\mu})$:

$$V_{q\bar{q}}^{Q_2}(\mu\tilde{\mu})=4\varkappa t_Q\sum_\sigma {}^{Q}\mathcal{Y}_2(\mu\sigma)\eta(\mu\sigma)p_\gamma(\tilde{\sigma}\mu)$$

$$=-4\varkappa^2 t_Q{}^2\sum_\sigma\frac{E_{\sigma\mu}|{}^{Q}\mathcal{Y}_2(\mu\sigma)|^2}{E_{\sigma\mu}^2-\omega_\gamma{}^2}\xi(\mu\sigma)\eta(\mu\sigma)\,. \tag{4·16}$$

As is well known, the single-particle matrix elements ${}^{Q}\mathcal{Y}_2(\mu\sigma)$ are large for such orbit pairs $(\mu\sigma)$ that differ by $\Delta n_3=0$ and $\Delta\Lambda=2$ with respect to the asymptotic quantum numbers $[N_{\rm osc}n_3\Lambda\Omega]$ of the Nilsson orbits. These groups of orbits form a subshell characterized by the same values of $(N_{\rm osc}, n_3)$. We also know that the pairing factor $\eta(\mu\sigma)=u_\mu u_\sigma-v_\mu v_\sigma$ involved in (4·16) strongly depends on the position of the Fermi surface relative to the orbit pair $(\mu\sigma)$. Now, let us consider the case illustrated in Fig. 7(a), where the chemical potential $\lambda_{\rm F}$ is situated midway between the orbits μ and σ which have a large value of ${}^{Q}\mathcal{Y}_2(\mu\sigma)$. In this case $\eta(\mu\sigma)\approx 0$, so that the contribution from the pair $(\mu\sigma)$ is diminished. On the other hand, in the situation illustrated in Fig. 7(b) where the $\lambda_{\rm F}$ is located just above (or below) such an orbit pair $(\mu\sigma)$, the factor $\eta(\mu\sigma)$ is rather large. Furthermore, we often have a few orbits σ which are connected to the orbit μ by large values of ${}^{Q}\mathcal{Y}_2(\mu\sigma)$. In this case, owing to the subshell structure, these orbits contribute additively resulting in a large value of $V_{q\bar{q}}^{Q_2}(\mu\tilde{\mu})$.

Figure 8 displays the numerical examples of $V_{q\bar{q}}(\mu\tilde{\mu})$ for Er isotopes. In $^{160}{\rm Er}_{92}$, the chemical potential for neutrons $\lambda_{\rm F}$ is located between the two subshells $(N_{\rm osc}=4, n_3=0)$ and $(N_{\rm osc}=5, n_3=2)$. This situation corresponds to the case illustrated in Fig. 7(b). As is expected, the values of $V_{q\bar{q}}^{Q_2}(\mu\tilde{\mu})$ for the orbits $\mu=[400, 1/2]$, $[402, 3/2]$ and $[521, 1/2]$ are particularly large in this nucleus. As the neutron number increases, the $\lambda_{\rm F}$ enters into the subshell $(N_{\rm osc}=5, n_3=2)$ so that the situation illustrated in Fig. 7(a) occurs in $^{166}{\rm Er}_{98}$. We see indeed that the value for $\mu=[521, 1/2]$ is diminished. With further increasing numbers of neutrons, the $\lambda_{\rm F}$ goes to the position intermediate between the subshells $(N_{\rm osc}=5, n_3=2)$ and $(N_{\rm osc}=5, n_3=1)$, again realizing the situation of Fig. 7(b). Accordingly, the values for the orbits belonging to these subshells become large (in magnitude) in $^{170}{\rm Er}_{102}$. As for the sign of $V_{q\bar{q}}^{Q_2}(\mu\tilde{\mu})$, we see that they are negative (positive) for the orbits μ lying above (below) the chemical potential $\lambda_{\rm F}$. This property is easily understood from the sign of the pairing factor $\eta(\mu\sigma)$ involved in Eq. (4·16).

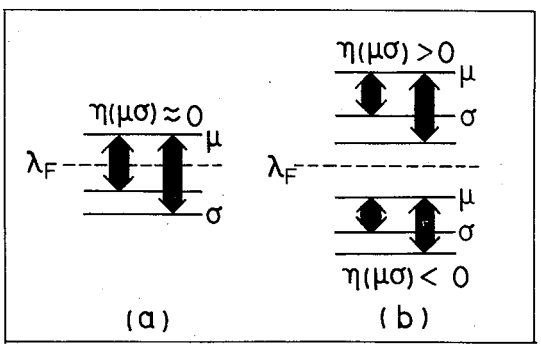

Fig. 7. (a) The case when the chemical potential $\lambda_{\rm F}$ lies in the middle of the subshell. (b) The case when the $\lambda_{\rm F}$ lies between the two groups of subshell.

In Er isotopes, the proton subshell $(N_{\rm osc}=4, n_3=1)$ is partially occupied.

This situation corresponds to Fig. 7(a) so that the values of $V_{q\tilde{q}}^{QJ^2}(\mu\tilde{\mu})$ for proton orbits are small.

Couplings with individual modes

Although the properties of $V_{q\tilde{q}}(\mu\tilde{\mu})$ represented in Fig. 8 are already suggestive to the strong isotope dependence of the coupling vertices $V_{q\tilde{q}}(\lambda)$, we need to investigate the properties of the RPA phonon amplitudes $\psi_\lambda(\mu\tilde{\mu})$ and $\varphi_\lambda(\mu\tilde{\mu})$ as well, in order to understand, for instance, the difference between ^{160}Er and ^{170}Er in the microscopic origins of the anharmonicity coefficient b_4 (shown in Fig. 5).

Let us first consider the couplings with the neutron pairing vibrational modes. As is well known, their amplitudes $\psi_\delta(\mu\tilde{\mu})$*) are proportional to $\eta(\mu\mu)/(E_{\mu\mu}-\omega_\delta)$. As seen in the numerical example for ^{170}Er listed in Table III, therefore, their signs are almost always the same with those of $V_{q\tilde{q}}(\mu\tilde{\mu})$. As a consequence of the phase coherence between the two quantities, the mode-mode coupling vertex $V_{q\tilde{q}}(\delta)$ for the neutron pairing vibration can become very large in ^{170}Er. We note that this mechanism is essentially the same as that of generating the anomalous 0^+ excited states in Ge and Se isotopes.[10] In contrast to ^{170}Er, the subshell structure near the chemical potential in $^{160}Er_{92}$ has a character that makes the above-mentioned mechanism ineffective. In this nucleus, there appear near the Fermi surface several orbits that belong neither to the subshell ($N_{\rm osc}=4$, $n_3=0$) nor to ($N_{\rm osc}=5$, $n_3=2$); for example, [642, 5/2], [651, 3/2] and [505, 11/2]. Consequently, the amplitudes $\psi_{\nu,\delta}(\mu\tilde{\mu})$ of the neutron pairing-vibration are large for these orbits. On the other hand, the matrix elements $V_{q\tilde{q}}(\mu\tilde{\mu})$ are large for the orbits like [400, 1/2], [402, 3/2] and [521, 1/2] belonging to the subshells. Thus, as is evident from Table III, coherence

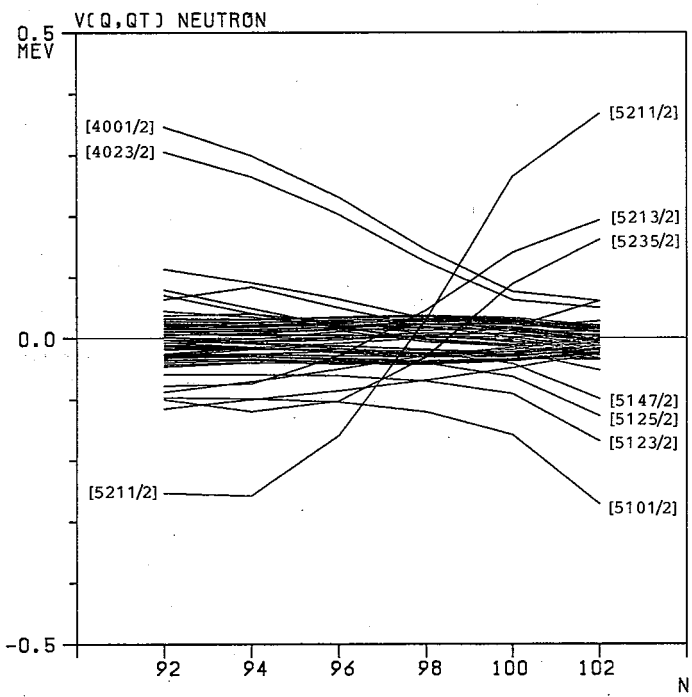

Fig. 8. Values of the matrix elements $V_{q\tilde{q}}(\mu\tilde{\mu})$ for neutron orbits μ. Numerical examples for Er isotopes with $N=92\sim102$.

*) We denote the pairing vibration by "δ" meaning that it is a fluctuation mode of the pairing gap Δ.

between $\phi_{\nu,\delta}(\mu\bar{\mu})$ and $V_{q\bar{q}}(\mu\bar{\mu})$ is not strong in ^{160}Er.

Next, let us consider the couplings with the β-vibrations. The condition for the appearance of the collective β-vibration is known to be the occurrence of near-lying single-particle orbits with different quadrupole moments.[5] This condition is well fulfilled in ^{160}Er and ^{162}Er. The orbits which have large values of the RPA amplitude $\phi_\beta(\mu\bar{\mu})$ are [660, 1/2], [651, 3/2] and [505, 11/2] for neutrons in ^{160,162}Er. Thus, coherence between $\phi_\beta(\mu\bar{\mu})$ and $V_{q\bar{q}}(\mu\bar{\mu})$ is also weak in these nuclei (see Table III).

When the overlaps between the collective $K^\pi=0^+$ modes and the coupling-source operator $\hat{V}_{q\bar{q}}$ are small in spite of the existence of orbits having large values of $V_{q\bar{q}}(\mu\bar{\mu})$, as we have seen above for ^{160,162}Er, the couplings to the non-collective $K^\pi=0^+$ modes associated with such orbits (with large value of $V_{q\bar{q}}(\mu\bar{\mu})$) tend to become important. In general, there exist several such non-collective modes. Thus, the coupling strengths $V_{q\bar{q}}(\lambda)$ distribute over many $K^\pi=0^+$ modes including both collective and non-collective ones, rather than concentrating on a particular collective mode. This is the main reason for the difference between ^{160,162}Er and ^{170}Er in the microscopic origin of the anharmonicity coefficient b_4 displayed in Fig. 5.

Summary of this subsection

Similar analyses can be made for the other coupling vertices $V_{pq}(\lambda)$ and $V_{p\bar{p}}(\lambda)$.[9] We can also make similar analysis for the contributions of the pairing force and the $K=0$ component of the Q″Q″ force to these vertices.*) These investigations indicate that the $K=\pm2$ components of the Q″Q″ force play the major role in the $K^\pi=0^+$ couplings, and lead us to the following conclusions:

Table III. Matrix elements $V_{q\bar{q}}(\mu\bar{\mu})$ for the coupling-source operator, the forward-going amplitudes $\phi_\beta(\mu\bar{\mu})$ of the RPA β-vibration, and $\phi_{\nu,\delta}(\mu\bar{\mu})$ for the neutron pairing vibration. Only the neutron components are listed.

^{160}Er				^{170}Er		
μ	$V_{q\bar{q}}(\mu\bar{\mu})$[MeV]	$\phi_\beta(\mu\bar{\mu})$	$\phi_{\nu,\delta}(\mu\bar{\mu})$	μ	$V_{q\bar{q}}(\mu\bar{\mu})$[MeV]	$\phi_{\nu,\delta}(\mu\bar{\mu})$
[402, 5/2]	.114	−.052	−.040	[521, 3/2]	.194	.084
[404, 7/2]	.045	−.061	−.045	[523, 5/2]	.162	.113
[400, 1/2]	.347	−.227	−.134	[521, 1/2]	.368	.591
[402, 3/2]	.305	−.255	−.149			
				[512, 5/2]	−.127	−.600
[521, 3/2]	−.078	−.188	.488	[514, 7/2]	−.098	−.249
[523, 5/2]	−.100	−.173	.211	[510, 1/2]	−.271	−.044
[521, 1/2]	−.253	−.055	.071	[512, 3/2]	−.168	−.042
[660, 1/2]	.064	.288	−.179	[642, 5/2]	−.004	.098
[651, 3/2]	.017	.409	−.480	[633, 7/2]	−.035	.353
[642, 5/2]	−.025	.133	.392	[624, 9/2]	−.012	.190
[633, 7/2]	.028	−.062	.086			
				[505, 11/2]	−.025	.040
[505, 11/2]	−.114	−.485	−.251	[651, 1/2]	.021	−.026
[532, 3/2]	.070	.035	−.146			
[530, 1/2]	.080	.034	−.115			

*) We plan to perform a more detailed investigation concerning the dependence of the mode-mode couplings on the residual interactions used in the calculation.

(a) When the Fermi surface is located inside a subshell having large values of $\mathcal{Y}_2(\mu\sigma)$ (see Fig. 7(a)), the couplings with the $K^\pi=0^+$ modes are relatively weak. (b) When the Fermi surface is situated just above (and/or below) the subshell (see Fig. 7(b)), the couplings can become strong. This situation may be further classified into two cases: (b1) When the orbits belonging to the subshell are the dominant ones above (below) the Fermi surface, the coupling with the pairing-vibrational mode is strong. (b2) When there exist many other orbits (near the Fermi surface) in addition to those belonging to the subshell, the mode-mode coupling strengths tend to be distributed over many $K^\pi=0^+$ modes.

4.3. *Couplings with the $K^\pi=4^+$ modes*

From the expressions of $V_{\tilde{q}\tilde{q}}(\mu\nu)$ and $V_{p\tilde{q}}(\mu\nu)$ in Eqs. (4·4) and (4·5) for the $K^\pi=4^+$ couplings, we can easily confirm that these matrix elements become large only for the orbit pairs $(\mu\tilde{\nu})$ with $\Delta n_3=0$ and $\Delta\Lambda=4$. The orbit pairs $(\mu\nu)$ satisfying this condition are, e.g., ([400, 1/2], [404, 7/2]), ([402, 3/2], [402, 5/2]), ([521, 1/2], [523, 5/2]), ([521, 1/2], [523, 7/2]), ([512, 5/2], [512, 3/2]), ([514, 9/2], [510, 1/2]), ([505, 11/2], [501, 3/2]) for neutrons and ([413, 7/2], [411, 1/2]) for protons. Since we are not taking into account the residual hexadecapole interactions and thus the RPA $K^\pi=4^+$ modes are non-collective, the mode-mode coupling vertices $V_{\tilde{q}\tilde{q}}(\lambda)$ and $V_{p\tilde{q}}(\lambda)$ are entirely determined by the matrix elements $V_{\tilde{q}\tilde{q}}(\mu\nu)$ and $V_{p\tilde{q}}(\mu\nu)$.

We can easily see from Eqs. (4·4) and (4·5) that these coupling matrix elements are diminished when the pairing factors $\eta(\mu\sigma)$ and $\eta(\sigma\nu)$ become small. In fact, these values for the neutron orbit pair $(\mu\nu)=([521, 3/2], [523, 5/2])$ become small at ^{166}Er, since the chemical potential is located between $\mu=[521, 3/2]$ and $\sigma=[521, 1/2]$, and at the same time between $\sigma=[521, 1/2]$ and $\nu=[523, 5/2]$, which are the major contributors to the sums on the r.h.s. of Eqs. (4·4) and (4·5). This mechanism explains the isotope dependence of the quantity $b_4(K=\pm4)$ displayed in Fig. 5(b).

§ 5. Properties of the double γ-vibrational states in ^{164,166,168}Er

5.1. *Effects of the mode-mode couplings*

As described in Part I, we quantize the classical collective Hamiltonian (3·1) by replacing the collective variables $(\eta^*, \eta, \tilde{\eta}^*, \tilde{\eta})$ with the boson operators $(B^\dagger, B, \tilde{B}^\dagger, \tilde{B})$ and by taking the normal ordering. Then, diagonalizing the resulting quantum Hamiltonian in the boson space, we obtain excitation spectra and $E2$-transition probabilities. In this section we discuss how the properties of the double γ-vibrational states in Er isotopes are affected by the dynamical anharmonicity term $\mathcal{H}^{(4)}_{\rm dyn}$ which was neglected in the calculation reported in Part I.

Figures 9(a) and (b) compare the results of two calculations for ^{168}Er with and without including the dynamical anharmonicity effects. We can clearly see that the excitation energies are greatly lowered by these effects. It should be stressed here that these effects cannot be simulated by a mere change of the quadrupole-force strength χ. This point is seen by comparing Fig. 9(b) with (c) which is the result of calculation similar to Fig. 9(a) but with an increased value of χ. In fact, the prediction for the splitting between the $K=0$ and $K=4$ states is significantly different between the two calculations. The importance of the collective-noncollective couplings in lowering the excitation energies of the collective states has been emphasized by Kishimoto and Tamura[11] in their

extensive calculations for transitional nuclei by means of the boson expansion method. The result exhibited in Fig. 9 is qualitatively consistent with their argument. It should be stressed, however, that the (η^*, η) expansion method enables us to remove a number of arbitrary approximations adopted by them in treating the mode-mode couplings.

Figure 10 shows the ratios of the excitation energies and the $E2$-transition amplitudes of the double γ-vibrational states ($K=0$ and 4) to those of the single γ-vibrational states in ^{168}Er as functions of the quadrupole-force strength $\varkappa$. Similarly to Fig. 2 of Part I in which $\mathcal{H}^{(4)}_{\rm dyn}$ was neglected, we see that the properties of the $K=4$ state acquire a similarity to those of the corresponding $K=4$ state in the triaxial rigid-rotor model, as the value of $\varkappa$ increases. We find that the dynamical anharmonicity effects enhance this trend.

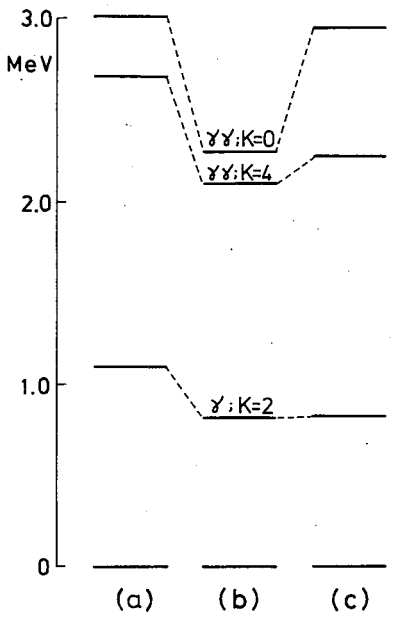

Fig. 9. Excitation energies of the single and double γ-vibrational states in ^{168}Er. (a) The result of calculation with $\varkappa=0.00525[\hbar\omega_0 b_0^{-4}]$ neglecting the dynamical anharmonicity term $\mathcal{H}^{(4)}_{\rm dyn}$. (b) The same as (a) but including $\mathcal{H}^{(4)}_{\rm dyn}$. (c) The same as (a) but with $\varkappa=0.00580[\hbar\omega_0 b_0^{-4}]$.

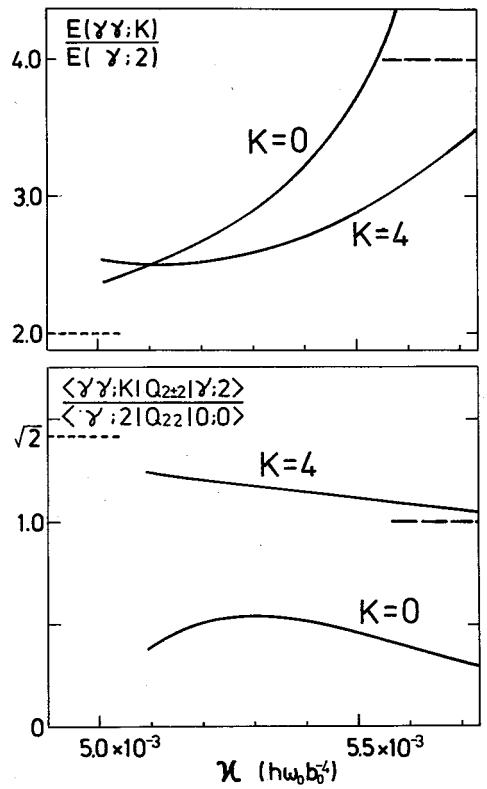

Fig. 10. The upper part: The ratio of the excitation energies of the double γ-vibrational states ($K=0$ and 4) to those of the single γ-vibrational states are plotted for the case of ^{168}Er as functions of the quadrupole-force strength $\varkappa$. The broken and dotted lines indicate the triaxial rigid-rotor limit for the $K=4$ state and the harmonic-vibrational limit for both the $K=0$ and $K=4$ states, respectively. The lower part: The same as above, but for the quadrupole-transition amplitudes between the single- and double-γ vibrational states. Compare with Fig. 2 of Ref. 1) in which the dynamical anharmonicity effects are neglected.

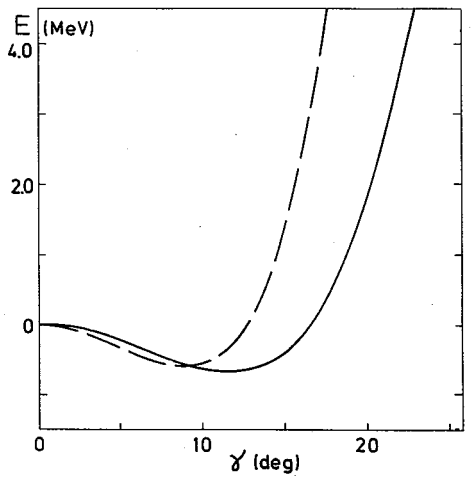

Fig. 11. The collective potential $V_{\rm coll}(\gamma)$. The solid (broken) line represents the result of calculation with (without) including the dynamical anharmonicity $\mathcal{H}^{(4)}_{\rm dyn}$.

Figure 11 compares the collective potentials $V_{\rm coll}(\gamma)$ calculated with and without including $\mathcal{H}^{(4)}_{\rm dyn}$. As is formulated in Part I, the $V_{\rm coll}(\gamma)$ are calculated by transforming the quantized boson Hamiltonian into the Bohr-Mottelson-type collective Hamiltonian represented by the polar coordinates and momenta (γ, φ, p_γ, p_φ). We see in Fig. 11 that the potential wall is significantly lowered by the dynamical anharmonicity effects. The calculated values of the anharmonicity parameters (D, C_2, C_4, ε_1, ε_2, ε_3) for the Bohr-Mottelson-type collective Hamiltonian (see Eqs. (4·9) and (4·10) of Part I) are listed in Table IV together with the values of (α, β, b_1, b_2, b_3, b_4).

5.2. *Theoretical spectra for the anharmonic γ-vibrations*

The theoretical spectra for the γ-vibrational states in ^{164,166,168}Er are displayed in Fig. 12. Because of the reason accounted for in § 4, the position of the $K=0$ state is most sensitive to the change of the neutron number. Comparing Fig. 12 to the result of calculation without including $\mathcal{H}^{(4)}_{\rm dyn}$ (Fig. 4 of Part I), we see indeed that the dynamical anharmonicities greatly lower the excitation energies of the $K=0$ states, the magnitude of which considerably changes according to different isotopes. Thus, experimental data for the excitation energies of the double γ-vibrational $K^\pi=0^+$ states should be very valuable to pin down the dynamical anharmonicity effects under discussion. On the other hand, as soon as we go outside the region of Er isotopes with $N=96\sim100$, where the condition of subshell structure for enhancement of the γ-collectivity is well fulfilled, the couplings between the double γ-vibrational states and the other $K^\pi=0^+$ collective modes become so strong (see Fig. 4) that the C_4 becomes negative indicating an instability of the fourth-

Table IV. Coefficients of the Bohr-Mottelson-type collective Hamiltonian, Eq. (4·9) of Part I, and those of the classical collective Hamiltonian (3·1) evaluated for ^{164,166,168}Er by taking the dynamical anharmonicity effects into account. Parameters used are the same as in Fig. 12.

	D	C_2	C_4	ε_1	ε_2	ε_3
^{164}Er	216.	−3.59	32.1	−4.58	−4.78	−0.147
^{166}Er	247.	−6.18	54.4	−5.61	−5.60	−0.143
^{168}Er	320.	−4.35	51.7	−7.49	−9.61	−0.179
	$[\hbar^2/\hbar\omega_0]$	$[\hbar\omega_0]$	$[\hbar\omega_0]$			$[\hbar\omega_0]^{-1}$

	α	β	b_1	b_2	b_3	b_4
^{164}Er	0.208	−0.231	−0.0164	0.0232	0.0053	−0.0240
^{166}Er	0.179	−0.233	−0.0139	0.0232	0.0088	−0.0102
^{168}Er	0.178	−0.194	−0.0159	0.0208	0.0108	−0.0235

all in $[\hbar\omega_0]$

order collective potential $V_{\rm coll}(\gamma)$ with respect to the collective coordinate γ. As discussed in § 4, when a specific collective mode plays a predominant role in the mode-mode couplings (as in ^{170}Er), such an instability might be removed by explicitly introducing the collective coordinate and momentum corresponding to this degree of freedom. On the other hand, when many non-collective modes play equally important roles (as in ^{160,162}Er), this problem calls for a much more detailed investigation on the stability of the collective submanifold. For this study, we should also improve our residual interactions.

§ 6. Concluding remarks

We have carried out a detailed analysis of the dynamical anharmonicity effects arising from the couplings between the RPA γ-vibrations and the other $K=0$ and ±4 modes, and found that they are very important as well as the kinematical anharmonicity effects arising from the Pauli principle between the γ-vibrational phonons themselves. Special emphasis has been put on elucidating the microscopic structure of the mode-mode couplings. We have found that the $K=\pm2$ components of the Q″Q″ force play a major role in the couplings with the $K=0$ modes, and that the coupling vertices sensitively depend on the relative position between the Fermi surface and the subshells of the Nilsson diagram. As a general rule, we

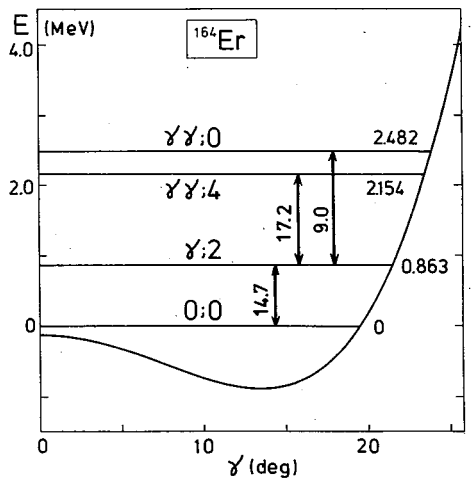

(a)

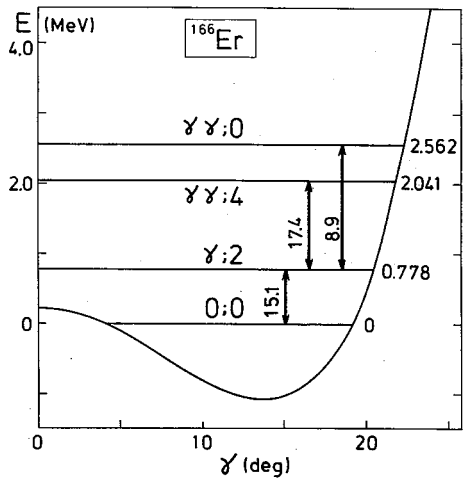

(b)

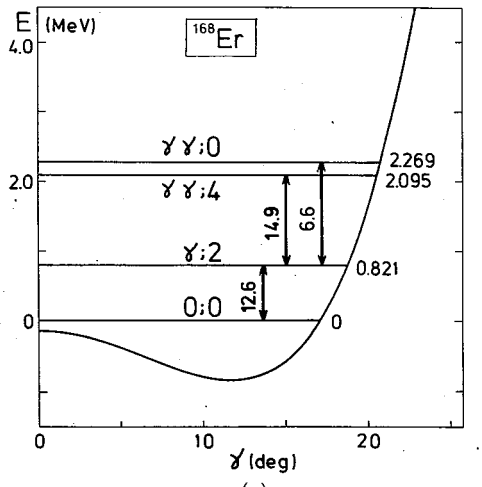

(c)

Fig. 12. The excitation energies in MeV and quadrupole transition amplitudes ($\langle\gamma;2|\hat{Q}_{22}|0;0\rangle$ and $\langle\gamma\gamma;K|\hat{Q}_{22}|\gamma;2\rangle$) in $b_0^2=\hbar/M\omega_0$ for the single- and double γ-vibrational states in ^{164}Er(a), ^{166}Er(b) and ^{168}Er(c). The parameters used in the calculation are the same as those listed in Table II except for the quadrupole-force strengths χ, which are 0.00530 for ^{164}Er, 0.00545 for ^{166}Er and 0.00525 for ^{168}Er in units of $[\hbar\omega_0 b_0^{-4}]$.

can expect that the couplings become very strong when the Fermi surface is situated midway between the two subshells both having large matrix elements for the $K=\pm 2$ quadrupole operator $r^2 Y_{2\pm 2}$. Thus, a strong isotope dependence of the properties of the double γ-vibrational states is predicted.

In this analysis, we have taken into account the couplings with all the $K^\pi=0^+$ and $\pm 4^+$ modes, and demonstrated that the accumulated effects from a large number of non-collective modes (whose individual contributions are small) are very important. On the other hand, the couplings with the low-lying pairing vibrations become in some situations too strong to be treated within the fourth-order approximation of the (η^*, η) expansion. It seems likely that we need to explicitly introduce one more collective variable corresponding to the pairing vibrations in such cases. We can also imagine other situations where the resonances between different RPA modes occur, i.e., the denominator of the expression (2·17) for the mode-mode couplings vanishes. Although we have not encountered such a resonance problem in this paper since the RPA frequencies ω_γ actually adopted for the γ-vibrations are zero or imaginary, this problem should be overcome in order to extend the applicability of the (η^*, η) expansion method. Generally speaking, it is an open and important subject to clarify the dynamical conditions which determine the stability of the collective submanifold associated with the collective motion under consideration.[12] We believe that the convergence property of the (η^*, η) expansion is closely related to the stability of the collective submanifold against the mode-mode couplings.

Since the major aim of this paper was to explicitly see how the SCC method incorporates the mode-mode couplings among different RPA modes in determining the collective submanifold for the anharmonic γ-vibrations, we have not discussed experimental data in detail. For a quantitative comparison of the theoretical calculations with experimental data, it will be necessary to improve our residual interaction by including the quadrupole-pairing force and the three-body forces which arise as a natural extension of the Q″Q″ force.[13),14] We plan to perform such improved calculations in a forthcoming paper, where the couplings with the pairing-rotational modes are also taken into account.

Acknowledgements

We thank Dr. Y. R. Shimizu, Mr. H. Sakamoto and the members of the 1985 annual research project on "microscopic theories of large-amplitude collective motions" organized by RIFP, Kyoto University, for helpful discussions. The computer calculation for this work has been supported in part by RCNP, Osaka University.

References

1) M. Matsuo and K. Matsuyanagi, Prog. Theor. Phys. **74** (1985), 1227.
2) T. Marumori, T. Maskawa, F. Sakata and A. Kuriyama, Prog. Theor. Phys. **64** (1980), 1294.
3) A. Bohr and B. R. Mottelson, Physica Scripta **25** (1982), 28.
4) T. S. Dumitrescu and I. Hamamoto, Nucl. Phys. **A383** (1982), 205.
5) A. Bohr and B. R. Mottelson, *Nuclear Structure,* Vol. II (Benjamin, 1975).
6) M. Matsuo, Y. R. Shimizu and K. Matsuyanagi, *Proc. of the Niels Bohr Centennial Conference on Nuclear Structure, Copenhagen, 1985,* ed. R. Broglia, G. Hageman and B. Herskind (North-Holland, 1985), p. 161.
7) T. Marumori, K. Takada and F. Sakata, Prog. Theor. Phys. Suppl. No. 71 (1981), 1.
8) D. R. Bes, Prog. Theor. Phys. Suppl. Nos. 74 & 75 (1983), 1.

9) M. Matsuo, Genshikaku Kenkyu (in Japanese) **31** (1985), 45.
10) F. Sakata, S. Iwasaki, T. Marumori and K. Takada, Z. Phys. **A286** (1978), 195.
S. Iwasaki, T. Marumori, F. Sakata and K. Takada, Prog. Theor. Phys. **56** (1976), 1140.
11) T. Kishimoto and T. Tamura, Nucl. Phys. **A270** (1976), 317.
12) F. Sakata, T. Marumori, K. Muramatsu and Y. Hashimoto, Prog. Theor. Phys. **74** (1985), 51.
13) T. Kishimoto, *Proc. 1980 RCNP Int. Symp. Highly Excited States in Nuclear Reactions, Osaka,* p. 145.
14) E. R. Marshalek, Phys. Rev. **C29** (1984), 640.

Prog. Theor. Phys. Vol. 77, No. 6, June 1987, Progress Letters

Signature Dependence of $M1$ and $E2$ Transitions in Rotating Triaxial Odd-A Nuclei

Masayuki MATSUZAKI, Yoshifumi R. SHIMIZU*
and Kenichi MATSUYANAGI

Department of Physics, Kyoto University, Kyoto 606
**Department of Physics, Kyushu University, Fukuoka 812*

(Received December 18, 1986)

Effects of both the static and the dynamic triaxial deformations on the signature dependence of $B(M1)$ and $B(E2)$ in odd-A nuclei are studied by applying the RPA formalism based on the rotating shell model to odd-A nuclei. Numerical examples are presented for ^{165}Lu and ^{157}Ho. The observed $M1$ properties of the high-spin region of ^{165}Lu are well reproduced, while the extremely strong signature dependence of $B(E2)$ in ^{157}Ho is not reproduced by the calculation.

In recent years, strong signature dependence of the $B(M1)$ and $B(E2)$ values has been observed[1),2)] in the $\Delta I=1$ transitions between high-spin states in odd-A nuclei. These experimental data have been discussed in connection with the occurrence of triaxial deformations.[3),4)] The theoretical calculations have been done mainly in terms of the particle-rotor model.[3)~5)] In addition to the effects of the static triaxial deformations, those of the γ-vibrations have also been discussed, within the framework of the macroscopic Bohr-Mottelson model, in some cases.[6),7)]

The purpose of our work is to develop, on the basis of the Rotating Shell Model (RSM), a microscopic description of odd-A high-spin states along the line parallel to the phenomenological particle-rotor model. In this letter, we report a few typical results obtained by applying the RPA formalism based on the RSM[8)] to odd-A nuclei. One of the advantages of our approach is that it can easily be applied to high-spin states with many aligned quasiparticles, while it has a limitation that the γ-vibrations and the wobbling modes are treated within the small amplitude approximation. The main steps of our microscopic approach are as follows:

1) We construct a diabatic quasiparticle representation for the rotating triaxially deformed potential that is obtained by transforming the single-particle potential of the Nilsson plus BCS form into a uniformly rotating frame of reference with a given value of the rotational frequency $\omega_{\rm rot}$. This step provides us with the diabatic basis for the RSM.

2) The residual interactions consisting of the monopole-pairing and the doubly-stretched quadrupole forces are treated by means of the RPA in the rotating frame,[8)] and normal modes of vibration are determined.

3) For odd-A nuclei, the couplings of the aligned quasiparticles with the γ-vibrations in the rotating frame are treated in a way similar to the traditional quasiparticle-phonon coupling models.[9)] The γ-vibrations are taken into account up to the two-phonon states, and the Pauli principle effects stemming from the two-quasiparticle structure of the γ-vibration are neglected.

4) We extend Marshalek's treatment[10] of the Nambu-Goldstone modes, $\Gamma^{\dagger}$ and Γ, of the RPA to odd-A nuclei. Namely, we make the following replacement,

$$\left.\begin{aligned}\Gamma^{\dagger}&\to\frac{1}{\sqrt{2I}}(\hat{I}_{-}-\hat{J}_{-}^{(\mathrm{qp})}),\\ \Gamma&\to\frac{1}{\sqrt{2I}}(\hat{I}_{+}-\hat{J}_{+}^{(\mathrm{qp})}),\end{aligned}\right\}\tag{1}$$

where $\hat{I}_{\pm}$ represents the total angular momentum and $\hat{J}_{\pm}^{(\mathrm{qp})}$ the quasiparticle angular momentum. This ansatz is the most crucial point of our approach. The motive of this replacement is to develop a microscopic model in which the state vectors are constructed, as in the particle-rotor model, in a direct-product form of the rotational and the internal wave functions. A similar ansatz was previously adopted by Hara and Kusuno[11] for the case $\omega_{\mathrm{rot}}=0$. Once the replacement (1) is admitted, it is straightforward to extend Marshalek's procedure[10] for constructing the state vectors in the laboratory frame to odd-A nuclei.

By means of the above procedure, we obtain effective electromagnetic operators acting on the internal wave functions of odd-A nuclei as follows:

M1 transitions with $\Delta I=-1$

$$\hat{\mu}_{-1}=(g_l-g_{\mathrm{RPA}})\,\hat{l}_{-1}^{(\mathrm{qp})}+(g_s^{(\mathrm{eff})}-g_{\mathrm{RPA}})\,\hat{s}_{-1}^{(\mathrm{qp})}+\text{vibrational terms},\tag{2}$$

where $\hat{\boldsymbol{l}}^{(\mathrm{qp})}$ and $\hat{\boldsymbol{s}}^{(\mathrm{qp})}$ denote the orbital and spin angular momenta of quasiparticles, and the vibrational contributions consist of the linear terms with respect to the RPA phonon creation and annihilation operators (see Ref. 10)). The effective g-factor of the RPA vacuum state, g_{RPA}, is given by

$$g_{\mathrm{RPA}}=\frac{\langle\hat{\mu}_x\rangle}{\langle\hat{J}_x\rangle},\tag{3}$$

where the expectation values are taken with respect to the RPA vacuum states.

E2 transitions with $\Delta I=-1$

$$\frac{1}{i}\hat{Q}_{2-1}=-\sqrt{\frac{3}{2}}\langle Q_0\rangle\frac{\hat{J}_z^{(\mathrm{qp})}}{I}+\langle Q_2\rangle\left(2\frac{i\hat{J}_y^{(\mathrm{qp})}}{I}+\frac{\hat{J}_z^{(\mathrm{qp})}}{I}\right)+\text{vibrational terms},\tag{4}$$

where the quadrupole operator $\hat{Q}_{2\mu}$ is quantized along the rotation axis (the x-axis), and $\langle Q_K\rangle$ $(K=0,2)$ represent the expectation values of the quadrupole operators Q_{2K} whose quantization axis is the z-axis. The vibrational terms consist of the linear terms with respect to the RPA phonon operators. When the triaxial deformation is small, Eq. (4) can be rewritten in a good approximation as

$$\frac{1}{i}\hat{Q}_{2-1}=\left\{-\sqrt{\frac{3}{2}}\langle Q_0\rangle+\langle Q_2\rangle\left(1+2(-1)^{I-j}\left|\frac{\Delta E}{\hbar\omega_{\mathrm{rot}}}\right|\right)\right\}\frac{\hat{J}_z^{(\mathrm{qp})}}{I}+\text{vibrational terms},\tag{5}$$

where ΔE denotes the signature splitting of the quasiparticle energies. For the quasiparticles associated with the j-shell, ΔE may be written as

$$\Delta E \equiv E\left(\alpha=\frac{1}{2}\right)-E\left(\alpha=-\frac{1}{2}\right)=(-1)^{j+1/2}|\Delta E|\,, \tag{6}$$

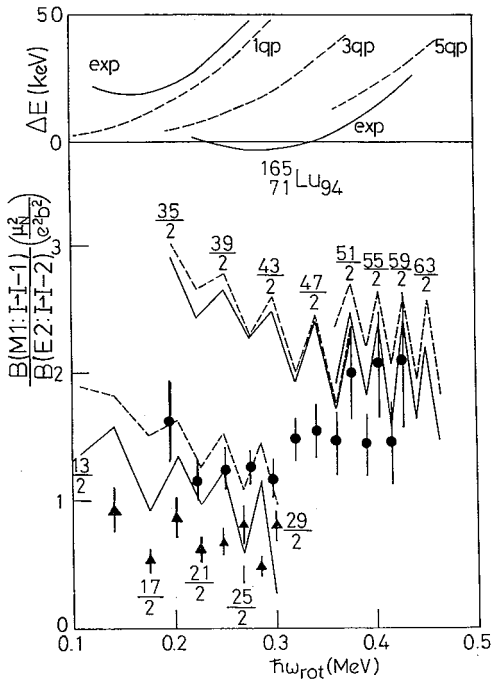

Fig. 1. The ratios $B(M1; I\to I-1)/B(E2; I\to I-2)$ plotted as a function of ω_{rot}. The solid triangles and the solid circles with error bars denote the experimental data.[1] The solid (broken) lines represent the results of calculation with (without) taking into account the couplings with the γ-vibrations. The experimental values for $I=31/2$ and $33/2$ lying in the band crossing region are omitted from the figure. The triaxial deformation parameters are assumed to be $\gamma_0=18°$, $10°$ and $0°$ for the one-, three- and five-quasiparticle bands, respectively. Note that our definition of the sign of γ_0 is opposite to the Lund convention.[3] Other parameters of calculation are: $\beta=0.21$, $g_s^{(eff)}=0.7g_s^{(free)}$, $\Delta_p=1.20$ MeV, $\Delta_n=1.16$ MeV for the one-quasiparticle band, $\Delta_p=1.18$ MeV, $\Delta_n=0.72$ MeV for the three-quasiparticle band, and $\Delta_p=1.18$ MeV, $\Delta_n=0$ for the five-quasiparticle band. In the upper portion of this figure, calculated values for the signature-splittings of the quasiparticle energies are compared with the experimental ones.

where j is related to the signature α by $j=\alpha+$even. The expression (5) reduces to that of Hamamoto[3] when $j=1/2$, because in this case the factor $(-1)^{I-j}|\Delta E/\hbar\omega_{rot}|$ becomes $(-1)^{I-1/2}$. Note that the factor multiplying $\langle Q_2\rangle$ in Eq. (5) always takes larger values for the favoured states (whose $I=j+$even) than for the unfavoured states (whose $I=j+$odd). Note also that the ratio $|\Delta E/\hbar\omega_{rot}|$ is smaller than unity in general.

Below we present typical results of numerical calculations for ^{165}Lu and ^{157}Ho, for which most detailed experimental data are available. In these calculations, the same static triaxial deformation parameters as in Refs. 3) and 4) are used for the sake of comparison with these works, except for the five-quasiparticle aligned band of ^{165}Lu where $\gamma_0=0°$ is assumed. For the sake of reference, we also mention that the static triaxial deformations which we calculated by using the method of Ref. 12) are $\gamma_0=0°\sim8°$ for the one-quasiparticle band, $\gamma_0=6°\sim11°$ for the three-quasiparticle band and $\gamma_0\approx0°$ for the five-quasiparticle band. (Note that our definition of the sign of γ_0 is opposite to the Lund convention.[3]) These values of γ_0 smoothly change as a function of ω_{rot} within individual bands. The principle of fixing other parameters entering in the calculation is the same as in Ref. 8), and the details will be given in a forthcoming paper.

Figure 1 shows the ratios $B(M1; I\to I-1)/B(E2; I\to I-2)$ for ^{165}Lu as a

function of ω_{rot}. The solid (broken) lines represent the ratios calculated with (without) taking the couplings with the γ-vibrations into account. The observed rotational bands may be roughly divided into three groups according to the number of aligned quasiparticles. The first group ($15/2 \lesssim I \lesssim 29/2$) involves the aligned quasiparticle A_p or B_p. The second ($35/2 \lesssim I \lesssim 51/2$) involves the quasiparticle configuration $A_pA_nB_n$ or $B_pA_nB_n$. The third ($I \gtrsim 59/2$) involves $A_pA_nB_nC_nD_n$ or $B_pA_nB_nC_nD_n$. Here A_p, B_p and A_n, B_n, C_n, D_n are the familiar notations[1] denoting the aligned quasiparticle states associated with the $\pi h_{11/2}$ and $\nu i_{13/2}$ shells, respectively. Note that we obtain the crossing between the second and the third configurations at $\hbar\omega_{rot} \simeq 0.4$ MeV in good agreement with the suggestion from the experiment.[1] The interactions between the two configurations are neglected in our calculation with the diabatic approximation, although the experimental data indicate that these are rather strong. The selfconsistently calculated neutron pairing gaps are $\Delta_n = 0.72$ MeV at $\hbar\omega_{rot} = 0.2$ MeV for the three-quasiparticle band and $\Delta_n = 0$ for the five-quasiparticle band,*) when the pairing-force strength G is fixed at the ground state to reproduce the odd-even mass difference. We see in Fig. 1 that the signature dependence is well reproduced especially in the highest-spin region. Another interesting feature of Fig. 1 is that the ratio increases when the $i_{13/2}$ neutrons align. This trend is easily understandable from Eqs. (2) and (3), since the aligned $i_{13/2}$ neutrons decrease the value of g_{RPA}.[13)~15)] The calculated values of g_{RPA} are $0.29 \sim 0.27$ for the one-quasiparticle band, $-0.12 \sim -0.04$ for the three-quasiparticle bands, and $-0.05 \sim -0.04$ for the five-quasiparticle band. These values of g_{RPA} smoothly change as a function of ω_{rot} within individual bands.

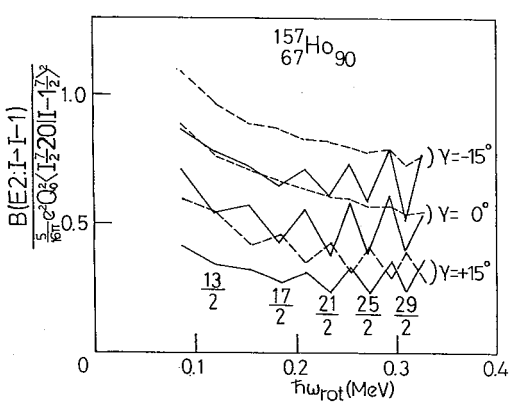

Fig. 2. The calculated values of $B(E2; I \to I-1)$ divided by $(5/16\pi)e^2\langle Q_0\rangle^2\langle I, 7/2, 2, 0|I-1, 7/2\rangle^2$. The three cases with different γ_0 values ($\gamma_0 = \pm 15°, 0°$) are displayed. The solid (broken) lines show the results with (without) taking the couplings with the γ-vibrations into account. The deformation parameters used are $\beta = 0.20$, $\Delta_p = 1.21$ and $\Delta_n = 1.25$ MeV.

Figure 2 shows the calculated values of $B(E2; I \to I-1)$ for ^{157}Ho divided by $(5/16\pi)e^2\langle Q_0\rangle^2\langle I, 7/2, 2, 0|I-1, 7/2\rangle^2$. It is seen that the signature dependence originating from the couplings with the γ-vibrations is stronger than that from the static triaxial deformations. Consequently, the $B(E2; I \to I-1)$ from the favoured states (whose $I = j + \text{even}$) become always larger than those from the unfavoured states (whose $I = j + \text{odd}$), in agreement with the experimental data.[2] On the other hand, the calculated signature dependence of $B(E2)$ is smaller in magnitude than experimental data. Also, the large experimental values[2] of the ratio $B(E2; I \to I-1)/B(E2; I \to I-2)$ could not be reproduced. In this connection, we note

*) As shown in Ref. 8), the pairing gaps depend only weakly on ω_{rot} within each rotational band defined by the diabatic quasiparticle representation. Therefore, we used constant pairing gaps for each band in Fig. 1.

that the calculated values of the factor $\Delta E/\hbar\omega_{\rm rot}$ are 0.43, 0.08 and -0.05 for $\gamma_0=15°$, 0° and $-15°$, respectively, at $\hbar\omega_{\rm rot}=0.2$ MeV in ^{157}Ho, which are considerably smaller than unity. Thus, the signature dependence originating from the static triaxial deformations is significantly suppressed in this nucleus.

The results presented above are in qualitative agreement*) with those of Refs. 3), 4), 6), 7) and 15) except for 1) the case $\gamma=15°$ in Fig. 2**) and 2) the highest-spin region of ^{165}Lu, for which the calculation including the five aligned quasiparticles was carried out for the first time. The microscopic model outlined in this paper may be regarded as a kind of extension of the particle-rotor model, since the basis of the intrinsic state vectors is determined by the RSM as a function of $\omega_{\rm rot}$. One of the merits of this approach is that multi-nucleon-aligned bands can be easily treated, whereas, in the conventional particle-rotor model, the treatment of such bands becomes increasingly difficult with increasing number of aligned nucleons. The results of calculation presented here show the feasibility of our approach. A systematic calculation for many high-spin data is being performed, and will be reported in a forthcoming paper in which the details of formulation will also be given.

The computer calculation for this work has been financially supported by Research Center for Nuclear Physics, Osaka University.

1) P. Frandsen et al., Phys. Lett. **B177** (1986), 287.
2) G. B. Hagemann et al., Nucl. Phys. **A424** (1984), 365.
3) I. Hamamoto, *Proc. Niels Bohr Centennial Conf. on Nuclear Structure, Copenhagen 1985*, ed. R. Broglia, G. B. Hagemann and B. Herskind (North-Holland, 1985), p. 129, and references therein.
4) I. Hamamoto and B. Mottelson, Phys. Lett. **167B** (1986), 370.
5) F. Dönau and S. Frauendorf, *Proc. Conf. on High Angular Momentum Properties of Nuclei , Oak Ridge 1982,* ed. N. R. Johnson (Harwood, New York, 1983), p. 143.
6) A. Ikeda, Nucl. Phys. **A439** (1985), 317.
7) N. Onishi, I. Hamamoto, S. Åberg and A. Ikeda, Nucl. Phys. **A452** (1986), 71.
8) Y. R. Shimizu and K. Matsuyanagi, Prog. Theor. Phys. **70** (1983), 144; **72** (1984), 799.
9) L. S. Kisslinger and R. A. Sorensen, Rev. Mod. Phys. **35** (1963), 853.
10) E. R. Marshalek, Nucl. Phys. **A275** (1977), 416.
11) K. Hara and S. Kusuno, Nucl. Phys. **A245** (1975), 147.
12) Y. R. Shimizu and K. Matsuyanagi, Prog. Theor. Phys. **71** (1984), 960.
13) M. Sano, T. Takemasa and M. Wakai, *Proc. Int. Conf. on Nuclear Moments and Nuclear Structure, Osaka 1972,* ed. H. Horie and K. Sugimoto, J. Phys. Soc. Jpn. **34** Suppl. (1973), 365.
14) S. Frauendorf, Phys. Lett. **100B** (1981), 219.
15) Y. S. Chen, P. B. Semmes and G. A. Leander, Phys. Rev. **C34** (1986), 1935.

*) According to Ref. 7), the couplings with the γ-vibrations enhance the $B(E2; I\to I-1)$ from the unfavoured states over those from the favoured states. We confirmed that a similar result is obtained also in our approach if the chemical potential lies, as in their case, below the $K=1/2$ states associated with the high-j orbit. Since the chemical potential lies near the $K=7/2$ orbit in the case ^{157}Ho, there is no contradiction between the results shown in Fig. 2 and that of Ref. 7).

**) The reason for the disagreement between our result and that of Ref. 3) in the $\gamma=15°$ case of ^{157}Ho is not clear.

Progress of Theoretical Physics, Vol. 78, No. 3, September 1987

Microscopic Description of Anharmonic Gamma-Vibrations by Means of the Selfconsistent-Collective-Coordinate Method. III

Masayuki MATSUO*) and Kenichi MATSUYANAGI

Department of Physics, Kyoto University, Kyoto 606

(Received April 8, 1987)

Properties of the anharmonic gamma-vibrations and their (N, Z)-dependence are investigated in a wide region of the rare-earth deformed nuclei. The effective Hamiltonian which contains, in addition to the monopole-pairing plus (doubly-stretched) quadrupole-quadrupole interactions, the quadrupole-pairing interaction and the effective three-body force is used in the microscopic calculation. Dynamical anharmonicity effects arising from the mode-mode couplings are analysed in detail in relation to these effective interactions. The couplings between the gamma-vibrations and the pairing rotations are also taken into account in order to recover the nucleon-number conservation. The numerical calculation indicates that the properties of the anharmonic gamma-vibrations significantly change from one nucleus to another reflecting the subshell structure near the Fermi surface. A characteristic (N, Z)-dependence of the double gamma-vibrational states is predicted for some Dy and Er isotopes.

§ 1. Introduction

The γ-vibrations of deformed even-even nuclei are typical examples that exhibit non-linear dynamics of nuclear collective motions. In particular, large anharmonicities of the double γ-vibrational states were suggested[1),2)] in ^{168}Er and have been investigated from various viewpoints.[3)~5)] In Part I[6)] of this series of paper we formulated a micrsocopic theory describing the anharmonic γ-vibrations on the basis of the selfconsistent-collective-coordinate (SCC) method.[7)] The SCC method can take into account the most remarkable feature of the large-amplitude non-linear collective motion: The internal structure of the collective variables changes selfconsistently depending on the amplitude of the collective motion. This dynamical mechanism is caused by the couplings between different kinds of the RPA excitation modes. It should be recalled here that the RPA defines the normal modes of excitation under the linear approximation which is valid only in the small amplitude limit. In Part II,[8)] we investigated how this dynamical mechanism affects the properties of the anharmonic γ-vibrations in Er isotopes and analysed in detail the microscopic structure of the mode-mode couplings. We found that the dynamical effects arising from the mode-mode couplings are quite sensitive to the subshell structure of the Nilsson single-particle levels near the Fermi surface.

The first aim of this paper, Part III, is to perform a detailed and systematic study of the anharmonic γ-vibrations over a wide region of the nuclear chart in the rare-earth region. From the analysis of Part II, we expect that dynamics of the anharmonic γ-vibrations have characteristic (N, Z)-dependence. Therefore, investigation on the (N, Z)-dependence of their properties is indispensable to understand the nature

*) Present address: Cyclotron Laboratory, The Institute of Physical and Chemical Research, Wakō-shi, Saitama 351-01.

of the anharmonic γ-motions.

The second aim of this paper is to perform the numerical calculations by using an improved model Hamiltonian. In Parts I and II, we employed the effective interaction composed of the pairing and the doubly stretched quadrupole ($P+Q''Q''$) forces. In this paper, we take into account the quadrupole-pairing interaction and the effective three-body force in addition to the $P+Q''Q''$ forces. Importance of the quadrupole-pairing interaction has been emphasized in the microscopic descriptions of the low-lying quadrupole motions of the transitional nuclei.[9),10)] On the other hand, the three-body force is naturally derived as a higher-order term of the $Q''Q''$ force. This force is an extension of the similar three-body force[11)] (appropriate for use in the spherical basis) into the case of using the deformed basis. Importance of the ordinary three-body force in describing the mode-mode couplings has been emphasized[11)] by Kishimoto in connection with the deformation splitting of the giant quadrupole resonances. Since various kinds of mode-mode coupling play the central role in our theory, it is also indispensable to examine how the coupling matrix elements are modified by these interactions neglected in Parts I and II.

The third aim of this paper is to improve our theoretical framework for treating the nucleon-number conservation. We use the extended formulation of the SCC method recently proposed by one of the authors (M. M.).[12)] In this formulation, the number-conservation law violated by the use of the quasiparticle representation is recovered in average by taking into account the coupling effects between the γ-vibrations and the pairing rotational motions.

Details of the improved model Hamiltonian is described in § 2. The extended formulation of the SCC method which satisfies the number conservation in average is briefly described in § 3. In this section, we also evaluate the additional contribution to the collective Hamiltonian that comes from the couplings between the γ-vibrations and the pairing rotational motions. Sections 4 and 5 are devoted to the analysis of the effects of the quadrupole-pairing interaction and the effective three-body force on the properties of the anharmonic γ-vibrations. In § 6, the (N, Z)-dependence of the properties of the anharmonic γ-vibrations is discussed. Concluding remarks are given in § 7.

§ 2. The Hamiltonian

We employ the Hamiltonian $\hat{H}$ expressed as

$$\hat{H}=\hat{h}_{\rm def}+\hat{H}_{\rm int}+\hat{H}_{\rm int}^{\rm 3\text{-}body}, \tag{2·1}$$

$$\hat{H}_{\rm int}=-\sum_{\tau=n,p}G_0^{(\tau)}\hat{P}_{00}^{(\tau)\dagger}\hat{P}_{00}^{(\tau)}-\sum_{\tau=n,p}G_2^{(\tau)}\sum_{K=-2}^{2}\hat{P}_{2K}^{(\tau)\dagger}\hat{P}_{2K}^{(\tau)}-\frac{1}{2}\kappa\sum_{K=-2}^{2}(-1)^K\hat{Q}''_{2K}\hat{Q}''_{2-K}, \tag{2·2}$$

$$\hat{H}_{\rm int}^{\rm 3\text{-}body}=\kappa_3\Big\{\frac{1}{2}\hat{R}''\sum_{K=-2}^{2}(-1)^K\hat{Q}''_{2K}\hat{Q}''_{2-K} -\frac{1}{3!}\sqrt{\frac{56\pi}{5}}\sum_{K_1,K_2}\langle 2K_12K_2|2,K_1+K_2\rangle(-1)^{2-K_1-K_2}\hat{Q}''_{2K_1}\hat{Q}''_{2K_2}\hat{Q}''_{2-K_1-K_2}\Big\}, \tag{2·3}$$

where

$$\hat{P}_{2K}^{(\tau)\dagger}=\frac{1}{2}\sum_{\substack{\mu\nu \\ \text{(neutron or proton)}}}\langle\mu|r^2Y_{2K}|\nu\rangle c_\mu^\dagger c_{\bar{\nu}}^\dagger\,, \qquad (\tau=n,\,p) \tag{2·4}$$

$$\hat{R}''=:\sum_{\mu\nu}\langle\mu|(r^2)''|\nu\rangle c_\mu^\dagger c_\nu:\,, \tag{2·5}$$

and the other notations are the same as given in Part I. The second term of the r.h.s. of Eq. (2·2) represents the quadrupole-pairing interaction (hereafter abbreviated as P_2 interaction). The effective three-body interaction $\hat{H}_{\text{int}}^{3\text{-body}}$ is similar to that proposed by Kishimoto,[11] except for the difference that it is here defined in terms of the doubly stretched operators $\hat{R}''$ and $\hat{Q}''_{2K}$.*)

We use in the numerical calculation exactly the same Nilsson Hamiltonian $\hat{h}_{\text{def}}$ and the single-particle model space as used in Parts I and II. Namely, the neutron major-shells with $N_{\text{osc}}=4\sim6$ and the proton major-shells with $N_{\text{osc}}=3\sim5$ are taken into account. Because of the deformation of the equilibrium shape, the BCS treatment of $\hat{H}$ brings about the quadrupole-pairing gap $\Delta_2^{(\tau)}\equiv G_2^{(\tau)}\langle\hat{P}_{20}^{(\tau)\dagger}\rangle$ as well as the monopole pairing gap $\Delta_0^{(\tau)}\equiv G_0^{(\tau)}\langle\hat{P}_{00}^{(\tau)\dagger}\rangle$.

The force-strengths of the residual interactions are fixed in the following way. The roles of the P_2 interaction have been known through the $L=2$ components of the two-nucleon transfer reactions for spherical nuclei in the Pb region,[13),14)] the enhancement of $(p,\,t)$ cross sections for deformed nuclei in the actinide region,[15),16)] rotational moments of inertia,[17)~19)] blocking effects on the band-crossing angular frequency in deformed odd-nuclei,[19)~21)] etc. Through these analyses, the P_2 force strength is estimated to be about $G_2\approx 10A^{-4/3}G_0$ fm^{-4}. We thus assume that**)

$$G_2^{(\tau)}=18R^{-4}G_0^{(\tau)}\,, \qquad (R=1.2A^{1/3}\text{fm}) \tag{2·6}$$

where $G_0^{(\tau)}$ is the strength of the monopole-pairing interaction and is written as

$$G_0^{(\tau)}=g_0^{(\tau)}/A \qquad [\text{MeV}]\,. \tag{2·7}$$

We determine the constant $g_0^{(\tau)}$ for each isotope such that the calculated minimum quasiparticle energies coincide in average with the experimental odd-even mass differences.***) The constants $g_0^{(\tau)}$ determined in this way are; $g_0^{(\tau)}=(16,\,23)$ MeV (for $\tau=n$ and p, respectively) for Gd, Dy, Er; (17, 25) for Yb; (18, 25) for Hf; (18, 26) for W; (20, 29) for Os. Typical values of the calculated gap parameters are $\Delta_0^{(\tau)}=(0.64,\,0.77)$ MeV and $\Delta_2^{(\tau)}=(0.038,\,0.027)$ MeV·fm^{-2} (for $\tau=n$ and p, respectively) for ^{168}Er.

*) In Ref. 11), the three-body force is derived for the nucleus with spherical shape. It is to be noted that the doubly stretched quadrupole-quadrupole interaction, the third term of the r.h.s. of Eq. (2·2), already includes some parts of the three-body interaction defined in the spherical basis. The doubly-stretched three-body force, Eq. (2·3), includes not only the remaining part of the three-body interaction but also some contributions from the four-body force defined in the spherical basis.

**) Estimation from the multipole expansion of the zero-range δ-interaction[18] gives $G_2=(28\pi/3)R^{-4}G_0$.

***) When the quadrupole-pairing gap Δ_2 is rather large, the pairing gap $\Delta(\mu)=\Delta_0+\langle\mu|r^2Y_{20}|\mu\rangle\Delta_2$ sensitively depends on the quadrupole moment of the single-particle orbit. Therefore, we consider it appropriate to determine G_0 with some averaging procedure instead of determining it for each nucleus.

These values are consistent with the result of the recent extensive analysis of the quasiparticle spectrum.[19]

The three-body interaction $\hat{H}_{\rm int}^{\rm 3\text{-}body}$ is derived from the idea of the selfconsistent average potential associated with the quadrupole collective motions.[11] It is well known that the average potential which satisfies the volume conservation and the selfconsistency to the nuclear density is generated by the doubly-stretched quadrupole ($Q''Q''$) interaction with the selfconsistent force strength $\kappa^{(\rm self)}=4\pi M\omega_0{}^2/3R^2$.[23),24)] This is valid, however, only for small-amplitude vibrations about the deformed equilibrium shape. For larger amplitude vibrations, more rigorous selfconsistency condition is required and is satisfied by including the three-body force with the selfconsistent strength $\kappa_3{}^{(\rm self)}=20\pi M\omega_0{}^2/9R^4$.[11] When the single-particle model space is truncated in numerical calculation, we should employ instead of $\kappa_3{}^{(\rm self)}$ the force strength κ_3 given by

$$\kappa_3=(\kappa/\kappa^{(\rm self)})^2\kappa_3{}^{(\rm self)} \tag{2·8}$$

and the $Q''Q''$ force strength κ given later. The above relation is derived from the following consideration. Let us consider the time-dependent potential associated with the γ-vibrations. The contribution of the $Q''Q''$ interaction and the three-body interaction to the time-dependent potential δV are

$$\delta\hat{V}^{Q''Q''}=-\kappa^{(\rm self)}\alpha^{(\rm full)}(\hat{Q}''_{22}+\hat{Q}''_{2-2}) \tag{2·9a}$$

and

$$\delta\hat{V}^{\rm 3\text{-}body}=\kappa_3{}^{(\rm self)}(\alpha^{(\rm full)})^2\left(\hat{R}''-\sqrt{\frac{16\pi}{5}}\hat{Q}''_{20}\right), \tag{2·9b}$$

where the vibrational amplitude $\alpha^{(\rm full)}\equiv\langle\hat{Q}''_{22}\rangle$ should be calculated in the full space without truncation. As is well known, the potential δV gives rise to the coupling between the single-particle motion and the collective motion, and the particle-vibration coupling strengths are given by $\kappa^{(\rm self)}\alpha^{(\rm full)}$ and $\kappa_3{}^{(\rm self)}(\alpha^{(\rm full)})^2$. When the numerical calculation is done in a truncated model space, we consider it of primary importance that the correct particle-vibration coupling strengths are reproduced in the calculation. This requirement is easily met by adjusting the force strengths κ and κ_3 such that the relations $\kappa\alpha=\kappa^{(\rm self)}\alpha^{(\rm full)}$ and $\kappa_3\alpha^2=\kappa^{(\rm self)}(\alpha^{(\rm full)})^2$ are satisfied, where $\alpha=\langle\hat{Q}''_{22}\rangle$ on the l.h.s. of these equations is calculated in the truncated model space. Then, eliminating α and $\alpha^{(\rm full)}$, we get Eq. (2·8) from these relations. The well-known fact that the quadrupole core-polarization effect can be renormalized in a model space consisting of a single major-shell with $\kappa=2\kappa^{(\rm self)}$ and $\alpha=\alpha^{(\rm full)}/2$ may be considered as an example of the above renormalization procedure. Thus, only the strength κ of the $Q''Q''$ interaction is an adjustable parameter in our model Hamiltonian. As was done in Parts I and II, we fix the value of κ so as to reproduce the observed band-head energy of the gamma band with $K^\pi=2^+$ for each nucleus.

§ 3. Approximate treatment of the nucleon-number conservation

In this section we describe a method of approximately treating the nucleon-number conservation. This is done by developing a framework that explicitly treats the couplings between the γ-vibrations and the pairing rotations. The pairing rotation is a kind of the Nambu-Goldstone mode that arises to recover the rotational symmetry in the gauge space (i.e., symmetry with respect to the phases of wave functions) broken by the Hartree-Fock-Bogoliubov ground state. Thus, the broken symmetry is recovered by taking the couplings with the pairing rotation into account. The TDHB state vector suitable for this purpose is written as[12]

$$|\phi(\eta_i^*, \eta_i, N_\tau, \varphi_\tau)\rangle=\Big(\prod_{\tau=n,p} e^{-i\varphi_\tau \hat{N}_\tau}\Big) e^{i\hat{G}(\eta_i^*, \eta_i, N_\tau)}|\phi_0\rangle \tag{3·1}$$

in place of the one defined by Eq. (I.3·2). Here, the collective variables $(\eta_i^*, \eta_i)\equiv(\eta^*, \eta, \tilde{\eta}^*, \tilde{\eta})$ represent the γ-vibration. The conjugate variables (φ_τ, N_τ) describe the pairing rotations of neutrons and protons $(\tau=n, p)$, where φ_τ represents the rotation angle in gauge space and N_τ means the total number of neutrons (or protons) which corresponds to the operator $\hat{N}_\tau$. The $|\phi_0\rangle$ is the deformed BCS ground state having the average nucleon number $N_{\tau,0}$. The operator $i\hat{G}$ is expanded as

$$\begin{aligned} i\hat{G}(\eta_i^*, \eta_i, N_\tau)=&\sum_\tau\{G_\lambda(\eta_i^*, \eta_i, N_\tau)\hat{X}_\lambda^\dagger - G_\lambda^*(\eta_i^*, \eta_i, N_\tau)\hat{X}_\lambda\} \\ &+\sum_{\tau'=n,p}\{G_{N\tau}(\eta_i^*, \eta_i, N_\tau)\hat{N}_{\tau',A}+G_{\theta\tau}(\eta_i^*, \eta_i, N_\tau)\hat{\Theta}_{\tau'}\}, \end{aligned} \tag{3·2}$$

where $\hat{X}_\lambda^\dagger$ and $\hat{X}_\lambda$ are the RPA phonon creation and annihilation operators defined by Eqs. (I.2·13)~(I.2·19). The operators $\hat{N}_{\tau,A}$ and $\hat{\Theta}_\tau$ for the RPA pairing-rotational modes

$$\hat{\Theta}_\tau=\sum_{\mu<\nu}\theta_\tau(\mu\nu)(a_\mu^\dagger a_\nu^\dagger - a_{\bar{\nu}}a_{\bar{\mu}}), \tag{3·3a}$$

$$\hat{N}_{\tau,A}=\text{the } a_\mu^\dagger a_\nu^\dagger \text{ and } a_\nu a_\mu \text{ part of } \hat{N}_\tau \tag{3·3b}$$

are determined by the RPA equations

$$[\hat{H}, \hat{N}_{\tau,A}]_{\mathrm{RPA}}=0, \tag{3·4a}$$

$$[\hat{H}, \hat{\Theta}_\tau]_{\mathrm{RPA}}=\sum_{\tau'} g_{\tau\tau'}\hat{N}_{\tau',A}, \tag{3·4b}$$

$$\langle\phi_0|[\hat{N}_{\tau,A}, \hat{\Theta}_{\tau'}]|\phi_0\rangle=\delta_{\tau\tau'}. \tag{3·4c}$$

The unknown functions G_λ, G_λ^*, $G_{N\tau}$ and $G_{\theta\tau}$ as well as the collective Hamiltonian are determined by the following basic equations of the SCC method;[12] (i) the equation of the collective submanifold

$$\delta\langle\phi_0|\Big\{e^{-i\hat{G}}\hat{H}e^{i\hat{G}}-\sum_{i=1,2}\Big(\frac{\partial\mathcal{H}}{\partial\eta_i^*}\hat{O}_i^\dagger+\frac{\partial\mathcal{H}}{\partial\eta_i}\hat{O}_i\Big)-\sum_{\tau=n,p}\Big(\frac{\partial\mathcal{H}}{\partial N_\tau}e^{-i\hat{G}}\hat{N}_\tau e^{i\hat{G}}\Big)\Big\}|\phi_0\rangle=0 \tag{3·5}$$

with

$$\hat{O}_i{}^{\dagger}=e^{-i\hat{G}}\frac{\partial}{\partial\eta_i}e^{i\hat{G}} \quad \text{and} \quad \hat{O}_i=-e^{-i\hat{G}}\frac{\partial}{\partial\eta_i{}^*}e^{i\hat{G}}\,, \tag{3·6}$$

(ii) the definition of the collective Hamiltonian

$$\mathcal{H}(\eta_i{}^*,\,\eta_i,\,N_\tau)=\langle\phi_0|e^{-i\hat{G}}\hat{H}e^{i\hat{G}}|\phi_0\rangle-\langle\phi_0|\hat{H}|\phi_0\rangle\,, \tag{3·7}$$

and (iii) the canonical-variables conditions

$$\left.\begin{aligned}&\langle\phi_0|\hat{O}_i{}^{\dagger}(\eta_i{}^*,\,\eta_i,\,N_\tau)|\phi_0\rangle=\frac{1}{2}\eta_i{}^*\,,\\&\langle\phi_0|\hat{O}_i(\eta_i{}^*,\,\eta_i,\,N_\tau)|\phi_0\rangle=\frac{1}{2}\eta_i\,,\end{aligned}\right\} \tag{3·8}$$

$$\langle\phi_0|e^{-i\hat{G}(\eta_i{}^*,\eta_i,N_\tau)}\hat{N}_\tau e^{i\hat{G}(\eta_i{}^*,\eta_i,N_\tau)}|\phi_0\rangle=N_\tau\,, \tag{3·9}$$

$$\langle\phi_0|e^{-i\hat{G}(\eta_i{}^*,\eta_i,N_\tau)}\frac{\partial}{\partial N_\tau}e^{i\hat{G}(\eta_i{}^*,\eta_i,N_\tau)}|\phi_0\rangle=0\,. \tag{3·10}$$

In the previous papers (Parts I and II) the collective variables φ_τ and N_τ were not introduced and the second term of the r.h.s. of Eq. (3·2), which represents the component of the pairing rotational mode, was neglected. Correspondingly, the basic equations are modified so that the third term newly appear in the bracket of Eq. (3·5) together with the new equations, (3·9) and (3·10). Equation (3·9) gives the constraint that the average nucleon number for the TDHB state vector (2·1) should coincide with the variable N_τ and be independent of the variables $(\eta_i{}^*,\,\eta_i)$ for the γ-vibration. This means that the average nucleon number is conserved in this formalism.

The basic equations are solved according to the $(\eta^*,\,\eta)$-expansion technique whose general procedure is given in Ref. 12). We adopt the same boundary condition and the same Hartree approximation as adopted in Parts I and II. Up to the third order of the expansion for the operator $i\hat{G}$, the solution is exactly the same as those given in Part I*) except that we have now the contributions in Eq. (3·2) from the pairing rotational components

$$G_{N_\tau}^{(2)}=0\,, \tag{3·11a}$$

$$G_{\theta_\tau}^{(2)}=-\frac{1}{2}\langle\phi_0|[[\hat{N}_\tau,\,i\hat{G}^{(1)}],\,i\hat{G}^{(1)}]|\phi_0\rangle\,. \tag{3·11b}$$

The resultant fourth-order collective Hamiltonian takes the following form:**)

$$\begin{aligned}\mathcal{H}&=\mathcal{H}^{(2)}+\mathcal{H}^{(4)}\\&=\alpha(\eta^*\eta+\bar{\eta}^*\bar{\eta})+\beta(\eta^*\bar{\eta}^*+\eta\bar{\eta})+b_1(\eta^*\eta^*\bar{\eta}^*\bar{\eta}^*+\text{c.c.})\\&\quad+b_2(\eta^*\bar{\eta}^*\eta^*\eta+\eta^*\bar{\eta}^*\bar{\eta}^*\bar{\eta}+\text{c.c.})+b_3(\eta^*\eta^*\eta\eta+\bar{\eta}^*\bar{\eta}^*\bar{\eta}\bar{\eta})+b_4\eta^*\bar{\eta}^*\eta\bar{\eta}\,.\end{aligned} \tag{3·12}$$

*) Equation (I.3·33) for $G_\gamma^{(3)}$ should be replaced by Eq. (II.2·8).

**) Since the collective variables N_τ representing the total neutron (proton) numbers are the constants of motion, we can substitute the ground-state values $N_{\tau,0}$ for N_τ. For simplicity of notation, we omit the constants $N_{\tau,0}$ hereafter.

Table I. Contributions of each term in Eq. (3·13) to the fourth-order coefficients $b_i(i=1\sim4)$ for ^{168}Er.

	b_1	b_2	b_3	b_4 all in $[\hbar\omega_0]$
$\mathcal{H}^{(4)}_{\rm tru}$	−.0022	.0169	.0198	.0282
$\mathcal{H}^{(4)}_{\rm dyn}$	−.0064	−.0066	−.0072	−.0368
$\mathcal{H}^{(4)}_{\rm PR}$	−.0005	.0011	.0028	.0047
total	−.0090	.0113	.0154	−.0039

The fourth-order term $\mathcal{H}^{(4)}$ can be decomposed as

$$\mathcal{H}^{(4)}=\mathcal{H}^{(4)}_{\rm tru}+\mathcal{H}^{(4)}_{\rm dyn}+\mathcal{H}^{(4)}_{\rm PR}\,, \tag{3·13}$$

where the first two terms are the same as given in Part II. The third term results from the contribution of $G^{(2)}_{N\tau}$ and $G^{(2)}_{\theta\tau}$ in Eq. (3·2), and represents the effect of the mode-mode coupling between the γ-vibration and the pairing rotation. The relative importance of each term in Eq. (3·13) in determining the coefficients $b_i(i=1\sim4)$ is seen in Table I. This numerical example for ^{168}Er indicates that the contribution of $\mathcal{H}^{(4)}_{\rm PR}$ is rather small in comparison with those of $\mathcal{H}^{(4)}_{\rm tru}$ and $\mathcal{H}^{(4)}_{\rm dyn}$. As discussed in Part II, $\mathcal{H}^{(4)}_{\rm dyn}$ represents the dynamical anharmonicity due to the mode-mode couplings between the RPA γ-vibrations and the other $K^\pi=0^+,\pm4^+$ RPA modes, and $\mathcal{H}^{(4)}_{\rm tru}$ mainly stands for the Pauli principle effect among the RPA γ-vibrations. We found that similar conclusions hold also for other nuclei as far as the low-lying states up to the double excitations of the γ-vibrations are concerned. The reason why the effect of $\mathcal{H}^{(4)}_{\rm PR}$ is small can be, explicitly seen as follows. If the couplings to the pairing rotations are neglected, i.e., if we put $G^{(2)}_{N\tau}=G^{(2)}_{\theta\tau}=0$, the collective representation of the neutron (proton) number $\hat{N}_\tau$ is given by

$$\mathcal{N}_\tau\equiv\langle\phi|\hat{N}_\tau|\phi\rangle=N_{\tau,0}+n_\tau{}^{(1100)}(\eta^*\eta+\tilde{\eta}^*\tilde{\eta})+n_\tau{}^{(1010)}(\eta^*\tilde{\eta}^*+\eta\tilde{\eta})+\cdots\,. \tag{3·14}$$

The second and the higher-order terms represent the deviations from the ground-state value $N_{\tau,0}$. A numerical example for these coefficients is

$$(n_\tau{}^{(1100)},\ n_\tau{}^{(1010)})=\begin{cases}(-0.20,\ 0.05) & \text{for neutrons}\\ (-0.06,\ 0.02) & \text{for protons}\end{cases},$$

in the case of ^{168}Er. We found that these coefficients become small when the quasiparticle components of the RPA γ-vibrations $\hat{X}_\gamma{}^\dagger=\sum_{\mu<\nu}\{\psi_\gamma(\mu\nu)a_\mu{}^\dagger a_\nu{}^\dagger+\varphi_\gamma(\mu\nu)a_{\bar{\nu}}a_{\bar{\mu}}\}$ evenly distribute over both sides of the Fermi surface. This case always holds in nuclei where low-frequency γ-vibrations are observed.

After the quantization and transforming into the polar-coordinate representation by means of the procedure described in Part I, we obtain the Bohr-Mottelson-type collective Hamiltonian for anharmonic γ-vibrations:

$$H_{\rm coll}=T_{\rm coll}+V_{\rm coll}\,, \tag{3·15}$$

$$T_{\rm coll}=-\frac{\hbar^2}{2D}\left(\frac{\partial^2}{\partial\gamma^2}+\frac{1}{\gamma}\frac{\partial}{\partial\gamma}+\frac{1}{4\gamma^2}\frac{\partial^2}{\partial\varphi^2}\right)+\varepsilon_1\frac{\hbar^2}{2D}\left(\gamma^2\frac{\partial^2}{\partial\gamma^2}+3\gamma\frac{\partial}{\partial\gamma}+1\right)$$

$$+\varepsilon_2\frac{\hbar^2}{2D}\cdot\frac{1}{4}\frac{\partial^2}{\partial\varphi^2}+\varepsilon_3\left(\frac{\hbar^2}{2D}\right)^2\left(\frac{\partial^2}{\partial\gamma^2}+\frac{1}{\gamma}\frac{\partial}{\partial\gamma}+\frac{1}{4\gamma^2}\frac{\partial^2}{\partial\varphi^2}\right)^2, \tag{3·16}$$

$$V_{\rm coll}=\frac{1}{2}C_2\gamma^2+C_4\gamma^4, \tag{3·17}$$

where the mass parameter D, the restoring-force parameter C_2,*) and the anharmonicity coefficients (ε_1, ε_2, ε_3 and C_4) are derived from the microscopic quantities such as the Nilsson single-particle energies and the strengths of the residual interactions.

§ 4. Effects of the quadrupole-pairing interaction

In this section, we investigate the effects of the quadrupole-pairing (P_2) interactions on the properties of the anharmonic γ-vibrations. Since the dynamical anharmonicities caused by the mode-mode couplings between the RPA γ-vibrations and the other RPA modes with $K^\pi=0^+$ and $\pm4^+$ play crucial roles in our theory, we first analyse the effect on the dynamical anharmonicities in detail, and then discuss the effects on energy spectra and transition probabilities.

4.1. *Effects on dynamical anharmonicities*

The strengths κ and $G_2^{(\tau)}$ of the $Q''Q''$ and P_2 interactions enter into the coupling matrix elements,**) which generate the couplings between the γ-vibrational modes and other ones, as

$$V_\gamma(\underset{K=2}{\mu\nu};\underset{K=2}{\tau;\sigma})=\frac{1}{4}\mathcal{Q}_2(\mu\tilde{\nu})\mathcal{Q}_2(\sigma\tau)\Big\{\kappa(u_\mu v_\nu+v_\mu u_\nu)(u_\sigma u_\tau-v_\sigma v_\tau)$$
$$-G_2^{(\tau)}\left(\frac{\omega_0}{\omega_\perp}\right)^4(u_\mu v_\nu u_\sigma u_\tau-v_\mu u_\nu v_\sigma v_\tau)\Big\}, \tag{4·1}$$

where $\mathcal{Q}_2(\mu\nu)=\langle\mu|(r^2Y_{22})''|\nu\rangle$ and all single-particle labels are for neutrons (or protons). When the orbit dependence of the uv-factors can be neglected in the above equation, the contribution of the P_2 interaction (the second term on the r.h.s. of Eq. (4·1)) cancels that of the $Q''Q''$ interaction (the first term) if the $Q''Q''$ force strength κ and the P_2 force strength $G_2^{(\tau)}$ satisfy the relation $G_2\approx2\kappa(\omega_\perp/\omega_0)^4\approx3\kappa$. This kind of cancellation mechanism was previously discussed by Andō, Bandō and Nagata[22] in the case of spherical nuclei. The actual force strengths adopted in our calculation are $G_2^{(\tau)}\approx0.05[\hbar\omega_0b_0^{-4}]$ and $\kappa\approx0.05[\hbar\omega_0b_0^{-4}]$. It is expected from this argument that the mode-mode couplings can be reduced up to about 2/3 by the P_2 interaction, and hence the dynamical anharmonicity may be reduced to about half.

Figure 1 presents a numerical example for Er isotopes. This figure shows the effect of the P_2 interaction on the coefficients of the dynamical anharmonicity terms of the collective Hamiltonian, which arises from the mode-mode couplings to the K^π

*) The numbers for $\frac{1}{2}C_2$ were erroneously listed in Table III of Part I and in Table IV of Part II, and therefore should be multiplied by a factor 2.

**) The matrix elements $V_\gamma(\mu\nu\sigma;\rho)$ of the two-body residual interaction are diagrammatically defined in Fig. 2 of Part II.

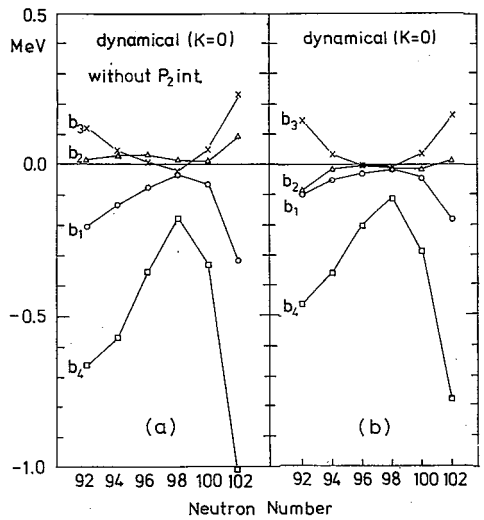

Fig. 1. Contributions of the dynamical anharmonicities arising from the couplings to the $K^\pi=0^+$ RPA modes to the coefficients of the fourth-order collective Hamiltonian for Er isotopes. In (a) the P_2 interaction is neglected, while (b) shows the result of full calculation. The $Q''Q''$ force strength κ and the pairing-force strength G_0 used in (a) are the same as in Fig. 4 of Part II.

$=0^+$ RPA modes. It is seen that the P_2 interaction systematically reduces the dynamical anharmonicities. We find similar reductions also for the dynamical anharmonicities due to the couplings to the $K^\pi=\pm4^+$ modes and for other nuclei. We note here that the effect (about 20% reduction) is not so strong as is expected from the simple estimation made above. This is because the orbit dependence of the *uv*-factors is strong in deformed nuclei so that the cancellation mechanism mentioned above is significantly diminished. The P_2 interaction not only affects the matrix elements V_Y but also modifies the *nv*-factors through the quadrupole pairing gap Δ_2. Of course, it also affects the RPA γ-vibrations, the RPA $K^\pi=0^+$ and $\pm4^+$ modes themselves. It should be noted that the effect of the P_2 interaction displayed in Fig. 1 results from the complicated combination of all these mechanisms. Thus, we have found that the P_2 interaction does not change the qualitative feature of the dynamical anharmonicity which is determined[8] by the $Q''Q''$ interaction.

4.2. *Effects on energy spectra and transition probabilities*

In discussing these effects, we must mention two kinds of ambiguity associated with the use of the P_2 interaction. The first ambiguity is that its strength is not definitely established although a large number of suggestions are available.[13)~21)] The second ambiguity is concerned with the deformation dependence of this interaction. In this connection, several authors[16),19)] employ the stretched quadrupole matrix elements for deformed nuclei, i.e., the ordinary quadrupole matrix elements appearing in $\hat{P}^{(\tau)\dagger}_{2K}$, Eq. (2·4), are replaced by the stretched ones $\langle\mu|(r^2Y_{2K})_{x_i\to x_i'}|\nu\rangle$ where $x_i'=(\omega_i/\omega_0)^{1/2}x_i$. Hereafter we abbreviate this stretched quadrupole-pairing interaction as P_2' interaction.

In order to estimate how the above-mentioned ambiguities of this interaction affect the calculated results, we perform the analysis for the following three cases; (a) the case where the P_2 interaction is neglected, (b) the case where the P_2 interaction is employed and (c) the case where the P_2' interaction is used. The force strength G_2 in Case (c) is fixed by the condition that it gives almost the same quadrupole-pairing gap Δ_2 as that in Case (b). We find that the prescription $G_2=(28\pi/3)R^{-4}G_0$ approximately satisfies this requirement and therefore we use this value in Case (c). The force strengths determined by the above prescription are, for instance, ($G_2^{(n)}$, $G_2^{(p)}$)

$=(0.00380, 0.00546)[\hbar\omega_0 b_0^{-4}]$ in Case (b) and (0.00696, 0.00967) in Case (c) for ^{166}Er. As $\hat{P}'^{\dagger}_{22}=(\omega_\perp/\omega_0)\hat{P}^{\dagger}_{22}\approx 1.1\hat{P}^{\dagger}_{22}$, Case (c) approximately corresponds to the calculation of Case (b) with the $K=2$ part of the P_2 interaction enhanced by about a factor of two.

Figure 2 compares the calculated excitation energies of the γ-vibrational states in ^{166}Er for the three cases mentioned above. This figure shows that the quadrupole-pairing interaction compresses the scale of the energy spectra. Similar effects on the low-lying quadrupole motions in transitional nuclei have been discussed by Kishimoto and Tamura.[9] We show in Table II the calculated coefficients of the Bohr-Mottelson-type collective Hamiltonian, Eq. (3·15). It is seen that the compression of the energy spectra is related to the increase of the collective mass parameter D. (Since the coefficients ε_1 and ε_2 are proportional to D by definition, their increase is a secondary effect.) This role of the quadrupole-pairing interaction is quite in contrast to that of the $Q''Q''$ interaction which mainly affects the collective potential. It is interesting to recall here that the quadrupole-pairing interaction increases also the rotational moment of inertia.[17)~19)]

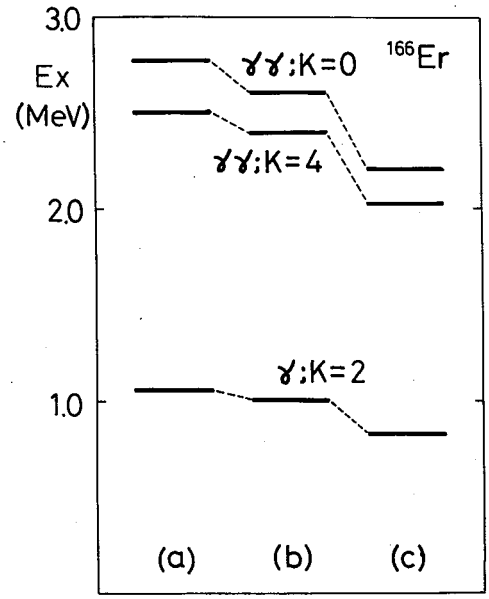

Fig. 2. Effects of the quadrupole-pairing interaction on the excitation energies of the single- and the double-γ vibrational states of ^{166}Er. The quadrupole-pairing interaction is neglected in (a), while the P_2 and the P_2' interactions are taken into account in (b) and (c), respectively. The $Q''Q''$ force strength is $\kappa=0.00510[\hbar\omega_0 b_0^{-4}]$.

Figure 3 shows calculated excitation energies of the double γ excited states, where the $Q''Q''$ force strengths κ are adjusted so as to reproduce the observed single-γ excitation energy. We see that the position of the $K=0$ double γ-vibrational state sensitively depends on the quadrupole-pairing interaction in comparison with that of the $K=4$ state. When the quadrupole-pairing interaction is neglected (Case (a)), we have to employ the $Q''Q''$ interaction with

Table II. Effects of the quadrupole-pairing interaction on the coefficients of the Bohr-Mottelson-type collective Hamiltonian, Eqs. (3·16) and (3·17):
(a) The result calculated with neglecting the P_2 force,
(b) the result calculated with including the P_2 force,
(c) the same as (b) except that the P_2' force is used instead of the P_2 force.
The parameters used in the numerical calculation are the same as in Fig. 2.

	D $[\hbar^2/\hbar\omega_0]$	C_2 $[\hbar\omega_0]$	C_4 $[\hbar\omega_0]$	ε_1	ε_2	ε_3 $[\hbar\omega_0]^{-1}$
(a)	299.	−7.67	73.5	−5.34	−5.51	−0.11
(b)	403.	−7.64	94.8	−7.09	−7.79	−0.03
(c)	521.	−7.98	94.4	−8.28	−9.63	0.05

Table III. Calculated $B(E2)$ values for ^{166}Er with various treatments of the quadrupole-pairing interaction. For the meaning of the notations (a), (b) and (c), see the caption to Table II. Numbers in the parentheses indicate the ratios to the $B(E2; 0_{gs}\to 2_\gamma)$. The parameters used in the numerical calculation are the same as in Fig. 3.

	$\frac{B(E2; 0_{gs}\to 2_\gamma)}{B_{sp}}$	$\frac{B(E2; 2_\gamma\to 4_{\gamma\gamma}(K=4))}{B_{sp}}$	$\frac{B(E2; 0_{\gamma\gamma}(K=0)\to 2_\gamma)}{B_{sp}}$
(a)	17.0	11.3 (0.66)	5.7 (0.34)
(b)	14.0	9.6 (0.68)	5.3 (0.38)
(c)	9.9	7.3 (0.74)	4.7 (0.47)

$$B_{sp}=2B_w=\frac{2}{4\pi}\left(\frac{3}{5}\right)^2\times R^4[e^2\mathrm{fm}^4],\ R=1.2A^{1/3}[\mathrm{fm}]\,.$$

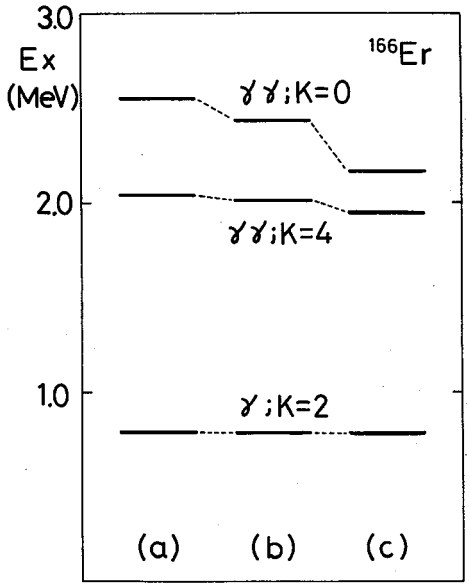

Fig. 3. Excitation energies of the double γ-vibrational states of ^{166}Er calculated with various treatment of the quadrupole-pairing interaction. For the meaning of the notations (a), (b) and (c), see the caption to Fig. 2. The $Q''Q''$ force strengths used are $\kappa=0.00543$, 0.00546 and $0.00518[\hbar\omega_0 b_0^{-4}]$ for (a), (b) and (c), respectively.

relatively large strength. Then, the anharmonicity of the double γ-vibrational state, especially the $K=0$ state, becomes stronger than Cases (b) and (c). We calculate the reduced $E2$ transition probabilities between the γ-vibrational states as (see Ref. 2))

$$\left.\begin{aligned} &B(E2; 0_{gs}\to 2_\gamma)\\ &\quad=2|\langle\gamma; 2|Q_{22}^{(\mathrm{charge})}|0; 0\rangle|^2\,,\\ &B(E2; 2_\gamma\to 4_{\gamma\gamma}(K=4))\\ &\quad=|\langle\gamma\gamma; 4|Q_{22}^{(\mathrm{charge})}|\gamma; 2\rangle|^2\,,\\ &B(E2; 0_{\gamma\gamma}(K=0)\to 2_\gamma)\\ &\quad=2|\langle\gamma; 2|Q_{22}^{(\mathrm{charge})}|\gamma\gamma; 0\rangle|^2 \end{aligned}\right\} \quad (4\cdot 2)$$

without using the effective charge. These three $B(E2)$ values coincide in the limit of harmonic vibration. Table III shows that the $B(E2)$ values associated with the single- and the double-γ excited states are reduced by the quadrupole-pairing interaction. The origin of this reduction is essentially the same as that known[25),26)] in the RPA description of the quadrupole states.

§ 5. Effects of the three-body interaction

We now investigate how the effective three-body interaction contributes to the mode-mode couplings between the γ-vibrational modes and the low-lying $K^\pi=0^+$ and $\pm 4^+$ modes. For this purpose, let us analyse the contribution of the three-body interaction, Eq. (2·3), to the coupling-source operators defined by Eq. (2·30) of Part II. It is easily seen that the three-body interaction contributes only to the coupling-source operator $\hat{V}_{q\bar{q}}$ for the $K^\pi=0^+$ modes:

$$\hat{V}_{q\bar{q}}^{3\text{-body}} = -\kappa_3 t_Q^2 \left\{ \hat{R}'' - \sqrt{\frac{16\pi}{5}} \hat{Q}_{20}'' \right\}, \tag{5·1}$$

where t_Q is defined by (II.4·6). It should be noted that the square-radius operator $\hat{R}''$ is approximately orthogonal to the $K^\pi=0^+$ RPA modes under consideration.*) Therefore the first term on the r.h.s. of this equation is not important, and the mode-mode coupling is mainly determined by the second term in the bracket of Eq. (5·1). Since it is proportional to the operator $\hat{Q}_{20}''$, we expect that the three-body interaction is effective to the couplings with the $K^\pi=0^+$ modes having β-vibrational character. The diagonal matrix elements of $\hat{V}^{3\text{-body}}$ are approximately written as

$$V_{q\bar{q}}^{3\text{-body}}(\mu\bar{\mu}) \approx -\kappa_3 t_Q^2 \sqrt{\frac{16\pi}{5}} {}^{Q}\mathcal{Y}_0(\mu\mu)\xi(\mu\mu), \tag{5·2}$$

where ${}^{Q}\mathcal{Y}_0(\mu\mu)=\langle\mu|(r^2Y_{20})''|\mu\rangle$ and $\xi(\mu\mu)=2u_\mu v_\mu$. We can qualitatively evaluate the effect of the three-body force on the mode-mode couplings as follows. Let us recall that, for prolate deformation, the larger the quadrupole moment of a single-particle orbit the smaller the single-particle energy becomes. Accordingly, the matrix element $V_{q\bar{q}}^{3\text{-body}}(\mu\bar{\mu})$ is positive (negative) when the single-particle orbit μ is located above (below) the Fermi surface. On the other hand, the contribution of the $Q''Q''$ interaction, $V_{q\bar{q}}^{Q_2Q_2}(\mu\bar{\mu})$, (II.4·16), is opposite in sign to that of $V_{q\bar{q}}^{3\text{-body}}(\mu\bar{\mu})$. As a result of this cancellation, the magnitude of the matrix elements of the coupling-source operator is reduced. Thus, the three-body interaction reduces the dynamical anharmonicity effect on the γ-vibration.

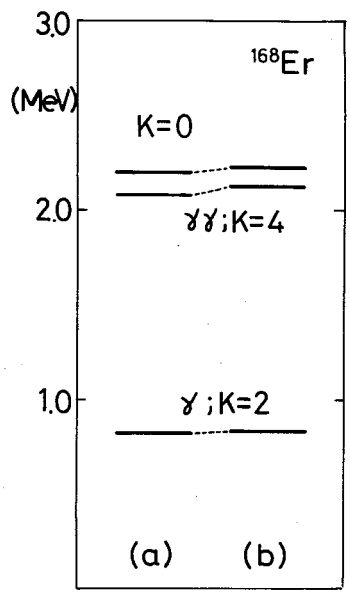

Fig. 4. Effects of the effective three-body force on the γ-vibrational excitation energies in ^{168}Er. The result of full calculation is shown in (a), while the three-body interaction is neglected in (b). The $Q''Q''$ force strength used is $\kappa=0.00546[\hbar\omega_0 b_0^{-4}]$.

By comparing Fig. 1(a) which takes into account the three-body interaction with Fig. 4(b) of Part II (where only the $P+Q''Q''$ interactions are used), we can examine the effect of the three-body interaction. It is found that the effect amounts to only about 20 % for the typical coefficient b_4. We found that situations are similar also for other nuclei. (Qualitatively, the effect varies from several percent to 30% depending on the nucleus.) This is because the three-body interaction mainly affects the couplings to the $K^\pi=0^+$ modes with β-vibrational character whose contributions to dynamical anharmonicity are relatively small parts of the whole.

Let us examine how the three-body

*) The operator $\hat{R}''$ has properties similar to the number operator, which corresponds to the pairing rotation and is orthogonal to the other $K^\pi=0^+$ RPA modes.

interaction affects the γ-vibrational spectra. Figure 4 shows the spectra for ^{168}Er calculated with and without taking into account the three-body interaction. As is expected from the consideration above, we see that the effect of the three-body interaction is in fact rather small. It should be stressed here, however, that this result does not imply that the three-body interaction is unimportant in general. Because of the symmetry property related to the K-quantum number, the collective Hamiltonian, Eq. (3·12), does not have the third-order terms which would be affected by the three-body force. There is a suggestion that the three-body force plays an important role in the third-order terms of the collective Hamiltonian describing the quadrupole motions in spherical and transitional nuclei.[27]

§ 6. (N, Z)-dependence of the anharmonic γ-vibration

It is expected from the analysis in Part II that the γ-vibration is quite sensitive to the subshell structure of the Nilsson diagram. Therefore, it is very important to investigate the (N, Z)-dependence of the anharmonic γ-vibration. For this purpose we perform numerical calculations for all stable even-even deformed nuclei in the rare-earth region (from Gd to Os isotopes).

In order to see the general characteristics of the (N, Z)-dependence, we first perform the calculation by using the $Q''Q''$ force strength κ having the standard mass-number dependence; $\kappa = f\kappa^{(\mathrm{self})}$, where $\kappa^{(\mathrm{self})} = 120A^{-7/3}\mathrm{MeV}\cdot\mathrm{fm}^{-4}$ and a constant $f=1.65$. Figure 5 shows the calculated RPA frequency ω_γ and the fourth-order anharmonicity coefficient b_4. The former is related to the second-order coefficients α and β of the collective Hamiltonian (3·12) through $\omega_\gamma{}^2 = \alpha^2 - \beta^2$ and the latter quantity is most sensitive to the dynamical anharmonicity effects. The strong (N, Z)-dependence of the coefficient b_4 is remarkable. In two regions, (i) $N \approx 98$, $Z \approx 68$ (Dy, Er) and (ii) $N \approx 112$, $Z \approx 76$, the absolute magnitude of the coefficient is relatively small. On the other hand, in the other regions it enhances considerably and becomes almost divergent in some cases. There are two origins of this behaviour. First, we should recall the subshell structure effect on the mode-mode coupling which was found in Part II. In the region (i), the neutron Fermi surface is located just in the middle of

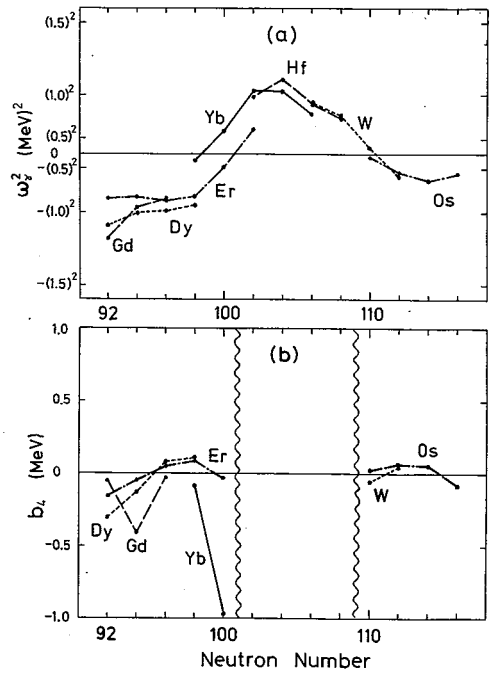

Fig. 5. (a) Squares of the excitation energies of the RPA γ-vibrations calculated for rare-earth deformed nuclei with the $Q''Q''$ force strength $\kappa = 1.65\,\kappa^{(\mathrm{self})}$. (b) Calculated fourth-order coefficients b_4 of the collective Hamiltonian. In the region between the two wavy lines, the coefficients exhibit a divergent behaviour.

the subshell $(N_{\rm osc}, n_3)=(5, 2)$ and, similarly, the proton subshell $(N_{\rm osc}, n_3)=(4, 2)$ is also partially occupied. In this situation, the couplings between the γ-vibrational modes and the $K^\pi=0^+$ RPA modes are rather weak. A similar situation occurs in the region (ii) with respect to neutron subshells $(N_{\rm osc}, n_3)=(5, 1)$ and $(5, 0)$ and the proton subshell $(N_{\rm osc}, n_3)=(4, 0)$. On the contrary, in the other region where the Fermi surface is located between different subshells the mode-mode couplings enhance. Consequently, the fourth-order coefficient b_4 becomes strongly (N, Z)-dependent. The other origin of the divergent behaviour in the region sandwitched between wavy lines in Fig. 5(b) is related to the "resonance problem". In this region, the neutron subshell $(N_{\rm osc}, n_3)=(5, 2)$ and the proton subshell (4, 2) are almost occupied and therefore the collectivity of the γ-vibrational mode is weak. On the other hand, as was discussed in Part II, the fourth-order coefficients of the collective Hamiltonian include the energy denominator $1/(\omega_\lambda-2\omega_\gamma)$ where ω_λ is the RPA frequency of the $K^\pi=0^+$ or $\pm4^+$ modes. Therefore, the coefficients become unphysically large when the RPA frequency ω_γ approximately satisfies the resonance condition $2\omega_\gamma=\omega_\lambda$. When $\omega_\gamma>\Delta_0$, this resonance problem occurs rather generally, because the level density of the $K^\pi=0^+$ and $\pm4^+$ RPA modes is high in the energy region greater than $2\Delta_0$. As is seen in Fig. 5(a), this situation actually occurs in the region between the two wavy lines in Fig. 5(b) where the collectivity of the γ-vibration is weak. Because of the problem mentioned above, it would be safe to restrict the application of our theoretical framework to nuclei which have strong collectivity and where the RPA frequency ω_γ is very small or imaginary. These nuclei are just those most interesting to us.

In order to quantitatively investigate the anharmonic γ-vibration in each nucleus, we next perform the calculation by using the $Q''Q''$ force strength which reproduces the observed single-γ excitation energy. Figures 6 and 7 and Table IV display the calculated results for nuclei for which the collective Hamiltonian reproducing the experimental single-γ excitation energies are successfully constructed. In Gd~Er region with $92\lesssim N\lesssim94$, we could not find such κ values within a reasonable range because the mode-mode coupling effects become too strong. It should be remarked also that the predictions for the Os region are not as reliable as those for Dy~Er region because of the following reason. The Os isotopes belong to the γ-unstable nuclei where the γ-degree are not necessarily bound to the nearby region of $\gamma=0$, whereas our formalism is based on the fourth-order (η^*, η)-expansion with the boundary condition at the prolate BCS ground state. Thus, in the following,

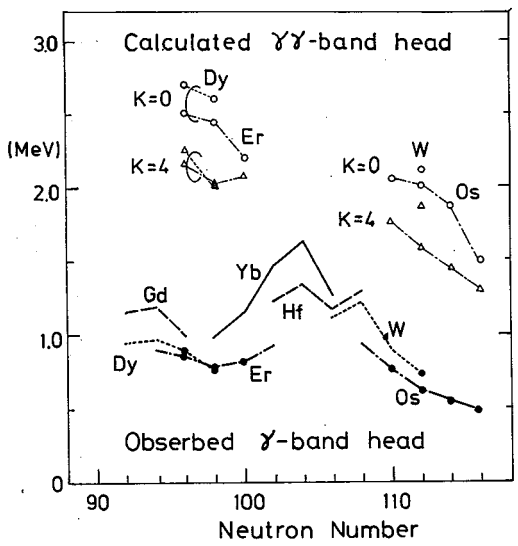

Fig. 6. Predicted excitation energies of the double γ-vibrational states. The $Q''Q''$ force strength is chosen to reproduce the observed single γ-excitation energy in each nucleus, which is also plotted in this figure.

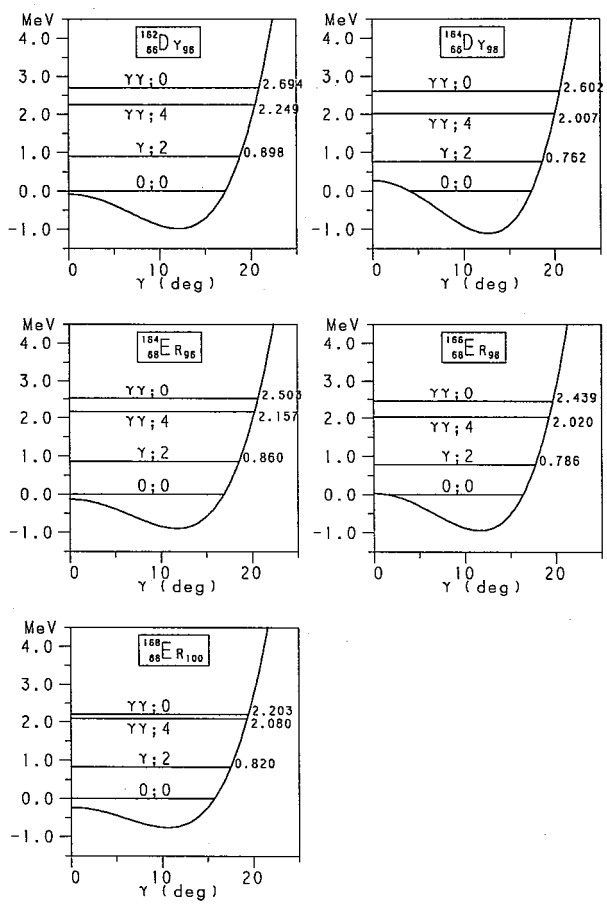

Fig. 7. Calculated collective potentials and predicted γ-vibrational spectra for Dy and Er isotopes.

Table IV. Calculated excitation energies and the $B(E2)$ values of the double γ-vibrational states. Adopted $Q''Q''$ force strengths are listed in the rightmost column in units of the selfconsistent value $\kappa^{(\mathrm{self})}=120A^{-7/3}[\mathrm{MeV}\cdot\mathrm{fm}^{-4}]$.

	$E(\gamma\gamma;K)$ [MeV]		$E(\gamma\gamma;K)/E(\gamma)$		$\frac{B(E2;0_{gs}\to 2_\gamma)}{B_{sp}}$	$\frac{B(E2;2_\gamma\to 4_{\gamma\gamma})}{B(E2;0_{gs}\to 2_\gamma)}$	$\frac{B(E2;0_{\gamma\gamma}\to 2_\gamma)}{B(E2;0_{gs}\to 2_\gamma)}$	$\kappa/\kappa^{(\mathrm{self})}$
	$K=4$	$K=0$	$K=4$	$K=0$				
^{162}Dy	2.248	2.694	2.50	3.00	14.1	0.67	0.37	1.64
^{164}Dy	2.007	2.602	2.64	3.42	15.8	0.66	0.33	1.70
^{164}Er	2.157	2.503	2.51	2.91	13.9	0.68	0.37	1.63
^{166}Er	2.021	2.079	2.57	3.10	14.1	0.68	0.38	1.67
^{168}Er	2.080	2.203	2.54	2.69	11.1	0.68	0.25	1.65
^{186}W	1.871	2.121	2.53	2.87	12.2	0.75	0.43	1.64
^{186}Os	1.770	2.057	2.30	2.68	15.7	0.72	0.43	1.65
^{188}Os	1.589	2.013	2.51	3.18	17.9	0.70	0.39	1.68
^{190}Os	1.464	1.876	2.63	3.37	17.9	0.68	0.37	1.68
^{192}Os	1.313	1.513	2.69	3.10	17.0	0.68	0.34	1.66

we focus our discussion on the Dy~Er region.

Calculated collective potentials for these nuclei, shown in Fig. 7, have a common feature that is characteristic to nuclei lying in the transitional region between the axial symmetric prolate deformation and the triaxial equilibrium deformation. We also notice in Fig. 6 that excitation energy of the $K=0$ double-γ vibrational state exhibits remarkable (N, Z)-dependence. The ratio $E(\gamma\gamma; K)/E(\gamma)$ for the $K=0$ state varies from 2.69 to 3.42 depending on the nucleus (see Table IV). On the other hand the ratio for the $K=4$ double-γ vibrational state depends on (N, Z) only weakly. We can see in Table IV a similar behaviour also for the $B(E2)$ ratios. In contrast to the almost constant value (≈ 0.67) for the $K=4$ states, the $B(E2)$ ratio for the $K=0$ states remarkably changes from one nucleus to another. Such behaviours are evidently caused by the strong (N, Z)-dependence of the dynamical anharmonicity effects which we have seen in Fig. 6.

By comparing Fig. 7 with Fig. 12 of Part II, we can see that the property of the potential energy function and the predicted excitation spectra for ^{168}Er are almost the same between the two calculations.

§ 7. Concluding remarks

In this paper, Part III, we have first improved our calculation made in Part II for anharmonic γ-vibrations in the following two points. 1) The conservation of average nucleon number is guaranteed by taking into account the couplings between the γ-vibrations and the pairing rotational modes. 2) The quadrupole-pairing and the effective three-body forces are taken into account in addition to the $P+Q''Q''$ force. We have examined that the coupling effects with the pairing rotations are small for the anharmonic γ-vibrational modes under consideration. We have also found that the dynamical anharmonicities resulting from both the quadrupole-pairing and the effective three-body interactions are small in comparison with those resulting from the $Q''Q''$ interaction. Hence the characteristic properties of the mode-mode couplings discussed in Part II again hold also when the improved model Hamiltonian (2·1) is employed.

We have next performed a systematic analysis of the properties of the anharmonic γ motions over a wide region of the rare-earth nuclei. Since the collective variables in the selfconsistent-collective-coordinate method is defined dynamically not only in the small-amplitude (RPA) limit but also in the large-amplitude region, the internal structure of the collective variables develops depending on the amplitude of the collective motion. The structure change is caused by the mode-mode couplings between different kinds of the RPA normal modes. The dynamical anharmonicity effects associated with the γ-vibration are found to change considerably from nucleus to nucleus reflecting the subshell structure of the Nilsson orbits. In the Dy~Er region with $Z\approx 66$ and $N\approx 98$ and in the W~Os region with $Z\approx 76$ and $N\approx 112$, the dynamical anharmonicities manifest themselves as the characteristic (N, Z)-dependence of the $K=0$ double γ-vibrational states. For nuclei outside of the two regions, however, the mode-mode couplings become extremely strong so that we could not construct a physically meaningful fourth-order collective Hamiltonian.

In Part II and in this paper, we have definitely seen a growth of a simple regularity in the complicated anharmonicity effects. Namely, the tendency toward the triaxial equilibrium shape and the characteristics of the γ motions associated with such systems develop as the strength of the $Q''Q''$ force increases, and this tendency is enhanced by the dynamical anharmonicity effects. Thus, we can say that the microscopic model, which is based on the SCC method and developed in this series of paper, successfully incorporates some basic ingredients of non-linear dynamics associated with the anharmonic γ-vibrations.

We have presented theoretical predictions for the properties of the anharmonic γ-vibrations in nuclei for which our microscopic calculations have been successfully performed. We have found that the position of the $K^\pi=0^+$ double γ-vibrational state is particularly sensitive to the dynamical anharmonicity effects. It is thus especially desired to experimentally identify the double γ-vibrational states in order to check the accuracy of the theoretical predictions for Dy and Er isotopes.

Besides the successful cases, we have also suggested two situations for which we need to improve our theoretical framework. In the first case, the mode-mode couplings are too strong so that the magnitudes of the fourth-order coefficients of the collective Hamiltonian become too large. In the second case, the resonance problem between the RPA γ-vibrations and the other $K^\pi=0^+, \pm 4^+$ modes occurs. In both cases, the (η^*, η) expansion in its present form might diverge. These difficult problems may be intimately connected with the stability of the collective submanifold extracted by the (η^*, η) expansion method, and remain as a challenging future subject. It is of course instructive to learn in experiment what the actual situations are in nuclei for which we have encountered the theoretical problem mentioned above.

Acknowledgements

We thank Dr. H. Sakamoto for fruitful discussions on the effective three-body interaction. The computer calculation for this work has been supported in part by the Research Center for Nuclear Physics, Osaka University.

References

1) W. F. Davidson et al., J. of Phys. **G7** (1981), 455, 843.
2) A. Bohr and B. R. Mottelson, Physica Scripta **25** (1982), 28.
3) T. S. Dumitrescu and I. Hamamoto, Nucl. Phys. **A383** (1982), 205.
4) V. G. Soloviev and N. Yu. Shirikova, Z. Phys. **A301** (1981), 263; Yadern. Fiz. **36** (1982), 1376 [Sov. J. Nucl. Phys. **36** (1982), 799].
V. G. Soloviev, Pis'ma Zh. Eksp. Teor. Fiz. **40** (1984), 398 [JETP Lett. **40** (1984), 1216].
5) N. Yoshinaga, Y. Akiyama and A. Arima, Phys. Rev. Lett. **17** (1986), 1116.
6) M. Matsuo and K. Matsuyanagi, Prog. Theor. Phys. **74** (1985), 1227.
7) T. Marumori, T. Maskawa, F. Sakata and A. Kuriyama, Prog. Theor. Phys. **64** (1980), 1294.
8) M. Matsuo and K. Matsuyanagi, Prog. Theor. Phys. **76** (1986), 93.
9) T. Kishimoto and T. Tamura, Nucl. Phys. **A270** (1976), 317.
10) K. Takada and S. Tazaki, Nucl. Phys. **A448** (1986), 56.
11) T. Kishimoto, *Proc. 1980 RCNP Int. Symp. Highly Excited States in Nuclear Reactions, Osaka,* p. 145.
12) M. Matsuo, Prog. Theor. Phys. **76** (1986), 372.
13) D. R. Bes and R. A. Broglia, Phys. Rev. **C3** (1971), 2349.
14) R. A. Broglia, D. R. Bes and B. S. Nilsson, Phys. Lett. **50B** (1974), 213.

15) D. R. Bes, R. A. Broglia and B. Nilsson, Phys. Lett. **40B** (1972), 338.
16) I. Ragnarsson and R. A. Broglia, Nucl. Phys. **A263** (1976), 315.
17) M. Wakai and A. Faessler, Nucl. Phys. **A295** (1978), 86.
18) I. Hamamoto, Nucl. Phys. **A232** (1974), 445.
19) M. Diebel, Nucl. Phys. **A419** (1984), 221.
20) J. D. Garrett et al., Phys. Lett. **118B** (1982), 297.
21) J. C. Bacelar et al., Phys. Lett. **152B** (1985), 157.
22) K. Andō, H. Bandō and S. Nagata, Prog. Theor. Phys. **52** (1974), 928.
23) T. Kishimoto et al., Phys. Rev. Lett. **35** (1975), 552.
24) A. Bohr and B. R. Mottelson, *Nuclear Structure* (Benjamin, 1975), vol. 2.
25) D. R. Bes, G. G. Dussel and J. Gratton, *Proc. Int. Nucl. Phys. Conf. 1966, Gatlinburg,* ed. R. L. Becker (Academic Press, New York).
26) H. Bandō, Prog. Theor. Phys. **36** (1966), 551.
27) H. Sakamoto, private communication.

Progress of Theoretical Physics, Vol. 79, No. 4, April 1988

Quasiparticle-Vibration Couplings in Rotating Triaxial Odd-A Nuclei

Masayuki MATSUZAKI, Yoshifumi R. SHIMIZU*
and Kenichi MATSUYANAGI

Department of Physics, Kyoto University, Kyoto 606
**Department of Physics, Kyushu University, Fukuoka 812*

(Received October 19, 1987)

A new microscopic model which takes into account both the static and dynamic triaxial deformations in the high-spin states of odd-A nuclei is developed. The model is based on the rotating shell model and treats the quasiparticle-vibration couplings in the uniformly rotating frame of reference. Effects of the static and dynamic triaxial deformations on the signature splitting of the quasiparticle energies and on the signature dependence of $B(M1)$, $B(E2; I \to I-1)$ and $B(E2; I \to I-2)$ for the transitions within the unique-parity bands in odd-A nuclei are discussed. Numerical examples are presented for odd-Z nuclei ^{157}Ho, ^{159}Tm and ^{161,165}Lu, and for odd-N nuclei ^{161}Dy, ^{167}Er and ^{161,163,167}Yb to which experimental data for $B(M1)$ and $B(E2)$ are available.

§ 1. Introduction

The main purpose of this paper is to extend the traditional quasiparticle-vibration coupling model for non-rotating nuclei[1),2)] into the case of rapidly rotating nuclei by formulating it in the reference frame which is uniformly rotating with rotational frequency $\omega_{\rm rot}$. It is intended to use this model for analyzing the dynamical interplay in odd-A nuclei between aligned quasiparticle excitations and vibrational excitations in the near-yrast region with large angular momentum. In this paper, among the various vibrational modes, we focus our attention on the "gamma" vibrations which represent dynamical shape fluctuations in the gamma degree of freedom. Since we treat odd-A nuclei whose equilibrium shapes are (in general) triaxial and which are rotating, the "gamma" vibrational modes do not have definite K quantum number and may contain the components corresponding to the wobbling modes[3)] characteristic to nuclei having static triaxial shapes. We, therefore, call these vibrations "generalized-gamma vibrations" in order to distinguish them from the familiar gamma vibrations with $K=\pm 2$ which represent the shape fluctuations away from the axially symmetric equilibrium shape.

The motive for developing this model lies in the recent experimental progress[4)~13)] in measuring both the stretched and non-stretched $E2$ transition probabilities as well as the $M1$ transitions between very high-spin states in odd-A nuclei in the rare-earth region. As was pointed out by Hamamoto and Mottelson,[14),15)] these experimental data contain information useful to identify the static and dynamic triaxial deformations and their relations to rapid rotations.

Our model is based on the rotating shell model (RSM)[16),17)] which is an extension of the familiar cranked shell model[18),19)] in that the variation of the pairing gap Δ and the deformation parameters (β, γ) as functions of $\omega_{\rm rot}$ is taken into account for each

rotational band. One of the merits of our microscopic approach is that it can be easily applied to high-spin states involving many aligned quasiparticles. On the other hand, its main limitation is that the generalized-gamma vibrations are treated within the small-amplitude approximation of the RPA. Thus, our microscopic model may be best suited to the description of rotational bands in the near-yrast region of odd-A nuclei which have rather stable minimum somewhere in the (β, γ) plane.

The formulation of our model consists of the following four steps:

1) Our first task is to construct a diabatic quasiparticle representation for a deformed single-particle potential which is uniformly rotating about the x-axis with rotational frequency $\omega_{\rm rot}$. The diabatic basis for the RSM enables us to unambiguously specify individual rotational bands in which internal structures of the quasiparticle state vectors smoothly change as functions of $\omega_{\rm rot}$.[19]

2) The residual interactions between quasiparticles are treated by means of the RPA in the rotating frame. This step determines the normal modes of vibration in even-even nuclei.

3) Then we treat the couplings in odd-A nuclei between the aligned quasiparticles and the generalized-gamma vibrations (obtained above) in the same manner as in the traditional quasiparticle-vibration coupling models.[1),2)]

4) The most crucial point of our approach is the treatment of the "Nambu-Goldstone modes", $\Gamma^\dagger$ and Γ, in the RPA, which reorient the angular momentum of the collective rotation. We extend Marshalek's prescription[20] into odd-A nuclei and replace these modes with the exact angular-momentum operators. This replacement corresponds to the fact that the state vectors in the laboratory frame are constructed in a direct product form of the rotational and the internal wave function in just the same manner as in the well-known particle-rotor model.[3] Thus, our model may also be regarded as a particular version of the particle-rotor model, in which the basis of the internal state vectors is determined by the RSM as a function of $\omega_{\rm rot}$.

Details of the formulation in each step mentioned above are given in § 2. In this section, we also give microscopic expressions for the intrinsic $E2$ and $M1$ operators. These formulae may be useful to the analysis of 1) the effects of static and dynamic triaxial deformations on the $B(E2)$ values with $\Delta I=1$ which connect the favoured bands to the unfavoured bands (and v.v.), and 2) the effects of aligned quasiparticles on $B(M1)$ values. Details of the computational procedure are described in § 3. Some typical results of numerical calculation are presented in § 4 for 1) nuclei with the $h_{11/2}$ odd protons and 2) nuclei with the $i_{13/2}$ odd neutrons. Concluding remarks are given in § 5.

§ 2. Formulation of model

2.1. *Diabatic quasiparticle basis for use in the rotating shell model*

We start from a single-particle potential $\hat{h}_{\rm sp}$ which is deformed with respect to both the pairing and the quadrupole degrees of freedom:

$$\hat{h}_{\rm sp}=\hat{h}_{\rm def}-\Delta(\hat{P}^\dagger+\hat{P})-\lambda\hat{N}\,, \tag{2·1}$$

where $\hat{h}_{\rm def}$ is the modified-harmonic-oscillator potential defined by

$$\hat{h}_{\rm def}=\hat{h}_{\rm sph}(\boldsymbol{x}\to\tilde{\boldsymbol{x}},\boldsymbol{p}), \tag{2·2}$$

$$\hat{h}_{\rm sph}=\sum_{n=1}^{A}\left\{\frac{\boldsymbol{p}^2}{2M}+\frac{1}{2}M\omega_0{}^2\boldsymbol{x}^2+v_{ls}\boldsymbol{l}\cdot\boldsymbol{s}+v_{ll}(\boldsymbol{l}^2-\langle\boldsymbol{l}^2\rangle_N)\right\}_n. \tag{2·3}$$

Here, $\hat{P}$ and $\hat{N}$ are the conventional nucleon-pair and nucleon-number operators, respectively. They are treated separately for protons and neutrons. In Eq. (2·2) the notation $\boldsymbol{x}\to\tilde{\boldsymbol{x}}$ means that the coordinates $x_i(i=1, 2, 3)$ are replaced by the doubly stretched coordinates $\tilde{x}_i\equiv(\omega_i/\omega_0)x_i$. We consider triaxial quadrupole deformations so that the frequencies ω_i with $i=1, 2$ and 3 of the modified-harmonic-oscillator are not equal in general.

Let us consider a situation where the nucleus is uniformly rotating with rotational frequency $\omega_{\rm rot}$ about the x-axis (the 1st axis) defined with respect to the single-particle potential $\hat{h}_{\rm sp}$. To describe such a uniformly rotating nucleus, we consider a time-dependent state vector which has a form familiar in the Hartree-Bogoliubov theory:

$$|\phi(I,\theta)\rangle=e^{-i\theta\hat{J}_x}e^{i\hat{G}}|\phi_0\rangle, \tag{2·4}$$

where $|\phi_0\rangle$ is the BCS ground state for $\hat{h}_{\rm sp}$ and $\theta=\omega_{\rm rot}t$. We expand the unknown one-body operator $\hat{G}$ in a power series of $\omega_{\rm rot}$, i.e.,

$$\hat{G}=\hat{G}^{(0)}+\omega_{\rm rot}\hat{G}^{(1)}+\omega_{\rm rot}^2\hat{G}^{(2)}+\cdots, \tag{2·5}$$

and successively determine $\hat{G}^{(n)}$ so as to satisfy the following basic equations:

$$\text{(i)}\quad I=-\frac{\partial\mathcal{H}'}{\partial\omega_{\rm rot}}$$

$$\text{with}\quad \mathcal{H}'=\langle\phi_0|e^{-i\hat{G}}(\hat{h}_{\rm sp}-\omega_{\rm rot}\hat{J}_x)e^{i\hat{G}}|\phi_0\rangle, \tag{2·6}$$

$$\text{(ii)}\quad \delta\langle\phi_0|e^{-i\hat{G}}(\hat{h}_{\rm sp}-\omega_{\rm rot}\hat{J}_x)e^{i\hat{G}}|\phi_0\rangle=0, \tag{2·7}$$

$$\text{(iii)}\quad \left.\begin{aligned}&\langle\phi_0|e^{-i\hat{G}}\hat{J}_xe^{i\hat{G}}|\phi_0\rangle=I,\\&\langle\phi_0|e^{-i\hat{G}}\frac{\partial}{\partial\omega_{\rm rot}}e^{i\hat{G}}|\phi_0\rangle=0.\end{aligned}\right\} \tag{2·8}$$

The above basic equations are derived by applying the selfconsistent-collective-coordinate method[21] to the particular problem under consideration. A method of solving this set of equations is described in detail in Ref. 22) (see also Ref. 23)). It is found[23] that a cutoff of the $\omega_{\rm rot}$-expansion in Eq. (2·5) results in a diabatic level diagram (in place of the adiabatic one) for the quasiparticle energies in the rotating frame. As is well known, the diabatic basis enables us to unambiguously specify individual rotational bands whose internal wave functions smoothly change as functions of $\omega_{\rm rot}$.[19] In this way, we obtain a single-particle Hamiltonian $\hat{h}'_{\rm sp}$ describing independent quasiparticle motions in the deformed potential $\hat{h}_{\rm sp}$ which is now rotating with the rotational frequency $\omega_{\rm rot}$:

$$\hat{h}'_{\rm sp}={\rm const}+\sum_{\mu}E_\mu a_\mu^\dagger a_\mu+\sum_{\bar{\mu}}E_{\bar{\mu}}a_{\bar{\mu}}^\dagger a_{\bar{\mu}}, \tag{2·9}$$

where $(a_\mu^\dagger, a_\mu)$ and $(a_{\bar{\mu}}^\dagger, a_{\bar{\mu}})$ are the diabatic quasiparticle creation and annihilation operators with signature $\alpha=1/2$ ($r\equiv e^{-i\pi\alpha}=-i$) and $\alpha=-1/2$ ($r=+i$), respectively. They are determined, together with their energies E_μ and $E_{\bar{\mu}}$, as smooth functions of $\omega_{\rm rot}$.*)

To describe individual rotational bands, we have to carefully identify the quasiparticle configurations across the band-crossing region such that their internal structures smoothly change as functions of $\omega_{\rm rot}$. This is done in the following way. Let us denote the quasiparticles defined with respect to the yrast configuration $|\phi_{\rm y}\rangle$ by $(\mathring{a}_\mu^\dagger, \mathring{a}_{\bar{\nu}}^\dagger)$; i.e.,

$$\mathring{a}_\mu|\phi_{\rm y}\rangle=\mathring{a}_{\bar{\nu}}|\phi_{\rm y}\rangle=0\,, \tag{2·10}$$

where $|\phi_{\rm y}\rangle$ is constructed to be the lowest-energy configuration at a given value of $\omega_{\rm rot}$. Then, the quasiparticle configurations describing individual rotational bands take in general the following form:

$$|\phi_{\rm band}\rangle=\Big(\prod_{\mu=1}^{n_+}\mathring{a}_\mu^\dagger\Big)\Big(\prod_{\bar{\nu}=1}^{n_-}\mathring{a}_{\bar{\nu}}^\dagger\Big)|\phi_{\rm y}\rangle \quad \text{for } \omega_{\rm cri}^{(i)}<\omega_{\rm rot}<\omega_{\rm cri}^{(j)}\,. \tag{2·11}$$

Note that the explicit form of $|\phi_{\rm band}\rangle$ changes whenever the rotational band under consideration crosses with another band; for instance, the configuration corresponding to the g-band changes as

$$|\phi_g\rangle=\begin{cases} |\phi_{\rm y}\rangle\,, & 0\le\omega_{\rm rot}\le\omega_{\rm cri}^{(1)}\,,\\ \mathring{a}_A^\dagger\mathring{a}_{\bar{B}}^\dagger|\phi_{\rm y}\rangle\,, & \omega_{\rm cri}^{(1)}\le\omega_{\rm rot}\le\omega_{\rm cri}^{(2)}\,,\\ \mathring{a}_A^\dagger\mathring{a}_{\bar{D}}^\dagger|\phi_{\rm y}\rangle\,, & \omega_{\rm cri}^{(2)}\le\omega_{\rm rot}\le\omega_{\rm cri}^{(3)}\,,\\ \cdots & . \end{cases} \tag{2·12}$$

On the other hand, the configuration for the s-band changes as

$$|\phi_s\rangle=\begin{cases} \mathring{a}_A^\dagger\mathring{a}_{\bar{B}}^\dagger|\phi_{\rm y}\rangle\,, & 0\le\omega_{\rm rot}\le\omega_{\rm cri}^{(1)}\,,\\ |\phi_{\rm y}\rangle\,, & \omega_{\rm cri}^{(1)}\le\omega_{\rm rot}\le\omega_{\rm cri}^{(4)}\,,\\ \cdots & . \end{cases} \tag{2·13}$$

Here the suffices A, B, $\cdots$ are the familiar notations[24] labelling the quasiparticle states with unique-parity.

The equilibrium deformations are determined as functions of $\omega_{\rm rot}$ for each rotational band in even-even nuclei to simultaneously satisfy the following self-consistency conditions:

$$G\langle\phi_{\rm band}|\hat{P}|\phi_{\rm band}\rangle=\Delta\,,\qquad \langle\phi_{\rm band}|\hat{N}|\phi_{\rm band}\rangle=N$$
$$\text{for both protons and neutrons}\,, \tag{2·14}$$

$$(\omega_1^{\rm eff})^2\langle\phi_{\rm band}|\sum_{n=1}^{A}(x_1)_n{}^2|\phi_{\rm band}\rangle=(\omega_2^{\rm eff})^2\langle\phi_{\rm band}|\sum_{n=1}^{A}(x_2)_n{}^2|\phi_{\rm band}\rangle$$
$$=(\omega_3^{\rm eff})^2\langle\phi_{\rm band}|\sum_{n=1}^{A}(x_3)_n{}^2|\phi_{\rm band}\rangle\,, \tag{2·15}$$

*) Their precise definitions are given by Eq. (2·19) below.

under the volume-conservation condition $\omega_1^{\rm eff}\omega_2^{\rm eff}\omega_3^{\rm eff}=\omega_0^3$, where $\omega_i^{\rm eff}=\sqrt{\omega_i^2-\omega_{\rm rot}^2}$ for $i=2$ and 3, and $\omega_1^{\rm eff}=\omega_1$. Equation (2·15) results from the semiclassical requirement that the velocity distribution in the rotating frame be isotropic in average.[25] This equation determines the frequency ω_i of the potential, from which the ordinary deformation parameters (β, γ) are immediately obtained.[25]

In this way, we obtain the diabatic quasiparticle representation whose equilibrium deformations are selfconsistently determined as functions of $\omega_{\rm rot}$.

2.2. *The RPA in the uniformly rotating frame*

The residual interactions that are consistent, in the sense of the Landau-Migdal theory, with the single-particle Hamiltonian (2·9) are given by

$$\hat{H}_{\rm int}=\hat{H}_{\rm P}+\hat{H}_{\rm QQ}\,, \tag{2·16}$$

$$\hat{H}_{\rm P}=-G\tilde{P}^{\dagger}\tilde{P} \qquad \text{for both protons and neutrons}\,, \tag{2·17}$$

$$\hat{H}_{\rm QQ}=-\frac{1}{2}\sum_{K=0,1,2}\kappa_K^{(+)}\tilde{Q}_K^{(+)\dagger}\tilde{Q}_K^{(+)}-\frac{1}{2}\sum_{K=1,2}\kappa_K^{(-)}\tilde{Q}_K^{(-)\dagger}\tilde{Q}_K^{(-)}\,, \tag{2·18}$$

where $\tilde{P}\equiv\hat{P}-\langle\phi_{\rm band}|\hat{P}|\phi_{\rm band}\rangle$ and $\tilde{Q}_K^{(\pm)}$ are the quadrupole operators that are defined in terms of the doubly stretched coordinates x_i'' associated with the rotating deformed potential, i.e., $x_i''\equiv(\omega_i^{\rm eff}/\omega_0)x_i$. At the equilibrium deformation where Eq. (2·15) holds, we have the properties $\langle\tilde{Q}_K^{(\pm)}\rangle=0$ for all K.

To describe vibrational excitations built on a given rotational band $|\phi_{\rm band}\rangle$ in even-even nuclei, it is convenient to use the quasiparticle operators $(a_\mu^\dagger, a_{\bar\nu}^\dagger)$ defined with respect to this band:

$$\begin{aligned} &a_\mu|\phi_{\rm band}\rangle=0\,; \qquad \mu=1, 2, \cdots, \Omega-n_{\rm B}\,,\\ &a_{\bar\nu}|\phi_{\rm band}\rangle=0\,; \qquad \bar\nu=1, 2, \cdots, \Omega+n_{\rm B}\,, \end{aligned} \tag{2·19}$$

where $n_{\rm B}$ is the blocking number of this band. These new quasiparticle operators are obtained from those defined by Eq. (2·10) through the following procedure.[16),17] Let 2Ω be the total number of single-particle states. Then, as is well known, the Hartree-Bogoliubov equation has 4Ω solutions. If we identify Ω positive-energy solutions as physical solutions for both signature sectors ($\alpha=1/2$ and $-1/2$), the quasiparticle vacuum coincides with the yrast configuration. Let $(n_\mu, n_{\bar\nu})$ be the occupation numbers of the quasiparticles $(\mathring{a}_\mu^\dagger, \mathring{a}_{\bar\nu}^\dagger)$ in the configuration $|\phi_{\rm band}\rangle$. Then the quasiparticle operators defined by (2·19) are obtained from the original quasiparticles by the following replacements:

$$\left.\begin{aligned} &(-E_\mu,\ \boldsymbol{V}_\mu,\ \boldsymbol{U}_\mu)\longrightarrow(E_{\overline{\Omega+\mu}},\ \bar{\boldsymbol{U}}_{\Omega+\mu},\ \bar{\boldsymbol{V}}_{\Omega+\mu})\,,\\ &(-E_{\bar\nu},\ \bar{\boldsymbol{V}}_\nu,\ \bar{\boldsymbol{U}}_\nu)\longrightarrow(E_{\Omega+\nu},\ \boldsymbol{U}_{\Omega+\nu},\ \boldsymbol{V}_{\Omega+\nu}) \end{aligned}\right\} \tag{2·20}$$

for the states with $n_\mu=1$ and $n_{\bar\nu}=1$, respectively. The other states with $n_\mu=n_{\bar\nu}=0$ remain the same. Thus, the annihilation operators $\mathring{a}_\mu(\mathring{a}_{\bar\nu})$ for the states with $n_\mu=1$ $(n_{\bar\nu}=1)$ are now replaced by the creation operators $a_{\overline{\Omega+\mu}}^\dagger(a_{\Omega+\nu}^\dagger)$ with negative energies and with opposite signature.

The RPA excitation operators $X_n^{(\pm)\dagger}$ are constructed in terms of the new quasiparticle operators as

$$X_n^{(\pm)\dagger}=\sum_{(\alpha\beta)}\{\psi_n^{(\pm)}(\alpha\beta)a_\alpha^\dagger a_\beta^\dagger+\varphi_n^{(\pm)}(\alpha\beta)a_\beta a_\alpha\}\,, \tag{2·21}$$

where $(\alpha\beta)=(\mu\bar{\nu})$ for the $\alpha=0$ $(r=+1)$ sector, and $(\alpha\beta)=(\mu\nu)$ or $(\bar{\mu}\bar{\nu})$ for the $\alpha=1$ $(r=-1)$ sector. The excitation energies $\hbar\omega_n^{(\pm)}$ and the amplitudes, $\psi_n^{(\pm)}(\alpha\beta)$ and $\varphi_n^{(\pm)}(\alpha\beta)$, are determined by solving the RPA equation of motion $[\hat{h}'_{\rm sp}+\hat{H}_{\rm int}, X_n^{(\pm)\dagger}]_{\rm RPA}=\hbar\omega_n^{(\pm)}X_n^{(\pm)\dagger}$ and by the normalization condition $\langle\phi_{\rm band}|[X_n^{(\pm)}, X_{n'}^{(\pm)\dagger}]|\phi_{\rm band}\rangle=\delta_{nn'}$. In this way, we obtain normal modes of vibration built on a given rotational band $|\phi_{\rm band}\rangle$.

2.3. *Quasiparticle-vibration couplings in the rotating frame*

For the description of rotational bands in odd-A nuclei, it is always possible to adopt a basis constituted by one-quasiparticle excitations from rotational bands of even-even nuclei. Namely, the basic state vectors of the rotating shell model can be always written in the form $a_\mu^\dagger|\phi_{\rm band}\rangle$, where the quasiparticle operators and their vacuum $|\phi_{\rm band}\rangle$ are defined by Eq. (2·19). We now consider the couplings between the quasiparticles $a_\mu^\dagger$ and the RPA normal modes $X_n^{(\pm)\dagger}$ defined by Eq. (2·21) with respect to the rotational bands in even-even nuclei (see Fig. 1). Following essentially the same procedure as in the well-known quasiparticle-vibration coupling models for non-rotating nuclei,[1),2)] we can derive from the original Hamiltonian, $\hat{H}'=\hat{h}'_{\rm sp}+\hat{H}_{\rm int}$, an effective Hamiltonian for odd-A nuclei in the rotating frame:

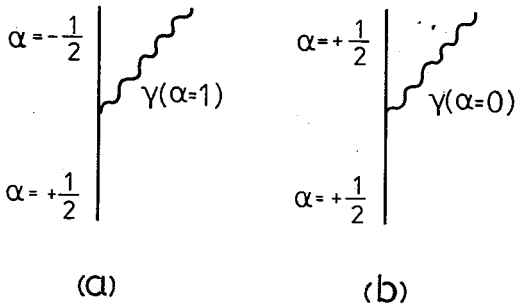

Fig. 1. Diagrammatic illustrations of the couplings between the quasiparticles (solid lines) and the generalized-gamma vibrations (wavy lines). The signatures α of these modes are indicated.

$$\hat{H}_{\rm odd}=\text{const}+\sum_\mu E_\mu a_\mu^\dagger a_\mu+\sum_{\bar{\mu}}E_{\bar{\mu}}a_{\bar{\mu}}^\dagger a_{\bar{\mu}}$$
$$+\sum_n\hbar\omega_n^{(+)}X_n^{(+)\dagger}X_n^{(+)}+\sum_n\hbar\omega_n^{(-)}X_n^{(-)\dagger}X_n^{(-)}+\hat{H}_{\rm coupl}\,, \tag{2·22}$$

where*)

$$\hat{H}_{\rm coupl}=\sum_n{\sum_{\mu\nu}}''\Lambda_n^{(+)}(\mu\nu)(X_n^{(+)\dagger}a_\mu^\dagger a_\nu+X_n^{(+)}a_\nu^\dagger a_\mu)$$
$$+\sum_n\sum_{\mu\bar{\nu}}\Lambda_n^{(-)}(\mu\bar{\nu})(X_n^{(-)\dagger}a_\mu^\dagger a_{\bar{\nu}}+X_n^{(-)}a_{\bar{\nu}}^\dagger a_\mu)$$
$$+\sum_n\sum_{\mu\bar{\nu}}\Lambda_n^{(-)}(\bar{\nu}\mu)(X_n^{(-)\dagger}a_{\bar{\nu}}^\dagger a_\mu+X_n^{(-)}a_\mu^\dagger a_{\bar{\nu}})\,. \tag{2·23}$$

*) The double primes attached to Σ denote that when the component $(\mu\nu)$ is summed, its signature partner $(\bar{\mu}\bar{\nu})$ should also be summed.

Explicit expressions for the quasiparticle-vibration-coupling vertices $\Lambda_n^{(\pm)}$ are

$$\Lambda_n^{(+)}(\mu\nu)=-\sum_{K=0,1,2}(-1)^K\kappa_K^{(+)}Q_K^{(+)}(n)Q_K^{(+)}(\mu\nu)\,,$$

$$\Lambda_n^{(-)}(\mu\bar{\nu})=\sum_{K=1,2}(-1)^K\kappa_K^{(-)}Q_K^{(-)}(n)Q_K^{(-)}(\mu\bar{\nu})\,,$$

$$\Lambda_n^{(-)}(\bar{\nu}\mu)=-\sum_{K=1,2}\kappa_K^{(-)}Q_K^{(-)}(n)Q_K^{(-)}(\mu\bar{\nu})\,, \tag{2·24}$$

where $Q_K^{(\pm)}(n)$ are the quadrupole transition amplitudes associated with the vibrational modes $X_n^{(\pm)}$ and are given by

$$Q_K^{(+)}(n)=\sum_{\mu\bar{\nu}}\{\psi_n^{(+)}(\mu\bar{\nu})Q_K^{(+)}(\mu\bar{\nu})-(-1)^K\varphi_n^{(+)}(\mu\bar{\nu})Q_K^{(+)}(\mu\bar{\nu})\}\,,$$

$$Q_K^{(-)}(n)=\sum_{\mu<\nu}{}''\{\psi_n^{(-)}(\mu\nu)Q_K^{(-)}(\mu\nu)+(-1)^K\varphi_n^{(-)}(\mu\nu)Q_K^{(-)}(\mu\nu)\}\,. \tag{2·25}$$

In the above equations, $Q_K^{(\pm)}(\mu\nu)$ and $Q_K^{(\pm)}(\mu\bar{\nu})$ are the quasiparticle matrix elements of the (doubly-stretched) quadrupole operators $\tilde{Q}_K^{(\pm)}$ and are defined as

$$\tilde{Q}_K^{(\pm)}=\hat{Q}_K^{(\pm\mathrm{A})}+\hat{Q}_K^{(\pm\mathrm{B})}\,, \tag{2·26}$$

$$\left.\begin{aligned}\hat{Q}_K^{(+\mathrm{A})}&=\sum_{\mu\bar{\nu}}Q_K^{(+)}(\mu\bar{\nu})(A_{\mu\bar{\nu}}^{\dagger}+(-1)^KA_{\mu\bar{\nu}})\,,\\ \hat{Q}_K^{(-\mathrm{A})}&=\sum_{\mu<\nu}{}''Q_K^{(-)}(\mu\nu)(A_{\mu\nu}^{\dagger}-(-1)^KA_{\mu\nu})\,,\end{aligned}\right\} \tag{2·27}$$

$$\left.\begin{aligned}\hat{Q}_K^{(+\mathrm{B})}&=\sum_{\mu\nu}{}''Q_K^{(+)}(\mu\nu)B_{\mu\nu}^{\dagger}\,,\\ \hat{Q}_K^{(-\mathrm{B})}&=\sum_{\mu\bar{\nu}}Q_K^{(-)}(\mu\bar{\nu})(B_{\mu\bar{\nu}}^{\dagger}-(-1)^KB_{\mu\bar{\nu}})\,,\end{aligned}\right\} \tag{2·28}$$

where

$$A_{\mu\nu}^{\dagger}=a_\mu^{\dagger}a_\nu^{\dagger}\,,\qquad B_{\mu\nu}^{\dagger}=a_\mu^{\dagger}a_\nu\,,\quad\text{etc.} \tag{2·29}$$

We note that the operators $\hat{Q}_K^{(\pm\mathrm{A})}$ can be rewritten in terms of the RPA normal modes as follows:

$$\hat{Q}_K^{(\pm\mathrm{A})}=\sum_n\{Q_K^{(\pm)}(n)X_n^{(\pm)\dagger}\pm(-1)^KQ_K^{(\pm)}(n)X_n^{(\pm)}\} \tag{2·30}$$

with $Q_K^{(\pm)}(n)$ being defined by Eq. (2·25) above. The quasiparticle-vibration-coupling Hamiltonian $\hat{H}_{\mathrm{coupl}}$ has been derived from the cross terms between the above $\hat{Q}_K^{(\pm\mathrm{A})}$ parts and the $\hat{Q}_K^{(\pm\mathrm{B})}$ parts of the quadrupole operators (2·26) when they are inserted into the quadrupole-quadrupole interaction (2·18). In fact, there are contributions to the coupling vertices (2·24) also from the residual pairing interaction (2·17). Although we actually take into account these contributions in this work, they are omitted in the expression (2·24) since they are not important for the generalized-gamma vibrations on which we focus our attention hereafter.

The quantities $(E_\mu, \hbar\omega_n^{(\pm)}, \Lambda_n^{(\pm)})$ and the operators $(a_\mu, X_n^{(\pm)})$ appearing in the above equations are defined with respect to a given band $|\phi_{\mathrm{band}}\rangle$, and are functions of ω_{rot}. It is important to notice that $\Lambda_n^{(-)}(\bar{\nu}\mu)\neq\Lambda_n^{(-)}(\mu\bar{\nu})$.

In this paper, we are particularly interested in the couplings to the generalized-gamma vibrations that evolve from the ordinary gamma vibrations (built on the ground states). Due to the effects of the triaxiality of the static single-particle potential and also due to the Coriolis couplings in the rotating frame, the generalized-gamma vibrations do not have definite K quantum number but still contain the $|K|=2$ components as the largest components in the angular-momentum region investigated here. Neglecting the other vibrational modes and denoting the generalized-gamma vibrational modes with the signatures $\alpha=0$ ($r=+1$) and $\alpha=1$ ($r=-1$) as $X_\gamma^\dagger$ and $X_{\bar\gamma}^\dagger$, respectively, the internal state vectors of odd-A nuclei can be written as superpositions of the quasiparticle and the generalized-gamma vibrational excitations:

$$
\begin{aligned}
|\chi_n(\omega_{\rm rot})\rangle=&\sum_\mu \psi_n^{(1)}(\mu)a_\mu^\dagger|\phi\rangle \\
&+\sum_\mu \psi_n^{(3)}(\mu\gamma)a_\mu^\dagger X_\gamma^\dagger|\phi\rangle+\sum_{\bar\mu} \psi_n^{(3)}(\bar\mu\,\bar\gamma)a_{\bar\mu}^\dagger X_{\bar\gamma}^\dagger|\phi\rangle \\
&+\sum_\mu \psi_n^{(5)}(\mu\gamma\gamma)\frac{1}{\sqrt{2}}a_\mu^\dagger X_\gamma^\dagger X_\gamma^\dagger|\phi\rangle+\sum_\mu \psi_n^{(5)}(\mu\bar\gamma\,\bar\gamma)\frac{1}{\sqrt{2}}a_\mu^\dagger X_{\bar\gamma}^\dagger X_{\bar\gamma}^\dagger|\phi\rangle \\
&+\sum_{\bar\mu} \psi_n^{(5)}(\bar\mu\gamma\bar\gamma)a_{\bar\mu}^\dagger X_\gamma^\dagger X_{\bar\gamma}^\dagger|\phi\rangle \\
&\qquad\text{for the } \alpha=1/2\ (r=-i)\text{ sector},
\end{aligned}
\tag{2·31}
$$

where the generalized-gamma vibrations are taken into account up to double excitations. The internal state vectors for the $\alpha=-1/2(r=+i)$ sector take a form similar to above, except that the suffices μ are to be replaced by $\bar\mu$. The amplitudes $\psi_n^{(1)}(\mu)$, $\psi_n^{(3)}(\mu\gamma)$, etc. are determined by treating the quasiparticle and the vibrational modes as fermions and bosons, respectively, and by diagonalizing the Hamiltonian (2·22) in the model space (2·31). The diagonalization is carried out for each signature sector ($\alpha=+1/2$ and $-1/2$) separately.

It is important to note that the state vector (2·31) contains, in general, many quasiparticles that are defined with respect to the yrast configuration, i.e., the quasiparticles ($\mathring{a}_\mu^\dagger$, $\mathring{a}_\nu^\dagger$). For instance, it contains three such quasiparticles when the s-band (which involves two quasiparticle excitations from the g-band) is adopted as the vacuum $|\phi_{\rm band}\rangle$ for the quasiparticles ($a_\mu^\dagger$, $a_\nu^\dagger$). When we discuss experimental data in § 4, we use the familiar terms like one-quasiparticle (1qp) bands and three-quasiparticle (3qp) bands by counting the number of quasiparticles defined with respect to the g-band before the first band crossing.

2.4. *Microscopic expressions for the intrinsic E2 and M1 operators*

In the previous subsection, we constructed the internal wave functions defined in the rotating frame. In order to calculate the $E2$ and $M1$ transition probabilities, however, we have to construct the total wave functions defined in the laboratory frame. We do this in a manner similar to the familiar particle-rotor model. Namely, we construct the state vectors in the laboratory frame in a direct product form of the rotational D-function $|IM\kappa\rangle$ and the internal wave function $|\chi_n(\omega_{\rm rot})\rangle$:

$$|\Psi_{nIM\kappa}(\omega_{\rm rot})\rangle = |IM\kappa\rangle \otimes |\chi_n(\omega_{\rm rot})\rangle \,. \tag{2·32}$$

Note, however, that the projection κ is defined here with respect to the x-axis which coincides with the rotation axis in the rotating shell model.

It is convenient to adopt the Holstein-Primakoff-type boson representation for the D-functions, which were invented by Marshalek.[26] In this representation, for instance, the rotational D-functions $|IM\kappa\rangle$ can be written in the subspace $\kappa = I$ in the following simple form:

$$|II_0I\rangle = \frac{1}{\sqrt{2\pi}} e^{i(I-I_0)\Phi} \frac{1}{\sqrt{(I-I_0)!}} (b^\dagger)^{I-I_0} |I_0 I_0 I_0\rangle \,. \tag{2·33}$$

Here the boson operator $b^\dagger$ transfers $\Delta M = -1$ and the operator $e^{i\Phi}$ transfers $\Delta I = \Delta M = \Delta\kappa = +1$. The angular-momentum shift operator $\hat{I}_-^{\rm (lab)}$ with respect to the laboratory frame is expressed as

$$\begin{aligned} \hat{I}_-^{\rm (lab)} &= \hat{I}_y^{\rm (lab)} - i\hat{I}_z^{\rm (lab)} \\ &= b^\dagger \sqrt{2\hat{I} - b^\dagger b} \quad \text{with } \hat{I} = I_0 - i\frac{\partial}{\partial \Phi} \,. \end{aligned} \tag{2·34}$$

As is evident from the above expressions, the Holstein-Primakoff-type boson representation is suited to an expansion in terms of $1/I_0$.

It is here very important to distinguish three frames of reference; the laboratory (lab) frame, the principal axis (PA) frame and the uniformly rotating (UR) frame.[27] They are related by

$$\hat{O}_{\lambda\mu}^{\rm (lab)} = e^{i\mu\Phi} \hat{O}_{\lambda\mu}^{\rm (UR)} = \sum_\kappa \hat{D}_{\mu\kappa}^{\lambda} \hat{O}_{\lambda\kappa}^{\rm (PA)} \,, \tag{2·35}$$

where $\hat{O}_{\lambda\mu}^{\rm (lab)}$, $\hat{O}_{\lambda\mu}^{\rm (UR)}$ and $\hat{O}_{\lambda\kappa}^{\rm (PA)}$ are the tensor operators of rank λ defined in the lab-, UR- and PA- frame, respectively. Thus, for instance, we have the following relations for the quadrupole operators:

$$\hat{Q}_{2-1}^{\rm (UR)} = e^{i\Phi} \hat{Q}_{2-1}^{\rm (lab)} = e^{i\Phi} \sum_\kappa \hat{D}_{-1\kappa}^{2} \hat{Q}_{2\kappa}^{\rm (PA)} \,. \tag{2·36}$$

Expanding the $\hat{D}$-operator in terms of $1/I_0$ and retaining the terms up to the $I_0^{-1/2}$ order,*) we obtain

$$\hat{Q}_{2-1}^{\rm (UR)} \approx \sqrt{\frac{3}{2}} \frac{\hat{I}_-^{\rm (UR)}}{I_0} \hat{Q}_{20}^{\rm (PA)} - \frac{\hat{I}_+^{\rm (UR)}}{I_0} \hat{Q}_{2-2}^{\rm (PA)} + \hat{Q}_{2-1}^{\rm (PA)} \,, \tag{2·37}$$

where

$$\hat{I}_\pm^{\rm (lab)} = e^{\pm i\Phi} \hat{I}_\pm^{\rm (UR)} \,. \tag{2·38}$$

In order to calculate the $E2$ transition probabilities, we need to know the microscopic expressions for the intrinsic operators $\hat{Q}_{20}^{\rm (PA)}$, $\hat{Q}_{2-2}^{\rm (PA)}$ and $\hat{Q}_{2-1}^{\rm (PA)}$ acting on the internal wave functions $|\chi_n(\omega_{\rm rot})\rangle$. For this aim, we extend Marshalek's treatment[20] of the

*) Up to the order $I_0^{-1/2}$, they are given[20),26)] by

$\hat{D}_{-12}^{2} \approx 0$, $\hat{D}_{-11}^{2} \approx 0$, $\hat{D}_{-10}^{2} \approx \sqrt{3/2} \cdot \hat{I}_-^{\rm (lab)}/I_0$, $\hat{D}_{1-1}^{2} \approx e^{-i\Phi}$, $\hat{D}_{1-2}^{2} \approx -e^{-2i\Phi} \hat{I}_+^{\rm (lab)}/I_0$.

"Nambu-Goldstone modes" ($\Gamma^\dagger$ and Γ) to odd-A nuclei. These are the modes that reorient the angular momentum of the collective rotation:

$$\Gamma^\dagger=\frac{1}{\sqrt{2I_c}}\hat{J}_-^{(\mathrm{RPA})}=\frac{1}{\sqrt{2I_c}}(\hat{J}_y^{(\mathrm{RPA})}-i\hat{J}_z^{(\mathrm{RPA})}), \tag{2·39}$$

where $I_c=\langle\hat{J}_x\rangle$ and the superscript denotes that they are evaluated in the RPA.*) Hereafter, the expectation values are taken with respect to the RPA vacuum $|\phi_{\mathrm{band}}\rangle$. These modes appear among the RPA normal modes. The quadrupole operator $\hat{Q}_{2-1}$ is then expressed in terms of the RPA normal modes $\{X_n^{(-)\dagger}, X_n^{(-)}, \Gamma^\dagger, \Gamma\}$ and the quasiparticle operators $(B_{\mu\bar{\nu}}^\dagger, B_{\mu\bar{\nu}})$ as follows:

$$\hat{Q}_{2-1}^{(\mathrm{RPA})}=\langle\hat{Q}_{20}\rangle\sqrt{\frac{3}{I_c}}\Gamma^\dagger-\langle\hat{Q}_{22}\rangle\sqrt{\frac{2}{I_c}}\Gamma+\hat{Q}_{2-1}^{(\mathrm{vib})}+\hat{Q}_{2-1}^{(\mathrm{qp})}, \tag{2·40}$$

where $\hat{Q}_{2-1}^{(\mathrm{vib})}$ and $\hat{Q}_{2-1}^{(\mathrm{qp})}$ are the vibrational and quasiparticle terms, respectively,

$$\hat{Q}_{2-1}^{(\mathrm{vib})}=\sum_n\{Q_{-1}^{(\mathrm{UR})}(n)X_n^{(-)\dagger}+Q_{+1}^{(\mathrm{UR})}(n)X_n^{(-)}\}, \tag{2·41}$$

$$\hat{Q}_{2-1}^{(\mathrm{qp})}=\sum_{\mu\bar{\nu}}\{Q_{-1}^{(\mathrm{qp})}(\mu\bar{\nu})B_{\mu\bar{\nu}}^\dagger+Q_{+1}^{(\mathrm{qp})}(\mu\bar{\nu})B_{\mu\bar{\nu}}\} \tag{2·42}$$

with

$$Q_{\pm1}^{(\mathrm{UR})}(n)=\frac{i}{\sqrt{2}}(Q_1^{(-)}(n)\pm Q_2^{(-)}(n)), \tag{2·43}$$

$$Q_{\pm1}^{(\mathrm{qp})}(\mu\bar{\nu})=\frac{i}{\sqrt{2}}(Q_1^{(-)}(\mu\bar{\nu})\pm Q_2^{(-)}(\mu\bar{\nu})). \tag{2·44}$$

The subscripts in the above notations refer to the x-axis except for $Q_{K=1,2}^{(-)}(n)$ and $Q_{K=1,2}^{(-)}(\mu\bar{\nu})$ where K denotes the z-component. Marshalek discussed[20] a formal unitary transformation which replaces the "Nambu-Goldstone modes" $(\Gamma^\dagger, \Gamma)$ with the exact angular-momentum operators $(\hat{I}_-, \hat{I}_+)/\sqrt{2I_c}$. Extending his argument to odd-A nuclei, we now assume that the following replacements are possible:

$$\left.\begin{aligned}\Gamma^\dagger&\longrightarrow\frac{1}{\sqrt{2I_c}}(\hat{I}_-^{(\mathrm{UR})}-\hat{J}_-^{(\mathrm{qp})}),\\ \Gamma&\longrightarrow\frac{1}{\sqrt{2I_c}}(\hat{I}_+^{(\mathrm{UR})}-\hat{J}_+^{(\mathrm{qp})}),\end{aligned}\right\} \tag{2·45}$$

where $\hat{J}_\pm^{(\mathrm{qp})}$ are the angular-momentum operators acting on the odd quasiparticles $(a_\mu^\dagger, a_{\bar{\nu}}^\dagger)$. A similar ansatz was previously adopted by Hara and Kusuno[28] for the case $\omega_{\mathrm{rot}}=0$. Then, Eq. (2·40) may be rewritten as

*) Note that I_0 for odd-A nuclei differs from I_c for even-even nuclei by $\langle\hat{J}_x^{(\mathrm{qp})}\rangle=I_0-I_c$, which represents the contribution from the last odd quasiparticle. We assume that the difference is small in comparison with I_0 itself so that it is possible to expand the functions of I_0 in terms of $\langle\hat{J}_x^{(\mathrm{qp})}\rangle/I_c$.

$$\hat{Q}_{2-1}^{(\mathrm{RPA})}=\langle\hat{Q}_{20}\rangle\sqrt{\frac{3}{2}}\frac{1}{I_c}(\hat{I}_-^{(\mathrm{UR})}-\hat{J}_-^{(\mathrm{qp})})-\langle\hat{Q}_{22}\rangle\frac{1}{I_c}(\hat{I}_+^{(\mathrm{UR})}-\hat{J}_+^{(\mathrm{qp})})$$
$$+\hat{Q}_{2-1}^{(\mathrm{vib})}+\hat{Q}_{2-1}^{(\mathrm{qp})}\,. \tag{2·46}$$

We now require that the above $\hat{Q}_{2-1}^{(\mathrm{RPA})}$ should be equivalent to the $I_0^{-1/2}$ order approximation of $\hat{Q}_{2-1}^{(\mathrm{UR})}$, Eq. (2·37). It should be recalled here that our microscopic calculation is done in the UR frame and that the RPA takes into account the $I_c^{-1/2}$ order corrections to the independent-quasiparticle limit of the rotating shell model. By comparing the coefficients in Eqs. (2·37) and (2·46) of the angular-momentum operators $\hat{I}_\pm^{(\mathrm{UR})}$, we obtain the microscopic expressions in the RPA order for the intrinsic operators $\hat{Q}_{2\nu}^{(\mathrm{PA})}$ to be used in the expression (2·37) for $Q_{2-1}^{(\mathrm{UR})}$:

$$\hat{Q}_{20}^{(\mathrm{PA})}=\langle\hat{Q}_{20}\rangle\,,$$
$$\hat{Q}_{2-2}^{(\mathrm{PA})}=\langle\hat{Q}_{22}\rangle\,,$$
$$\hat{Q}_{2-1}^{(\mathrm{PA})}=\hat{Q}_{2-1}^{(\mathrm{vib})}+\hat{Q}_{2-1}^{(\mathrm{qp})}-\langle\hat{Q}_{20}\rangle\sqrt{\frac{3}{2}}\frac{1}{I_c}\hat{J}_-^{(\mathrm{qp})}+\langle\hat{Q}_{22}\rangle\frac{1}{I_c}\hat{J}_+^{(\mathrm{qp})}\,. \tag{2·47}$$

In the same way, we can derive the microscopic expressions for the intrinsic $M1$ operators $\hat{\mu}_{1\kappa}^{(\mathrm{PA})}$ defined by

$$\hat{\mu}_{1-1}^{(\mathrm{UR})}=e^{i\Phi}\hat{\mu}_{1-1}^{(\mathrm{lab})}=e^{i\Phi}\sum_\kappa\hat{D}_{-1\kappa}^1\hat{\mu}_{1\kappa}^{(\mathrm{PA})}\,. \tag{2·48}$$

Expanding the $\hat{D}$-operator in terms of $1/I_0$ and retaining the terms up to the $I_0^{-1/2}$ order,*) we obtain

$$\hat{\mu}_{1-1}^{(\mathrm{UR})}\approx\hat{\mu}_{1-1}^{(\mathrm{PA})}+\frac{1}{\sqrt{2}}\frac{1}{I_0}\hat{I}_-^{(\mathrm{UR})}\hat{\mu}_{10}^{(\mathrm{PA})}\,. \tag{2·49}$$

On the other hand, the $M1$ operator $\hat{\mu}_{1-1}$ is represented by the RPA normal modes in the UR frame as

$$\hat{\mu}_{1-1}^{(\mathrm{RPA})}=\frac{1}{\sqrt{I_c}}\langle\hat{\mu}_x\rangle\Gamma^\dagger+\hat{\mu}_{1-1}^{(\mathrm{vib})}+\hat{\mu}_{1-1}^{(\mathrm{qp})}\,, \tag{2·50}$$

where $\hat{\mu}_{1-1}^{(\mathrm{vib})}$and $\hat{\mu}_{1-1}^{(\mathrm{qp})}$ are the vibrational and quasiparticle terms, respectively,

$$\hat{\mu}_{1-1}^{(\mathrm{vib})}=\sum_n\{\mu_{-1}^{(\mathrm{UR})}(n)X_n^{(-)\dagger}+\mu_{+1}^{(\mathrm{UR})}(n)X_n^{(-)}\}\,, \tag{2·51}$$

$$\hat{\mu}_{1-1}^{(\mathrm{qp})}=\sum_{\mu\bar{\nu}}\{\mu_{-1}^{(\mathrm{qp})}(\mu\bar{\nu})B_{\mu\bar{\nu}}^\dagger+\mu_{+1}^{(\mathrm{qp})}(\mu\bar{\nu})B_{\mu\bar{\nu}}\} \tag{2·52}$$

with

$$\mu_{-1}^{(\mathrm{UR})}(n)=\langle[X_n^{(-)},\,\hat{\mu}_{1-1}]\rangle\,,$$
$$\mu_{+1}^{(\mathrm{UR})}(n)=\langle[\hat{\mu}_{1-1},\,X_n^{(-)\dagger}]\rangle\,. \tag{2·53}$$

As before, the components of $\hat{\mu}$ refer to the x-axis. In deriving Eq. (2·50), we have

*) Up to the order $I_0^{-1/2}$, they are given[20),26)] by
$\hat{D}_{-11}^1\approx 0$, $\hat{D}_{-10}^1\approx\hat{I}_-^{(\mathrm{lab})}/\sqrt{2}I_0$, $\hat{D}_{-1-1}^1\approx e^{-i\Phi}$.

used the identity $\langle\hat{\mu}_x\rangle/\sqrt{I_c}=\langle[\Gamma,\hat{\mu}_{1-1}]\rangle$. Following the prescription (2·45) for the replacement of the "Nambu-Goldstone modes", we can rewrite Eq. (2·50) as

$$\hat{\mu}_{1-1}^{\{\mathrm{RPA}\}}=\frac{1}{\sqrt{2}}\langle\hat{\mu}_x\rangle\frac{1}{I_c}(\hat{I}_-^{(\mathrm{UR})}-\hat{J}_-^{(\mathrm{qp})})+\hat{\mu}_{1-1}^{\{\mathrm{vib}\}}+\hat{\mu}_{1-1}^{\{\mathrm{qp}\}}. \tag{2·54}$$

Requiring that the above $\hat{\mu}_{1-1}^{\{\mathrm{RPA}\}}$ should be equivalent to the $I_0^{-1/2}$-order approximation of $\hat{\mu}_{1-1}^{\{\mathrm{UR}\}}$, Eq. (2·49), we obtain

$$\begin{aligned}&\hat{\mu}_{10}^{\{\mathrm{PA}\}}=\langle\hat{\mu}_x\rangle,\\&\hat{\mu}_{1-1}^{\{\mathrm{PA}\}}=\hat{\mu}_{1-1}^{\{\mathrm{vib}\}}+\hat{\mu}_{1-1}^{\{\mathrm{qp}\}}-g_{\mathrm{RPA}}\hat{J}_{-1}^{(\mathrm{qp})},\end{aligned} \tag{2·55}$$

where

$$g_{\mathrm{RPA}}=\langle\hat{\mu}_x\rangle/I_c \tag{2·56}$$

and $\hat{J}_{-1}^{(\mathrm{qp})}=\hat{J}_-^{(\mathrm{qp})}/\sqrt{2}$. Microscopic expressions in the RPA order for other components of the $E2$ and $M1$ operators, $\hat{Q}_{2\mu}$ and $\hat{\mu}_{1\mu}$, can be obtained in a similar manner.

After obtaining the explicit expressions for the intrinsic operators, it is straightforward to calculate the $B(M1)$ and $B(E2)$ values by using the total wave function defined by Eq. (2·32) with $K=I$.

2.5. *Effects of triaxial deformations on* $B(E2;I\to I-1)$

In this subsection, we discuss the effects of triaxial deformations on the $B(E2;I\to I-1)$ values between the signature partners in the odd-A, unique-parity bands. As is evident from the expressions (2·36) and (2·37), the intrinsic operator $\hat{Q}_{2-1}^{\{\mathrm{PA}\}}$ is responsible for such signature-changing transitions with $\Delta I=1$. Let us rewrite this operator into a form, by means of which we can easily identify the effects of static triaxial deformation on the $E2$ transitions. Expressing the expectation values of the quadrupole operators $\langle\hat{Q}_{20}\rangle$ and $\langle\hat{Q}_{22}\rangle$ in terms of $Q_0\equiv\langle\hat{Q}_{K=0}^{\{+\}}\rangle$ and $Q_2\equiv\langle\hat{Q}_{K=2}^{\{+\}}\rangle/\sqrt{2}$, whose components are defined with respect to the z-axis, and using $\hat{J}_\pm^{(\mathrm{qp})}=\hat{J}_y^{(\mathrm{qp})}\pm i\hat{J}_z^{(\mathrm{qp})}$, the intrinsic operator $\hat{Q}_{2-1}^{\{\mathrm{PA}\}}$ in Eq. (2·47) is rewritten as

$$\frac{1}{i}\hat{Q}_{2-1}^{\{\mathrm{PA}\}}=\frac{1}{i}\hat{Q}_{2-1}^{\{\mathrm{vib}\}}+\frac{1}{i}\hat{Q}_{2-1}^{\{\mathrm{qp}\}}-\sqrt{\frac{3}{2}}Q_0\frac{\hat{J}_z^{(\mathrm{qp})}}{I_c}+Q_2\left(2\frac{i\hat{J}_y^{(\mathrm{qp})}}{I_c}+\frac{\hat{J}_z^{(\mathrm{qp})}}{I_c}\right). \tag{2·57}$$

We can eliminate $i\hat{J}_y^{(\mathrm{qp})}$ from the above expression by making use of the approximate relation

$$i\hat{J}_y^{(\mathrm{qp})}\approx(-1)^{I_i-j}\frac{|\Delta E|}{\hbar\omega_{\mathrm{rot}}}\hat{J}_z^{(\mathrm{qp})}, \tag{2·58}$$

where I_i denotes the angular-momentum of the initial state. Here ΔE is defined by $\Delta E=E(\alpha=1/2)-E(\alpha=-1/2)$ and represents the signature splitting of the quasiparticle energies associated with the unique-parity orbit j. The phase factor $(-1)^{I_i-j}$ in the above relation is obtained by assuming the normal phase rule $\Delta E=(-1)^{j+1/2}|\Delta E|$, and implies that it is positive (negative) for the transitions from the favoured (unfavoured) states whose angular-momentum $I_i=j+$even (odd). The relation (2·58)

is easily derived[14] by taking the quasiparticle matrix elements of the commutator between the cranking Hamiltonian $\hat{h}'_{\rm sp}=\hat{h}_{\rm sp}-\omega_{\rm rot}\hat{J}_x$ and the operator $\hat{J}_z$, and holds almost exactly in the axial symmetric limit except for the small corrections resulting from the doubly stretched $\boldsymbol{l}^2$ and $\boldsymbol{l}\cdot\boldsymbol{s}$ terms. Inserting (2·58) into (2·57), we obtain

$$\frac{1}{i}\hat{Q}^{\{\rm PA\}}_{2-1}=\frac{1}{i}\hat{Q}^{\{\rm vib\}}_{2-1}+\frac{1}{i}\hat{Q}^{\{\rm qp\}}_{2-1}+\left\{-\sqrt{\frac{3}{2}}Q_0+Q_2\left(1+2(-1)^{I_i-j}\left|\frac{\Delta E}{\hbar\omega_{\rm rot}}\right|\right)\right\}\frac{\hat{J}_z{}^{\rm (qp)}}{I_c}\,. \tag{2·59}$$

The above expression clearly shows that the signature dependent effect arises when the static triaxiality Q_2 is non-zero. The phase factor $(-1)^{I_i-j}$ implies that the $B(E2;\ I_i\to I_i-1)$ values are enhanced for the transitions from the favoured (unfavoured) states to the unfavoured (favoured) states when Q_2 is negative (positive). According to Bohr and Mottelson's definitions[3] of γ_0, i.e., $\tan\gamma_0\equiv\langle\hat{Q}^{(+)}_{K=2}\rangle/\langle\hat{Q}^{(+)}_{K=0}\rangle$, γ_0 is positive (negative) when Q_2 is positive (negative). Note that this sign convention for γ_0 is opposite to that of the Lund convention.[14] If the vibrational and the quasiparticle contributions, $\hat{Q}^{\{\rm vib\}}_{2-1}$ and $\hat{Q}^{\{\rm qp\}}_{2-1}$, are neglected, Eq. (2·59) reduces to the expression derived by Hamamoto and Mottelson[14),15] when $j=1/2$ because $|\Delta E|=\hbar\omega_{\rm rot}$ in this special case.

In addition to the static triaxial deformation $Q_2\neq 0$, the vibrational term $\hat{Q}^{\{\rm vib\}}_{2-1}$ also brings about signature dependent effects in the $B(E2;\ I\to I-1)$. This is caused by the mixings of the generalized-gamma vibration with signature $\alpha=1$ ($r=-1$) in the one-quasiparticle states, illustrated in Fig. 1(a). Microscopic structure of the coupling vertices $\Lambda_n{}^{(\pm)}$ appearing in Fig. 1 and defined by Eq. (2·24) will be investigated in detail in a separate paper.[29] We here only mention that they involve the matrix elements of $\hat{Q}^{(-)}_{K=1}$ and $\hat{Q}^{(-)}_{K=2}$ between the aligned quasiparticle states with different signatures, for which an approximate relation

$$\hat{Q}^{(-)\{\rm qp\}}_{K=2}\approx-(-1)^{I_i-j}\frac{|\Delta E|}{\hbar\omega_{\rm rot}}\hat{Q}^{(-)\{\rm qp\}}_{K=1} \tag{2·60}$$

holds under certain conditions. The above relation plays a role similar to the relation (2·58) between $i\hat{J}_y{}^{\rm (qp)}$ and $\hat{J}_z{}^{\rm (qp)}$ in deriving a phase rule for the signature dependent effects. It should be emphasized here that such an interplay between the $K=1$ and 2 components of the quadrupole motion is an interesting new feature of the generalized-gamma vibrations created in rotating triaxial nuclei.[30]

Thus, we expect in general that the signature dependence of $B(E2;\ I\to I-1)$ is very sensitive to whether effects of static and dynamic gamma deformations result in constructive coherence or destructive coherence. The degree of the competition (or the cooperation) between the static and dynamic effects depends, of course, on the magnitude of the γ_0 and the strengths of the quasiparticle-vibration-coupling vertices $\Lambda^{(-)}$.

2.6. *Effects of aligned quasiparticles on $B(M1)$*

The intrinsic operator $\hat{\mu}^{\{\rm PA\}}_{1-1}$ defined by Eq. (2·55) is responsible for the $M1$ transitions between the signature-partner bands. This operator may be rewritten as

$$\hat{\mu}_{1-1}^{(\mathrm{PA})}=(g_l-g_{\mathrm{RPA}})\,\hat{l}_{-1}^{(\mathrm{qp})}+(g_s-g_{\mathrm{RPA}})\,\hat{s}_{-1}^{(\mathrm{qp})}+\hat{\mu}_{1-1}^{(\mathrm{vib})}\,, \tag{2·61}$$

in terms of the expressions $\hat{\mu}_{1-1}^{(\mathrm{qp})}=g_l\,\hat{l}_{-1}^{(\mathrm{qp})}+g_s^{\mathrm{eff}}\,\hat{s}_{-1}^{(\mathrm{qp})}$ and $\hat{J}_{-1}^{(\mathrm{qp})}=\hat{l}_{-1}^{(\mathrm{qp})}+\hat{s}_{-1}^{(\mathrm{qp})}$. The g-factor of the RPA vacuum, g_{RPA}, appearing in the above equation is defined by Eq. (2·56) and may be rewritten into a more explicit form,[31)~33)]

$$g_{\mathrm{RPA}}=g_R+(g_i-g_R)\frac{i}{R+i}\,, \tag{2·62}$$

where $R\equiv\langle\hat{J}_x\rangle_g$, $i\equiv\langle\hat{J}_x\rangle-\langle\hat{J}_x\rangle_g$, $g_RR\equiv\langle\hat{\mu}_x\rangle_g$ and $g_ii\equiv\langle\hat{\mu}_x\rangle-\langle\hat{\mu}_x\rangle_g$, with the suffix g denoting the expectation value with respect to the g-band configuration. We see from the expression (2·62) that g_{RPA} decreases (increases) when the $i_{13/2}$ neutron ($h_{11/2}$ proton) alignment takes place, since g_i is negative (positive) in this case. This change in the g_{RPA} value associated with the alignment will, in turn, bring about a remarkable change in the $M1$ transition probabilities under consideration. Thus, in the case of odd-Z nuclei with the $h_{11/2}$ odd proton, the $B(M1)$ values will increase (decrease) when one goes from the 1qp band to the 3qp band involving the aligned $i_{13/2}$ neutrons ($h_{11/2}$ protons). On the other hand, for odd-N nuclei with the $i_{13/2}$ odd neutron, the $B(M1)$ values will increase (decrease) when the $h_{11/2}$ proton ($i_{13/2}$ neutron) alignment takes place.

§ 3. Details of numerical calculation

The procedure of numerical calculation is basically the same as in Ref. 17) except that the new method of constructing the diabatic quasiparticle representation[22),23)] is used for the first time in this work. We adopt the second-order approximation with respect to the power of the ω_{rot} expansion for determining the operator iG in Eq. (2·5). The parameters v_{ls} and v_{ll} of the modified-harmonic-oscillator potential are taken from Bohr and Mottelson's textbook.[3)] The three major shells with $N_{\mathrm{osc}}=3, 4, 5$ ($N_{\mathrm{osc}}=4, 5, 6$) are explicitly taken into accont for protons (neutrons),*) and the $\Delta N_{\mathrm{osc}}=2$ Coriolis coupling terms are neglected in the calculation. The equilibrium deformation parameters (β_0, γ_0) are determined by using the same method as in Ref. 25).*) This method makes use of the semiclassical requirement that the velocity distribution should be isotropic in average when seen in the rotating frame.

The pairing-force strengths used are $G_n=2.64/A$ and $G_P=3.51/A$ in units of $\hbar\omega_0$. These values are determined by the requirement that the calculated pairing gaps at $\hbar\omega_{\mathrm{rot}}=0$ reproduce the odd-even mass differences between ^{165}Lu and its even-even neighbours. The pairing gaps Δ_n and Δ_p are selfconsistently calculated as functions of ω_{rot} in each quasiparticle configuration for even-even nuclei. It turned out, however, that the Δ_n for the s-band configuration rapidly decreases in the region $\hbar\omega_{\mathrm{rot}}\gtrsim 0.3$ MeV. In such a case, we simply set the pairing gaps to be constant in such a region in order to avoid the difficulty associated with the pairing phase transition. These constant values are shown by thin dash-dotted lines in Fig. 4.

The quadrupole-force strengths $\kappa_K^{(\pm)}$ are determined in the following way. In the

*) The contributions from the nucleons outside the model space are taken into account in the same way as in Ref. 25). They are indispensable for reproducing the experimental data for β_0 in the calculations.

RPA calculation for the vibrations built on the g-band, we determine the values of $\kappa_0^{(+)}$ and $\kappa_2^{(+)}$ in each nucleus so as to reproduce at $\hbar\omega_{\rm rot}=0$ the average excitation energies of the lowest $K=0$ and 2 vibrational states in the neighbouring even-even nuclei. On the other hand, the values of $\kappa_1^{(\pm)}$ and $\kappa_2^{(-)}$ are determined at $\hbar\omega_{\rm rot}=0$ so as to restore in the RPA the rotational symmetry broken by the deformed single-particle potential $\hat{h}_{\rm def}$. Since the equilibrium deformation parameters (β_0, γ_0) are different between the g-band and the s-band configurations, the strengths $\kappa_K^{(\pm)}$ of the residual quadrupole-force are also slightly different between these configurations. In the RPA calculation for the vibrations built on the s-band, we assume, for simplicity, that $\kappa_0^{(+)}=\kappa_1^{(\pm)}=\kappa_2^{(\pm)}=\kappa$ and determine the value of κ at $\hbar\omega_{\rm rot}=0.2$ MeV such that the excitation energy $\hbar\omega_{\rm NG}$ of the "Nambu-Goldstone mode" (that reorients the angular momentum of the collective rotation) is correctly reproduced in the calculation at $\hbar\omega_{\rm NG}=\hbar\omega_{\rm rot}$.

In the treatment of the quasiparticle-vibration couplings, we take into account the lowest 10 quasiparticle states (with unique-parity) for each signature sector, $\alpha=\pm 1/2$. Thus, we diagonalize the 60×60 matrix for each signature at every value of $\omega_{\rm rot}$.

The $M1$ and $E2$ transition matrix elements are evaluated at the average value of $\omega_{\rm rot}$'s between the initial and the final states.*) In the calculation, the effective spin g-factor of $g_s^{\rm eff}=0.7g_s^{\rm free}$ is used, but no $E2$ effective charge is used. The rotational g-factor, g_R, appearing in Eq. (2·62) is usually calculated in a microscopic way. However, for the cases where it is apparent that a better agreement between calculated results and experimental data is obtainable if we phenomenologically modify the g_R value, we shall present the results of calculation using the phenomenological g_R values. These cases occur in nuclei involving the $i_{13/2}$ odd neutrons, and are explicitly mentioned in § 4.

It should be emphasized that we are going to do calculations which essentially contain no adjustable parameter. Since our major purpose in this paper is to examine the general characteristics of the prediction of the microscopic model formulated in § 2, we shall not attempt, except for a few cases mentioned above, in the next section to phenomenologically search for the optimal parameters entering in the numerical calculations. Of particular important one is the triaxiality parameter γ_0 characterizing the single-particle potential $\hat{h}_{\rm def}$. Since we use in this paper a very simple method of evaluating γ_0, there is room to improve the calculation especially with regard to the determination of the most appropriate values of γ_0 for individual bands. We leave such a task of elaborating our calculation in order to make a detailed comparison with experimental data for a future work.

§ 4. Some examples of numerical calculation

In this section, we present some results of numerical calculation for the unique-parity bands of odd-Z nuclei, ^{157}Ho, ^{159}Tm, ^{161,165}Lu, and of odd-N nuclei, ^{161}Dy, ^{167}Er and ^{161,163,167}Yb for which experimental data for $B(M1)$ and/or $B(E2)$ are available. Before presenting these results, we first test our theoretical values of $g_{\rm RPA}$ in ^{168}W, since a result of direct measurement of the g-factors of both the g-band and the s-band has

*) Since the wave functions in the diabatic basis change only smoothly as functions of $\omega_{\rm rot}$, we expect that this is a good approximation.

recently been reported[34] for the first time for this nucleus.

4.1. *g-factors of the g- and the s-band in* ^{168}W

Calculated and experimental values of the g-factors for the g- and the s-band in ^{168}W are compared in Fig. 2. As expected, the g-factor for the s-band suddenly decreases to about -0.2 due to the alignment of the $i_{13/2}$ neutrons. The calculation successfully reproduces this change in the g-factors before and after the band crossing. Equation (2·61) indicates that the $B(M1)$ values of odd-A nuclei sensitively depend on the g-factors of the even-even "core". Thus, the agreement displayed in Fig. 2 is quite encouraging to proceed to the discussion on the $B(M1)$ and $B(E2)$ values in odd-A nuclei.

4.2. *Nuclei with the* $h_{11/2}$ *odd-proton*

Figure 3 presents the deformation parameters (β_0, γ_0) for the 1qp and 3qp bands in ^{157}Ho, ^{159}Tm and ^{161,165}Lu. These deformation parameters are equivalent to the $(\beta^{(\mathrm{pot})}, \gamma^{(\mathrm{pot})})$ defined in Ref. 25) that characterize the deformed potential in $\hat{h}_{\mathrm{def}}$ for the even-even "cores" (the averages of the neighbouring even-even nuclei) of the odd-Z nuclei under consideration. These values are calculated by means of the semiclassical method described in § 2, and are used in the quasiparticle-vibration coupling calculations for evaluating the $M1$ and $E2$

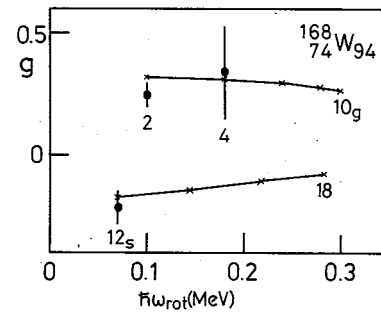

Fig. 2. Comparison of the calculated values of g_{RPA} with the corresponding experimental data[34] in ^{168}W. The calculated deformation parameters (β_0, γ_0) are $\beta_0=0.177\sim0.186$ and $\gamma_0=1.1°\sim9.3°$ for the g-band, and $\beta_0=0.182\sim0.187$ and $\gamma_0=0.8°\sim4.2°$ for the s-band, in the range $0.1\lesssim\hbar\omega_{\mathrm{rot}}\lesssim0.3$ MeV.

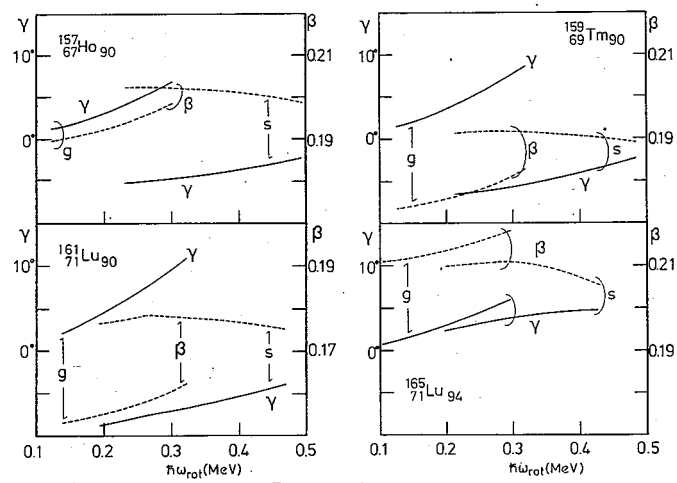

Fig. 3. Calculated deformation parameters (β_0, γ_0) for the g-band and the s-band configuration are plotted as functions of ω_{rot}. These values characterize the deformation of the "cores" (the averages of the even-even neighbours) of the odd-Z nuclei; ^{157}Ho, ^{159}Tm, ^{161}Lu and ^{165}Lu. Note that our definition of the sign of γ_0 is opposite to the Lund convention.[14]

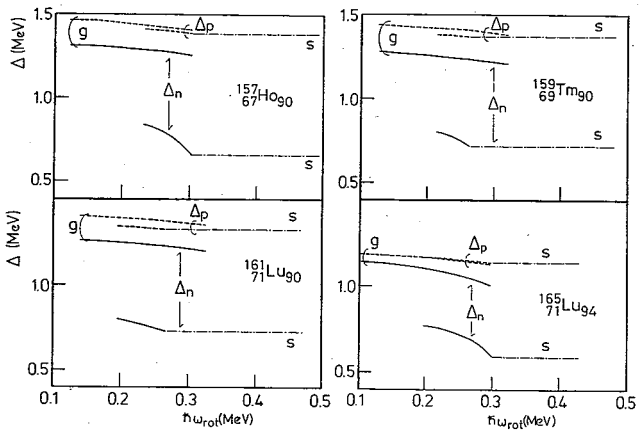

Fig. 4. Calculated pairing gaps (Δ_p, Δ_n) for the g-band and the s-band configurations are plotted as functions of ω_{rot}. These values characterize the pairing deformation of the "cores" (the averages of the even-even neighbours) of the odd-Z nuclei; ^{157}Ho, ^{159}Tm, ^{161}Lu and ^{165}Lu.

transition properties within the unique-parity bands.

It is seen in Fig. 3 that the β_0 values do not significantly change when one goes from the g-band to the s-band. On the other hand, the sign of γ_0 changes, in the case of the $N=90$ isotones, from positive to negative due to the excitation of the aligned $i_{13/2}$ neutrons. (Note that our definition of the sign of γ_0 is opposite to the Lund convention[14]).

Results of the numerical calculation for the ratios $B(M1)/B(E2)$ in the $N=90$ isotones, ^{157}Ho, ^{159}Tm and ^{161}Lu, with the $h_{11/2}$ odd-proton are displayed in Figs. 5~7. In these figures, the solid (broken) lines show the results of calculation in which the coupling effects with the generalized-gamma vibrations are taken into account (neglected). The solid triangles and the solid circles with error bars denote the experimental data before and after the first band crossings, respectively. In the upper parts of these figures, calculated values for the signature splittings ΔE of the quasiparticle energies are compared with the experimental data.

A remarkable feature of the observed $M1$ transition properties in these nuclei is that the $B(M1)$ values increase when one goes from the 1qp band to the 3qp band. The reason for this enhancement is easily understood from the expression (2·62): The g-factor associated with the aligned $i_{13/2}$ neutrons, g_i, is about -0.18 so that the g_{RPA} values considerably decreases when one goes from the 1qp band to the 3qp band. This reduction of g_{RPA}, on the other hand, brings about an enhancement of the $B(M1)$ values under consideration, as is easily seen from the expression (2·61).

It is furthermore seen from Figs. 5~7 that the calculated values of the ratio $B(M1)/B(E2)$ for the 3qp bands increase as Z increases from 67 to 71. There are two causes for this trend. One is the slight increase of the $B(M1)$ values associated with the decrease of the g_{RPA} values; i.e., $g_{RPA}=-0.029$, -0.045 and -0.062 at $\hbar\omega_{rot}=0.4$ MeV for ^{157}Ho, ^{159}Tm and ^{161}Lu, respectively. The other cause is the decrease of the $B(E2)$ values associated with the decrease of the deformation parameter β_0; i.e., $B(E2; I \to I-2)=0.83, 0.77$ and 0.67 $[e^2b^2]$ at $\hbar\omega_{rot}=0.4$ MeV for ^{157}Ho, ^{159}Tm and ^{161}Lu, respectively (see Fig. 3 for the β_0 values). The theoretical result that the ratio

$B(M1)/B(E2)$ in the $N=90$ isotones increases with increasing Z is in agreement with the experiments. On the other hand, the theoretical pattern as a function of $\omega_{\rm rot}$ is qualitatively similar for these isotopes, and do not explain the variations that are seen in the experimental data when one goes from one isotone to another.

As is well known,[14] the signature dependence of the $B(M1)$ is closely correlated with the signature splitting ΔE of the quasiparticle energies. On the other hand, this quantity ΔE is a rather sensitive function of the triaxiality parameter γ_0. Our γ_0 values used in Figs. 5~7 are qualitatively consistent with those evaluated by Frauendorf and May,[35] and by Hamamoto and Mottelson.[14] However, quantitatively, the absolute magnitudes of our γ_0 are much smaller than their values. As mentioned in § 3, there is room for elaborating our calculation especially with respect to the determination of γ_0. For example, the polarization effects of the odd quasiparticle are not fully taken into account in the present calculation (since our (β_0, γ_0) values are evaluated in the neighbouring even-even nuclei), although a part of such polarization effects may be taken into account in our model through the quasiparticle-vibration

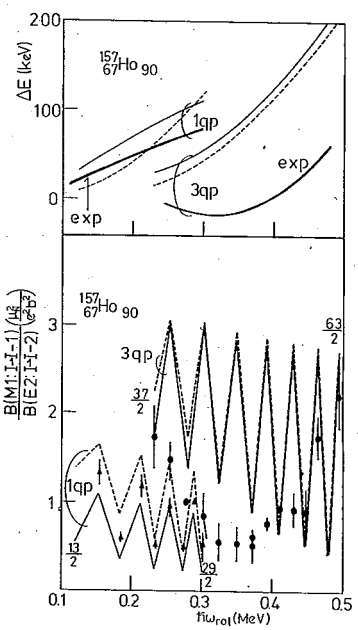

Fig. 5. Ratios $B(M1; I\to I-1)/B(E2; I\to I-2)$ and the signature splittings ΔE for ^{157}Ho, plotted as functions of $\omega_{\rm rot}$. The solid (broken) lines represent the results of calculation with (without) taking into account the couplings with the generalized-gamma vibrations. The solid triangles and the solid circles with error bars denote the experimental ratios[4),8)] before and after the first band crossings, respectively. The experimental data for the signature splitting ΔE are shown by the bold lines in the upper part of this figure, where all lines are drawn by smoothly interpolating the experimental and theoretical values.

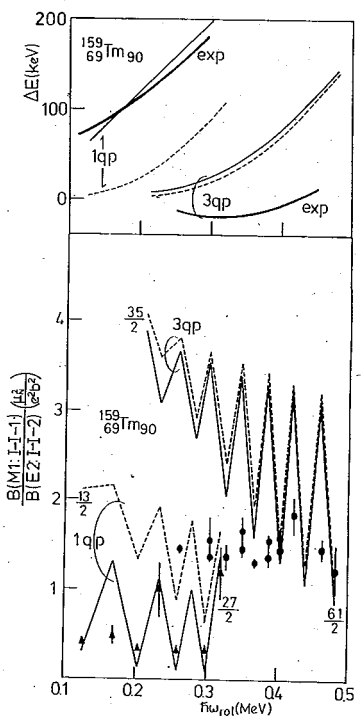

Fig. 6. Same as Fig. 5 but for ^{159}Tm. Experimental data are taken from Refs. 7) and 8).

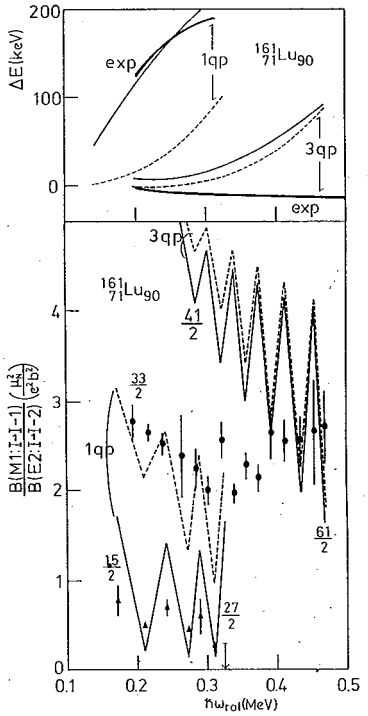

Fig. 7. Same as Fig. 5 but for ^{161}Lu. Experimental data are taken from Ref. 8).

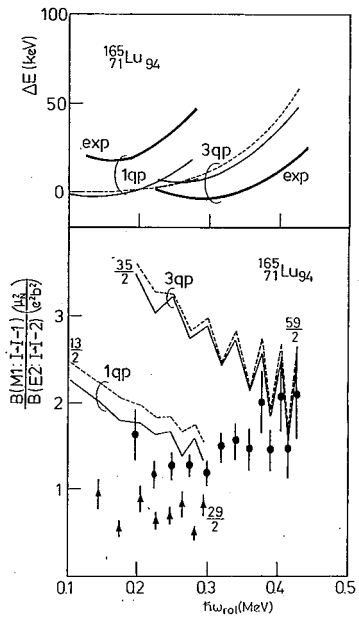

Fig. 8. Same as Fig. 5 but for ^{165}Lu. Experimental data are taken from Ref. 9). Note that the experimental data for $\hbar\omega_{\rm rot}\gtrsim 0.4$ MeV might correspond to the 5qp band.[9),36)]

couplings.

A similar theoretical pattern is also seen in ^{165}Lu with $N=94$ (see Fig. 8). In this nucleus, the magnitude of the ratios $B(M1;I\to I-1)/B(E2;I\to I-2)$ is somewhat overestimated. The calculated values for the collective g-factor, g_R defined in Eq. (2·62), are $0.32\sim 0.27$ in the range $0.1\lesssim\hbar\omega_{\rm rot}\lesssim 0.3$ MeV. The experimental ratios can be reproduced, however, if we use the phenomenological value 0.4 adopted in Ref. 14) in place of the microscopically calculated g_R, except for the 3qp band in the region $0.2\lesssim\hbar\omega_{\rm rot}\lesssim 0.3$ MeV where the experimental values are remarkably smaller than the calculated values. In this nucleus, it seems likely that the experimental data for $\hbar\omega_{\rm rot}\gtrsim 0.4$ MeV correspond to the $M1$ transitions associated with the 5qp band. This possibility was discussed in Ref. 9) and in our previous paper.[36)]

It is seen from Figs. 5~8 that the main effect of the couplings with the generalized-gamma vibrations on the $M1$ transition properties is to decrease the magnitudes of the $B(M1)$ values to some extent. A direct origin of this reduction is that the 1qp amplitude $\psi_n^{(1)}(\mu)$ in Eq. (2·31) becomes less than one due to the coupling effects. This reduction effect is found to be stronger in the 1qp band than in the 3qp band. Some numerical examples for the amplitudes characterizing the internal wave function defined by Eq. (2·31) are presented in Table I.

Calculated $E2$ transition rates for ^{157}Ho and ^{159}Tm are presented in Figs. 9 and 10, respectively. Comparing the solid lines (in which the coupling effects of the generalized-gamma vibrations are taken into account) with the broken lines (where

Table I. Calculated values for the amplitudes of the internal wave functions, defined by Eq. (2·31), valid for the 1qp and the 3qp band at $\hbar\omega_{\rm rot}=0.26$ MeV in ^{159}Tm. Only the major amplitudes (among the 60 components) are listed.

	1qp band		3qp band	
amplitudes	$\alpha=1/2$ (unfavored)	$\alpha=-1/2$ (favored)	$\alpha=1/2$ (unfavored)	$\alpha=-1/2$ (favored)
$\psi^{(1)}(\mu)$ or $\psi^{(1)}(\bar{\mu})$	0.889	0.780	0.989	0.992
$\psi^{(3)}(\mu\gamma)$ or $\psi^{(3)}(\bar{\mu}\gamma)$	0.141	0.416	−0.010	−0.014
$\psi^{(3)}(\bar{\mu}\bar{\gamma})$ or $\psi^{(3)}(\mu\bar{\gamma})$	−0.250	0.048	0.110	0.092
$\psi^{(5)}(\mu\gamma\gamma)$ or $\psi^{(5)}(\bar{\mu}\gamma\gamma)$	0.019	0.175	−0.003	−0.003
$\psi^{(5)}(\mu\bar{\gamma}\bar{\gamma})$ or $\psi^{(5)}(\bar{\mu}\bar{\gamma}\bar{\gamma})$	−0.045	−0.007	0.015	0.012
$\psi^{(5)}(\bar{\mu}\gamma\bar{\gamma})$ or $\psi^{(5)}(\mu\gamma\bar{\gamma})$	−0.110	0.034	0.001	0.001

these effects are neglected), we see a drastic effect of the generalized-gamma vibrations on the $B(E2)$ values with $\Delta I=1$ which connect the unfavoured states to the favoured states with one aligned proton in the $h_{11/2}$ orbit. The signature dependence of the $B(E2;\Delta I=1)$ follows the rule expected from Eq. (2·52) when the vibrational contributions are neglected. For ^{157}Ho and ^{159}Tm where the chemical potentials are situated about the middle of the Nilsson states associated with the $h_{11/2}$ orbit, we have found that the vibrational effects are always such that the transitions from the favoured states are enhanced in comparison with those from the unfavoured states. This signature dependence of $B(E2;I\to I-1)$ is in agreement with the experimental data. The major origin of this signature dependent effect can be attributed to the mixing of the generalized-gamma vibrations with the signature $\alpha=1$ in the unfavoured states. The microscopic mechanism of this signature dependent effect will be discussed in detail in a separate paper.[29] The vibrational effects clearly seen in the 1qp band are much reduced in the 3qp band, because the collectivity of the generalized-gamma vibration becomes weaker in the 3qp band.

Experimental values[4] for the ratio $Q_t^{(1)}/Q_t^{(2)}$ in ^{157}Ho are greater than one, and thus much larger than the calculated values shown in Fig. 9. The experimental signature dependence is also stronger, about a factor of two, than the calculated result. It is hard, however, to obtain such large values for this ratio in the theoretical calculation. In this connection, we note that our calculation well reproduces the magnitudes of the $E2$-transition moments with $\Delta I=2$ in the neighbouring nucleus ^{159}Tm (see Fig. 10) for which both the stretched and unstretched $E2$-transition rates have been determined recently by life-time measurements.[7]

Calculated results for the ratio $Q_t^{(1)}/Q_t^{(2)}$ of the unstretched and stretched $E2$-transition moments in ^{165}Lu are displayed and compared with the recent experimental data[8] in Fig. 11. It is seen that the calculation correctly reproduces the experimental magnitudes of this ratio. It is also seen that the signature dependence is weak in this nucleus with $N=94$.

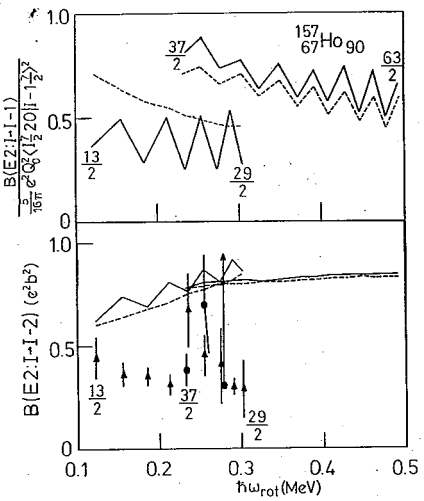

Fig. 9. $B(E2; I\to I-1)$ and $B(E2; I\to I-2)$ for ^{157}Ho, plotted as functions of ω_{rot}. The solid (broken) lines show the results of calculation in which the coupling effects of the generalized-gamma vibrations are taken into account (neglected). The solid triangles and the solid circles with error bars denote the experimental data[4] for the 1qp and the 3qp band, respectively. The $B(E2; I\to I-1)$ values are shown in units of the rigid-rotor values $(5/16\pi)\times\langle eQ_0\rangle^2\langle I, 7/2, 20|I-1, 7/2\rangle^2$ in order to clearly exhibit the signature dependence. The experimental values for this quantity are larger than one and thus off scale.

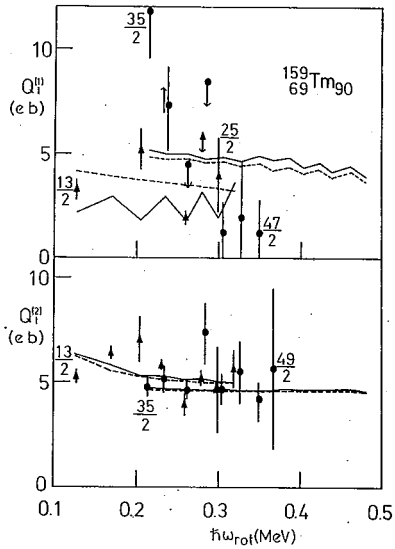

Fig. 10. $E2$-transition moments $Q_t^{(1)}$ and $Q_t^{(2)}$ for ^{159}Tm, plotted as functions of ω_{rot}. They are defined by

$$Q_t^{(\Delta I)}=\sqrt{\frac{(16\pi/5)B(E2; I\to I-\Delta I)}{\langle IK20|I-\Delta I, K\rangle^2}}.$$

The value $K=7/2$ is used. Other notations are the same as in Fig. 9. Experimental data are taken from Ref. 7).

We note here that the calculated results presented above are consistent with those of Ikeda[37] and Onishi et al.,[38] who previously pointed out the importance of the contributions from the gamma-vibrations to the $M1$ and $E2$ transition matrix elements by treating them within the framework of the macroscopic Bohr-Mottelson-type collective models.

In the calculation presented in Figs. 9~11, it is possible that the vibrational effects are overestimated. The crucial quantities determining the magnitudes of these effects are the quasiparticle-vibration-coupling vertices defined by Eq. (2·24). It is known[39),40] that the RPA calculation using the 5-major shells significantly overestimates the $B(E2)$ values between the gamma-vibrational states and the ground states in rare-earth nuclei. On the other hand, it seems reasonable to require that the calculated coupling vertices should be independent of the truncation of the Nilsson model space.[41] Then, it can be argued[42] that the 3-major shell calculation overestimates the magnitude of these vertices via the use of the force-strengths $\kappa_K^{(\pm)}$ (that reproduce the experimental excitation energies of the β and γ vibrations within this truncated model space) about 50% larger than those for the 5-major shell calculation, even when the calculated $E2$ transition matrix elements $Q_K^{(\pm)}(n)$ correctly reproduce

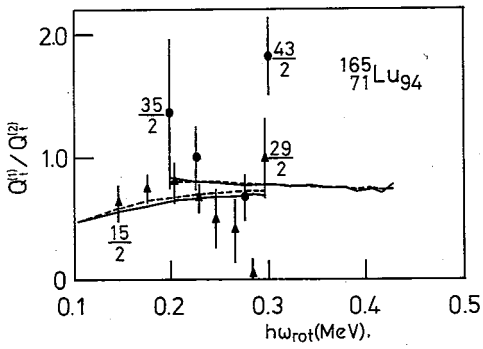

Fig. 11. Ratio $Q_t^{(1)}/Q_t^{(2)}$ of $E2$-transition moments for ^{165}Lu, plotted as a function of ω_{rot}. The value $K=9/2$ is used. Other notations are the same as in Fig. 9. Experimental data are taken from Ref. 8).

(within the 3-major shells) the experimental $B(E2)$ values between the gamma band and the g-band.

Experimental data for the $M1$ and $E2$ properties at a higher angular-momentum region are becoming available,[8] where various kinds of 5qp configurations may come into play. In this region of angular momentum, the transition from the superconducting to the normal phases of the pairing correlation is expected to take place. It remains to be an interesting subject to examine the applicability of the quasiparticle-vibration coupling model presented in this paper to such a transition region by taking into account the contributions from the pairing vibrational modes as well as the generalized-gamma vibrations.

4.3. *Nuclei with the $i_{13/2}$ odd neutron*

The deformation parameters (β_0, γ_0) calculated for the g-band configurations in ^{161}Dy, ^{167}Er and ^{161,163,167}Yb are presented in Figs. 12 and 14. These values are used in the quasiparticle-vibration-coupling calculations for the unique-parity bands associated with the $i_{13/2}$ odd neutron. For these 1qp bands, the triaxiality parameter γ_0 is

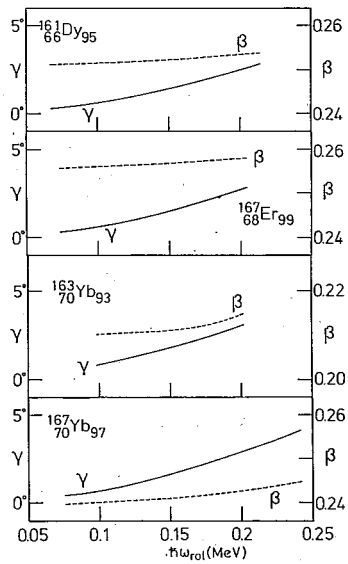

Fig. 12. Deformation parameters (β_0, γ_0) for the g-band configurations calculated as functions of ω_{rot}. These values characterize the deformations of the "cores" of the odd-N nuclei; ^{161}Dy, ^{167}Er and ^{163,167}Yb. Note that our definition of the sign of γ_0 is opposite to the Lund convention.[14]

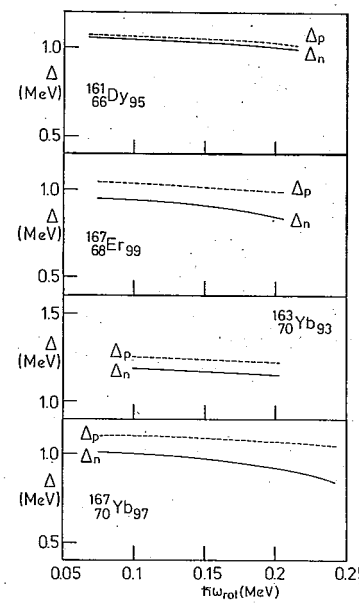

Fig. 13. Pairing gaps (Δ_p, Δ_n) for the g-band configurations calculated as functions of ω_{rot}. These values characterize the pairing deformations of the "cores" of the odd-N nuclei; ^{161}Dy, ^{167}Er and ^{163,167}Yb.

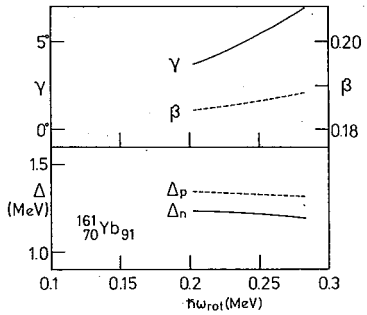

Fig. 14. Same as Figs. 12 and 13 but for ^{161}Yb.

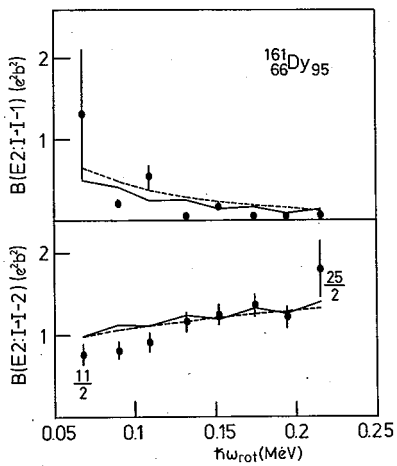

Fig. 16. $B(E2; I\rightarrow I-1)$ and $B(E2; I\rightarrow I-2)$ for ^{161}Dy, plotted as functions of ω_{rot}. The solid circles with error bars denote the experimental data.[10] Other notations are the same as in Fig. 9.

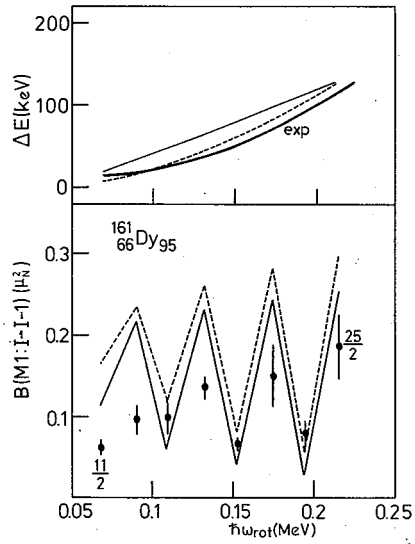

Fig. 15. $B(M1; I\rightarrow I-1)$ and the signature splittings ΔE (absolute magnitudes) for ^{161}Dy, plotted as functions of ω_{rot}. Notations are the same as in Fig. 5. Experimental data are taken from Ref. 10). Theoretical $B(M1)$ values are those calculated by using $g_R=0.21$. The sign of ΔE is negative, since the favoured signature α_f is $+1/2$ for the $i_{13/2}$ odd-quasiparticle in contrast to the $h_{11/2}$ odd-quasiparticle for which it is $-1/2$.

positive (negative in the Lund convention) and gradually increases as a function of ω_{rot}, but its magnitude remains small in the angular momentum region under consideration.

For the stable nuclei,[161] Dy and [167] Er, the $B(M1; I\rightarrow I-1)$, $B(E2; I\rightarrow I-1)$ and $B(E2; I\rightarrow I-2)$ values are separately known by Coulomb excitation experiments.[10),11)] Calculated results for these quantities are shown in Figs. 15~18 and compared with the experimental data. Concerning the calculation of the $B(M1)$ values, we remark that the microscopically calculated values for the collective g_R-factor defined by Eq. (2·56) are 0.37~0.36 for ^{161}Dy and 0.32~0.28 for ^{167}Er in the rotational-frequency region under consideration. However, for the magnitude of $B(M1)$, we find that much better agreement with the experimental data is obtainable if the phenomenologically determined values, 0.21 for ^{161}Dy and 0.18 for ^{167}Er, are used in place of the microscopically calculated g_R. (The possible origins of decreasing the g_R values in these nuclei are discussed in the textbook of Bohr and Mottelson.[3)]) Thus, the $B(M1)$ values obtained by using the phenomenological g_R are presented in Figs. 15 and 17. It is seen that the signature dependence is well reproduced in the calculation.

Figures 16 and 18 clearly show that the magnitudes of the calculated $B(E2; I\rightarrow I-1)$ and $B(E2; I\rightarrow I-2)$ are in good agreement with the experimental data. In

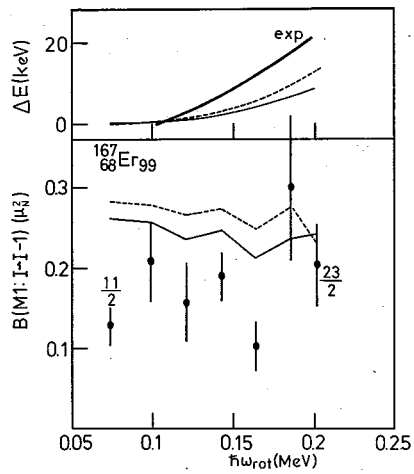

Fig. 17. Same as Fig. 15 but for ^{167}Er. Experimental data are taken from Ref. 11). Theoretical $B(M1)$ values are those calculated by using $g_R=0.18$.

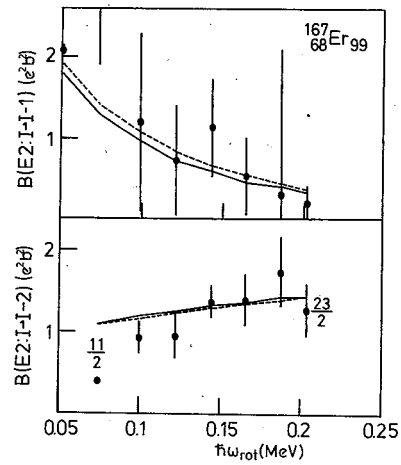

Fig. 18. Same as Fig. 16 but for ^{167}Er. Experimental data are taken from Ref. 11).

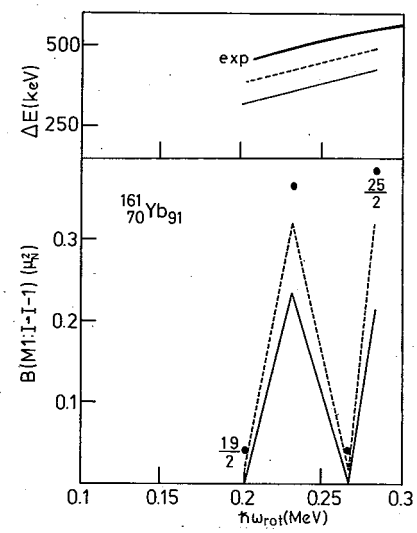

Fig. 19. Same as Fig. 15 but for ^{161}Yb. Experimental $B(M1)$ values are those[12),13)] obtained by assuming appropriate values for $B(E2; I\rightarrow I-2)$. Theoretical $B(M1)$ values are those calculated by using $g_R=0.2$.

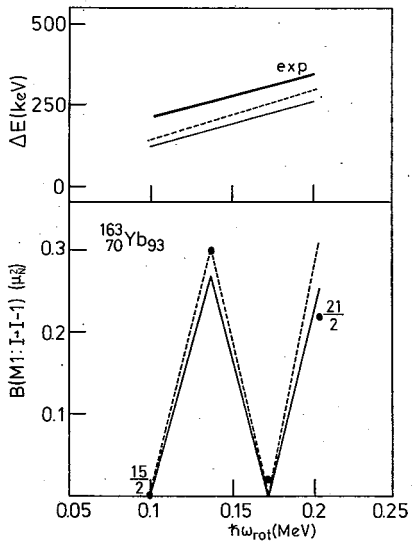

Fig. 20. Same as Fig. 19 but for ^{163}Yb.

the calculation we find that the signature dependence of $B(E2; I\rightarrow I-1)$ is weak in the case of ^{161}Dy and ^{167}Er. This is because the static triaxiality γ_0 is small and also because the coupling effects from the generalized-gamma vibrations are weak in these nuclei. To test this result of calculation, we need more accurate data for $B(E2; I\rightarrow I-1)$ in ^{167}Er. Of course, experimental data for the $M1$ and $E2$ properties of the 3qp bands in these odd-N nuclei are very much desired.

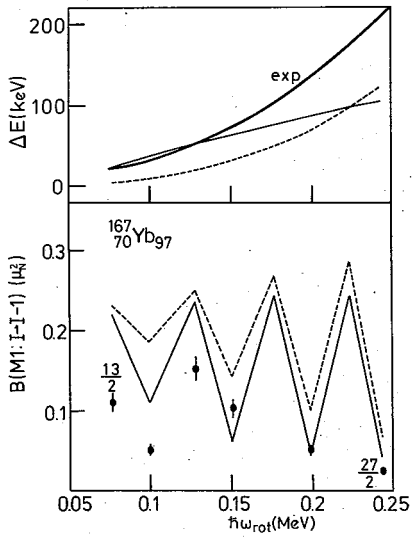

Fig. 21. Same as Fig. 19 but for ^{167}Yb.

Figures 19~21 show the calculated results for $B(M1; I \to I-1)$ in ^{161,163,167}Yb. In these calculations, the phenomenological value $g_R=0.2$ is used for the rotational g-factor. We see that the calculated signature splittings ΔE decrease as the neutron number increases from 91 to 97, in agreement with the experimental trend. The signature dependence of the $B(M1)$ values is also well reproduced in the calculation. The decrease of ΔE is a simple consequence of the increase of the deformation parameter β with increasing N (see Figs. 12 and 14).

§ 5. Concluding remarks

We have developed a microscopic model which takes into account both the static and dynamic triaxial deformations in the description of high-spin states of odd-A nuclei. The model is based on the rotating shell model and treats the quasiparticle-vibration couplings in the uniformly rotating frame of reference. With the use of this model, we have discussed the effects of the static and dynamic triaxial deformations on the signature splitting of the quasiparticle energies and on the signature dependence of $B(M1)$, $B(E2; I \to I-1)$ and $B(E2; I \to I-2)$ values for the transitions within the unique-parity bands in the rare-earth odd-A nuclei to which experimental data are available.

It has been shown that both the static and dynamic triaxial deformations bring about characteristic signature dependences in the $E2$-transition matrix elements. Thus, the $B(E2; I \to I-1)$ values are, in general, sensitive to whether these signature-dependent matrix elements add coherently or destructively. It has also been shown that the major effects of aligned quasiparticles on the $B(M1)$ values are easily taken into account through the change in the g_{RPA} values. In particular, the increase of the $B(M1)$ values associated with the alignment of the $i_{13/2}$ neutrons in odd-Z nuclei is qualitatively reproduced in the calculation. Thus, the microscopic model developed in this paper is useful to study the relation between the alignment and the triaxial deformations as well as their effects on the $M1$ and $E2$ transition properties at high-spin.

It is certainly a very interesting subject to further refine the microscopic model described in this paper; for instance, by taking into account higher-order quasiparticle-vibration-coupling diagrams. In view of the present status of experimental data, however, it seems for us more important to carry out a systematic comparison between theoretical calculations and experimental data within the framework of the model presented. More accurate and systematic data for the signature splittings, $B(M1)$, $B(E2; I \to I-1)$ and $B(E2; I \to I-2)$ are needed in order to identify

the static and dynamic triaxial deformations and to understand their roles in characterizing the high-spin spectra in the near-yrast region.

Acknowledgements

We are deeply indebted to J. D. Garrett, G. B. Hagemann, I. Hamamoto and B. R. Mottelson for valuable discussions and for giving us useful comments on this work, to G. B. Hagemann and M. Ohshima for providing us with their experimental data prior to publication. Two of us (Y.R.S. and K.M.) are grateful to the Niels Bohr Institute for the financial support to our stay in the NBI during the summer of 1987, where the final version of this paper was written. The computer calculation for this work has been supported in part by the Research Center for Nuclear Physics, Osaka University, and in part by the Institute for Nuclear Study, University of Tokyo.

References

1) L. S. Kisslinger and R. A. Sorensen, Rev. Mod. Phys. **35** (1963), 853.
2) V. G. Soloviev, *Theory of Complex Nuclei* (Nauka, Moskow, 1971 [Transl. Pergamon Press, 1976]).
3) A. Bohr and B. R. Mottelson, *Nuclear Structure,* vol. 2 (Benjamin, New York, 1975).
4) G. B. Hagemann et al., Nucl. Phys. **A424** (1984), 365.
5) A. J. Larabee et al., Phys. Rev. **C29** (1984), 1934.
6) R. Holtzmann et al., Phys. Rev. **C31** (1985), 421.
7) J. Gascon et al., Nucl. Phys. **A467** (1987), 539.
8) G. B. Hagemann, private communication.
9) P. Frandsen et al., Phys. Lett. **B177** (1986), 287.
10) M. Oshima et al., to be published.
11) M. Ohshima et al., Nucl. Phys. **A436** (1985), 518.
12) N. Roy et al., Nucl. Phys. **A382** (1982), 125.
13) J. Kownacki et al., Nucl. Phys. **A394** (1983), 269.
14) I. Hamamoto, *Proc. Niels Bohr Centennial Conf. on Nuclear Structure, Copenhagen 1985,* ed. R. Broglia, G. B. Hagemann and B. Herskind (North-Holland, 1985), p. 129, and references therein.
15) I. Hamamoto and B. Mottelson, Phys. Lett. **132B** (1983), 7.
16) Y. R. Shimizu and K. Matsuyanagi, Prog. Theor. Phys. **70** (1983), 144.
17) Y. R. Shimizu and K. Matsuyanagi, Prog. Theor. Phys. **72** (1984), 799.
18) R. Bengtsson and S. Frauendorf, Nucl. Phys. **A327** (1979), 139.
19) S. Frauendorf, in *Nuclear Physics,* ed. C. H. Dasso, R. A. Broglia and A. Winther (North-Holland, 1982), p. 111.
20) E. R. Marshalek, Nucl. Phys. **A275** (1977), 416.
21) T. Marumori, T. Maskawa, F. Sakata and A. Kuriyama, Prog. Theor. Phys. **64** (1980), 1294.
22) Y. R. Shimizu, to be published.
23) Y. R. Shimizu and K. Matsuyanagi, Prog. Theor. Phys. **74** (1985), 1346, and to be published.
24) J. D. Garrett, G. B. Hagemann and B. Herskind, Annu. Rev. Nucl. and Part. Sci. **36** (1986), 419.
25) Y. R. Shimizu and K. Matsuyanagi, Prog. Theor. Phys. **71** (1984), 960.
26) E. R. Marshalek, Phys. Rev. **C11** (1975), 1426.
27) E. R. Marshalek, Nucl. Phys. **A331** (1979), 429.
28) K. Hara and S. Kusuno, Nucl. Phys. **A245** (1975), 147.
29) M. Matsuzaki, Y. R. Shimizu and K. Matsuyanagi, in preparation.
30) D. Janssen and I. N. Mikhailov, Nucl. Phys. **A318** (1979), 390.
31) S. Frauendorf, Phys. Lett. **100B** (1981), 219.
32) I. Hamamoto and B. Mottelson, Phys. Lett. **167B** (1986), 370.
33) Y. S. Chen, P. B. Semmes and G. A. Leander, Phys. Rev. **C34** (1986), 1935.
34) J. Billowes et al., Phys. Lett. **178B** (1986), 145.
35) S. Frauendorf and F. R. May, Phys. Lett. **125B** (1983), 245.
36) M. Matsuzaki, Y. R. Shimizu and K. Matsuyanagi, Prog. Theor. Phys. **77** (1987), 1302.
37) A. Ikeda, Nucl. Phys. **A439** (1985), 317.
38) N. Onishi, I. Hamamoto, S. Åberg and A. Ikeda, Nucl. Phys. **A452** (1986), 71.
39) T. S. Dumitrescu and I. Hamamoto, Nucl. Phys. **A383** (1982), 205.

40) Y. R. Shimizu and K. Matsuyanagi, Prog. Theor. Phys. **72** (1984), 1017.
41) M. Matsuo and K. Matsuyanagi, Prog. Theor. Phys. **78** (1987), 591.
42) I. Hamamoto, private communication.

Note added in proof:

1) The operators $\hat{D}^{\lambda}_{\mu\nu}$ used in Eq. (2·35) are equivalent to the $\hat{D}^{\lambda}_{\bar{\nu}\mu}$ operators of Ref. 20).
2) The quadrupole matrix elements, $Q^{(-)}_{K}(\mu\bar{\nu})$ and $Q^{(-)}_{K}(n)$, appearing in Eqs. (2·43) and (2·44) should be distinguished from the doubly stretched ones appearing in Eqs. (2·24)~(2·30), although the same notations are used for these different quantities.
3) In the actual numerical calculation, the angular momentum I_0 defined by Eq. (2·33) is used in place of the $I_c \equiv \langle \hat{J}_x \rangle$ appearing in the expressions for the intrinsic $E2$ operator $Q^{(\mathrm{PA})}_{2K}$. This replacement may be allowed for the Ho, Tm and Lu nuclei, in which the difference $(I_0 - I_c)$ arising from the aligned angular momentum of the $h_{11/2}$ proton is rather small ($1 \sim 2\hbar$). When this difference cannot be neglected, more careful treatment of these quantities will be required.

Progress of Theoretical Physics, Vol. 81, No. 3, March 1989

Analysis of Collective-Noncollective Couplings in a Degenerate Many j-Shell Model

Hirokazu AIBA and Kenichi MATSUYANAGI

Department of Physics, Kyoto University, Kyoto 606

(Received September 17, 1988)

The selfconsistent-collective-coordinate method is applied to anharmonic quadrupole vibrations in a degenerate many j-shell model with the pairing-plus-quadrupole force. By comparing the result obtained by this method with that obtained by the boson-expansion method, it is shown that
1) the selfconsistent-collective-coordinate method yields, after a suitable canonical quantization, the result that agrees to order $(j+1/2)^{-1}$ with that obtained by the boson-expansion method, in the limit that the time-dependent Hartree-Bogoliubov space is truncated to the multiphonon space built out of the 2^+ phonons, and
2) the couplings between the RPA 2^+ phonons and the other modes (the pairing rotations and the noncollective modes) considerably modify the fourth-order boson Hamiltonian obtained by the conventional boson-expansion method.

§ 1. Introduction

This is the first report from work which aims at systematically studying anharmonic quadrupole vibrations in transitional nuclei by means of the selfconsistent-collective-coordinate (SCC) method.[1] The SCC method has been developed into a form applicable to nuclear collective phenomena by Matsuo and one of the present authors (K. M.),[2),3)] and successfully applied to the problem of two-phonon states of the anharmonic gamma-vibrations in axially symmetric deformed nuclei.[3)] The method has been further developed by Matsuo[4)] to restore the nucleon-number conservation which is broken by the use of the BCS quasiparticle representation. This is done by taking the coupling effects of the pairing rotational modes into account.

Microscopic study of anharmonic vibrational spectra in transitional nuclei by means of the boson-expansion method (BET) has long history.[5)] As was emphasized by Lie and Holzwarth,[6)] Holzwarth, Janssen and Jolos, [7)] and Kishimoto and Tamura,[8)] one of the major open problems is how to treat the mode-mode coupling effects between the lowest-frequency 2^+ phonons and the other modes, which are usually neglected by the truncation of the quasiparticle Hilbert space to the subspace built out of the multiphonon states associated with the collective 2^+ phonons. Kishimoto and Tamura took into account the collective-noncollective coupling effects by means of a projection-operator method with some physical assumptions, and demonstrated the importance of these effects.[8)] The SCC method developed in recent years provides us with a selfconsistent scheme which renormalizes the collective-noncollective coupling effects into the collective Hamiltonian. Thus, it has become possible to take a new step forward in the microscopic description of anharmonic vibrations beyond the level reached by the works referred to above.

In this paper, we employ a degenerate many j-shell model with the conventional pairing-plus-quadrupole ($P+QQ$) force,[9)] and explicitly see how the SCC method

renormalizes the coupling effects between different RPA modes into the collective Hamiltonian for anharmonic quadrupole vibrations. As a matter of course, detailed subshell structure plays a crucial role in determining properties of anharmonic vibrations in individual nuclei. It would be instructive, however, to study the degenerate limit before investigating such realistic situations, since this model provides us with a limiting situation where quadrupole collectivity in the RPA is concentrated in the lowest 2^+ phonon and, accordingly, the other 2^+ modes remain at the unperturbed two-quasiparticle energy. Of course, the RPA 4^+ modes are also completely noncollective. Furthermore, the pairing vibrational 0^+ modes vanish in the degenerate limit. Thus, distinction between the lowest 2^+ phonon and the other RPA modes is quite pronounced in this model.

Major subjects of this paper are 1) to examine validity of the quantization procedure which was formulated in Ref. 2) and used in Ref. 3), 2) to explicitly see the contributions from the couplings of the pairing rotations to the quadrupole collective Hamiltonian, and 3) to explicitly see how the coupling effects of the noncollective RPA modes with angular momenta 2 and 4 affect the quadrupole vibrational spectra. Up to now, the point 1) was examined for a schematic $SU(3)$ model in Ref. 2). Also, the point 2) was studied in Ref. 4) for an $O(4)$ model. This paper is an extension of those works to a more realistic situation. The point 3) is here studied by the SCC method for the first time.

After defining the model in § 2, we apply the SCC method and the modified Marumori (mM) boson-expansion method[5),6)] to it in §§ 3 and 4, respectively. The above three points are discussed in § 5 where the results obtained in §§ 3 and 4 are compared and used to clarify these points. Some numerical examples are given in § 6 to quantitatively examine these points.

§ 2. A degenerate many j-shell model

We consider a system composed of N_p protons and N_n neutrons moving within many shells which have common values of the angular momenta, j_p and j_n, respectively, and are degenerate in energy. We denote the numbers of the j_p- and j_n-shells as k_p and k_n, respectively (see Fig. 1), and assume that the nucleons are interacting with the familiar $P+QQ$ force.[9)] In the BCS quasiparticle representation, our model Hamiltonian is written as

$$H=\sum_{\tau=p,n}(H_{0\tau}+H_{P\tau})+H_{QQ}\,, \tag{2·1}$$

$$H_{0\tau}=E_\tau\sum_{i=1}^{k_\tau}\sum_m a_{\tau im}^\dagger a_{\tau im}\,, \tag{2·2}$$

$$H_{P\tau}=-\frac{1}{4}G_\tau(\tilde{P}_{\tau+}^\dagger\tilde{P}_{\tau+}+\tilde{P}_{\tau-}^\dagger\tilde{P}_{\tau-})\,, \tag{2·3}$$

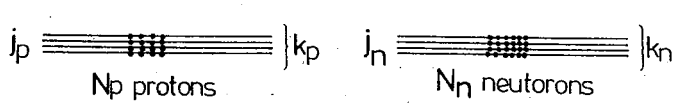

Fig. 1.

$$H_{QQ}=-\frac{1}{2}\chi\sum_{\mu}Q_{2\mu}^{\dagger}Q_{2\mu}\,, \tag{2·4}$$

where $(a_{\tau im}^{\dagger}, a_{\tau im})$ are the quasiparticle operators with τ denoting the protons or the neutrons, and i labelling the different j_τ shells. In terms of the bilinear quasiparticle operators defined by

$$A_{\tau\lambda\mu}^{\dagger}(ii')=\frac{1}{\sqrt{2}}\sum_{mm'}\langle j_\tau m j_\tau m'|\lambda\mu\rangle a_{\tau im}^{\dagger}a_{\tau i'm'}^{\dagger}\,, \tag{2·5}$$

$$B_{\tau\lambda\mu}^{\dagger}(ii')=-\sum_{mm'}\langle j_\tau m j_\tau m'|\lambda\mu\rangle a_{\tau im}^{\dagger}\tilde{a}_{\tau i'm'}\,, \tag{2·6}$$

where $\tilde{a}_{\tau im}\equiv(-1)^{j_\tau-m}a_{\tau i-m}$, the pairing and the quadrupole operators $\tilde{P}_{\tau\pm}^{\dagger}$ and $Q_{2\mu}^{\dagger}$ are written as

$$\tilde{P}_{\tau+}^{\dagger}=2\sqrt{\Omega_\tau}\,\eta_\tau\sum_{i=1}^{k_\tau}(A_{\tau 00}^{\dagger}(ii)+A_{\tau 00}(ii))-2\sqrt{\Omega_\tau}\,\xi_\tau\sum_{i=1}^{k_\tau}B_{\tau 00}^{\dagger}(ii)\,, \tag{2·7}$$

$$\tilde{P}_{\tau-}^{\dagger}=\sqrt{\Omega_\tau}\sum_{i=1}^{k_\tau}(A_{\tau 00}^{\dagger}(ii)-A_{\tau 00}(ii))\,, \tag{2·8}$$

$$Q_{2\mu}^{\dagger}=\sum_{\tau}Q_{\tau 2\mu}^{\dagger}\,, \tag{2·9}$$

$$Q_{\tau 2\mu}^{\dagger}=q_\tau\xi_\tau\sum_{i,i'=1}^{k_\tau}(A_{\tau 2\mu}^{\dagger}(ii')+A_{\tau 2\mu}(ii'))+q_\tau\eta_\tau\sum_{i,i'=1}^{k_\tau}(B_{\tau 2\mu}^{\dagger}(ii')+B_{\tau 2\mu}(ii'))\,. \tag{2·10}$$

Here $\Omega_\tau\equiv j_\tau+1/2$ and $q_\tau\equiv\langle j_\tau\|r^2Y_2\|j_\tau\rangle/\sqrt{5}$. The quantities $(E_\tau, \xi_\tau, \eta_\tau)$ associated with the pairing correlations are given in the BCS approximation by

$$E_\tau=\frac{1}{2}G_\tau k_\tau\Omega_\tau\quad,\quad\xi_\tau=\sqrt{2}u_\tau v_\tau\quad,\quad\eta_\tau=\frac{1}{2}(u_\tau^2-v_\tau^2) \tag{2·11}$$

with $v_\tau^2=N_\tau/(2k_\tau\Omega_\tau)$ and $u_\tau^2=1-v_\tau^2$. The above η_τ -factor should not be confused with the collective variables η_μ introduced later. In order to avoid inessential complications, we consider a particular case $j_p=j_n\equiv j$, $k_p=k_n\equiv k$, $G_p=G_n\equiv G_0$ and $q_p=q_n\equiv q$ in the following.

§ 3. Application of the SCC method

As collective variables, we take five complex variables (η_μ^*, η_μ) with $\mu=-2, -1, 0, 1$ and 2 representing quadrupole collective motions, and two sets of number-angle variables (N_τ, φ_τ) with $\tau=p, n$ to describe the pairing rotations. Following Ref. 4), we write the time-dependent Hartree-Bogoliubov (TDHB) state vectors in the following form:

$$|\phi(\eta_\mu^*, \eta_\mu, N_\tau, \varphi_\tau)\rangle=e^{-i\varphi_p\hat{N}_p}e^{-i\varphi_n\hat{N}_n}e^{i\hat{G}(\eta_\mu^*,\,\eta_\mu,\,N_\tau)}|\phi_0\rangle \tag{3·1}$$

with

$$i\hat{G}(\eta_\mu^*, \eta_\mu, N_\tau)=\sum_{\tau\lambda\mu}\{G_{\tau\lambda}(\eta_\mu^*, \eta_\mu, N_\tau)X_{\tau\lambda\mu}^{\dagger}-G_{\tau\lambda}^{*}(\eta_\mu^*, \eta_\mu, N_\tau)X_{\tau\lambda\mu}\}$$
$$+\sum_{\tau}\{G_{\tau N}(\eta_\mu^*, \eta_\mu, N_\tau)\hat{N}_\tau^{(\mathrm{RPA})}+G_{\tau\theta}(\eta_\mu^*, \eta_\mu, N_\tau)\hat{\Theta}_\tau^{(\mathrm{RPA})}\}\,, \tag{3·2}$$

where $\hat{N}_p$ and $\hat{N}_n$ are the number operators for protons and neutrons, respectively and $|\phi_0\rangle$ is the BCS vacuum. The operator $i\hat{G}$ is expanded in terms of the RPA vibrational modes

$$X^{\dagger}_{\tau\lambda\mu}=\sum_{\tau}\sum_{ii'}\{\psi_{\tau\lambda\tau}(ii')A^{\dagger}_{\tau\lambda\mu}(ii')+\varphi_{\tau\lambda\tau}(ii')A_{\tau\,\widetilde{\lambda\mu}}(ii')\} \tag{3·3}$$

and the RPA number and angle operators

$$\hat{N}_{\tau}^{(\mathrm{RPA})}=\xi_{\tau}\sqrt{2\Omega}\sum_{i}\{A^{\dagger}_{\tau 00}(ii)+A_{\tau 00}(ii)\}\,, \tag{3·4}$$

$$\hat{\Theta}_{\tau}^{(\mathrm{RPA})}=\frac{1}{2\xi_{\tau}k\sqrt{2\Omega}}\sum_{i}\{A^{\dagger}_{\tau 00}(ii)-A_{\tau 00}(ii)\}\,. \tag{3·5}$$

Here r labels different modes with the same multipolarity $(\lambda\mu)$. In the particular model under consideration, the pairing vibrational modes with $\lambda=0$ disappear, and there is only one collective vibrational mode with $\lambda=2$ (aside from the degeneracy with respect to the magnetic quantum number μ) in the RPA. We denote these collective vibrational modes as $(X^{\dagger}_{c2\mu}, X_{c2\mu})$.

The $G_{r\lambda}$, $G_{\tau N}$ and $G_{\tau\theta}$ appearing in Eq. (3·2) are functions of collective variables $(\eta_\mu{}^*, \eta_\mu, N_\tau)$, and determine a collective submanifold embedded in the phase space associated with the general TDHB state vectors. The basic equations of the SCC method, which determine the functions $G_{r\lambda}$, $G_{\tau N}$ and $G_{\tau\theta}$, are

i) *equations of collective submanifold*

$$\delta\langle\phi_0|e^{-i\hat{G}}\Big(H+\sum_{\mu}\Big(\frac{\partial\mathcal{H}}{\partial\eta_\mu}\frac{\partial}{\partial\eta_\mu{}^*}-\frac{\partial\mathcal{H}}{\partial\eta_\mu{}^*}\frac{\partial}{\partial\eta_\mu}\Big)-\sum_{\tau}\frac{\partial\mathcal{H}}{\partial N_\tau}\hat{N}_\tau\Big)e^{i\hat{G}}|\phi_0\rangle=0\,, \tag{3·6}$$

ii) *canonical-variable conditions*

$$\langle\phi_0|e^{-i\hat{G}}\frac{\partial}{\partial\eta_\mu}e^{i\hat{G}}|\phi_0\rangle=\frac{1}{2}\eta_\mu{}^*\,, \tag{3·7}$$

$$\langle\phi_0|e^{-i\hat{G}}\frac{\partial}{\partial\eta_\mu{}^*}e^{i\hat{G}}|\phi_0\rangle=-\frac{1}{2}\eta_\mu\,, \tag{3·8}$$

$$\langle\phi_0|e^{-i\hat{G}}\hat{N}_\tau e^{i\hat{G}}|\phi_0\rangle=N_\tau\,, \tag{3·9}$$

$$\langle\phi_0|e^{-i\hat{G}}\frac{\partial}{\partial N_\tau}e^{i\hat{G}}|\phi_0\rangle=0\,. \tag{3·10}$$

Here $\mathcal{H}$ is a classical collective Hamiltonian defined by

$$\begin{aligned}\mathcal{H}(\eta_\mu{}^*, \eta_\mu, N_\tau)&=\langle\phi_0|e^{-i\hat{G}}He^{i\hat{G}}|\phi_0\rangle-\langle\phi_0|H|\phi_0\rangle\\&\equiv\mathcal{H}_0+\mathcal{H}_P+\mathcal{H}_{QQ}\,,\end{aligned} \tag{3·11}$$

where $\mathcal{H}_0$, $\mathcal{H}_P$ and $\mathcal{H}_{QQ}$ represent the contributions from H_0, H_P and H_{QQ}, respectively. In accordance with the use of separable interaction, we evaluate $\mathcal{H}_{QQ}$ by

$$\mathcal{H}_{QQ}=-\frac{1}{2}\chi\sum_{\mu}Q^{*}_{2\mu}(\eta_\mu{}^*, \eta_\mu, N_\tau)Q_{2\mu}(\eta_\mu{}^*, \eta_\mu, N_\tau)\,, \tag{3·12}$$

where $Q^{*}_{2\mu}(\eta_\mu{}^*, \eta_\mu, N_\tau)=\sum_{\tau}Q^{*}_{\tau 2\mu}(\eta_\mu{}^*, \eta_\mu, N_\tau)$ are classical collective representations

for the quadrupole operators and are defined by

$$Q^{*}_{\tau 2\mu}(\eta_\mu{}^*, \eta_\mu, N_\tau) \equiv \langle\phi_0|e^{-i\hat{G}} Q^{\dagger}_{\tau 2\mu} e^{i\hat{G}}|\phi_0\rangle \,. \tag{3·13}$$

We solve the basic equations (3·6)~(3·10) by expanding $G_{\tau\lambda}$, $G_{\tau N}$ and $G_{\tau\theta}$ in power series of $\eta_\mu{}^*$, η_μ and $N_\tau - N_{0\tau}$, where $N_{0\tau} = \langle\phi_0|\hat{N}_\tau|\phi_0\rangle$. Requiring that anharmonic vibrations of the system under consideration reduce to the RPA phonons ($X^{\dagger}_{c2\mu}$, $X_{c2\mu}$) in the small-amplitude limit, we can set the first-order term as

$$i\hat{G}^{(1)} = \sum_{\mu}(G^{(1)}_{c2} X^{\dagger}_{c2\mu} - G^{*(1)}_{c2} X_{c2\mu}) \,, \tag{3·14}$$

$$G^{(1)}_{c2} = \sigma\eta_\mu + \tau\tilde{\eta}_\mu{}^* \,, \tag{3·15}$$

where $\tilde{\eta}_\mu \equiv (-1)^\mu \eta_{-\mu}$, and σ and τ are arbitrary complex numbers satisfying $|\sigma|^2 - |\tau|^2 = 1$. A choice of their values fixes our canonical coordinate system for describing the collective submanifold. We set $\sigma = (s + s^{-1})/2$ and $\tau = (s - s^{-1})/2$ with

$$s^4 = \sum_{ii'}(q_{c\tau}(ii'))^2 / \sum_{ii'}(p_{c\tau}(ii'))^2 \,. \tag{3·16}$$

This is the optimized RPA boundary condition introduced in Refs. 2) and 3). Here, $q_{c\tau}(ii')$ and $p_{c\tau}(ii')$ are the coefficients appearing in the RPA coordinate and momentum operators, respectively. They are given as linear combinations of the amplitudes $\psi_{c\tau}(ii')$ and $\varphi_{c\tau}(ii')$ defined by (3·3) when the RPA phonon frequency ω_c is real. They are also well defined for the case where ω_c is imaginary. Thus, we can go beyond the RPA critical point by the use of the phonon operators defined through the coordinate and momentum operators.[2),3)]

In the special case of degenerate many j-shells, the amplitudes $\psi_{c\tau}(ii')$ and $\varphi_{c\tau}(ii')$ are independent of the components (ii') and, consequently, the first-order term with the optimized RPA boundary condition reduces to an especially simple form:

$$i\hat{G}^{(1)} = \sum_{\mu}(\eta_\mu X^{\dagger}_{\mathrm{TD},2\mu} - \eta_\mu{}^* X_{\mathrm{TD},2\mu}) \,, \tag{3·17}$$

where $X^{\dagger}_{\mathrm{TD},2\mu}$ are just the Tamm-Dancoff phonons given by

$$X^{\dagger}_{\mathrm{TD},2\mu} = \frac{1}{k\xi}\sum_{\tau}\sum_{ii'}\xi_\tau A^{\dagger}_{\tau 2\mu}(ii') \tag{3·18}$$

with $\xi \equiv (\xi_p{}^2 + \xi_n{}^2)^{1/2}$.

Following the $(\eta_\mu{}^*, \eta_\mu, N_\tau - N_{0\tau})$ expansion procedure,[4)] we obtain the second-order solutions as follows:

$$G^{(2)*}_{c2\mu} = 0 \,, \tag{3·19}$$

$$G^{(2)*}_{\substack{\tau\lambda\mu \\ (\tau\neq c)}} = \begin{cases} g_\lambda{}^{(20)}(\eta^*\eta^*)_{\lambda\mu} + g_\lambda{}^{(11)}(\eta^*\tilde{\eta})_{\lambda\mu} + g_\lambda{}^{(02)}(\tilde{\eta}\tilde{\eta})_{\lambda\mu} & \text{for } \lambda = 2, 4 \,, \\ 0 \quad \text{for } \lambda = 0 \,, \end{cases} \tag{3·20}$$

$$G^{(2)*}_{N\tau} = 0 \quad , \quad G^{(2)*}_{\theta\tau} = g_{\theta\tau}{}^{(11)}(\eta^*\tilde{\eta})_{00} \,, \tag{3·21}$$

where

$$g_\lambda^{(20)}=-(6E-\beta)Z_\lambda/d\,, \tag{3·22}$$

$$g_\lambda^{(11)}=2(3E+\beta)Z_\lambda/d\,, \tag{3·23}$$

$$g_\lambda^{(02)}=\beta Z_\lambda/d\,, \tag{3·24}$$

$$g_{\theta\tau}^{(11)}=-4\sqrt{5}\xi\bar{\xi}_\tau^2\bar{\eta}_\tau\,. \tag{3·25}$$

Note that $G_{\tau\lambda\mu}^{(2)*}$ with $\tau\neq c$ are independent of r. Note also that the $(N_\tau-N_{0\tau})$-dependent terms are eliminated by taking the N_0 values which just coincide with the proton and neutron numbers N_τ of our system (see Ref. 4) for further discussion on this point). In the above equations, the following notations are used: $d\equiv(2E)^2-4(\alpha^2-\beta^2)$, $\alpha\equiv 2E+\beta$, $\beta\equiv-\chi q^2k^2\xi^2$, $\bar{\xi}_\tau\equiv\xi_\tau/\xi$, $\bar{\eta}_\tau\equiv\eta_\tau/\xi$,

$$Z_\lambda=\begin{cases}\dfrac{1}{\sqrt{n_2}}\bar{\xi}_p\bar{\xi}_n|\bar{\eta}_p-\bar{\eta}_n|x_2 & \text{for}\quad \lambda=2\,,\\[2ex] \dfrac{1}{\sqrt{n_4}}\sqrt{\bar{\xi}_p{}^2\bar{\xi}_p{}^2+\bar{\xi}_n{}^2\bar{\eta}_n{}^2}\,x_4 & \text{for}\quad \lambda=4\,,\end{cases} \tag{3·26}$$

$x_\lambda\equiv 20\beta W(22jj\,;\,\lambda j)$ with W being the Racah coefficients. The quantities n_λ denote the numbers of the noncollective RPA modes with $\lambda=2$ and 4, and are given by

$$n_\lambda=\begin{cases}k(k+1)-1 & \text{for}\quad \lambda=2\,,\\ k(k+1) & \text{for}\quad \lambda=4\,.\end{cases} \tag{3·27}$$

The notations $(\eta^*\eta^*)_{\lambda\mu}$, $(\eta^*\bar{\eta})_{\lambda\mu}$, etc. represent vector couplings; e.g.,

$$(\eta^*\bar{\eta})_{\lambda\mu}=\sum_{\mu_1\mu_2}\langle 2\mu_1 2\mu_2|\lambda\mu\rangle\eta_{\mu_1}^*\bar{\eta}_{\mu_2}\,. \tag{3·28}$$

The third-order solutions are given by

$$G_{c2\mu}^{(3)*}=\sum_{\lambda=2,4}g_{\lambda,\mathrm{dyn}}^{(30)}((\eta^*\eta^*)_\lambda\eta^*)_{2\mu}+\sum_\lambda g_\lambda^{(21)}((\eta^*\eta^*)_\lambda\bar{\eta})_{2\mu}$$
$$+\sum_{\lambda=2,4}\{g_{\lambda,\mathrm{dyn}}^{(12)}(\eta^*(\bar{\eta}\bar{\eta})_\lambda)_{2\mu}+g_{\lambda,\mathrm{dyn}}^{(12)'}((\eta^*\bar{\eta})_\lambda\bar{\eta})_{2\mu}\}\,, \tag{3·29}$$

where

$$g_{\lambda,\mathrm{dyn}}^{(30)}=-g_{\lambda,\mathrm{dyn}}^{(12)}=\frac{1}{2}g_{\lambda,\mathrm{dyn}}^{(12)'}=-\frac{1}{10}\hat{2}\hat{\lambda}n_\lambda g_\lambda^{(11)}(g_\lambda^{(20)}-g_\lambda^{(02)})\quad\text{for}\quad\lambda=2,4\ \text{only}\,, \tag{3·30}$$

$$g_\lambda^{(21)}=g_{\lambda,\mathrm{tru}}^{(21)}+g_{\lambda,\mathrm{dyn}}^{(21)}\,, \tag{3·31}$$

$$g_{\lambda,\mathrm{tru}}^{(21)}=\frac{1}{30}\hat{2}\hat{\lambda}C_\lambda\quad\text{for}\quad\lambda=0,2,4\,, \tag{3·32}$$

$$g_{\lambda,\mathrm{dyn}}^{(21)}=\begin{cases}-\dfrac{1}{5}\hat{2}\hat{\lambda}n_\lambda((g_\lambda^{(20)})^2-(g_\lambda^{(02)})^2) & \text{for}\quad\lambda=2,4\,,\\ 0 & \text{for}\quad\lambda=0\,.\end{cases} \tag{3·33}$$

Here $\hat{\lambda}\equiv\sqrt{2\lambda+1}$,

$$C_\lambda \equiv 50(\bar{\xi}_p{}^4 + \bar{\xi}_n{}^4) \begin{Bmatrix} j & j & 2 \\ j & j & 2 \\ j & j & \lambda \end{Bmatrix} \tag{3·34}$$

and the quantities with the subscript "dyn" represent the dynamical contributions from the collective-noncollective couplings of interest. The meaning of the subscript "tru" will be explained later in § 5. We omit explicit expressions for $G^{(3)}_{\tau+c,\lambda\mu}$, $G^{(3)}_{N\tau}$ and $G^{(3)}_{\theta\tau}$, since they do not contribute neither to the third-order collective representation $Q_{2\mu} = Q^{(1)}_{2\mu} + Q^{(2)}_{2\mu} + Q^{(3)}_{2\mu}$ nor the fourth-order collective Hamiltonian $\mathcal{H} = \mathcal{H}^{(2)} + \mathcal{H}^{(3)} + \mathcal{H}^{(4)}$.

Using the explicit solutions for iG obtained above, we can readily calculate collective representations of one-body operators and the collective Hamiltonian $\mathcal{H}$. We next perform the canonical quantization procedure with normal ordering.[2] Namely, we replace the classical collective variables $(\eta_\mu{}^*, \eta_\mu)$ with the quadrupole boson operators $(d_\mu{}^\dagger, d_\mu)$ and take normal ordering. Up to the third order, the pairing and quadrupole operators acting in the d-boson space are then given in the following form:

$$\mathring{\tilde{P}}^\dagger_{\tau+} = p^{(11)}_{\tau+} \hat{n}_d\,, \quad \mathring{\tilde{P}}^\dagger_{\tau-} = 0\,, \tag{3·35}$$

$$\mathring{\tilde{Q}}^\dagger_{\tau 2\mu} = q_\tau{}^{(10)}(d^\dagger_{2\mu} + \tilde{d}_{2\mu}) + q_\tau{}^{(11)}(d^\dagger \tilde{d})_{2\mu} + \sum_\lambda q^{(30)}_{\tau\lambda}\{(d^\dagger(d^\dagger d^\dagger)_\lambda)_{2\mu} + ((\tilde{d}\tilde{d})_\lambda \tilde{d})_{2\mu}\}$$
$$+ \sum_\lambda q^{(21)}_{\tau\lambda}\{((d^\dagger d^\dagger)_\lambda \tilde{d})_{2\mu} + (d^\dagger(\tilde{d}\tilde{d})_\lambda)_{2\mu}\}\,, \tag{3·36}$$

where $d_{\tilde{\mu}} \equiv (-1)^\mu d_{-\mu}$ and $\hat{n}_d \equiv \sum_\mu d_\mu{}^\dagger d_\mu$. The fourth-order collective Hamiltonian takes the following form:

$$\mathring{H} = h^{(11)} \hat{n}_d + h^{(20)} \sum_\mu (d^\dagger_{2\mu} \tilde{d}^\dagger_{2\mu} + \text{h. c.}) + h^{(21)} \sum_\mu \{d^\dagger_{2\mu}(d^\dagger \tilde{d})_{\widetilde{2\mu}} + \text{h. c.}\}$$
$$+ \sum_{\lambda\mu} h_\lambda{}^{(40)}\{(d^\dagger d^\dagger)_{\lambda\mu}(d^\dagger d^\dagger)_{\widetilde{\lambda\mu}} + \text{h. c.}\} + \sum_{\lambda\mu} h_\lambda{}^{(31)}\{(d^\dagger d^\dagger)_{\lambda\mu}(d^\dagger \tilde{d})_{\widetilde{\lambda\mu}} + \text{h. c.}\}$$
$$+ \sum_{\lambda\mu} h_\lambda{}^{(22)}(d^\dagger d^\dagger)_{\lambda\mu}(\tilde{d}\tilde{d})_{\widetilde{\lambda\mu}}\,. \tag{3·37}$$

Explicit expressions for the coefficients $p^{(ij)}_{\tau\pm}$, $q^{(ij)}_{\tau\lambda}$, $h_\lambda{}^{(ij)}$, etc. are given in § 5 in comparison with those obtained by the mM-BET. In derivation of $\mathring{H}$, we evaluate the contribution from the quadrupole force by means of the products of the quadrupole operators $\mathring{Q}_{2\mu} = \sum_\tau \mathring{Q}_{\tau 2\mu}$ with $\mathring{Q}_{\tau 2\mu}$ obtained above. Namely, we evaluate it as

$$\mathring{H}_{QQ} = -\frac{1}{2}\chi \sum_\mu \mathring{Q}^\dagger_{2\mu} \mathring{Q}_{2\mu}\,. \tag{3·38}$$

The motive for adopting this prescription is that we are consistently following the TDHB picture in which the quadrupole one-body fields generated by the quadrupole force play a basic role. In this prescription, bilinear boson terms arising from the contractions of the quartic boson terms in $\mathring{H}_{QQ}$ are included in the collective Hamiltonian $\mathring{H}$ above, except for specific terms renormalizing the spherical shell-model single-particle energies. We note here that a similar prescription was once used by Kuriyama[10] on the basis of consideration of the correspondence between the

TDHB method and the BET.

§ 4. Application of the mM-boson-expansion method

In the mM-BET,[5),6)] we first consider a multiphonon space built out of the Tamm-Dancoff phonons $X^{\dagger}_{\mathrm{TD},2\mu}$ defined by (3·18):

$$\left\{|n\alpha IM\rangle=\mathcal{N}^{(\mathrm{F})-1/2}_{n\alpha I}\frac{1}{\sqrt{n!}}(X^{\dagger}_{\mathrm{TD}})^{n}_{\alpha IM}|\phi_0\rangle\right\}, \tag{4·1}$$

where α labels different multiphonon states with the same number of phonons n and with the same number of angular momentum (IM), and $\mathcal{N}^{(\mathrm{F})}_{n\alpha I}$ is the norm defined by

$$\mathcal{N}^{(\mathrm{F})}_{n\alpha I}\equiv\frac{1}{n!}\langle\phi_0|(X_{\mathrm{TD}})^{n}_{\alpha IM}(X^{\dagger}_{\mathrm{TD}})^{n}_{\alpha IM}|\phi_0\rangle\,. \tag{4·2}$$

Corresponding to (4·1), we next define a d-boson space as

$$\left\{|n\alpha IM)\equiv\mathcal{N}^{(\mathrm{B})-1/2}_{n\alpha I}\frac{1}{\sqrt{n!}}(d^{\dagger})_{\alpha IM}|0)\right\}, \tag{4·3}$$

$$\mathcal{N}^{(\mathrm{B})}_{n\alpha I}\equiv\frac{1}{n!}(0|(d)^{n}_{\alpha IM}(d^{\dagger})^{n}_{\alpha IM}|0)\,, \tag{4·4}$$

where $|0)$ is a vacuum for the d-bosons. Using the mapping operator

$$U=\sum_{n\alpha IM}|n\alpha IM)(n\alpha IM|\,, \tag{4·5}$$

we can easily transform fermion operators acting in the multiphonon space into boson operators acting in the d-boson space. Thus, we obtain

$$\tilde{P}^{(\mathrm{B})\dagger}_{\tau+}\equiv U\tilde{P}^{\dagger}_{\tau+}U^{\dagger}=p^{(11)}_{\tau+,\mathrm{B}}\hat{n}_d\,,\quad \tilde{P}^{(\mathrm{B})\dagger}_{\tau-}\equiv U\tilde{P}^{\dagger}_{\tau-}U^{\dagger}=0\,, \tag{4·6}$$

$$\begin{aligned}Q^{(\mathrm{B})\dagger}_{\tau 2\mu}&\equiv UQ^{\dagger}_{\tau 2\mu}U^{\dagger}\\&=q^{(10)}_{\tau,\mathrm{B}}(d_{\mu}{}^{\dagger}+\tilde{d}_{\mu})+q^{(11)}_{\tau,\mathrm{B}}(d^{\dagger}\tilde{d})_{2\mu}+\sum_{\lambda=0,2,4}q^{(21)}_{\tau\lambda,\mathrm{B}}\{((d^{\dagger}d^{\dagger})_{\lambda}\tilde{d})_{2\mu}+(d^{\dagger}(\tilde{d}\tilde{d})_{\lambda})_{2\mu}\}\,,\end{aligned} \tag{4·7}$$

up to the third-order with respect to the power of the d-boson creation and annihilation operators. We designate quantities appearing in the mM-BET by subscript B or superscript (B). Explicit expresssions for the coefficients appearing in Eqs. (4·6) and (4·7) are given by

$$p^{(11)}_{\tau+,\mathrm{B}}=-2\sqrt{2}\xi\bar{\xi}_{\tau}{}^{3}\,, \tag{4·8}$$

$$q^{(10)}_{\tau,\mathrm{B}}=\bar{\xi}_{\tau}{}^{2}\,, \tag{4·9}$$

$$q^{(11)}_{\tau,\mathrm{B}}=-4\,\bar{\xi}_{\tau}{}^{2}\bar{\eta}_{\tau}w_2\,, \tag{4·10}$$

$$q^{(21)}_{\tau\lambda,\mathrm{B}}=\frac{1}{5}\bar{\xi}_{\tau}{}^{2}\hat{2}\hat{\lambda}\left\{\left(1-\frac{\bar{\xi}_{\tau}{}^{2}}{\bar{\xi}_{p}{}^{4}+\bar{\xi}_{n}{}^{4}}C_{\lambda}\right)\Big/\sqrt{1-C_{\lambda}}-1\right\}, \tag{4·11}$$

where $w_{\lambda}\equiv-\hat{2}\hat{\lambda}W(22jj;\lambda j)$ and $q^{(ij)}$ are given in units of $q_{\mathrm{eff}}\equiv kq\xi$. Note that the

coefficients $q_{\tau\lambda}^{(30)}$ are zero in the mM-BET.

The collective boson Hamiltonian $H^{(B)} \equiv UHU^{\dagger}$ takes in the fourth-order a form similar to $\mathring{H}$ defined ay (3·37) with the following coefficients:

$$h_B^{(11)} = \alpha - 2G_0\xi^2(\bar{\xi}_p{}^6 + \bar{\xi}_n{}^6) + 8\beta(\bar{\xi}_p{}^2\bar{\eta}_p + \bar{\xi}_n{}^2\bar{\eta}_n)^2 w_2{}^2 , \tag{4·12}$$

$$h_B^{(20)} = \frac{1}{2}\beta\sqrt{1-C_0} , \tag{4·13}$$

$$h_B^{(21)} = -4\beta(\bar{\xi}_p{}^2\bar{\eta}_p + \bar{\xi}_n{}^2\bar{\eta}_n)w_2 , \tag{4·14}$$

$$h_{\lambda,B}^{(22)} = 2\beta(\sqrt{1-C_\lambda}-1) - 2G_0\xi^2(\bar{\xi}_p{}^6 + \bar{\xi}_n{}^6) + 40\beta W(2222\,;2\lambda)(\bar{\xi}_p{}^2\bar{\eta}_p + \bar{\xi}_n{}^2\bar{\eta}_n)^2 w_2{}^2 , \tag{4·15}$$

$$h_{\lambda,B}^{(31)} = -\beta(\sqrt{1-C_\lambda}-1) , \tag{4·16}$$

and $h_{\lambda,B}^{(40)} = 0$. In the calculation of $H^{(B)}$, we have evaluated the quadrupole force in the following manner,

$$H_{QQ}^{(B)} \equiv UH_{QQ}U^{\dagger} = -\frac{1}{2}\chi\sum_{\mu} Q_{2\mu}^{(B)\dagger} Q_{2\mu}^{(B)} , \tag{4·17}$$

and neglected the renormalizations to the spherical single-particle energies in accordance with the philosophy of introducing such effective separable forces.[9]

§ 5. Comparison between the SCC method and the mM-boson expansion method

The subjects of this section are 1) to examine validity of the canonical quantization procedure adopted in § 3, 2) to see effects of the pairing rotations, and 3) to see effects of collective-noncollective couplings by means of comparison between the result of the SCC method and that of the mM-BET. Effects of the pairing rotations and of collective-noncollective couplings are selfconsistently renormalized into the collective Hamiltonian in the SCC method, while they are completely neglected in the BET. On the other hand, the latter method is a quantum theory so that we can test the accuracy of the canonical quantization procedure used in § 3 in the light of this method.

In order to separate the subject 1) from 2) and 3), we first neglect the terms representing contributions from the pairing rotations and collective-noncollective couplings in the SCC method. This means that we truncate the TDHB state space to

$$\{|\phi^{(tru)}\rangle = e^{i\hat{G}^{(tru)}}|\phi_0\rangle\} \tag{5·1}$$

with

$$i\hat{G}^{(tru)} = \sum_{\mu}\{\hat{G}_{c2}^{(tru)}(\eta_\mu{}^*, \eta_\mu)X_{c2\mu}^{\dagger} - G_{c2}^{*(tru)}(\eta_\mu{}^*, \eta_\mu)X_{c2\mu}\} . \tag{5·2}$$

Since the Tamm-Dancoff phonon $X_{TD,2\mu}^{\dagger}$ defined by (3·18) can be written as a linear combinations of the RPA phonon creation and annihilation operators $(X_{c2\mu}^{\dagger}, X_{c2\mu})$ in the degenerate many j-shell model under considereration, we see that the truncated

space (5·1) corresponds to the multiphonon space (4·1) considered in the BET. Within this truncated subspace, we obtain the following expressions for the coefficients appearing in the operators (3·35)~(3·37):

$$p^{(11)}_{\tau+,\mathrm{tru}}=p^{(11)}_{\tau+,\mathrm{B}}\,, \tag{5·3}$$

$$q^{(10)}_{\tau,\mathrm{tru}}=q^{(10)}_{\tau,\mathrm{B}}\,,\quad q^{(11)}_{\tau,\mathrm{tru}}=q^{(11)}_{\tau,\mathrm{B}}\,, \tag{5·4}$$

$$q^{(21)}_{\tau\lambda,\mathrm{tru}}=-\frac{1}{30}\bar{\xi}_\tau{}^2\left(\frac{4\bar{\xi}_\tau{}^2}{\bar{\xi}_p{}^4+\bar{\xi}_n{}^4}-1\right)2\hat{\lambda}C_\lambda\,, \tag{5·5}$$

$$h^{(11)}_{\mathrm{tru}}=h^{(11)}_{\mathrm{B}}\,,\quad h^{(21)}_{\mathrm{tru}}=h^{(21)}_{\mathrm{B}}\,, \tag{5·6}$$

$$h^{(20)}_{\mathrm{tru}}=\frac{1}{2}\beta\left(1-\frac{1}{2}C_0\right), \tag{5·7}$$

$$h^{(22)}_{\lambda,\mathrm{tru}}=-\beta C_\lambda-2G_0\xi^2(\bar{\xi}_p{}^6+\bar{\xi}_n{}^6)+40\beta W(2222\,;2\lambda)(\bar{\xi}_p{}^2\bar{\eta}_p+\bar{\xi}_n{}^2\eta_n)^2w_2{}^2\,, \tag{5·8}$$

$$h^{(31)}_{\lambda,\mathrm{tru}}=-\frac{1}{2}\beta C_\lambda\,, \tag{5·9}$$

where the subscript "tru" denotes the results obtained in the truncated subspace and the quantities with the subscript "B" are those obtained in § 4 by mM-BET. Since $\sqrt{1-C_\lambda}\approx 1-\frac{1}{2}C_\lambda$ and C_λ is a quantity of order Ω^{-1}, we can thus conclude that the fourth-order collective Hamiltonian obtained by the canonical quantization procedure with normal ordering agrees with that of the mM-BET up to order Ω^{-1} in the limit where the TDHB state space (3·1) is truncated to (5·1). In the same way, we find that the third-order pairing and quadrupole operators, $\tilde{P}^\dagger_{\tau\pm}$ and $\mathring{Q}^\dagger_{2\mu}=\sum_\tau\mathring{Q}^\dagger_{\tau 2\mu}$, agree with the corresponding operators, $\tilde{P}^{(\mathrm{B})\dagger}_{\tau\pm}$ and $Q^{(\mathrm{B})\dagger}_{2\mu}=\sum_\tau Q^{(\mathrm{B})\dagger}_{\tau 2\mu}$ given by Eqs. (4·6) and (4·7), up to order Ω^{-1} in the same limit. On the other hand, we note that $\mathring{Q}^\dagger_{\tau 2\mu}$ itself is slightly different from $Q^{(\mathrm{B})\dagger}_{\tau 2\mu}$ even in the $\Omega_\tau{}^{-1}$ order. This arises from the fact that, exactly speaking, the truncated TDHB space (5·1) is slightly larger than the multiphonon space (4·1). One can easily examine this point by expanding the former into a form of the Fock representation. This small difference is not important, however.

Next, let us proceed to discuss effects of the pairing rotations and collective-noncollective couplings, which are completely neglected in the mM-BET. The full expressions for the coefficients $p^{(ij)}$, $q^{(ij)}$ and $h^{(ij)}$ obtained with the use of the TDHB space (3·1) contain the terms representing these effects. They are given as follows:

$$p^{(11)}_{\tau+}=p^{(11)}_{\tau+,\mathrm{tru}}+p_{\tau+,\mathrm{pair}}\,, \tag{5·10}$$

$$p^{(11)}_{\tau+,\mathrm{pair}}=-4\sqrt{2}\xi\bar{\xi}_\tau\bar{\eta}_\tau{}^2\,, \tag{5·11}$$

$$q^{(10)}_{\tau}=q^{(10)}_{\tau,\mathrm{tru}}\,,\quad q^{(11)}_{\tau}=q^{(11)}_{\tau,\mathrm{tru}}\,, \tag{5·12}$$

$$q^{(21)}_{\tau\lambda}=q^{(21)}_{\tau\lambda,\mathrm{tru}}+q^{(21)}_{\tau\lambda,\mathrm{dyn}}+q^{(21)}_{\tau\lambda,\mathrm{pair}}\,, \tag{5·13}$$

$$\begin{aligned}q^{(21)}_{\tau\lambda,\mathrm{dyn}}=&\{\bar{\xi}_\tau{}^2(g^{(21)}_{\lambda,\mathrm{dyn}}+g^{(12)}_{\lambda,\mathrm{dyn}})-4\bar{\xi}_\tau\bar{\eta}_\tau\zeta_{\tau\lambda}\sqrt{n_\lambda}\,w_\lambda g^{(20)}_\lambda\}(1-\delta_{\lambda 0})\\&+\sum_{\lambda'=2,4}\hat{\lambda}\hat{\lambda}'W(2222\,;\lambda'\lambda)\{\bar{\xi}_\tau{}^2g'^{(12)}_{\lambda',\mathrm{dyn}}-4\bar{\xi}_\tau\bar{\eta}_\tau\zeta_{\tau\lambda'}\sqrt{n_{\lambda'}}\,w_{\lambda'}g^{(11)}_{\lambda'}\}\,,\end{aligned} \tag{5·14}$$

$$q^{(21)}_{\tau\lambda,\mathrm{pair}}=-4\hat{\lambda}\,\bar{\xi}_\tau{}^2\bar{\eta}_\tau{}^2/\sqrt{5}k\Omega\,, \tag{5·15}$$

$$q^{(30)}_{\tau\lambda}=q^{(30)}_{\tau\lambda,\mathrm{dyn}}=\begin{cases}\bar{\xi}_\tau{}^2 g^{(30)}_{\lambda,\mathrm{dyn}}-4\bar{\xi}_\tau\bar{\eta}_\tau\zeta_{\tau\lambda}\sqrt{n_\lambda}\,w_\lambda g^{(02)}_\lambda & \text{for } \lambda=2,4\,,\\ 0 \quad \text{for } \lambda=0\,,\end{cases} \tag{5·16}$$

$$h^{(11)}=h^{(11)}_{\mathrm{tru}}+h^{(11)}_{\mathrm{pair}}\,, \tag{5·17}$$

$$h^{(11)}_{\mathrm{pair}}=-2G_0\sum_\tau(\bar{\xi}_\tau{}^2\bar{\eta}_\tau{}^2+2\xi^2\bar{\xi}_\tau{}^4\bar{\eta}_\tau{}^2)\,, \tag{5·18}$$

$$h^{(20)}=h^{(20)}_{\mathrm{tru}}\,,\quad h^{(21)}=h^{(21)}_{\mathrm{tru}}\,, \tag{5·19}$$

$$h^{(22)}_\lambda=h^{(22)}_{\lambda,\mathrm{tru}}+h^{(22)}_{\lambda,\mathrm{dyn}}+h^{(22)}_{\lambda,\mathrm{pair}}\,, \tag{5·20}$$

$$\begin{aligned}h^{(22)}_{\lambda,\mathrm{dyn}}=&\{2\alpha n_\lambda((g^{(20)}_\lambda)^2+(g^{(02)}_\lambda)^2)-2En_\lambda((g^{(20)}_\lambda)^2-(g^{(02)}_\lambda)^2)\\ &-\beta n_\lambda g^{(11)}_\lambda(g^{(20)}_\lambda+g^{(02)}_\lambda)\}(1-\delta_{\lambda0})\\ &+\sum_{\lambda'=2,4}\hat{\lambda}'\hat{\lambda}'W(2222\,;\lambda'\lambda)\{2En_{\lambda'}g^{(11)}_{\lambda'}(2g^{(20)}_{\lambda'}+g^{(11)}_{\lambda'})\\ &+2\beta n_{\lambda'}g^{(11)}_{\lambda'}(g^{(20)}_{\lambda'}-g^{(11)}_{\lambda'}+g^{(02)}_{\lambda'})\}\,,\end{aligned} \tag{5·21}$$

$$h^{(22)}_{\lambda,\mathrm{pair}}=-4G_0\xi^2(\bar{\xi}_p{}^4\bar{\eta}_p{}^2+\bar{\xi}_n{}^4\bar{\eta}_n{}^2)-8\beta(\bar{\xi}_p{}^2\bar{\eta}_p{}^2+\bar{\xi}_n{}^2\bar{\eta}_n{}^2)/k\Omega\,, \tag{5·22}$$

$$h^{(31)}_\lambda=h^{(31)}_{\lambda,\mathrm{tru}}+h^{(31)}_{\lambda,\mathrm{dyn}}+h^{(31)}_{\lambda,\mathrm{pair}}\,, \tag{5·23}$$

$$h^{(31)}_{\lambda,\mathrm{dyn}}=\begin{cases}2En_\lambda\{g^{(20)}_\lambda(g^{(20)}_\lambda+g^{(11)}_\lambda+g^{(02)}_\lambda)+2g^{(11)}_\lambda g^{(02)}_\lambda\}\\ \qquad+\beta n_\lambda(g^{(20)}_\lambda+g^{(11)}_\lambda+g^{(02)}_\lambda)(g^{(20)}_\lambda-g^{(11)}_\lambda+g^{(02)}_\lambda) \quad \text{for } \lambda=2,4\,,\\ 0 \quad \text{for } \lambda=0\,,\end{cases} \tag{5·24}$$

$$h^{(31)}_{\lambda,\mathrm{pair}}=-20\beta\delta_{\lambda0}(\bar{\xi}_p{}^2\bar{\eta}_p{}^2+\bar{\xi}_n{}^2\bar{\eta}_n{}^2)/k\Omega\,, \tag{5·25}$$

$$h^{(40)}_\lambda=h^{(40)}_{\lambda,\mathrm{dyn}}=\begin{cases}2\alpha n_\lambda g^{(20)}_\lambda g^{(02)}_\lambda-\dfrac{1}{2}\beta n_\lambda g^{(11)}_\lambda(g^{(20)}_\lambda+g^{(02)}_\lambda) & \text{for } \lambda=2,4\,,\\ 0 \quad \text{for } \lambda=0\,,\end{cases} \tag{5·26}$$

where $q^{(ij)}$ are given in units of $q_{\mathrm{eff}}=kq\xi$ and

$$\zeta_{\tau\lambda}\equiv\begin{cases}\bar{\xi}_\tau\bar{\eta}_\tau/\sqrt{\bar{\xi}_p{}^2\bar{\eta}_p{}^2+\bar{\xi}_n{}^2\bar{\eta}_n{}^2} & \text{for } \lambda=4\,,\\ \bar{\xi}_\tau & \text{for } \lambda=2\end{cases} \tag{5·27}$$

with $\bar{\xi}_{\bar{p}}\equiv\bar{\xi}_n$ and $\bar{\xi}_{\bar{n}}\equiv-\bar{\xi}_p$. In Eqs. (5·14) and (5·21), the terms containing the Racah coefficients $W(2222;\lambda'\lambda)$ result from the recoupling of the angular momenta in the operators like $(d^\dagger(d^\dagger\tilde{d})_{\lambda'})_{2\mu}$ and $(d^\dagger\tilde{d})_{\lambda'\mu}(d^\dagger\tilde{d})_{\lambda'\mu}$ into the form $((d^\dagger d^\dagger)_\lambda d)_{2\mu}$ and $(d^\dagger d^\dagger)_{\lambda\mu}(\tilde{d}\tilde{d})_{\widetilde{\lambda\mu}}$. In the expressions for $p^{(11)}_{\tau+}$, $q^{(21)}_{\tau\lambda}$, $q^{(30)}_{\tau\lambda}$, $h^{(11)}$, $h^{(22)}_\lambda$, $h^{(31)}_\lambda$ and $h^{(40)}_\lambda$, the terms with the subscript "pair" represent contributions resulting from the couplings with the pairing rotations, while those with the subscript "dyn" represent dynamical anharmonic effects resulting from the collective-noncollective couplings. It is interesting to notice that the former effects result not only from the pairing force but also from the quadrupole force. In fact, $h^{(31)}_{\lambda,\mathrm{pair}}$ and the second term in $h^{(22)}_{\lambda,\mathrm{pair}}$ can be interpreted as representing change in the effective uv-factors of the BCS theory as the d-bosons are excited in the system. As discussed in detail in Ref. 11), this effect can

be represented by a $\hat{u}\,\hat{v}$-factor which depends on the d-boson number as

$$\hat{u}^2\,\hat{v}^2=u^2v^2\left\{1-\frac{(u^2-v^2)^2}{u^2v^2}\frac{1}{k\Omega}\hat{n}_d+\cdots\right\}. \tag{5·28}$$

Our results above include this effect up to the Ω^{-1} order. On the other hand, $h^{(11)}_{\text{pair}}$ and the first term in $h^{(22)}_{\lambda,\text{pair}}$ are associated with the pairing force and represent an effective decrease of quasiparticle-excitation energy in the presence of other quasiparticles.[11] Every pairing rotational term mentioned above is associated with the $G^{(2)}_{0\tau}$* term given by Eq. (3·21).

In the special case of degenerate many j-shells under consideration, only the pairing rotational modes among the $\lambda=0$ modes couple to the RPA 2^+ phonons and the other $\lambda=0$ modes decouple. Thus, as seen in expressions (5·14)~(5·26), the noncollective modes which couple to the collective 2^+ mode have an angular momentum $\lambda=2$ or 4. They are coupled by the quadrupole force and are taken into account through the second-order term $G^{(2)}_{r\lambda\mu}$ with $r\neq c$, Eq. (3·20), in the expansion for $i\hat{G}$. Since higher-order terms in the (η_μ^*, η_μ) expansion are iteratively determined, they of course affect also the third-order term $G^{(3)}_{c\lambda\mu}$ given by Eq. (3·29). These collective-noncollective coupling effects are diagrammatically represented in Fig. 2. We here note that each diagram in this figure does not correspond to one of the terms in $h^{(22)}_{\lambda,\text{dyn}}$, $h^{(31)}_{\lambda,\text{dyn}}$ and $h^{(40)}_{\lambda,\text{dyn}}$ above, but they are mixed up in these terms under the optimized RPA boundary condition (3·16). This boundary condition enables us, however, to go beyond the RPA critical point from where the RPA frequency becomes imaginary (see Ref. 3)). In fact, as is well known, anharmonic vibrational excitation spectra in transitional nuclei often correspond to the region slightly beyond the RPA critical point.

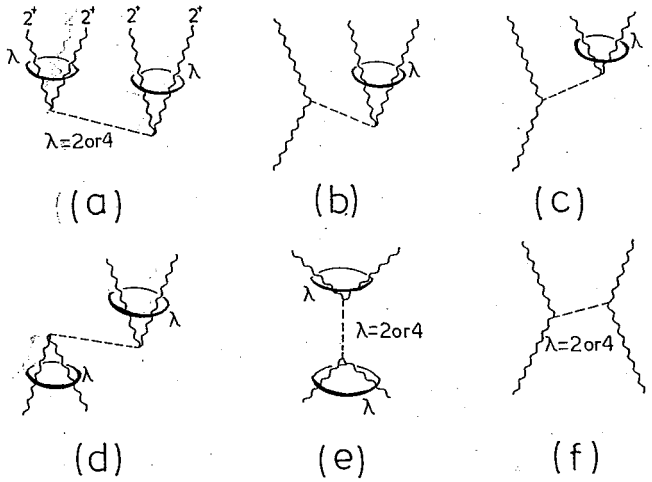

Fig. 2. Diagrammatic representation of the fourth-order dynamical anharmonicities associated with the couplings with the noncollective modes with $\lambda=2$ and 4. The wavy lines represent the RPA 2^+ modes, while the broken lines the noncollective modes.

§ 6. Numerical calculation

In this section, we evaluate the three points 1)~3) discussed in § 5 by numerical calculation. For the parameters of the model, we take $j=9/2$, $k=4$ and, accordingly, the maximum number of seniority, $k\Omega$, is 20 for both protons and neutrons. Evidently, similar results will be obtained for other values of j and k (as long as they are not considerably different from the above values). The pairing-force strength G_0 is fixed to yield the pairing gap $\Delta=\frac{1}{2}G_0k\Omega=1$ MeV, which is independent of the nucleon number. The quadrupole-force strength χ is fixed to be $\chi k^2q^2\xi^2=1.2$ MeV, which corresponds to the transitional region slightly beyond the RPA critical point ($\chi_c k^2q^2\xi^2=1.0$ MeV). As mentioned in § 3, our boundary condition enables us to go beyond the critical point. $B(E2)$ values are calculated using the electric quadrupole operator $\hat{Q}^{(E2)}_{2\mu}=\sum_\tau e_\tau Q_{\tau 2\mu}$ with effective charges $e_p=1.5\,e$ and $e_n=0.5\,e$.

In Fig. 3 we present a typical example of the anharmonic vibrational spectra calculated by fourth-order boson Hamiltonians with different approximations. Comparing the result of the mM-BET (Fig. 3(a)) with that of the truncated SCC method (Fig. 3(b)), we see that they agree very well. This is what we expect from the consideration in § 5 (i.e., the two methods agree to order Ω^{-1}), and indicates the accuracy of our canonical quantization procedure. This figure also shows that the collective-noncollective coupling effects lower the excitation energies of the 2_1^+ and 4_1^+ states, whereas the pairing-rotational effects slightly increase their energies.

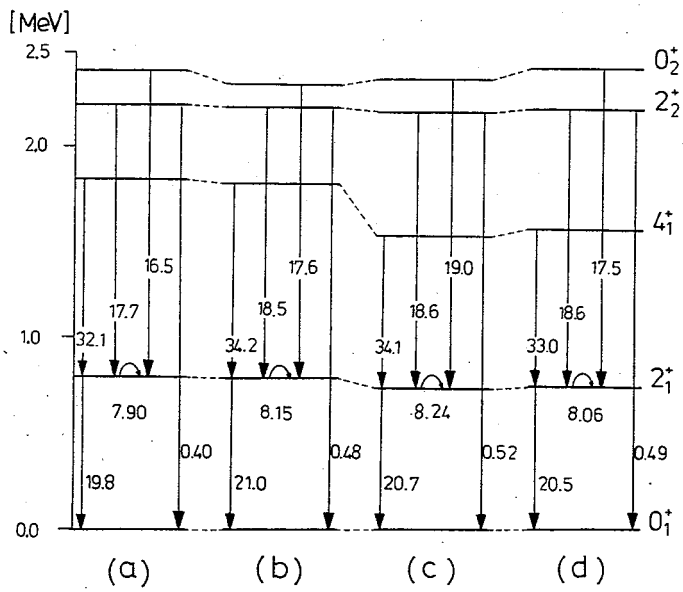

Fig. 3. Comparison of spectra obtained with different prescriptions for the fourth-order boson Hamiltonian; (a) mM-BET, (b) truncated SCC method with the coefficients $q^{(ij)}_{\tau\nu}$ and $h^{(ij)}_{\tau\nu}$, (c) SCC method with the pairing rotational effects neglected, (d) SCC method. The $B(E2)$ values and the quadrupole moments are given in units of e^2q^2 and eq, respectively. The parameters used are $j=9/2$, $k=4$, $N_p=12$, $N_n=14$, $G_0k\Omega=2$ MeV, $\chi k^2q^2\xi^2=1.2$ MeV, $e_p^{\rm eff}=1.5e$, $e_n^{\rm eff}=0.5e$.

Figures 4 and 5 show how the properties of the 0_2^+, 2_2^+ and 4_1^+ states change as the neutron number N_n changes. We notice that $B(E2\,;\,2_2^+\to 2_1^+)$ is most sensitive to N_n ; it decreases as one moves away from the mid-shell ($N_n=20$). This is connected with the well-known property of the particular terms in the collective Hamiltonian that change the d-boson number by one. Namely, this property is mainly associated with the change of the BCS occupation factor $\eta_n{}^2=\frac{1}{2}(u_n{}^2-v_n{}^2)$. In this connection we note that, although the d-boson numbers are considerably mixed in the eigenstates, the cross-over transitions $B(E2\,;\,2_2^+\to 0_1^+)$ remain small. We find that this is mainly because of the cancellation between the matrix elements associated with the $q^{(10)}$ term and those with the $q^{(11)}$ term in the quadrupole operator $\mathring{Q}_{2\mu}^{\dagger}$ defined by (3·36).

In these figures, the mode-mode coupling effects on the final results are not striking. This does not imply that they are unimportant, however. In fact, as shown in Figs. 6 and 7, they considerably affect the values of $q^{(ij)}$ and $h^{(ij)}$. For instance, the values of $q^{(21)}_{4,\mathrm{dyn}}$ and $q^{(30)}_{4,\mathrm{dyn}}$ are of the same order of magnitude as that of $q^{(21)}_{4,\mathrm{tru}}$. It is very interesting to notice that, although $h^{(22)}_{\lambda,\mathrm{tru}}$ are always positive, the signs of $h^{(22)}_{\lambda,\mathrm{dyn}}$ depend

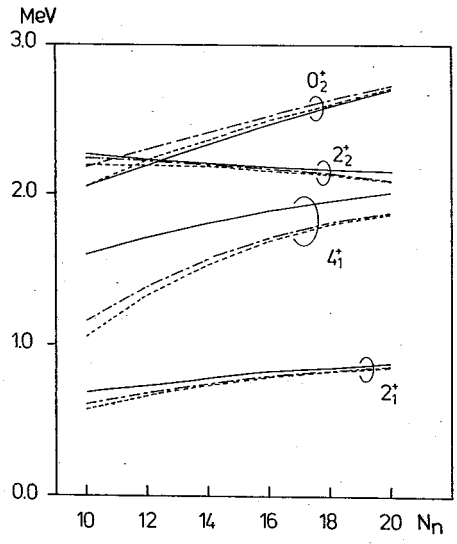

Fig. 4. Dependence of spectra on the neutron number. The full lines, the broken lines and the dash-dotted lines represent the results calculated with the truncated SCC method, the SCC method with the pairing rotational effects neglected, and the SCC method, respectively. The parameters used are the same as in Fig. 3 except that N_n is here varied.

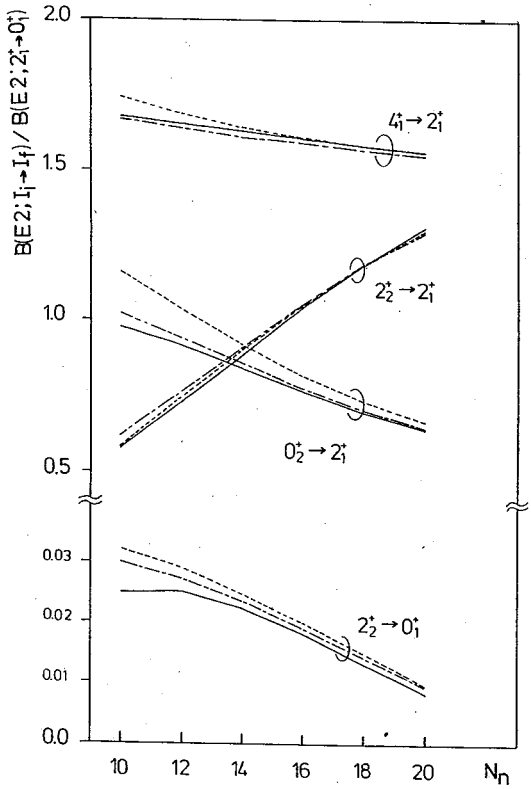

Fig. 5. Dependence of $B(E2)$ values on the neutron number. Ratios of $B(E2)$ to $B(E2\,;\,2_2^+\to 0_1^+)$ are shown. Notations and parameters used are the same as in Fig. 4. Note that $B(E2\,;\,2_2^+\to 0_1^+)$ are shown with a scale different from other transitions.

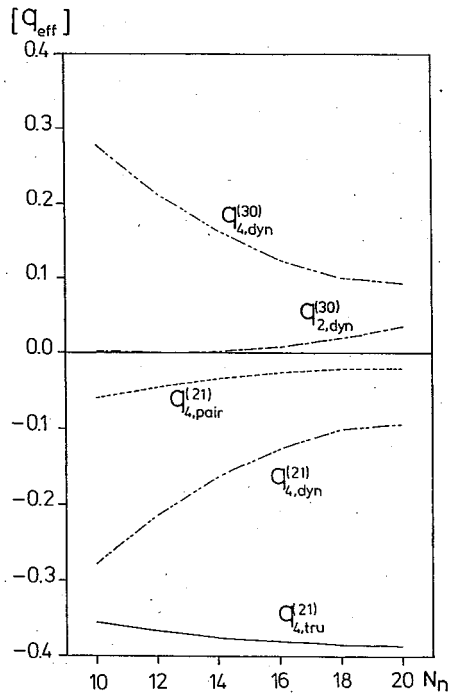

Fig. 6. Values of different terms in $q^{(21)}$ and $q^{(30)}$ and their dependences on the neutron number. Parameters used in the calculation are the same as in Figs. 4 and 5.

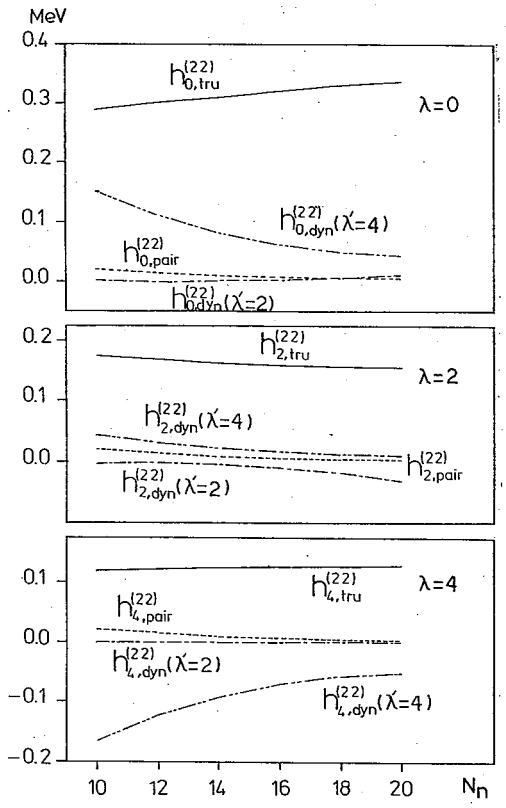

Fig. 7. Values of different terms in $h^{(22)}_{\lambda=0,2,4}$ and their dependences on the neutron number. $h^{(22)}_{\lambda',\mathrm{dyn}}$ ($\lambda=2$) and $h^{(22)}_{\lambda',\mathrm{dyn}}$ ($\lambda=4$) represent the contributions from the noncollective modes with $\lambda=2$ and 4, respectively. Parameters used in the calculation are the same as in Figs. 4~6.

on the angular momentum λ. Namely, $h^{(22)}_{\lambda=0,\mathrm{dyn}}$ is positive and $h^{(22)}_{\lambda=4,\mathrm{dyn}}$ is negative. Thus, the collective-noncollective couplings sometimes give rise to an effective repulsive force as well as an effective attractive force between the d-bosons. Consequently, the relative magnitudes of $h^{(22)}_{\lambda=0,2,4}$ are considerably modified by the collective-noncollective coupling effects. We also see in Figs. 6 and 7 that the effects become stronger as one moves away from the mid-shell ($N_n=20$). The reason is that the couplings are caused by the part of the quadrupole force that changes the quasiparticle number by two and accompanies the BCS occupation factor $\eta_n{}^2=\frac{1}{2}(u_n{}^2-v_n{}^2)$. In Fig. 7 the contributions from the noncollective modes with $\lambda=2$ and 4 are separately shown. We see that the contributions from the $\lambda=4$ modes are much larger than those from the $\lambda=2$ modes. It should be noted, however, that this might be a consequence of the special situation of the degenerate model in which the quadrupole collectivity in the RPA is completely concentrated in the 2^+ phonon $X^{\dagger}_{c2\mu}$.

The contributions from the pairing rotations, $h^{(22)}_{\lambda,\mathrm{pair}}$, on the fourth-order boson Hamiltonian are rather small and positive in sign, which corresponds to a *repulsive* force. It would be appropriate to understand this result in connection with other

effects emphasized in previous works:[11] It was found in Ref. 11) that the couplings between the quadrupole phonons and the pairing rotations give rise to an effective increase in absolute magnitude of the (u^2-v^2) factor as many phonons are excited in the system, and this effect greatly decreases the excitation energies, corresponding to an effective *attractive* force between the d-bosons. In fact, such a seniority-dependent effect of the (u^2-v^2) factor is represented as a correction to the third-order term with the coefficient $h^{(21)}$ and arises in the fifth-order terms. Thus, this effect is not taken into account in the fourth-order approximation.

§ 7. Concluding remarks

It has been shown that our canonical quantization procedure yields the result which agrees with that of the mM-BET to order Ω^{-1} in the truncated TDHB subspace (5·1). We note here that this agreement is achieved by adopting the prescription (3·38) where the one-body operators are treated as basic quantities generating the TDHB fields.

It has also been found that the mode-mode couplings considerably affect the coefficients $h^{(ij)}$ and $q^{(ij)}$ of the collective Hamiltonian $\mathring{H}$ and the operators $\mathring{Q}_{2\mu}$. Some parts of their contributions to the fourth-order boson Hamiltonian have repulsive character, and some other parts are attractive. Consequently, the relative magnitudes of $h^{(22)}_{\lambda=0,2,4}$, etc. are significantly modified from those given by the mM-BET. In realistic case, we should expect that relative magnitudes of various terms in $h^{(ij)}$ take quite different values in individual nuclei reflecting rather sensitively subshell structure near the Fermi surface. The numerical examples for the degenerate many j-shell model, presented in § 6, should therefore be understood in a qualitative sense; i.e., as providing an example which indicates the importance of renormalizing the mode-mode coupling effects to the quadrupole collective Hamiltonian $\mathring{H}$ and the operators $\mathring{Q}_{2\mu}$. In particular, we should expect that the pairing vibrational modes (which disappear in the degenerate model) play an important role in some realistic situations.

Acknowledgements

We are indebted to M. Matsuo for his useful comments on the original version of this paper. The computer calculation for this work has been supported in part by the Research Center for Nuclear Physics, Osaka University.

References

1) T. Marumori, T. Maskawa, F. Sakata and A. Kuriyama, Prog. Theor. Phys. **64** (1980), 1294.
2) M. Matsuo and K. Matsuyanagi, Prog. Theor. Phys. **74** (1985), 288.
3) M. Matsuo and K. Matsuyanagi, Prog. Theor. Phys. **74** (1985), 1227; **76** (1986), 93; **78** (1987), 591.
4) M. Matsuo, Prog. Theor. Phys. **76** (1986), 372.
5) P. Ring and P. Schuck, *The Nuclear Many-Body Problem* (Springer-Verlag, 1980).
6) S. G. Lie and G. Holzwarth, Phys. Rev. **C12** (1975), 1035.
7) G. Holzwarth, D. Janssen and R. V. Jolos, Nucl. Phys. **A261** (1976), 1.
8) T. Kishimoto and T. Tamura, Nucl. Phys. **A270** (1976), 317.
9) D. R. Bes and R. A. Sorensen, *The Pairing-Plus-Quadrupole Model, Advances in Nuclear Physics* (Plenum Press, 1969), vol. 2, p. 129.
10) A. Kuriyama, Prog. Theor. Phys. Suppl. Nos. 74 & 75 (1983), 66.
11) T. Suzuki, M. Fuyuki and K. Matsuyanagi, Prog. Theor. Phys. **62** (1979), 690; **65** (1981), 1667.

Prog. Theor. Phys. Vol. 83, No. 4, April 1990, Progress Letters

Octupole Vibrations Built on Superdeformed Rotational Bands

Shoujirou MIZUTORI, Yoshifumi R. SHIMIZU* and Kenichi MATSUYANAGI

Department of Physics, Kyoto University, Kyoto 606
**Department of Physics, Kyushu University, Fukuoka 812*

(Received November 24, 1989)

Strength functions for giant octupole resonances built on the superdeformed rotational bands are calculated by means of the RPA based on the cranking model. It is suggested that strongly collective octupole vibrational states appear within a few MeV from the superdeformed yrast line.

Since the discovery[1] of the superdeformed rotational band in ^{152}Dy, similar bands have been systematically found in neighbouring nuclei,[2] and their microscopic structures have been extensively studied mainly on the basis of the cranking model.[3)~5)] Also, a possible role of the giant dipole resonances has been discussed in connection with the population mechanism of the superdeformed band.[6] In this paper, we report a calculated result of the strength functions for octupole vibrations built on the superdeformed bands. We are interested in the question how large deformation and rapid rotation modify the properties of multipole vibrational modes. In particular, we are interested in the possibility that frequencies of some of the giant multipole resonances become low so that they might appear within a few MeV from the superdeformed yrast states. Although there is at present no clear-cut experimental data concerning elementary excitation modes built on the superdeformed states, we believe that such data will be obtained in the near future by means of new-generation gamma-ray detector systems planned now.

We start from the cranked Nilsson Hamiltonian,

$$h' = h_{\text{Nilsson}} - \omega_{\text{rot}} J_x \,,$$

and use the doubly-stretched multipole-multipole interactions as residual interactions:

$$H = h' - \frac{1}{2}\sum_{\lambda K} \chi_{\lambda K} Q''^{\dagger}_{\lambda K} Q''_{\lambda K} \,,$$

where $Q''_{\lambda K}$ are the multipole operators defined in terms of the doubly-stretched coordinates $x''_i = (\omega_i/\omega_0)x_i$ with $i=1$, 2 and 3. Here (ω_i/ω_0) denotes the ratios of the frequencies of the deformed harmonic-oscillator potential to that of the spherical one. The importance of the doubly-stretched multipole-multipole interaction for deformed nuclei was first pointed out by Kishimoto.[7] The force-strength $\chi_{\lambda K}$ can be determined by strictly imposing selfconsistency conditions between the potential and the density, once the single-particle potential at the equilibrium is given. In a recent publication by Sakamoto and Kishimoto,[8] they gave an improved version for the octupole coupling strength χ_{3K}:

$$\chi_{3K}=\frac{4\pi}{7}M\omega_0{}^2\Big\{\langle(r^4)''\rangle_0+\frac{2}{7}(4-K^2)\langle(r^4P_2)''\rangle_0 + \frac{1}{84}(K^2(7K^2-67)+72)\langle(r^4P_4)''\rangle_0\Big\}^{-1},$$

where P_l denotes the Legendre polynomial. We use this formula; the expectation values appearing on the r.h.s. are evaluated by using the calculated yrast configurations for the cranking Hamiltonian h'. We treat the residual interaction in the RPA, and calculate the strength functions for the multipole operators $Q_{\lambda K}$ through the response functions $R(Q_{\lambda K}^{\dagger}, Q_{\lambda K})$:

$$S(Q_{\lambda K};\omega)=\frac{1}{\pi}\mathrm{Im}R(Q_{\lambda K}^{\dagger}, Q_{\lambda K};\omega+i\epsilon) \overset{\epsilon\to 0}{\to} \sum_n \delta(\omega_n-\omega)|\langle n|Q_{\lambda K}|0\rangle|^2 .$$

The RPA-response functions are calculated from the unperturbed response functions R_0 through the well-known relation:

$$R=(1-R_0\chi)^{-1}R_0 ,$$

where R, R_0 and χ are to be regarded as matrices with respect to the indices (λK) denoting different multipole fields. Of course, χ is a diagonal matrix whose elements are $\chi_{\lambda K}$. In fact, we first calculate the response functions for the doubly-stretched multipole operators $Q''_{\lambda K}$ and then make a linear transformation into the representation in terms of the ordinary multipole operators $Q_{\lambda K}$. Details of this procedure can be found in Ref. 9). The strength functions thus obtained are those defined in the rotating frame. Within the uniform-rotation approximation inherent to the cranking model, the strength functions in the laboratory frame are obtained through the relation[9]

$$S(Q_{\lambda\mu};\omega)=\frac{1}{\pi}\mathrm{Im}R(Q_{\lambda\mu}^{\dagger}, Q_{\lambda\mu};\omega-\mu\omega_{\mathrm{rot}}) .$$

Here $Q_{\lambda\mu}$ are the multipole operators whose components μ are defined with respect to the rotation axis (x-axis). They are related to $Q_{\lambda K}$, with K being the symmetry axis (z-axis) component, by linear transformations.[9] We do not calculate the widths of giant resonances. Instead, we treat the imaginary part Γ of the energy as an energy-smoothing parameter in order to focus our attention on the gross features of the strength functions.

Procedure of numerical calculation is essentially the same as in Ref. 9). The parameters v_{ls} and v_{ll} of the Nilsson Hamiltonian are the same as in Ref. 10), except that we use the doubly-stretched coordinates also for the $(\boldsymbol{l}\cdot\boldsymbol{s})$- and $\boldsymbol{l}^2$-terms. The RPA calculation is done using 6 major shells; $N_{\mathrm{osc}}=3-8$ for neutrons and $N_{\mathrm{osc}}=2-7$ for protons. The pairing correlations and the hexadecapole deformations are neglected in this calculation. The equilibrium deformation is fixed to be $\delta_{\mathrm{osc}}=0.56$ for ^{152}Dy. This value was estimated by means of the Strutinsky method at $\omega_{\mathrm{rot}}/\omega_0=0.05$, and assumed to be independent of ω_{rot}. Numerical calculations have been carried out

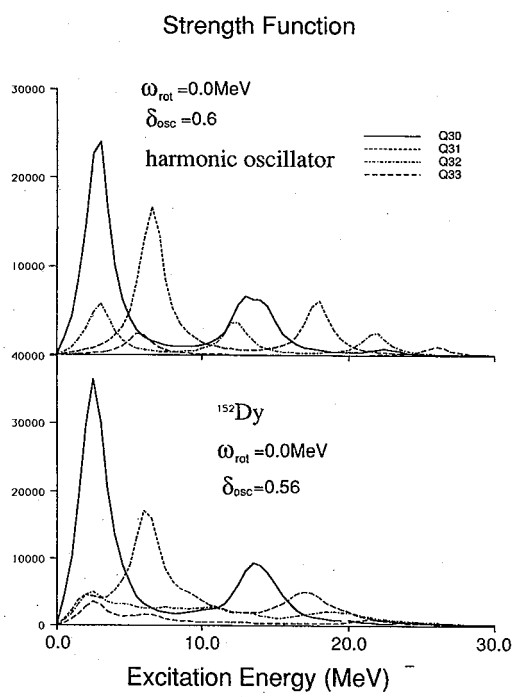

Fig. 1. Strength functions for the octupole operators r^3Y_{3K} with $K=0$, 1, 2 and 3. The upper part shows the result calculated for the harmonic-oscillator potential with $\delta_{osc}=0.6$ and for the nucleus with $Z=N=80$ (magic number of the 2 : 1 shell structure). The lower part shows the result calculated for the Nilsson potential with $\delta_{osc}=0.56$ and for ^{152}Dy. Energy-smoothing width $\Gamma=1$ MeV is used. The unit is $\pi(\hbar/M\omega_0)^3/\hbar\omega_0$.

for the isoscalar $\lambda=0$, 1, 2 and 3 modes and the isovector $\lambda=0$, 1 and 2 modes. Since we find that the result for the isoscalar octupole modes is most interesting and since the results for the $\lambda=0$, 1 and 2 modes were partly reported in Ref. 11), we focus our attention on the octupole vibrations in the following. We only mention here that our results for the $\lambda=0$, 1 and 2 modes are not qualitatively different from those reported in Refs. 12) and 13). It should be noted that although we call the modes associated with the Q''_{3K} fields "octupole modes" for brevity, they are in fact linear combinations of the ordinary octupole fields r^3Y_{3K} and the compressional dipole fields r^3Y_{1K}. As mentioned before, we have made linear transformations to obtain the strength functions for the r^3Y_{3K} fields, after obtaining the response function for the Q''_{3K} operators. It should also be mentioned that the spurious center of motion is separated out in the calculation.[14]

The lower part of Fig. 1 shows the octupole strength functions calculated for ^{152}Dy at $\omega_{rot}=0$. We clearly see a prominent peak of the $K=0$ component at about 3 MeV. The reason why we obtain the low-energy $K=0$ peak can be easily understood by examining the well-known 2 : 1 shell structure for the deformed harmonic-oscillator (h.o.) potential. For comparison, we present in the upper part of Fig. 1 the octupole strength functions calculated by using the h.o. potential. In this case, the $K=0$ peak is composed of coherent one-particle-one-hole excitations which transfer the asymptotic quantum numbers (N_{osc}, n_3, Λ) for the h.o. potential by $\Delta N_{osc}=1$, $\Delta n_3=1$, $\Delta\Lambda=0$. The unperturbed excitation energies of these configurations are $\hbar\omega_z\simeq 5$ MeV, and they are lowered by attractive octupole-octupole interactions. Apparently, the strength functions for the Nilsson potential are similar to those for the h.o. potential. The unperturbed particle-hole configurations contributing to the $K=0$ peak for the Nilsson potential are displayed in Fig. 2. We see that, in spite of the splittings due to the $(\boldsymbol{l}\cdot\boldsymbol{s})$- and $\boldsymbol{l}^2$- terms, the configurations in the h.o. potential cluster at about 5 MeV in excitation energy. They coherently contribute to forming a collective octupole vibration at about 3 MeV. Similar consideration is applied also for the low-energy $K=2$ peak, though its strength is weaker than that of $K=0$.

Figure 3 displays the strength functions defined in the laboratory frame. The

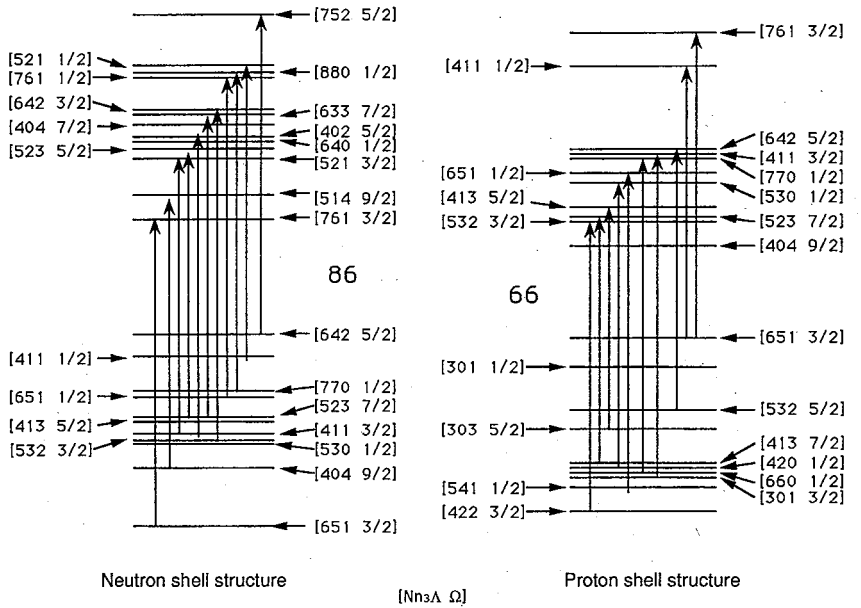

Fig. 2. Particle-hole configurations with respect to the closed shells, $Z=66$ and $N=86$, for the Nilsson potential with $\delta_{osc}=0.56$, which constitute the low-frequency $K=0$ octupole vibration.

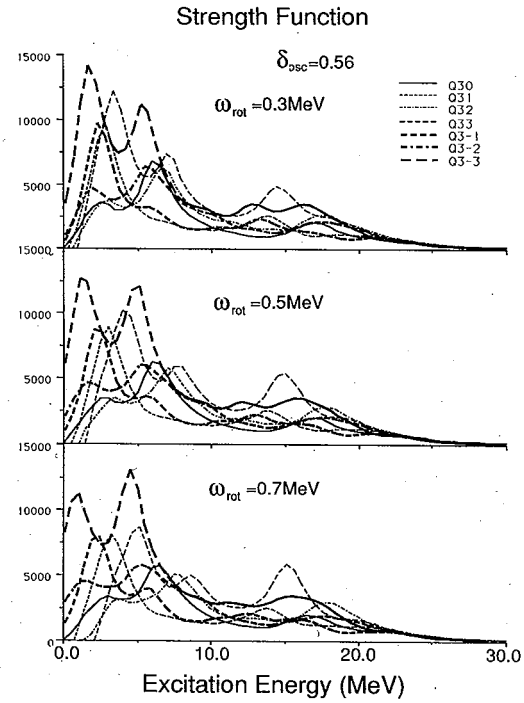

Fig. 3. Octupole strength functions in the laboratory frame. These are calculated for the Nilsson potential with $\delta_{osc}=0.56$ at $\hbar\omega_{rot}=0.3$ (the upper part), 0.5 (the middle part) and 0.7 MeV (the lower part). The component μ of the octupole operator $Q_{3\mu}$ denotes the projection on the rotation axis (x-axis). Energy-smoothing width $\Gamma=1$ MeV is used. The unit is $\pi(\hbar/M\omega_0)^3/\hbar\omega_0$.

upper, middle and lower parts of this figure show the results calculated at $\hbar\omega_{\rm rot}=0.3$, 0.5, and 0.7 MeV, respectively. Note that the octupole strength functions are here classified according to the x-axis component μ, intstead of the K-quantum number (z-component) used in Fig. 1. We see prominent low-energy peaks for the $\mu=\pm 3$ components. They are associated with the $K=0$ peak shown in Fig. 1 so that their physical origins are the same as discussed above. Note that the rotational band composed of these components of octupole one-phonon excitations has odd spin and negative parity, if the spin and parity of the superdeformed yrast band are assumed to be even and positive.[1)]

The computer calculation has been financially supported in part by the Grant-in-Aid for Scientific Research of the Japan Ministry of Education, Science and Culture (No. 01540245), and in part by Research Center for Nuclear Physics, Osaka University, and done partly by using the computer center of Institute for Nuclear Study, University of Tokyo.

---

1) P. J. Twin et al., Phys. Rev. Lett. **57** (1986), 811.
2) P. Fallon et al., Phys. Lett. **B218** (1989), 137, and references therein.
3) T. Bengtsson, I. Ragnarsson and S. Åberg, Phys, Lett. **B208** (1989), 39.
4) W. Nazarewicz, R. Wyss and A. Johnson, Phys. Lett. **B255** (1989), 208, and references therein.
5) Y. R. Shimizu, E. Viggezi and R. A. Broglia, Nucl. Phys. **A509** (1990), 80.
6) B. Herskind et al., Phys. Rev. Lett. **59** (1987), 2416.
7) T. Kishimoto et al., Phys. Rev. Lett. **35** (1975), 552.
8) H. Sakamoto and T. Kishimoto, Nucl. Phys. **A501** (1989), 205.
9) Y. R. Shimizu and K. Matsuyanagi, Prog. Theor. Phys. **72** (1984), 1087; **75** (86), 1161.
10) T. Bengtsson and I. Ragnarsson, Nucl. Phys. **A436** (1985), 14.
11) S. Mizutori, in *Proc. of the INS-NBI Workshop on Rotation and Vibration in Nuclei* [Genshikaku Kenkyuu **33** (1989), 109.]
12) M. Gallardo, M. Diebel, T. Døssing and R. A. Broglia, Nucl. Phys. **A443** (1985), 415.
13) S. Åberg, Nucl. Phys. **A472** (1987), 1.
14) J. L. Egido and H. Weidenmüller, Phys. Rev. **C39** (1989), 2398.

Progress of Theoretical Physics, Vol. 85, No. 2, February 1991

Diabatic Approach to Shape Coexistence Phenomena in Semi-Magic Nuclei. I

—— *Illustration of Basic Ideas* ——

Takahiro FUKUI, Masayuki MATSUO* and Kenichi MATSUYANAGI

Department of Physics, Kyoto University, Kyoto 606
**Yukawa Institute for Theoretical Physics, Kyoto University, Kyoto 606*

(Received July 7, 1990)

A new microscopic method based on the diabatic picture is proposed to describe the low-lying deformed excited 0^+ states in semi-magic nuclei. In this method, the couplings between anharmonic shape vibrations associated with different Hartree-Fock-Bogoliubov minima are diagonalized after constructing the diabatic basis. Basic ideas are illustrated for three kinds of exactly solvable models. Several examples are given which exhibit well localized deformed wave functions around the second minimum of the collective potential. It is possible that such deformed excited states well retain their identities against the mixing with the spherical configurations, even when their existence can hardly be expected from the properties of the adiabatic potential-energy functions.

§ 1. Introduction

In recent years, deformed excited states with $J^\pi=0^+$ have been systematically observed in semi-magic Sn isotopes[1)~5)] and Pb isotopes[6)~10)] whose ground states are spherical. They appear very low in excitation energy and retain their identities suggesting that mixings with the spherical ground states are small. These experimental data may therefore be regarded as typical examples of shape coexistence phenomena. The deformed excited 0^+ states are associated with proton two-particle-two-hole (2p-2h) excitations across the closed shells ($Z=50$ or 82).[11)~15)] Their excitation energies are drastically lowered mainly by the pairing correlations among the protons and by the quadrupole correlations between the protons and the neutrons.[11)~15)] In the Nilsson picture, we have down-sloping and up-sloping single-particle levels as functions of quadrupole deformation. It is then easily confirmed that the 2p-2h excited configurations, where two particles lie in the down-sloping levels and two holes in the up-sloping levels, have finite equilibrium deformations. In the adiabatic potential energy surface plotted as a function of quadrupole deformation, we expect to have second minimum corresponding to the 2p-2h excited configurations. The excitation energy of deformed excited state may be roughly estimated from the energy difference between the first and the second minima.

Quite recently, Bengtsson and Nazarewicz[16)] have shown that the diabatic potential-energy functions defined by switching off the interaction between the 2p-2h configuration and the ground-state configuration give more accurate estimate for the excitation energies of the deformed excited 0^+ states in Pb isotopes than the conventional adiabatic potential-energy functions. This suggests that the couplings between the deformed and the spherical states in semi-magic nuclei of interest will not be correctly described in terms of the conventional adiabatic theory of collective motions.

In this paper, we propose a new microscopic approach for treating the shape coexistence phenomena. This approach is based on the diabatic picture. Namely, we first define two diabatic configurations which correspond to the deformed and the spherical states, neglecting the couplings between them. The coupling between two kinds of states is then diagonalized in the second step. We use the (η^*, η) expansion method based on the selfconsistent-collective-coordinate (SCC) method[17] in order to describe collective motions associated with individual diabatic configurations. The couplings between the two kinds of collective motion are then treated in a manner similar to the well-known coupled channel method. Our method may thus be regarded as a coupled channel version of the SCC method. For convenience, in this paper we call our method "coupled-configuration SCC method". The formulation is given in § 2. We shall illustrate usefulness of our approach by applying our method to three kinds of exactly solvable models; i.e., the particle-plus-harmonic-core model (§ 3), the particle-plus-anharmonic-core model (§ 4) and the multi-$O(4)$ model (§ 5). These models may be useful to study various problems of collective dynamics accompanying level crossings in the single-particle spectrum. We shall present in §§ 3~5 typical examples that exhibit deformed excited states with localized wave functions. It is worth emphasizing that such localized wave functions exist even when their existence can hardly be expected from the properties of the adiabatic potential-energy functions. Conclusions are given in § 6.

§ 2. Outline of the method

We assume that the system under consideration has two local minima in the collective potential energy function. We proceed in two steps. In the first step, we construct classical collective Hamiltonians describing diabatic collective vibrations about the individual local minima. For this purpose, we use the (η^*, η) expansion method[17] about the individual Hartree-Bogoliubov (HB) stationary states corresponding to the local minima. In the second step, we construct the total Hamiltonian taking into account the coupling between the two diabatic collective vibrations and quantize it.

2.1. *Diabatic collective Hamiltonian for each configuration*

Let us express the individual HB vacua by $|\phi_i(0)\rangle$ with $i=1$ and 2. The time-dependent (TD) HB state vectors evolving from these static HB vacua can be written in the following form:

$$|\psi_i(\eta_i^*, \eta_i, \phi_i, N_i)\rangle = e^{-i\phi_i\hat{N}} e^{i\hat{G}_i(\eta_i^*, \eta_i, N_i)} |\phi_i(0)\rangle\,, \quad i=1, 2\,, \tag{2·1}$$

where η_i^* and η_i are time-dependent collective variables describing the collective vibrations around the i-th local minima. The operator $e^{-i\phi_i\hat{N}}$, $\hat{N}$ being the number operator, is introduced in order to eliminate the spurious number-fluctuations associated with the use of the TDHB approximation.[18] Here ϕ_i are the angle variables conjugate to the nucleon number N_i. They are treated as classical dynamical variables. The operator $i\hat{G}_i$ can be written in terms of the quasiparticle creation and

annihilation operators $(a_{i\mu}^{\dagger}, a_{i\nu})$, defined with respect to the individual static HB solutions $|\phi_i(0)\rangle$ and satisfying $a_{i\mu}|\phi_i(0)\rangle=0$, as follows:

$$i\hat{G}_i(\eta_i^*, \eta_i, N_i)=\sum_{\mu,\nu}\{G_{i\mu\nu}(\eta_i^*, \eta_i, N_i)a_{i\mu}^{\dagger}a_{i\nu}^{\dagger}-G_{i\mu\nu}^*(\eta_i^*, \eta_i, N_i)a_{i\nu}a_{i\mu}\}\,. \tag{2·2}$$

Note that the TDHB state vectors are normalized to unity and their time developments are here treated as a unitary transformation parametrized by the time-dependent collective variables $(\eta_i^*, \eta_i, \phi_i)$. The basic equations of the SCC method that determine the unknown functions $G_{i\mu}(\eta_i^*, \eta_i, N_i)$ are

1) Equations of collective submanifold

$$\delta\langle\phi_i(0)|e^{-i\hat{G}_i}\left(H-i\dot{\eta}_i\frac{\partial}{\partial\eta_i}-i\dot{\eta}_i^*\frac{\partial}{\partial\eta_i^*}-\dot{\phi}_i\hat{N}\right)e^{i\hat{G}_i}|\phi_i(0)\rangle=0\,, \tag{2·3}$$

where $\dot{\eta}_i\equiv d\eta_i/dt=-i\partial\mathcal{H}_i/\partial\eta_i^*$, $\dot{\eta}_i^*\equiv d\eta_i^*/dt=i\partial\mathcal{H}_i/\partial\eta_i$ and $\dot{\phi}_i\equiv d\phi_i/dt=\partial\mathcal{H}_i/\partial N_i$.

2) Canonical variables conditions

$$\langle\phi_i(0)|e^{-i\hat{G}_i}\frac{\partial}{\partial\eta_i}e^{i\hat{G}_i}|\phi_i(0)\rangle=\frac{1}{2}\eta_i^*\,,$$

$$\langle\phi_i(0)|e^{-i\hat{G}_i}\frac{\partial}{\partial\eta_i^*}e^{i\hat{G}_i}|\phi_i(0)\rangle=-\frac{1}{2}\eta_i\,,$$

$$\langle\phi_i(0)|e^{-i\hat{G}_i}\hat{N}e^{i\hat{G}_i}|\phi_i(0)\rangle=N_i\,,$$

$$\langle\phi_i(0)|e^{-i\hat{G}_i}\frac{\partial}{\partial N_i}e^{i\hat{G}_i}|\phi_i(0)\rangle=0\,, \tag{2·4}$$

where H is the microscopic Hamiltonian for the system under consideration. The collective Hamiltonian describing the vibrations about the individual HB local minima are defined as

$$\mathcal{H}_i(\eta_i^*, \eta_i, N_i)=\langle\phi_i(0)|e^{-i\hat{G}_i}He^{i\hat{G}_i}|\phi_i(0)\rangle\,. \tag{2·5}$$

The above basic equations are solved by expanding the unknown functions $G_{i\mu\nu}(\eta_i^*, \eta_i, N_i)$ in power series of the collective variables η_i^*, η_i and (N_i-N_0) as

$$G_{i\mu\nu}(\eta_i^*, \eta_i, N_i)=\sum_{rst}g_{i\mu\nu}^{(rst)}(\eta_i^*)^r(\eta_i)^s(N_i-N_0)^t\,, \tag{2·6}$$

where $N_0=\langle\phi_i(0)|\hat{N}|\phi_i(0)\rangle$. Correspondingly, the collective Hamiltonian $\mathcal{H}_i(\eta_i^*, \eta_i, N_i)$ are also expanded as

$$\mathcal{H}_i(\eta_i^*, \eta_i, N_i)=\sum_{rst}h_{i\mu\nu}^{(rst)}(\eta_i^*)^r(\eta_i)^s(N_i-N_0)^t\,. \tag{2·7}$$

The unknown coefficients $g_{i\mu\nu}^{(rst)}$ and $h_{i\mu\nu}^{(rst)}$ are determined such that the basic equations, (2·3) and (2·4), are satisfied in each order of the expansion. In fact, we can put $N_i-N_0=0$ so that the $t\neq0$ terms in the above expansions are unnecessary below.[18] The lowest-order terms of the expansion can be determined by the RPA type boundary condition.[19] In this paper, we consider up to the third order $(r+s\leq3)$ for $G_{i\mu\nu}$ and to the fourth order $(r+s\leq4)$ for $\mathcal{H}_i$. We shall see in §§ 3~5 that $\mathcal{H}_i$ thus constructed indeed describe diabatic collective vibrations about the individual HB

minima.

2.2. *Coupled-configuration collective Schrödinger equation*

Let us next consider the coupling between the collective vibrations $\{|\psi_i(\eta_i^*, \eta_i, \phi_i, N_i)\rangle;\ i=1, 2\}$ associated with the different diabatic configurations (coexisting HB minima). Now we suppose that the two collective variables, (η_1^*, η_1) and (η_2^*, η_2), describe essentially the same collective degrees of freedom which are connected with the quadrupole shape. The collective variables (ϕ_i, N_i) representing the pairing rotations should also be the same irrespective of the configuration i. On the basis of this idea, we introduce the collective coordinates (η^*, η, ϕ, N) which are globally defined over all the diabatic vibrations. The global collective coordinates (η^*, η, ϕ, N) must be connected with the diabatic collective coordinates $(\eta_i^*, \eta_i, \phi_i, N_i)$ by canonical transformations. Taking into account up to the linear order of the transformation, we assume the following relations:

$$\begin{pmatrix}\eta_i\\ \eta_i^*\end{pmatrix}=\begin{pmatrix}x_i & y_i\\ y_i & x_i\end{pmatrix}\begin{pmatrix}\eta-\eta_i^\circ\\ \eta^*-\eta_i^\circ\end{pmatrix},$$

$$\begin{pmatrix}\phi_i\\ N_i\end{pmatrix}=\begin{pmatrix}\phi\\ N\end{pmatrix}, \tag{2·8}$$

$$\begin{pmatrix}x_i\\ y_i\end{pmatrix}=\frac{z_i\pm z_i^{-1}}{2}. \tag{2·9}$$

Here the variables (η^*, η) represent the collective degrees of freedom related with the quadrupole shape motion of the nucleus, and (ϕ, N) represent the gauge angle and the nucleon number. The constants η_i° represent the equilibrium quadrupole deformations of the i-th HB states $|\psi_i(0)\rangle$, and are real because the HB states are static and time-even. The parameters $z_i(>0)$ are introduced so that scales of the collective coordinates (η_i^*, η_i) can be adjusted.

The constants η_i° and z_i can be determined in the following way. Expectation value $\langle\psi_i(\eta_i^*, \eta_i, \phi_i, N_i)|\hat{Q}|\psi_i(\eta_i^*, \eta_i, \phi_i, N_i)\rangle$ of the quadrupole moment $\hat{Q}$, which represents the shape of the nucleus, can be calculated for each diabatic configuration by means of the (η_i^*, η_i) expansion. It is then expressed in terms of the global collective coordinates (η^*, η, ϕ, N) by using Eq. (2·8) and can be Taylor-expanded:

$$Q_i(\eta^*, \eta)=\langle\psi_i(\eta_i^*, \eta_i, \phi_i, N_i)|\hat{Q}|\psi_i(\eta_i^*, \eta_i, \phi_i, N_i)\rangle\Big|_{\substack{\eta_i^*=\eta_i^*(\eta^*,\eta)\\ \eta_i=\eta_i(\eta^*,\eta)\\ \phi_i=\phi\\ N_i=N=N_0}}$$

$$=Q_i|_{\eta^*=\eta=0}+\frac{\partial Q_i}{\partial\eta}\Big|_{\eta^*=\eta=0}(\eta^*+\eta)+\cdots, \tag{2·10}$$

where $\eta_i(\eta^*, \eta)$ represents the right-hand side of Eq. (2·8) and we put $N=N_0$. The quadrupole moment should be zero at $\eta^*=\eta=0$ (spherical limit), and it should have the same dependence on the collective coordinates irrespective of the configurations

because it corresponds to the collective degree of freedom which is common to the diabatic configurations. Imposing these requirements on Eq. (2·10) up to the linear order, we get

$$Q_i|_{\eta^*=\eta=0}=0\,,$$

$$\left.\frac{\partial Q_i}{\partial \eta}\right|_{\eta^*=\eta=0}=\left.\frac{\partial Q_j}{\partial \eta}\right|_{\eta^*=\eta=0}. \quad (i\neq j) \tag{2·11}$$

These equations are enough to determine η_i° and z_i, provided that the scale of the global collective coordinates (η^*, η) is fixed. In the case when we have an (η_i^*, η_i) expansion expression for the quadrupole moment,

$$\langle\phi_i(\eta_i^*, \eta_i, \phi_i, N_i)|\hat{Q}|\phi_i(\eta_i^*, \eta_i, \phi_i, N_i)\rangle|_{N_i=N_0}=q_i^{(0)}+q_i^{(1)}(\eta_i^*+\eta_i)+\cdots\,, \tag{2·12}$$

Eq. (2·11) reads

$$q_i^{(0)}-2\eta_i^\circ q_i^{(1)}z_i=0\,,$$

$$q_i^{(1)}z_i=q_j^{(1)}z_j\,. \quad (i\neq j) \tag{2·13}$$

Thus η_i° and z_i are determined.

We can then express the diabatic wave packets associated with the i-th HB states in terms of the newly defined collective coordinates (η^*, η, ϕ, N):

$$|\tilde{\phi}_i(\eta^*, \eta, \phi, N)\rangle=e^{i\Gamma_i(\eta^*,\eta,N)}|\phi_i(\eta_i^*, \eta_i, \phi_i, N_i)\rangle\Big|_{\substack{\eta_i^*=\eta_i^*(\eta^*,\eta)\\ \eta_i=\eta_i(\eta^*,\eta)\\ \phi_i=\phi\\ N_i=N}}. \tag{2·14}$$

Here we introduced a phase factor $\Gamma_i(\eta^*, \eta, N)$ which is real and accounts for the relative phase of the diabatic wave packets (2·14) between different configurations. The canonical variable condition is known to restrict the phase of the wave packet, while Eq. (2·4) requires this condition to be fulfilled independently for each diabatic collective variables (η_i^*, η_i). We demand here that the diabatic wave packet $|\tilde{\phi}_i(\eta^*, \eta, \phi, N)\rangle$ expressed in terms of the global collective coordinates (η^*, η, ϕ, N) should satisfy the same canonical variable condition for all the diabatic configurations.

$$\langle\tilde{\phi}_i(\eta^*, \eta, \phi, N)|\frac{\partial}{\partial\eta}|\tilde{\phi}_i(\eta^*, \eta, \phi, N)\rangle=\frac{1}{2}\eta^*\,,$$

$$\langle\tilde{\phi}_i(\eta^*, \eta, \phi, N)|\frac{\partial}{\partial\eta^*}|\tilde{\phi}_i(\eta^*, \eta, \phi, N)\rangle=-\frac{1}{2}\eta\,,$$

$$\langle\tilde{\phi}_i(\eta^*, \eta, \phi, N)|\hat{N}|\tilde{\phi}_i(\eta^*, \eta, \phi, N)\rangle=N\,,$$

$$\langle\tilde{\phi}_i(\eta^*, \eta, \phi, N)|\frac{\partial}{\partial N}|\tilde{\phi}_i(\eta^*, \eta, \phi, N)\rangle=0\,. \tag{2·15}$$

These canonical variable conditions reduce to the equations for the phase factor $\Gamma_i(\eta^*, \eta, N)$:

$$\frac{\partial}{\partial\eta}\Gamma_i=\frac{1}{2i}\eta_i^\circ\,,$$

$$\frac{\partial}{\partial\eta^*}\Gamma_i=-\frac{1}{2i}\eta_i^\circ\,,$$

$$\frac{\partial}{\partial N}\Gamma_i=0\,, \tag{2·16}$$

where Eqs. (2·14), (2·8) and (2·4) are substituted in Eq. (2·15). Thus we get the phase factor

$$\Gamma_i(\eta^*,\eta,N)=\frac{1}{2i}\eta_i^\circ(\eta-\eta^*)\,. \tag{2·17}$$

In Eq. (2·17) we neglected an arbitrary constant because the constant phase has no relevant effect.

Next, let us consider the interaction energy between the diabatic wave packets $|\tilde{\phi}_i(\eta^*,\eta,\phi,N)\rangle$. It is expressed by

$$\begin{aligned}\tilde{\mathcal{H}}_{ij}(\eta^*,\eta)&=\langle\tilde{\phi}_i(\eta^*,\eta,\phi,N)|H|\tilde{\phi}_j(\eta^*,\eta,\phi,N)\rangle|_{N=N_0}\\&=e^{-i\Gamma_i+i\Gamma_j}\langle\phi_i(\eta_i^*(\eta^*,\eta),\eta_i(\eta^*,\eta),\phi,N_0)|H|\phi_j(\eta_j^*(\eta^*,\eta),\eta_j(\eta^*,\eta),\phi,N_0)\rangle\,.\end{aligned} \tag{2·18}$$

On the other hand, the energy expectation value of the i-th diabatic wave packet is given by

$$\begin{aligned}\tilde{\mathcal{H}}_i(\eta^*,\eta)&=\langle\tilde{\phi}_i(\eta^*,\eta,\phi,N)|H|\tilde{\phi}_i(\eta^*,\eta,\phi,N)\rangle|_{N=N_0}\\&=\mathcal{H}_i(\eta_i^*(\eta^*,\eta),\eta_i(\eta^*,\eta),N_0)\,.\end{aligned} \tag{2·19}$$

With use of these quantities, we introduce a quantized Schrödinger equation for eigenstates of the collective excitation incorporating the couplings between the diabatic configurations:

$$\begin{pmatrix}H_1(b^\dagger,b) & H_{12}(b^\dagger,b)\\ H_{21}(b^\dagger,b) & H_2(b^\dagger,b)\end{pmatrix}\begin{pmatrix}|\psi_1\rangle_b\\ |\psi_2\rangle_b\end{pmatrix}=E\begin{pmatrix}|\psi_1\rangle_b\\ |\psi_2\rangle_b\end{pmatrix}, \tag{2·20}$$

where $H_{ij}(b^\dagger,b)$ and $H_i(b^\dagger,b)$ are defined by replacing the collective variables (η^*,η) in $\tilde{\mathcal{H}}_{ij}(\eta^*,\eta)$ and $\tilde{\mathcal{H}}_i(\eta^*,\eta)$ with the boson operators $(b^\dagger,b)$ and taking the normal ordering. That is,

$$H_{ij}(b^\dagger,b)=:\tilde{\mathcal{H}}_{ij}(\eta^*,\eta)|_{\substack{\eta^*=b^\dagger\\ \eta=b}}:\,,$$

$$H_i(b^\dagger,b)=:\tilde{\mathcal{H}}_i(\eta^*,\eta)|_{\substack{\eta^*=b^\dagger\\ \eta=b}}:\,. \tag{2·21}$$

The coupled configuration collective Schrödinger equation (2·20) may be justified, provided that the orthogonality between the different diabatic configurations holds well. We are in fact interested in such cases where the orthogonality condition is fulfilled exactly or almost exactly. On the other hand, if the overlap between the two wave packets is not negligible, it might be necessary to generalize the above equations. In this connection, it would be interesting to investigate the relation of this

approach to the time-dependent resonating Hartree-Bogoliubov theory recently proposed by Fukutome and Nishiyama.[24),25)]

The coupled-configuration collective Schrödinger equation can be solved by expanding the boson basis states:

$$|\psi_i\rangle_b=\sum_{n=0}^{N_{b,i}} C_{ni}|n, i\rangle_b\,. \tag{2·22}$$

In defining the boson basis states

$$|n, i\rangle_b=\frac{1}{\sqrt{n!}}(b_i^\dagger)^n|0, i\rangle_b\,,\quad b_i|0, i\rangle_b=0\,, \tag{2·23}$$

we use boson operators $(b_i^\dagger, b_i)$ which are the quantum counterpart of the collective variables (η_i^*, η_i) associated with the i-th HB state $\{|\psi_i\rangle_b;\ i=1, 2\}$. Namely,

$$\begin{pmatrix} b_i \\ b_i^\dagger \end{pmatrix}=\begin{pmatrix} x_i & y_i \\ y_i & x_i \end{pmatrix}\begin{pmatrix} b-\eta_i^\circ \\ b^\dagger-\eta_i^\circ \end{pmatrix}, \tag{2·24}$$

which should be compared with Eq. (2·8). The maximum numbers $N_{b,i}$ of the boson basis in Eq. (2·22) represent the cutoff of the boson space (physical boson space) which may arise from the same origin as in the boson expansion theory.

For any one-body operator $\hat{F}$ which acts on many-fermion state space we can introduce a corresponding operator F^{cc} which acts on the coupled-configuration collective boson space $\{|\psi_i\rangle_b;\ i=1, 2\}$. It can be defined by

$$F^{cc}=\begin{pmatrix} F_{11}(b^\dagger, b) & F_{12}(b^\dagger, b) \\ F_{21}(b^\dagger, b) & F_{22}(b^\dagger, b) \end{pmatrix},$$

$$F_{ij}(b^\dagger, b)=:\mathcal{F}_{ij}(\eta^*, \eta)|_{\substack{\eta^*=b^\dagger \\ \eta=b}}:\,,$$

$$\mathcal{F}_{ij}(\eta^*, \eta)=\langle\tilde{\phi}_i(\eta^*, \eta, \phi, N)|\hat{F}|\tilde{\phi}_j(\eta^*, \eta, \phi, N)\rangle|_{N=N_0}\,. \tag{2·25}$$

The matrix element of F^{cc} between the collective excited states can be calculated in terms of the collective boson state vectors.

§ 3. Particle-plus-harmonic-core model

Let us consider a simple model system consisting of two valence particles and a deformable core. We explicitly consider two valence levels which cross with each other as the deformation of the core increases. The two valence particles can jump between the two levels by the monopole pairing force. In this section, we assume that the vibration of the core is harmonic. The case of anharmonic vibration will be treated in the next section.

The model Hamiltonian consists of four parts,

$$H=H_{\text{core}}+H_{\text{sp}}^\circ+H_{\text{coup}}+H_{\text{int}}\,, \tag{3·1}$$

where

$$H_{\text{core}}=\frac{1}{2}(P^2+Q^2)\,,\quad H_{\text{sp}}^{\circ}=\epsilon_{\circ}\sum_{k=1,2}\sigma_k\hat{N}_k\,,\tag{3·2}$$

$$H_{\text{coup}}=-\chi Q\sum_{k=1,2}\sigma_k\hat{N}_k\,,\quad H_{\text{int}}=-GA^{\dagger}A,\tag{3·3}$$

with

$$A^{\dagger}=\sum_{k=1,2}A_k^{\dagger}\,,\quad A_k^{\dagger}=\sum_{m>0}c_{km}^{\dagger}c_{\widetilde{km}}^{\dagger}\,,\quad \hat{N}_k=\sum_m c_{km}^{\dagger}c_{km}\,.\tag{3·4}$$

Here $P=-i(\partial/\partial Q)$ is the momentum conjugate to the deformation coordinate Q of the core. In the above Hamiltonian, H_{core} describes the harmonic vibration of the core, H_{sp}° the shell-model single-particle energies for the valence nucleons, H_{coup} the coupling between the valence nucleons and the core deformation Q, and H_{int} the monopole pairing interaction between the valence nucleons. The particle-core coupling strength and the pairing-force strength are denoted by χ and G, respectively. The suffix k labels different valence levels. We consider only two levels, and set $\sigma_k=-1$ and $+1$ for $k=1$ and 2, respectively. In the monopole-pair creation operator $A_k^{\dagger}$ and the nucleon-number operator $\hat{N}_k$ for level k, the suffix m labels degenerate single-particle states and $\widetilde{km}$ denotes the time reversed state of km. We assume, for simplicity, that the degeneracy is two-fold, i.e., $m=-1/2$ and $1/2$. The single-particle energies $\epsilon_k(Q)$ including the particle-core coupling are defined by

$$H_{\text{sp}}(Q)=H_{\text{sp}}^{\circ}+H_{\text{coup}}(Q)=\sum_k\epsilon_k(Q)\hat{N}_k\tag{3·5}$$

as functions of the deformation of the core. Due to the particle-core coupling, the first level $\epsilon_1(Q)=-\epsilon_{\circ}+\chi Q$ is up-sloping while the second level $\epsilon_2(Q)=\epsilon_{\circ}-\chi Q$ is down-sloping as a function of Q. They cross at $Q=\epsilon_{\circ}/\chi$. The two diabatic configurations are simply given by $A_1^{\dagger}|0\rangle\otimes|\phi_1^{\text{core}}\rangle$ and $A_2^{\dagger}|0\rangle\otimes|\phi_2^{\text{core}}\rangle$, where $|0\rangle$ represents the vacuum for valence nucleons and $|\phi_i^{\text{core}}\rangle$ the time dependent wave packets describing the collective vibration of the core. They are apparently orthogonal to each other, and are mixed by the pairing interaction H_{int}.

It is known that the equation of the collective manifold in the SCC method reduces to the ordinary time-dependent variational principle when we consider simple models involving only single boson-degree of freedom. For the present model with harmonic-vibrational core, the solutions of the time-dependent variational principle are obviously given by the time-dependent coherent states

$$|\phi_i^{\text{core}}(\eta_i^*,\,\eta_i)\rangle=e^{\eta_i b_i^{\dagger}-\eta_i^* b_i}|\phi_i^{\text{core}}(0)\rangle\,,\tag{3·6}$$

where time-dependence of the vibrational amplitudes $\eta_i(t)$ are given by $\eta_i(t)=\eta_i(0)e^{-i\omega t}$, and where

$$|\phi_i^{\text{core}}(0)\rangle=e^{\eta_i^{\circ}(b^{\dagger}-b)}|0\rangle\tag{3·7}$$

with $b=(Q+iP)/\sqrt{2}$, represent the equilibrium states of the core whose deformations are given by $\eta_i^{\circ}=-\chi$ and χ for $i=1$ and 2, respectively. They are the vacua for the shifted boson operators $b_i=b-\eta_i^{\circ}$ appearing in Eq. (3·6) and satisfying $b_i|\phi_i^{\text{core}}(0)\rangle=0$.

The relation (2·8) between the local collective variables (η_i^*, η_i) and the global ones (η^*, η) becomes very simple in this model, and is given by $\eta_i=\eta-\eta_i^\circ$. With respect to the diabatic configurations $A_i^\dagger|0\rangle\otimes|\phi_i^{\text{core}}\rangle$, the diagonal and off-diagonal matrix elements of the Hamiltonian are easily calculated to be $\mathcal{H}_i=(\eta^*\eta+(1/2))+2\epsilon_\circ\sigma_i-\sqrt{2}\,\chi\sigma_i(\eta^*+\eta)-G$ and $\langle\psi_1(\eta_1^*, \eta_1, \phi, N_0)|H|\psi_2(\eta_2^*, \eta_2, \phi, N_0)\rangle=-Ge^{-\chi(\eta-\eta^*)}$. Taking into account the phase factor defined by (2·14) and given by (2·17), we finally obtain the coupling matrix elements defined by (2·18) as $\mathcal{H}_{12}=\mathcal{H}_{21}=-G$.

Replacing the (η^*, η) with the boson operators $(b^\dagger, b)$, we obtain the requantized Hamiltonian

$$H=\begin{pmatrix}\left(b^\dagger b+\frac{1}{2}\right)-2\left(\epsilon_\circ-\chi\frac{b^\dagger+b}{\sqrt{2}}\right)-G & -G \\ -G & \left(b^\dagger b+\frac{1}{2}\right)+2\left(\epsilon_\circ-\chi\frac{b^\dagger+b}{\sqrt{2}}\right)-G\end{pmatrix}$$

$$=\frac{1}{2}(P^2+Q^2)\boldsymbol{1}+\epsilon_\circ\sum_k\sigma_k\boldsymbol{N}_k-\chi Q\sum_k\sigma_k\boldsymbol{N}_k+\boldsymbol{H}_{\text{int}}\,, \tag{3·8}$$

where $\boldsymbol{1}$ is the 2×2 unit matrix,

$$\boldsymbol{N}_k=\begin{pmatrix}\langle0|A_1\hat{N}_kA_1^\dagger|0\rangle & \langle0|A_1\hat{N}_kA_2^\dagger|0\rangle \\ \langle0|A_2\hat{N}_kA_1^\dagger|0\rangle & \langle0|A_2\hat{N}_kA_2^\dagger|0\rangle\end{pmatrix}=2\begin{pmatrix}\delta_{k1} & 0 \\ 0 & \delta_{k2}\end{pmatrix}, \tag{3·9}$$

$$\boldsymbol{H}_{\text{int}}=\begin{pmatrix}\langle0|A_1\hat{H}_{\text{int}}A_1^\dagger|0\rangle & \langle0|A_1\hat{H}_{\text{int}}A_2^\dagger|0\rangle \\ \langle0|A_2\hat{H}_{\text{int}}A_1^\dagger|0\rangle & \langle0|A_2\hat{H}_{\text{int}}A_2^\dagger|0\rangle\end{pmatrix}=-G\begin{pmatrix}1 & 1 \\ 1 & 1\end{pmatrix}, \tag{3·10}$$

which exactly coincides with the original Hamiltonian (3·1). Thus, we have

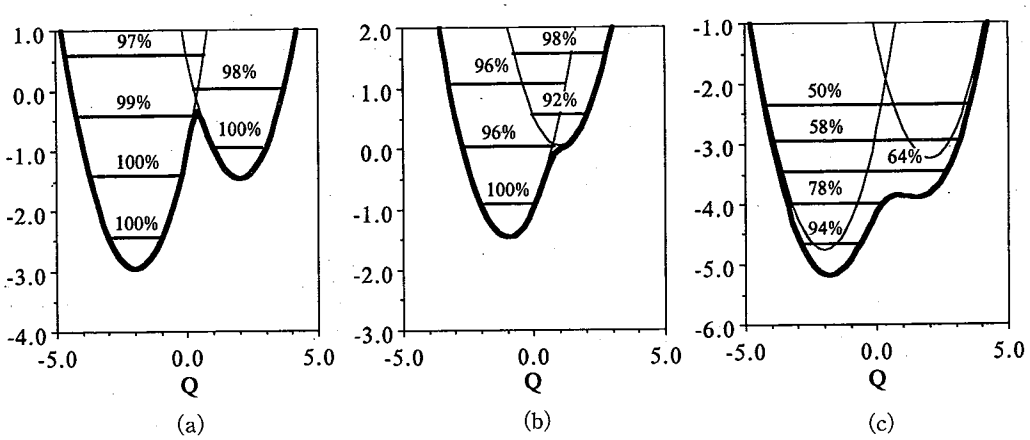

Fig. 1. Examples of the potential-energy functions and exact energy levels for the particle-plus-harmonic-core model. Thick and thin lines represent the adiabatic and the diabatic potentials respectively. Energy levels are drawn with respect to the diabatic potential in cases (a) and (b), and with respect to the adiabatic ones in case (c). The numbers on individual levels indicate the percentages of the main diabatic configurations in the wave functions obtained by diagonalizing the total Hamiltonian. The parameters used are $G=0.2$, $\chi=1.0$ for case (a), $G=0.2$, $\chi=0.5$ for case (b), $G=2.0$, $\chi=1.0$ for case (c), and $\epsilon_\circ=0.375$ for all cases.

confirmed that our theoretical scheme outlined in § 2 gives exact solutions for the case of simple model under consideration. It should be noted here that the matrix elements of the coupling Hamiltonian $\boldsymbol{H}_{\text{int}}$ become $-G$, in agreement with the exact solutions, owing to the phase factors $e^{i\Gamma_i}$ defined by (2·14) and given by Eq. (2·17).

We can simulate various situations concerning shape coexistence phenomena by varying three parameters $\epsilon_\circ$, G and χ of this model. In Fig. 1 we present typical examples of the collective potential-energy functions and the quantum levels obtained by exact diagonalizations. Cases (a) and (b) represent the situation with relatively weak pairing-force strength G, while case (c) that with very strong pairing force. Except for case (c), we can very clearly distinguish two kinds of vibrational states associated with the first and the second minima of the collective potential. They retain their identities even after the mixings due to the pairing force. It is striking that this characteristic holds for levels whose excitation energies lie much higher than the barrier of the adiabatic potential between the two local minima. Such phenomena, i.e., the existence of well localized wave functions around the local minima can hardly be expected from the properties of the adiabatic potential.

In Fig. 2 we compare the spectra obtained by means of the adiabatic approximation (Born-Oppenheimer approximation) with the exact solutions. They are obtained as follows. First we calculate the adiabatic potential by diagonalizing H for a given value of Q neglecting the collective kinetic energy of H_{core}. It is given by

$$V_{\text{ad}}(Q)=\frac{1}{2}Q^2+V_{\text{particle}}(Q) \tag{3·11}$$

with

$$V_{\text{particle}}(Q)=-G-\sqrt{4(\epsilon_\circ-\chi Q)^2+G^2}\,, \tag{3·12}$$

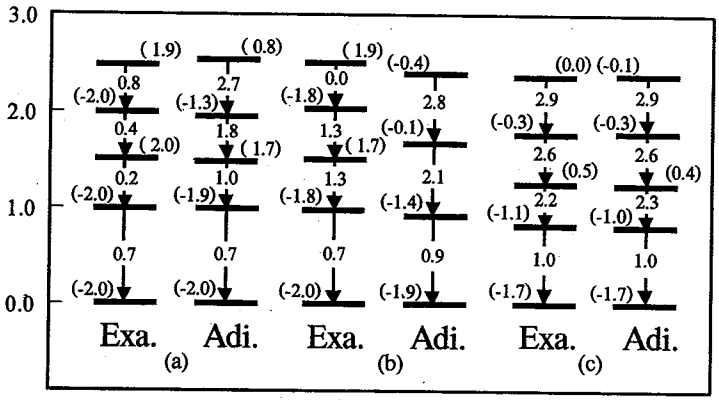

Fig. 2. Examples of excitation spectra and transition matrix elements $|\langle m|Q|n\rangle|$ for the particle-plus-harmonic-core model. Parameters used are the same as in Fig. 1, for cases (a), (b) and (c), respectively. "Exa." represents the spectra obtained by exact diagonalization of the Hamiltonian, and "Adi." those obtained by the adiabatic approximation. Numbers in parenthesis on each level indicate the expectation value of $\hat{Q}_p=\sum_k\sigma_k\hat{N}_k$. Note that we get $\langle\hat{Q}_p\rangle=\pm 2.0$ when there is no mixing between the lower and the upper configurations. Thus, these numbers indicate the diabaticity of the levels.

whose local minima occurs at $Q=\pm\chi$, when $G=0$. Secondly, we diagonalize $H_{\rm ad}=(1/2)P^2+V_{\rm ad}(Q)$ and obtain adiabatic spectra and wave functions. We see in Fig. 2 that the transition matrix elements are rather poorly reproduced by the adiabatic approximation in cases (a) and (b), while they are well reproduced in case (c) when we have very strong pairing force mixing the two diabatic configurations. The adiabatic approximation is thus found to overestimate the mixing between the two kinds of vibrations around the local minima in situations like cases (a) and (b) where the pairing-force strength G is relatively weak.

The following considerations may be helpful to understand the above result. The Landau-Zener transition probability P_{LZ} at the level crossing point between the down-sloping and up-sloping single-particle levels is given by

$$P_{\rm LZ}=e^{-2\gamma} \tag{3·13}$$

with

$$\gamma=\frac{\pi|V_{\rm int}|}{\left|\dot{Q}\frac{\partial}{\partial Q}(\epsilon_2-\epsilon_1)\right|}. \tag{3·14}$$

In the model under consideration, the interaction $V_{\rm int}$ between the two diabatic configurations is given by the pairing-force strength G. The single-particle-energy difference $\epsilon_2-\epsilon_1$ is given by $2(\epsilon_\circ-\chi Q)$. The time-dependence of the core deformation Q is given by $Q=Q_0e^{i\omega t}$ so that $|\dot{Q}|=\omega Q_0$, where we can set $Q_0=\omega=1$ for the ground state of $H_{\rm core}=(P^2+Q^2)/2$. For the parameters adopted in Fig. 1, we obtain $\gamma=0.17$, 0.34 and 1.7 for cases (a), (b) and (c), respectively. Thus, the condition for the validity of the adiabatic approximation, $\gamma>1$, is violated except for case (c). Namely, the Landau-Zener transition probability is rather large and the particles do not always follow the adiabatic level.

It should be mentioned here that we would also obtain $\gamma<1$ for the level crossings associated with the shape coexistence in Sn and Pb isotopes by making an analysis similar to above.

§ 4. Particle-plus-anharmonic-core model

Instead of postulating the collective variables (Q, P) for the core as in the previous section, we now derive them by means of the SCC method for a single-j model Hamiltonian with $O(4)$ symmetry. Namely, we consider the core whose Hamiltonian is given by

$$H_{\rm core}=-G_cA_c^\dagger A_c-\frac{1}{2}\chi\hat{Q}_c^\dagger\hat{Q}_c\,, \tag{4·1}$$

$$A_c^\dagger=\sum_{m>0}c_{cm}^\dagger c_{\tilde{cm}}^\dagger\,,\quad \hat{Q}_c=\sum_m\sigma_{cm}c_{cm}^\dagger c_{cm}\,, \tag{4·2}$$

where $\sigma_{cm}=+1$ for $|m|<\Omega/2$ and $\sigma_{cm}=-1$ for $|m|>\Omega/2$ with $\Omega=j+(1/2)$. The $c_{cm}^\dagger$ and c_{cm} are creation and annihilation operators of nucleons in the core. This model Hamiltonian may be regarded as a simplified version of the familiar pairing-plus-

quadrupole $(P+QQ)$-force model for the single j-shell. The operators $A_c^\dagger$, A_c, Q_c and their commutators form a Lie algebra of $O(4)$ symmetry. This model Hamiltonian has been used for schematic analysis of anharmonic quadrupole vibrations in transitional nuclei.[18),20),21)] It was shown in Ref. 18) that the fourth-order approximation of the (η^*, η) expansion well reproduces the low-lying collective states for the Hamiltonian (4·1). In accordance with the above $H_{\rm core}$, we consider the single-particle Hamiltonian

$$H_{\rm sp}=H_{\rm sp}^\circ+H_{\rm coup}=(\epsilon_\circ-\chi\hat{Q}_c)\sum_{i=1,2}\sigma_i\hat{N}_i\,, \tag{4·3}$$

where $H_{\rm sp}^\circ$ is given by (3·2). Note that Q in the previous subsection is here replaced with the simplified "quadrupole" operator $\hat{Q}_c$ for the core. The total Hamiltonian of this model is defined by $H=H_{\rm core}+H_{\rm sp}+H_{\rm int}$, where the interaction $H_{\rm int}$ between the valence particles is the same as in (3·3).

We apply our theoretical scheme outlined in § 2 to the model system consisting of two particles plus core with the $O(4)$ symmetry defined above. It is easily seen that there exists two HB minima corresponding to two valence configurations. The two diabatic configurations may be explicitly constructed as

$$|\phi_i(\eta_i^*, \eta_i, \phi_i, N_i)\rangle=A_i^\dagger|0\rangle\otimes|\phi^{\rm core}(\eta_i^*, \eta_i, \phi_i, N_i)\rangle\,, \quad (i=1, 2) \tag{4·4}$$

$$|\phi^{\rm core}(\eta_i^*, \eta_i, \phi_i, N_i)\rangle=e^{-i\phi_i\hat{N}_i}\ e^{G_i(\eta_i^*,\eta_i,N_i)B_i^\dagger-G_i^*(\eta_i^*,\eta_i,N_i)B_i}|\phi_i(0)\rangle\,, \tag{4·5}$$

$$B_i^\dagger=\sum_{m>0}\sigma_{im}a_{im}^\dagger a_{\tilde{i}\tilde{m}}^\dagger\,, \quad B_i=\sum_{m>0}\sigma_{im}a_{\tilde{i}\tilde{m}}a_{im}\,, \tag{4·6}$$

where $|\phi_i(0)\rangle$ are the HB vacua and $a_{im}^\dagger$ are the quasiparticles defined with respect to them:

$$a_{im}^\dagger=u_{im}c_{im}^\dagger-v_{im}c_{\tilde{i}\tilde{m}}\,, \quad a_{im}|\phi_i(0)\rangle=0\,. \tag{4·7}$$

The diabatic configurations (4·4) are obviously orthogonal to each other.

The unknown function $G_i(\eta_i^*, \eta_i, N_i)$ in Eq. (4·5) is determined by the (η_i^*, η_i) expansion method based on the SCC method. Assuming the existence of global collective variables (η^*, η) related with the collective variable (η_i^*, η_i) by Eq. (2·8), we then derive the coupled-configuration Schrödinger equation for the model under consideration following the procedure described in § 2. We adopt the fourth-order approximation in the (η_i^*, η_i) expansion when evaluating the diabatic collective Hamiltonians $\mathcal{H}_i(\eta_i^*, \eta_i)$, while the (η^*, η) dependence of the coupling matrix elements $\tilde{\mathcal{H}}_{ij}(\eta^*, \eta)$ is taken into account up to the first order in (η^*, η).

We show in Fig. 3 typical examples of the calculated potential-energy functions. In this figure, thin lines show the diabatic potentials while thick lines the adiabatic potentials. The horizontal lines indicate the zero-point vibrational amplitudes evaluated by means of the RPA based on the local HB minima. The adiabatic potentials are calculated in terms of the conventional Born-Oppenheimer approximation scheme. On the other hand, the diabatic potentials are calculated in the following way. First, we rewrite the collective Hamiltonian $\mathcal{H}_i(\eta_i^*, \eta_i)$ defined by (2·5) in terms of the collective coordinates $q_i=(\eta_i^*+\eta_i)/\sqrt{2}$ and the momenta $p_i=i(\eta_i^*-\eta_i)/\sqrt{2}$,

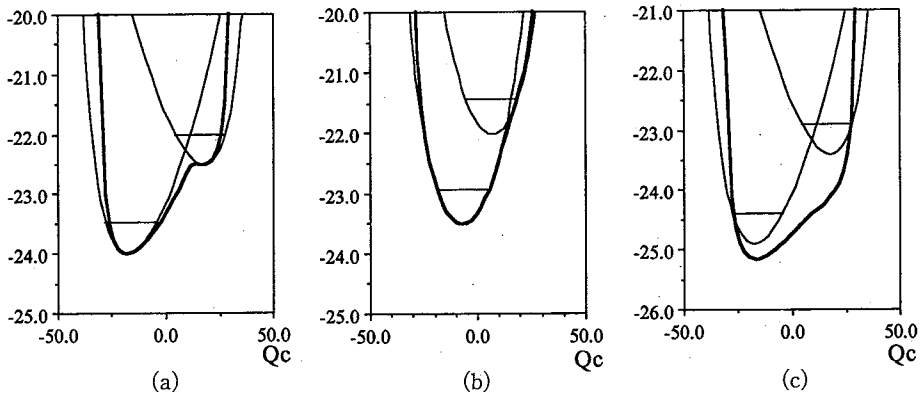

Fig. 3. Examples of the potential-energy functions for the particle-plus-anharmonic-core model. Thick lines represent the adiabatic potentials, while thin lines the diabatic potentials obtained by means of the SCC method. Parameters used are $\epsilon_c=0.375$, $G_c=0.06$, $\Omega=40$, $N_c=30$, and $G=0.1$, $\chi=0.03$ for case (a), $G=0.1$, $\chi=0.025$ for case (b), $G=1.0$, $\chi=0.03$ for case (c). The calculated pairing gap Δ of the core is 1.16 at the spherical point.

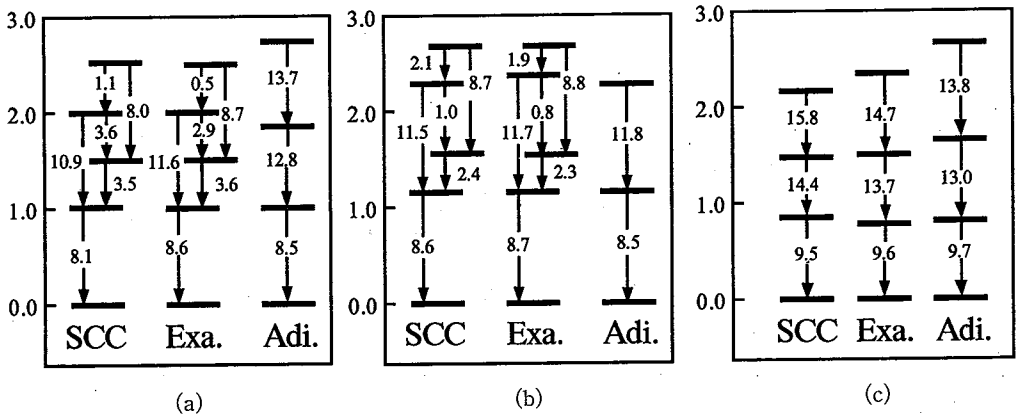

Fig. 4. Examples of excitation spectra and transition matrix elements $|\langle m|\hat{Q}_c|n\rangle|$ for the particle-plus-anharmonic-core model. The spectra denoted as "SCC" are obtained by means of the coupled-configuration SCC method, "Exa." by exact diagonalization, and those denoted as "Adi." are obtained by means of adiabatic approximation. Parameters used are the same as in Fig. 3, for cases (a), (b) and (c), respectively.

and define the momentum-independent part of it as the collective potential $V_i(q_i)$ associated with the i-th diabatic configuration. Secondly, we evaluate the expectation value Q_c of the "quadrupole operator" $\hat{Q}_c$ with respect to the core wave function (4·5), and expand it in terms of the collective coordinate up to the third order in q_i. Using the ralation between q_i and Q_c, we rewrite the $V_i(q_i)$ as a function of Q_c.

Cases (a), (b) and (c) in Fig. 3 correspond to those in Fig. 1. Namely, Figs. 3(a) and (b) represent the case of relatively weak pairing-force strength G, while Fig. 3(c) that of very strong G. We see that the fourth-order (η_i^*, η_i) expansion successfully yields the diabatic potential-energy functions incorporating the anharmonic effects of the core vibrations. It should be noted here that zero-point amplitude washes out the

second minimum that exists in case (a) in the adiabatic potential-energy function.

In Fig. 4 are compared the excitation spectra and transition moments obtained by the coupled-configuration SCC method with those of the exact solutions. Expectation values of the "quadrupole" operator $\hat{Q}_c$ and the percentages of the first diabatic configurations in the final wave functions obtained after taking the couplings into account are listed in Table I. Cases (a), (b) and (c) in Fig. 4 and Table I correspond to cases (a), (b) and (c) of Fig. 3, respectively. In Table I, Q_c represent the expectation values of the operator $\hat{Q}_c$ for the core, while Q_p those for the valence operator $\hat{Q}_p$ defined by $\hat{Q}_p=\sum_{k=1,2}\hat{Q}_k$ with $\hat{Q}_k=\sum_m \sigma_{km} c^{\dagger}_{km} c_{km}$. Note that $Q_p=-2$ and $+2$ for the first and the second diabatic configurations, respectively. They can therefore be used

Table I. Properties of the excited states in the particle-plus-anharmonic-core model obtained by exact diagonalization (Exact), the coupled-configuration SCC method (SCC) and the adiabatic approximation (Adiabatic). Parameters used are the same as in Fig. 4 for cases (a), (b) and (c), respectively. The numbers in the first column indicate the order of the levels counted from the lowest one. Numbers in the column "%" indicate the percentages of the lower diabatic configurations involved in the total wave functions. Numbers in the columns denoted as "Q_c" and "Q_p" indicate the expectation values of the operators $\hat{Q}_c$ and $\hat{Q}_p \equiv \sum_k \sigma_k \hat{N}_k$, respectively.

(a)

	Exact			SCC			Adiabatic	
	%	Q_c	Q_p	%	Q_c	Q_p	Q_c	Q_p
1	100	−15.2	−2.0	100	−17.7	−2.0	−12.7	−2.0
2	99	−7.9	−1.9	99	−12.9	−2.0	−1.9	−1.3
3	3	14.6	1.9	2	17.2	1.9	4.5	−0.0
4	98	−2.9	−1.9	99	−8.6	−2.0	−4.6	−0.8
5	1	8.2	2.0	1	13.1	2.0	—	—

(b)

	Exact			SCC			Adiabatic	
	%	Q_c	Q_p	%	Q_c	Q_p	Q_c	Q_p
1	100	−6.8	−2.0	100	−7.2	−2.0	−6.1	−1.9
2	97	−5.4	−1.9	97	−6.5	−1.9	−3.5	−1.6
3	3	6.5	1.9	3	6.8	1.9	0.2	−0.7
4	97	−4.0	−1.9	98	−6.1	−1.9	—	—
5	3	5.5	1.9	3	6.5	1.9	—	—

(c)

	Exact			SCC			Adiabatic	
	%	Q_c	Q_p	%	Q_c	Q_p	Q_c	Q_p
1	90	−12.8	−1.6	92	−15.0	−1.6	−10.1	−1.5
2	70	−1.1	−0.8	72	−5.0	−0.9	0.5	−0.7
3	58	2.3	−0.3	53	2.4	−0.1	1.7	−0.5
4	63	1.2	−0.5	62	0.4	−0.5	−0.6	−0.5

as a measure of the mixings of the two configurations in the total wave functions.

In Fig. 4, we also show the result calculated in terms of the adiabatic (Born-Oppenheimer) approximation. This calculation was done in the following way. We first apply the conventional constrained Hartree-Bogoliubov (CHB) method to the model under consideration by choosing the expectation value Q_c of the core "quadrupole" operator $\hat{Q}_c$ as a constraint. For a given value of Q_c, we diagonalize the pairing interaction H_{int} which mixes different eigenstates of the single-particle Hamiltonian $H_{sp}=(\epsilon_0-\chi Q_c)\sum_{k=1,2}\sigma_k\hat{N}_k$, and select the lowest energy configuration. The collective potential energy is then obtained as a sum of the core and the valence-particle contributions as follows:

$$V_{ad}(Q_c)=V_{core}(Q_c)+V_{particle}(Q_c)\,, \tag{4·8}$$

where

$$V_{core}(Q_c)=-\frac{G}{8}\{N_c(2\Omega-N_c)-Q_c^2+\sqrt{(N_c^2-Q_c^2)((2\Omega-N_c)^2-Q_c^2)}\}-\frac{1}{2}\chi Q_c^2 \tag{4·9}$$

with N_c being the number of particles in the core, and $V_{particle}(Q_c)$ is the same as in Eq. (3·12). Next, we evaluate the collective mass parameter as a function of Q_c by means of the conventional cranking procedure. Diagonalizing the Schrödinger equation obtained after quantization, we get the collective spectra in the adiabatic approximation.

It is clearly seen in Fig. 4 and Table I that the coupled-configuration SCC method successfully reproduces the main features of the exact spectra. In Figs. 4(a) and (b), the 1st, 2nd and 4th eigenstates are associated with the first (lower) diabatic configurations, while 3rd and 5th eigenstates correspond to the second (higher) configurations. It is striking that the diabatic collective vibrations well retain their identities in the 3rd and 5th eigenstates in spite of the fact that the second HB minima are completely washed out by the zero-point vibrational amplitudes (see Figs. 3(a) and (b)). As shown in Table I, the mixing probabilities of the first diabatic configurations are only a few percent in the 3rd and 5th eigenstates. This result is totally unexpected from the properties of the adiabatic potential energy functions. Indeed, the adiabatic (Born-Oppenheimer) approximation completely fails in reproducing the main characteristics of the 3rd and 5th eigenstates which are seen in the exact spectra and in the coupled-configuration SCC method. On the other hand, the adiabatic approximation works fairly well when the coupling matrix elements between the two diabatic configurations become stronger. This is shown in Fig. 4(c) and Table I(c) which exhibit the result for the case with very strong pairing force. In contrast to the adiabatic (Born-Oppenheimer) approximation, the coupled-configuration SCC method nicely reproduces the transition moments as well as the excitation spectra over the whole range of the pairing-force strength G.

§ 5. Multi-$O(4)$ model

The $O(4)$ model Hamiltonian for nucleons in a single j-shell, discussed in § 4 in

relation to the particle-plus-anharmonic-core model, may be easily generalized to the case of many j-shells as

$$H=\sum_k \epsilon_k^\circ \hat{N}_k - GA^\dagger A - \frac{1}{2}\chi \hat{Q}^\dagger \hat{Q}\,, \tag{5·1}$$

$$A^\dagger=\sum_k A_k^\dagger\,,\quad \hat{Q}=\sum_k q_k \hat{Q}_k\,,\quad \hat{N}=\sum_k \hat{N}_k\,, \tag{5·2}$$

$$A_k^\dagger=\sum_{m>0} c_{km}^\dagger c_{\tilde{k}\tilde{m}}^\dagger\,,\quad \hat{Q}_k=\sum_m \sigma_{km} c_{km}^\dagger c_{km}\,,\quad \hat{N}_k=\sum_m c_{km}^\dagger c_{km}\,, \tag{5·3}$$

where the suffix k distinguishes different j-shells, and $\sigma_{km}=\pm 1$ according to $|m|\gtrless \Omega/2$. The coefficients q_k in $\hat{Q}$ simulate the magnitude of the reduced quadrupole moments of the j-shell. This model Hamiltonian may be regarded as a simplified version of the conventional $P+QQ$ force model in the sense that only the $K=0$ component of the quadrupole deformation is considered. In the special case that single-particle levels ϵ_k° are equidistant, all q_k are equal, and all $\Omega_k=j_k+(1/2)=2$, this model reduces to the one used by Arve and Bertsch[22] in order to study collective mass parameters in finite superconducting systems. The single-particle energies $\epsilon_{km}(Q)$ corresponding to the Nilsson diagram may be defined by

$$H_{\rm sp}=\sum_{km}\epsilon_{km}(Q) c_{km}^\dagger c_{km}\,, \tag{5·4}$$

$$\epsilon_{km}(Q)=\epsilon_k^\circ-\chi Q q_k \sigma_{km}\,, \tag{5·5}$$

where Q represents the expectation value of $\hat{Q}$ with respect to the HB state vector. The levels with positive (negative) σ_{km} are down-sloping (up-sloping) as functions of Q. Corresponding to this classification of single-particle levels, let us define the following operators:

$$K_{k+}=\frac{1}{2}(A_k^\dagger+B_k^\dagger)\,,\quad L_{k+}=\frac{1}{2}(A_k^\dagger-B_k^\dagger)\,,$$

$$K_{k-}=\frac{1}{2}(A_k+B_k)\,,\quad L_{k-}=\frac{1}{2}(A_k-B_k)\,,$$

$$K_{k0}=\frac{1}{4}(\hat{N}_k+\hat{Q}_k-\Omega_k)\,,\quad L_{k0}=\frac{1}{4}(\hat{N}_k-\hat{Q}_k-\Omega_k)\,, \tag{5·6}$$

where $B_k^\dagger=\sum_{km>0}\sigma_{km} c_{km}^\dagger c_{\tilde{k}\tilde{m}}^\dagger$. The sets (K_{k+}, K_{k-}, K_{k0}) and (L_{k+}, L_{k-}, L_{k0}) form $SU(2)$ algebras, and they commute with each other. The former represents the nucleon pairs in the down-sloping levels, while the latter those in the up-sloping levels. Thus, the multi-$O(4)$ model is equivalent to the multi-$SU(2)\times SU(2)$ model. The $O(4)$ representation corresponds to the seniority-coupling scheme, while the $SU(2)\times SU(2)$ representation to the Nilsson-plus-BCS picture.[20] By choosing different values for the parameters ϵ_k°, q_k, Ω_k, G and χ, the model may be used to simulate a variety of situations where the pairing and quadrupole correlations compete with each other.

In the following, we consider a special case of the multi-$O(4)$ model to simulate the shape coexistence phenomena in semi-magic nuclei. For this purpose, we distinguish protons and neutrons, and consider two levels for protons and one level for neutrons.

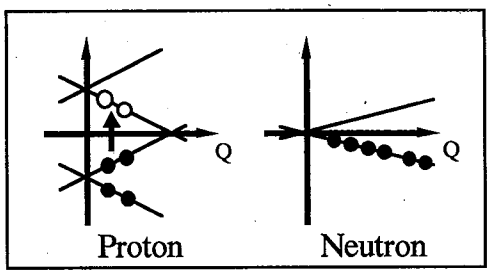

Fig. 5. Schematic illustration of the single-particle energies adopted in the multi-$O(4)$ model. The arrow shows the 2p-2h excitation of the protons.

The lower proton level is assumed to be fully occupied by protons and the neutron level is assumed to have large j and partially filled with neutrons (see Fig. 5). The model Hamiltonian is given by

$$H=H_p+H_n+H_{np}\,, \tag{5·7}$$

$$H_n=-G_nA_n^{\dagger}A_n-\frac{1}{2}\chi\hat{Q}_n^{\dagger}\hat{Q}_n\,, \tag{5·8}$$

$$H_p=\sum_{k=1,2}\epsilon_k^{\circ}\hat{N}_{pk}-G_pA_p^{\dagger}A_p -\frac{1}{2}\chi\hat{Q}_p^{\dagger}\hat{Q}_p\,, \tag{5·9}$$

$$H_{pn}=-\chi\hat{Q}_p\hat{Q}_n\,, \tag{5·10}$$

where the suffices p and n in the operators $A^{\dagger}$, $\hat{Q}^{\dagger}$ and $\hat{N}$ denote the levels for protons and neutrons, respectively. Here the proton 2p-2h excitations across the closed shell in Sn and Pb isotopes are simulated as excitations of two protons from the level $k=1$ to $k=2$. In accordance with this physical picture, we shall treat protons as being in normal phase while neutrons are treated as being in superconducting phase. It should be emphasized that the "protons" and "neutrons" in this model do not necessarily correspond to the actual ones. Rather, the "neutron" Hamiltonian H_n in (5·7) may be regarded as simulating not only neutron excitations but also proton excitations in the single-particle levels except for those explicitly treated by H_p. From this point of view, we can regard H_p, H_n and H_{pn} of (5·7) as corresponding to $H_{sp}^{\circ}+H_{\rm int}$, $H_{\rm core}$ and $H_{\rm coup}$ of the particle-plus-anharmonic-core model Hamiltonian (3·1). It should be emphasized, however, that we are now going to derive collective variables for the total model Hamiltonian (5·7) in contrast to the treatment in previous sections where the collective variables are assumed to describe the collective vibrations of the core. The model Hamiltonian (5·7) is similar to the one used in Ref. 14) in order to study the deformed excited states in Pb isotopes by means of the extended TDHF theory of Yamamura and Kuriyama.[23] A major difference between their approach and ours is that they neglect the mixings between the deformed and spherical configurations while we are interested in the problem how to correctly treat them.

Typical excitation spectra obtained by exact diagonalization of the model Hamiltonian (5·7) are displayed in Fig. 6. Here the parameters $N_p=N_{p1}+N_{p2}=4$, $\Omega_{p1}=\Omega_{p2}=2$ and $\Omega_n=40$ are adopted. We see that model produces the excited deformed configurations associated with the proton 2p-2h excitations, and that their excitation energies decrease with increasing neutron number N_n. This is because the model system under consideration becomes softer against deformation as N_n approaches mid-shell, which occurs at $N_n=40$ for $\Omega_n=j_n+(1/2)=40$. In this figure, we also see that the excited deformed configuration appears in doublets. This is because of symmetry properties of the multi-$O(4)$ model; namely, the system is invariant under the transformation $\hat{Q}_k\to-\hat{Q}_k$. This is analogous to the prolate-oblate degeneracy. The small splittings of the doublets may be interpreted as due to the tunnelings

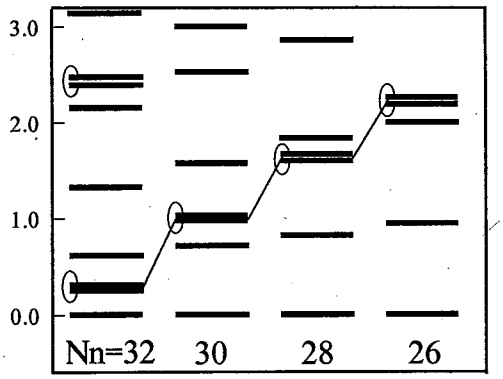

Fig. 6. Exact excitation spectra of the multi-$O(4)$ model plotted as functions of the neutron number N_n. The deformed excited states are connected by thin lines. Parameters used for protons are $G_p=0.1$, $q_1=q_2=2.0$, $\epsilon_1^2=-1.6$, $\epsilon_2^2=1.6$, and those for neutrons are the same as in the core Hamiltonian of the particle-plus-anharmonic-core model used for case (a) in Figs. 3 and 4 except for the neutron numbers, which are $N_n=26\sim32$ here.

between the "prolate" and the "oblate" configurations.

To this model we apply the coupled-configuration SCC method. We note here that the "prolate-oblate" symmetry of this model brings about three Hartree-Bogoliubov states $|\phi_i(0)\rangle$, which are spherical, "prolate" and "oblate". As the exact spectra indicates, however, the doublet states due to the "prolate-oblate" symmetry are almost degenerate. Thus, in applying the coupled-configuration SCC method, we neglect the couplings with the "oblate" configuration for simplicity, and take into account only the couplings between the spherical and the "prolate" configurations. The diabatic configuration $|\phi_i(\eta_i^*, \eta_i, \phi_i, N_i)\rangle$ associated with the spherical ($i=1$) and the "prolate" ($i=2$) HB states are constructed by the fourth-order (η_i^*, η_i) expansion. They are orthogonal to each other. We use the "quadrupole" operator $\hat{Q}=\hat{Q}_n+\hat{Q}_p$ when making the canonical transformation (2·8) between the diabatic collective coordinate $(\eta_i^*, \eta_i, \phi_i, N_i)$ and the global collective coordinates (η^*, η, ϕ, N). Along the line discussed in § 2, we calculate the coupling Hamiltonian $\tilde{\mathcal{H}}_{ij}(\eta^*, \eta)$ as well as $\tilde{\mathcal{H}}_i(\eta^*, \eta)$. The (η^*, η) dependence of the coupling matrix elements $\tilde{\mathcal{H}}_{ij}(\eta^*, \eta)$ is taken into account up to the first-order in (η^*, η), since the (η^*, η) dependence of them is found to be very weak.

In Fig. 7 we show the calculated potential energy functions. Thin lines represent the diabatic potentials while thick lines the adiabatic potentials calculated by means of the Born-Oppenheimer approximation. The diabatic potentials are evaluated in the same way as in Fig. 3 except that the core "quadrupole" moment Q_c is replaced with the total "quadrupole" moment $Q=\langle\hat{Q}_p+\hat{Q}_n\rangle$ here. It is apparently seen that the multi-$O(4)$ model under consideration produces the excited HB minimum. In this figure, the horizontal lines indicate the zero-point vibrational amplitudes of the RPA modes associated with individual diabatic configurations. It should be noted that the second HB minimum is not deep enough to accommodate the zero-point vibration within the second well. In Figs. 8(a) and (b), excitation spectra and transition matrix elements calculated by means of the coupled-configuration SCC method are denoted as SCC (A) and compared with the exact solutions. Here, the third eigenstates correspond to the deformed excited states associated with the second minima of the collective potential shown in Fig. 7. They involve the proton 2p-2h excitations and correspond to the doublets in the exact spectra. In Tables II(a) and (b), percentages of the first (spherical) diabatic configuration in the total wave functions are listed together with the expectation values of the $\hat{Q}$ operators. It is seen that the mixing

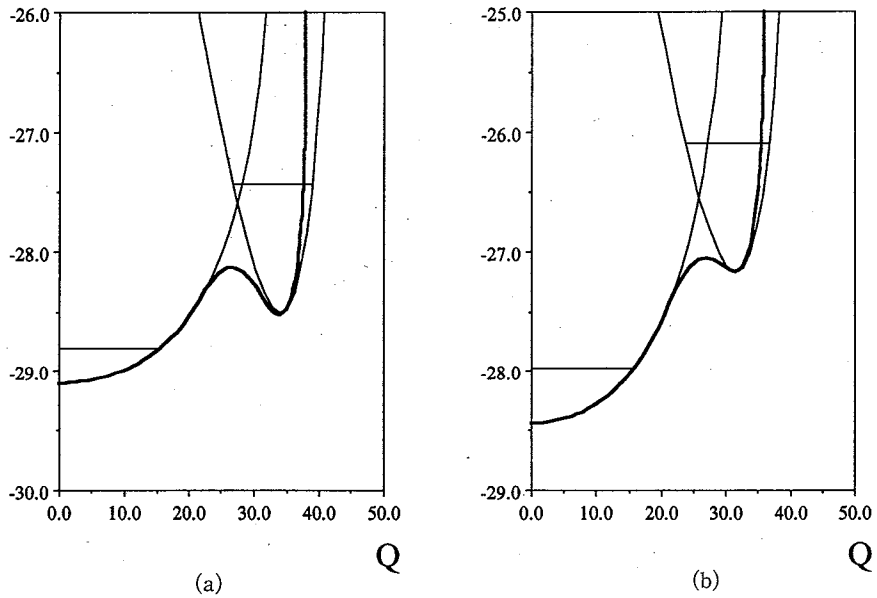

Fig. 7. Examples of the potential-energy functions for the multi-$O(4)$ model. Thick lines represent the adiabatic potentials, while thin lines the diabatic potentials obtained by means of the SCC method. The neutron numbers are $N_n=30$ for case (a), and $N_n=28$ for case (b). Parameters used are the same as in Fig. 6.

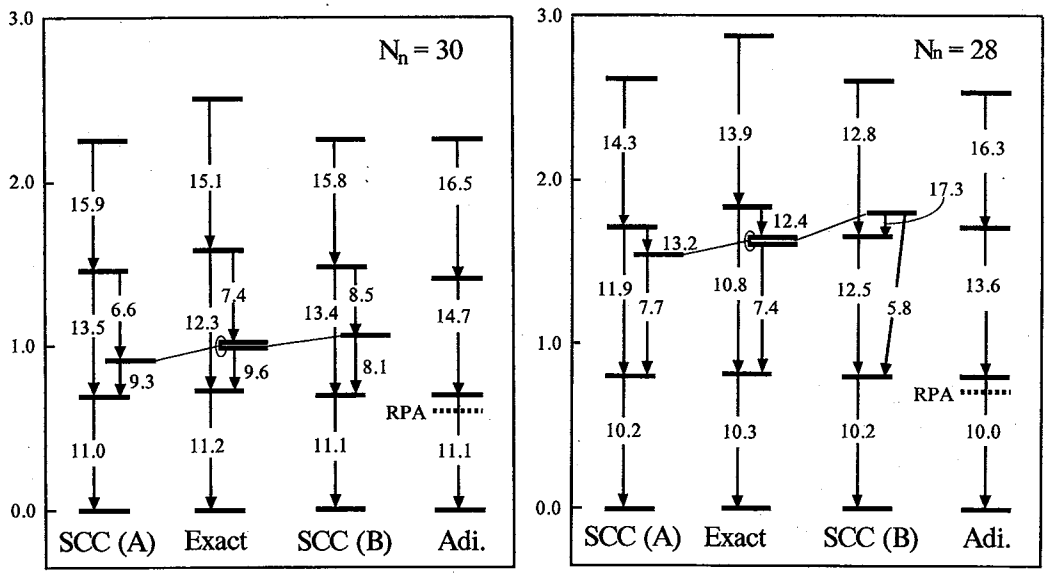

Fig. 8. Excitation spectra and transition matrix elements for the multi-$O(4)$ model calculated by various methods. The spectra denoted as "SCC(A)" and "SCC(B)" are obtained by means of the diabatic approaches described in the text. The deformed excited states are connected by thin lines. The spectra denoted as "Adi." show the results obtained by means of the adiabatic approximation. The RPA excitation energies are also shown by dashed lines. The numbers on the transition arrows indicate the transition matrix elements of the operator $\hat{Q}=\hat{Q}_n+\hat{Q}_p$. Parameters used are the same as in Fig. 7 for cases (a) and (b), respectively.

Table II. Properties of the excited states in the multi-$O(4)$ model obtained by exact diagonalization (Exa.), the coupled-configuration SCC method (SCC(A)), an alternative application of the SCC method (SCC(B)) and the adiabatic approximation (Adiabatic). Notations are essentially the same as in Table I. Parameters used are the same as in Fig. 7 for cases (a) and (b), respectively. Note that the third eigenstates in the columns "Exa.", SCC(A) and SCC(B) correspond to the deformed excited states, except for the column SCC(B) in case (b) where the fourth eigenstate corresponds to them. Note also that two numbers are written for the third eigenstates in the exact spectra, since they are in fact doublets.

(a)

	Exa.	SCC(A)			SCC(B)			Adiabatic	
	%	%	Q	Q_p	%	Q	Q_p	Q	Q_p
1	100	100	0.1	0.0	100	0.1	0.0	2.1	0.1
2	93	97	1.2	0.3	99	0.6	0.1	5.4	0.7
3	2, 7	4	32.6	7.7	4	33.7	7.7	11.6	2.2
4	98	100	0.2	0.0	98	0.7	0.2	5.9	2.1
5	99	100	0.0	0.0	100	0.2	0.0	—	—

(b)

	Exa.	SCC(A)			SCC(B)			Adiabatic	
	%	%	Q	Q_p	%	Q	Q_p	Q	Q_p
1	100	100	0.0	0.0	100	0.0	0.0	1.6	0.1
2	99	100	0.1	0.0	100	0.1	0.0	3.6	0.5
3	15, 1	10	28.3	7.2	83	5.4	1.3	10.6	1.9
4	95	91	2.9	0.7	17	26.7	6.6	9.7	2.5
5	99	100	0.1	0.0	100	0.2	0.0	—	—

between the first and the second (deformed diabatic configurations are small for the pairing-force strength G adopted, and thus the excited deformed configurations retain their identities very well in the third eigenstates. Thus, the expectation values of the $\hat{Q}$ operator, Q, are large only for the third eigenstates demonstrating their characters as deformed excited states.

For the matrix elements of the $\hat{Q}$ operators between the eigenstates of the multi-$O(4)$ model under consideration, the following remarks should be added. Because of the symmetry property with respect to the transformation $\hat{Q}_k \to -\hat{Q}_k$, the deformed excited states discussed above are in fact symmetric or antisymmetric superpositions of the "prolate" and "oblate" configurations. Thus, the expectation values of the $\hat{Q}$ operator in the exact solution always become zero even if they have large value of Q when the tunnelings are neglected. To indicate the deformed character of the calculated eigenstates, however, we have written in Tables II(a) and (b) the Q values that are obtained in the coupled-configuration SCC method by neglecting the tunneling effects. On the other hand, it is necessary to take into account the above symmetry property when we discuss the transition matrix elements between the "spherical" and

"deformed" configurations. One can easily confirm that the transition matrix elements of this kind get a factor $\sqrt{2}$ when we replace the "prolate" configuration with the linear combination of the "prolate" and "oblate" configurations satisfying the symmetry property of the Hamiltonian (5·7). This replacement has been done in Figs. 8(a) and (b). Needless to say, other transition matrix elements are unaffected by this replacement.

It is seen in Figs. 8(a) and (b), that the transition matrix elements between the deformed and the spherical configurations are of the same order of magnitude in spite of the small mixings. The reason is that the diagonal matrix elements of $\hat{Q}$ are much larger than the off-diagonal matrix elements contributing to the transitions between different states in the same diabatic configurations. Thus, even small mixings are sufficient to bring about strong transitions between the deformed and the spherical configurations.

For reference sake, we present in Figs. 8(a), (b), Tables II(a), (b) also the results of an alternative calculation denoted as SCC(B), which is done in the following way. First the SCC method is applied to the neutron Hamiltonian H_n, Eq. (5·8), and the fourth-order approximation of the (η^*, η) expansion on the spherical basis is adopted. The collective representation $\mathcal{H}_n(\eta^*, \eta)$ of H_n is then regarded as a collective Hamiltonian. Second the collective representation $Q_n(\eta^*, \eta)$ of the operator $\hat{Q}_n$ in H_{pn}, Eq. (5·10), is obtained. Third, the total Hamiltonian $\mathcal{H} = \mathcal{H}_n(\eta^*, \eta) + H_p - \chi\hat{Q}_p Q_n(\eta^*, \eta)$, which corresponds to (5·7), is diagonalized replacing the collective variables (η^*, η) with the boson operators and treating the proton operators H_p and $\hat{Q}_p$ exactly. In this approach, the proton and the neutron parts of the model Hamiltonian (5·7) are treated as the valence particles and the core, respectively. In the sense that the particle-core couplings are diagonalized in the spherical basis, this approximation procedure is analogous to the intermediate-coupling scheme. Although this procedure is not selfconsistent since the collective variables are determined by neglecting the valence particles and the particle-core couplings, it may be useful for situations where the division of the many j-shell into the valence and the core parts can be done without ambiguities in such a way that the collectivities are essentially attributed to the core part. In addition, it is applicable also to such cases where there are no well-defined second HB minima. It is seen in Figs. 8(a), (b) and Tables II(a) and (b) that this alternative procedure also successfully reproduces the major characteristics of the exact spectra.

In Figs. 8(a), (b), Tables II(a), (b), we also present the results obtained by means of the conventional adiabatic (Born-Oppenheimer) approximation. They are calculated in the following way. First, we adopt the constrained HB method by choosing the expectation value Q of the total "quadrupole" operator $\hat{Q} = \hat{Q}_n + \hat{Q}_p$ as a constraint to obtain the collective potential-energy functions displayed by the thick lines in Fig. 7. Second, we apply the conventional cranking procedure to evaluate the collective mass parameter as a function of Q. Finally, we solve the collective Schrödinger equation obtained after quantization. The resulting eigensolutions are denoted as "Adi." in these figures and tables. It is obvious that the adiabatic approximation completely fails in reproducing the deformed excited states that appear as the third eigenstates in the coupled-configuration SCC method.

§ 6. Concluding remarks

We have proposed a new microscopic method on the basis of the diabatic picture in order to study the shape coexistence phenomena in semi-magic nuclei. This method may be regarded as an extension of the SCC method to treating the couplings between diabatic vibrational modes associated with different HB minima. We have applied this method to three kinds of schematic models whose exact solutions exhibit two kinds of vibrational states coexisting in the same energy region. It is shown that our method well reproduces the main characteristics of the exact spectra of the systems, which is beyond the limit of applicability of the conventional adiabatic treatment. A particularly interesting suggestion for future study of the shape coexistence phenomena is that the two kinds of diabatic vibrational states associated with the first and the second minima of the collective potential-energy function may retain their identities even if their excitation energies are much higher than the barrier between the two local minima. A crucial quantity which determines whether such situations are realized or not is the matrix element of the pairing force between the two diabatic configurations. We shall apply the coupled-configuration SCC method proposed in this paper to the deformed excited 0^+ states in Sn and Pb isotopes in a succeeding paper, with particular attention to the strength of the interaction matrix elements between the spherical and the deformed configurations.

Acknowledgements

This work has been carried out as a part of the 1989 annual research project on "Nonlinear Dynamics of Nuclear Collective Motions" organized by RIFP, Kyoto University. It was also supported by the Grant-in-Aid for Scientific Research from the Ministry of Education, Science and Culture (No. 01540245 and No. 01790187). The computer calculation for this work has been supported in part by RCNP, Osaka University.

References

1) J. Bron, W. H. A. Hesselink, A. Van Poelgeest, J. J. A. Zalmstra, M. J. Uitzinger, H. Verheul, K. Heyde, M. Waroquier, H. Vincx and P. Van Isacker, Nucl. Phys. **A318** (1979), 335.
2) A. Bäcklin, N. G. Jonsson, R. Julin, J. Kantele, M. Luontama, A. Passoja and T. Poikolainen, Nucl. Phys. **A351** (1981), 490.
3) D. A. Viggars, H. W. Taylor, B. Singh and J. C. Waddington, Phys. Rev. **C36** (1987), 1006.
4) H. Harada, T. Murakami, K. Yoshida, J. Kasagi, T. Inamura and T. Kubo, Phys. Lett. **B207** (1988), 17.
5) H. Harada, M. Sugawara, H. Kusakari, H. Sinohara, Y. Ono, K. Furuno, T. Hosoda, M. Adachi, S. Matsuki and N. Kawamura, Phys. Rev. **C39** (1989), 132.
6) P. Van Duppen, E. Coenen, K. Deneffe, M. Huyse, K. Heyde and P. Van Isacker, Phys. Rev. Lett. **52** (1984), 1974.
7) P. Van Duppen, E. Coenen, K. Deneffe, M. Huyse and J. L. Wood, Phys. Lett. **B154** (1985), 354.
8) J. Kantele, M. Luontama, W. Trzaska, R. Julin, A. Passoja and K. Heyde, Phys. Lett. **B171** (1986), 151.
9) P. Van Duppen, E. Coenen, K. Deneffe, M. Huyse and J. L. Wood, Phys. Rev. **C35** (1987), 1861.
10) J. Penninga, W. H. A. Hesselink, A. Balanda, A. Stolk, H. Verheul, J. Van Klinken, H. J. Riezebos and M. J. A. de Voigt, Nucl. Phys. **A471** (1987), 535.
11) K. Heyde, P. Van Isacker, M. Waroquier, J. L. Wood and R. A. Mayer, Phys. Rep. **102** (1983), 291.

12) K. Heyde, J. Jolie, J. Moreau, J. Ryckebusch, M. Waroquier, P. Van Duppen, M. Huyse and J. L. Wood, Nucl. Phys. **A466** (1987), 189.
13) K. Heyde, C. de Coster, J. Ryckebusch and M. Waroquier, Phys. Lett. **B218** (1989), 287.
14) M. Yamamura, M. Huyse, P. Van Duppen and K. Heyde, Prog. Theor. Phys. **82** (1989), 287.
15) S. Iwasaki, Prog. Theor. Phys. **79** (1988), 730.
16) R. Bengtsson and W. Nazarewicz, Z. Phys. **A334** (1989), 269.
17) T. Marumori, T. Maskawa, F. Sakata and A. Kuriyama, Prog. Theor. Phys. **64** (1980), 1294.
18) M. Matsuo, Prog. Theor. Phys. **76** (1986), 372.
19) M. Matsuo and K. Matsuyanagi, Prog. Theor. Phys **74** (1985), 1227; **76** (1986), 93; **78** (1987), 591.
20) K. Matsuyanagi, Prog. Theor. Phys. **67** (1982), 1441; in *Nuclear Physics,* ed. C. H. Dasso (North-Holland, 1982), p. 29.
21) T. Suzuki and Y. Mizobuchi, Prog. Theor. Phys. **79** (1988), 480.
22) P. O. Arve and G. F. Bertsch, Phys. Lett. **B215** (1988), 1.
23) M. Yamamura and A. Kuriyama, Prog. Theor. Phys. Suppl. No. 93 (1987).
24) H. Fukutome, Prog. Theor. Phys. **81** (1989), 342.
25) S. Nishiyama and H. Fukutome, preprint.